Population Dynamics and Pattern Formation in an Info-chemical Mediated Tri-trophic Plankton Model

A Thesis presented for the degree of

Doctor of Philosophy

at the

Department of Mathematical Sciences

University of Essex

by

Tahani A.S Al-Karkhi

2018

Dedicated to

My affectionate parents and all who continually pray for my fortune.

Acknowledgements

I would like to take this opportunity to express my gratitude and extend my special thanks to all those who have made my time whilst I have been working on my Ph.D so enjoyable and who have provided me the with the opportunity to complete it. So first, I must sincerely thank my supervisors, Professor Edward A. Codling and Dr. Hadi Susanto, for all the support and guidance that they have provided.

In addition, I would like to thank Professor John Dowden for reading my earlier chapters. My gratitude also goes to the department of mathematical sciences for their help and enthusiasm throughout my stay at the University of Essex. I would like to thank my friends and colleagues from the University of Essex who offered stimulating suggestions and encouragement and, most importantly, kept me entertained throughout all this time. Especial thanks go to my friends, Frank and Philip, for their help and support in proofreading my thesis and in offering constructive criticisms on grammar and syntax.

Finally, I have to say that this thesis would not have been possible without the confidence, endurance and support of my lovely family. My husband Rasool, one of the great men of the world, who never lets me feel alone, and who always supports me. To the memory of my mother, and to my supportive father and siblings and to my children, I offer much love.

Abstract

In this thesis, we study a spatio–temporal prey–predator model of plankton. This model has spatial interaction terms which represent a plankton dynamics that includes info–chemical mediated trophic interactions. We consider both a simplified two species model which has been studied in the literature (mostly in biological terms) and an extended, four-species model. In the latter, the grazing pressure of microzooplankton (M) on phytoplankton (P) is controlled through external infochemical (C) mediated predation by copepods (Z). We undertake a stability analysis of both the two species model and the four species model and compare the system dynamics. In relation to this, the critical conditions for Turing instability are derived; these are necessary and sufficient. Furthermore, we consider the degenerated situation wherein Turing bifurcation and Hopf bifurcation occur simultaneously. We also consider under what conditions Turing patterns are exhibited and under what conditions spatiotemporal patterns are observed generally. The Transient Turing instability of spatial interactions –exhibited by the two species model–is introduced and investigated in a number of ways. We also study the effects of the paradox of enrichment. This paradox led to a loss of stability in the four species model after this was derived from the two species model by expansion and by the addition of resources. Further, a numerical continuation technique was used to determine the existence of multiple stationary patterns.

Declaration

The work in this thesis is based on research carried out at the Applied Mathematics group, Department of Mathematical Sciences, University of Essex, United Kingdom. No part of this thesis has been submitted elsewhere for any other degree or qualification, and it is all my own work, unless referenced, to the contrary, in the text.

List of Abbreviations

DMSP	Dimethylsulphoniopropionate
DMS	Dimethylsulphide
NPZ	Nutrient-Phytoplankton-Zooplankton
HP	Hopf-bifurcation
c.c	Complex conjugate
DZBC	Dars Zingst Bodden Chain
HAB	Harmful Algal Bloom.
POE	Paradox of Enrichment.
(P_e, M_e)	Phytoplankton and Microzooplankton equilibrium point.
(P_e, M_e, Z_e, C_e)	Phytoplankton, Microzooplankton, Zooplankton and Chemical release equilibrium point
H.O.T	High Order Term
$\mathcal{L}$	Linear Operator
D_P	Phytoplankton diffusion coefficient
D_M	Microzooplankton diffusion coefficient
D_Z	Zooplankton diffusion coefficient
D_C	Chemical release (Infochemical) diffusion coefficient

Contents

List of Figures

List of Tables

Chapter 1

Thesis Description

1.1 Thesis Overview

This thesis furthers our understanding, in mathematical terms, of biological processes. By deriving a complete mathematical description of the complex interactions which take place in a marine ecosystem we can enhance our understanding of the phenomena involved. Mathematics plays its part by providing insights into areas of biology in which the associated phenomena are difficult, impractical or impossible to measure experimentally [90]. For example, a mathematical model of algal and plankton blooms can be used to simulate and test various forms of interaction which occur in various different environments closely aligned to those found in marine waters. The purpose of the model need not necessarily be to describe the exact process in detail, which is sometimes impossible. However, the model may, nevertheless, provide valid, qualitative information about, say, the effect of chemical release on the grazing behaviours of higher predators or under what conditions phytoplankton blooms or dies.

The goal of a mathematical model can be both predictive and to understand the mechanisms which drive an observed behaviour. This is what is referred to as a two-branch approach. However, the validation of the model is a major requirement when applying such a two-branch approach. This validation can be in the form of physical observations used to examine the feasibility of the outcomes produced by the model, or it can be in the form of a comparison with experimental data. Either way, the biological process should first be

characterised using a mathematical description.

The mathematical stability of a solution is closely related to its physical perceptibility. A result which is unstable in relation to small perturbations will certainly not be perceptible in a spatial biological environment where small perturbations are intrinsic. However, before stability can be established, determining the range of all possible solutions to a model is the first step. Even the physically unrealistic solutions, which initially may be assumed to be irrelevant, can lead to insights when they are combined with stability. From a biological perspective, a model that supports nonphysical solutions should be treated with caution.

In this thesis, we focus on the existence and the stability of solutions for the dynamics of phytoplankton-zooplankton relationships within aquatic environments. The focus is on a model based on two species [143] and another, extended model, based on four species. Phytoplankton play a key role in ocean dynamics. They form the basis of all food sources in aquatic environments [60]. Zooplankton consume phytoplankton, and this forms the basis of all the prey predator associations in aquatic environments. Phytoplankton supply oxygen and absorb carbon dioxide, thus combating global warming effects [60]. Infochemicals play a vital role in food web interactions; they can assist in the avoidance of predators, and/or in finding prey or mates [142]. Phytoplankton possess trophic interactions which allow them to defend themselves against grazers by using deterrents and toxins; they also possess multi trophic interactions that indirectly influence the foraging behaviours of prominent predators [250], [219].

In this thesis, we also investigate, algebraically, the types of the system roots yielded and the corresponding Eigen-values using the Cardans and Ferrari Cardans methods. We further aim at demonstrating the spatial movements of planktonic systems in the presence of released infochemicals. Reaction-diffusion systems are used in this thesis to represent spatial interactions among the planktonic species. The research also investigates conditions which promote or deter the evolution of Turing patterns; this investigation includes the identification of the suitable parametric conditions. Diffusivity assumptions which are realistic in relation to natural planktonic systems are employed to simulate the spatiotemporal distributions of species biomass. The sustainability of biodiversity will be explained here using the overall results. Further, the sustainability of biodiversity is explained based on the influence of infochemicals released by the phytoplankton and zooplankton species.

1.2 Thesis Objectives

The objective of this thesis falls into three main parts. Note that Objectives 1, 2 and 3 are the main objectives of the thesis, whereas Objective 4 is a minor objectives and below is a brief description for each objective points.

- Objective **1**

  The first objective is to demonstrate the utility of the methods outlined in [197] and [198]. We determine the nature of the roots of the original cubic in the two species model and the number of inflections related to the model in [143] in chapter 4 and the nature of the roots of the quartic polynomial in the extended four species model in chapter 7. Furthermore, due to the complex nature of the model in [143] and the extended four species model, we used the methods in [197] and [198] to investigate, algebraically, the types of the roots in each region of the four-species system.

- Objective **2**

  The second objective is to investigate and prove the stability of the two species model in [143] by studying the parameter values and analysing the stability and bifurcation of the model by changing three main control parameters K phytoplankton carrying capacity, ν infochemical release and r growth rate, which will help us to construct the general stability diagram in section 4.5 chapter 4. Moreover, the results presented in Chapter 4 proved that the phytoplankton and microzoplankton densities stabilize at a certain levels of copepod predation as shown in section 4.7.

- Objective **3**

  The third objective is to investigate (in Chapter 5) the existence of pattern formation in the spatial model which is developed on the basis of the model equations from [143]; in addition, we look at the four species spatial model in Chapter 7. Due to the added complexity of these models, i.e., the spatial effects of plankton interactions, it is necessary to make certain assumptions regarding the validity of the numerically observed behaviour of the pattern formations: i.e., the effects of prey diffusion are small and cant exceed the effects of predator diffusion. However, under these assumptions we determined specific patterns which focused our analysis on the existence of novel pattern-formation solutions to

the models explored in Chapters 5 and 7.

- Objective **4**

  The fourth objective is to re-model the two species model [143] and the four species model by using a different set of functional responses, such as the Beddington-DeAngelis functional responses. Beddington-DeAngelis introduced responses related to the mutual interference of two predators predating on one prey. However, we set this objective as future work in relation to this thesis.

1.3 Thesis Outline

Each chapter of this thesis presents details of a specific interaction or of an environmental scenario. The chapters are outlined below.

1.3.1 Chapter 2 Biological background for the Prey-Predator model.

This chapter illustrates the biological background which discusses the primary production of plankton in the ecosystem. We explain different species of organisms within the marine environment. The section introduces the basics of plankton as they feature in the marine ecosystem. In this chapter, we also review the issue of the marine environment and how it affects the survival of plankton.

1.3.2 Chapter 3 Plankton Mathematical Modeling.

Here, we first present an overview of the uses of mathematical modeling in biology and ecology. The chapter is divided into sections and subsections in order to help outline and review this information. The topics covered include: the use of ordinary, non-spatial, plankton models, spatial plankton models, and the partial differential equations relating to these. Plankton population dynamics, including both the non-spatial interactions and the local interactions are presented. Detailed information concerning spatial plankton dynamics and Turing mechanisms in prey predator models is provided. This chapter also highlights data and information concerning chemical models related to plankton dynamics. The last section of the chapter discusses climate change models, including CLAW, with a focus on the modeling of plankton dynamics.

1.3.3 Chapter 4 Bloom Formation and the Hydra Effect in the non-Spatial Infochemical Mediated Plankton Model.

A two-species prey-predator plankton model from the literature [143] is studied, wherein the grazing pressure of microzooplankton on phytoplankton is controlled through external info-chemical mediated predation. The systems stability and bifurcation is explored and analysed in order to explain the conditions which are necessary for phytoplankton bloom formation. The system is illustrated by constructing a heat map for each species, reflecting the positive relationship between the carrying capacity and the population density of each species. The asymptotic method is used to derive the bifurcation curve which, in turn, proves the existence of a limit cycle. The interplay between the level of infochemicallymediated external predation and the phytoplankton carrying capacity of the system is considered; this illustrates the system dynamics for a range of realistic parameter values.

1.3.4 Chapter 5 Transient Turing patterns in the Spatial Infochemical Mediated Plankton Model.

We study a more developed version of [143] by introducing spatial effects into the prey-predator interactions. The work in Chapter 4 proves that the coexistence point is stable for the reaction in the non-spatial system but is unstable for the reaction in the diffusion system. This proof is demonstrated via the Turing instability mechanism and depends on the choice of value. Moreover, a perturbation with a given wave number is applied to obtain the dispersion relation. The short term transient behaviour indicates that a disturbance to a stable equilibrium will eventually diminish; at first such will grow rapidly in size and this growth will continue for a while but eventually the disturbance decays[1].

1.3.5 Chapter 6 PMZC Plankton Model.

Here, we investigate the behaviour of the two species by deriving, from this behaviour, a four species model and by defining a higher level trophic. Introducing the second trophic into the prey predator model and

[1]Both of chapter 4 and 5 combined and structured in paper format and submitted to Journal of Mathematical Biology Springer submission number $JOMB - D - 18 - 00108$.

adding the effects of infochemical release, as a function, could saturate for some level. Also, we study the stability and a bifurcation analysis of the four trophic interaction model and examine the properties of the functions F_i. These latter define the species responses and the types of interspecific interactions which exist. Furthermore, the functions, F_i, depend not only on the population densities but also on a number of parameters such as the birth/death rate(s), population carrying capacity(-ies), etc. These parameters provide an intrinsic scale for each of the variables. The four species model is valid over a long time scale and we attempt to reduce the derived four species model into a special case model and then compare the results from the two models (two-species and four-species), using the same range of parameter values. This is to discover whether these sets of results are consistent with each other.

1.3.6 Chapter 7 Non Turing Patterns in the PMZC Plankton Model.

Studying spatial patterns, or specifically spatio–temporal pattern formation in prey-predator models, is to examine something which is ubiquitous in nature and such a study aligns with the seminal work of Turing on morphogenesis. In Chapter 6, we demonstrate various different Non-Turing and chaos patterns generated by the four species model by using various different initial conditions. Interactions between individuals in the four species over a wide range of spatial and temporal scales are shown to modify the temporal dynamics as well as the stability properties of the population–whichcould be distributed over a natural landscape[2].

1.3.7 Chapter 8 Conclusion and Future Work.

The final chapter presents a general conclusion for this thesis and outlines some new and open research problems in the area of reaction diffusion models of two-dimensional PDEs.

[2]Both of chapter 6 and 7 combined and structured in paper format and submitted to the Journal of Applied Mathematical Modelling in Elsevier submission Ref. No. $APM - D - 18 - 00444$.

Chapter 2

Biological Background

2.1 Plankton in Marine Ecosystems

Plankton are a group of organisms, which includes algae, mollusks, bacteria, coelenterates, protozoans, and crustaceans [96], that live in large bodies of water –some are unable to swim [131]. The term has also been used to represent other phyla of animals. This chapter presents a basic review of the nature of plankton as it exists in marine ecosystems. We also include information about the primary means by which plankton is produced in the ecosystem, the marine food webs, trophic levels, and the biological background of plankton. Plankton consists of drifting organisms that live in the surface layers of the ocean and also in fresh water. These organisms live in the top layer of the ocean, which is called the epipelagic zone. They are not strong enough to swim against the ocean currents [203]. Holoplankton, which exist as plankton all their lives, include crustacean copepods; predatory chaetognaths or arrow worms; and tiny swimming gastropods for example pteropods or sea butterflies among many others [131]. The abundance of the plankton found in ponds, lakes, and oceans varies horizontally, seasonally, and vertically. One of the variables that affect the population level is the availability of light [224]. Plankton undergoes vigorous growth when conditions are favourable and when nutrients are abundant. The effects brought about by these two factors can result in changes in the ecosystem leading to a change in the types of species present [148]. A change in aquatic food density can affect human health (as a result of drastic changes in the food web). This is one of the reasons why

plankton dynamics has become a significant topic within the biological field. Plankton are a fundamental source of food for many large aquatic organisms such as fish and whales. The organisms which make up plankton are divided into 3 main types: Phytoplankton, Zooplankton and Bacterioplankton. The place of plankton in the food chain, particularly in the global carbon cycle, makes it important to the ecology of the ocean. Marine biology stratifies food webs into trophic levels; this stratification places the producers at the 1st level and the herbivorous consumers at the 2nd level [96]. Fig.2.1 demonstrates that food chains start at trophic level 1 (with primary producers such as plants), then comes level 2 (herbivores), level 3 (predators), and then typically they end with carnivores or apex predators at level 4 or 5.

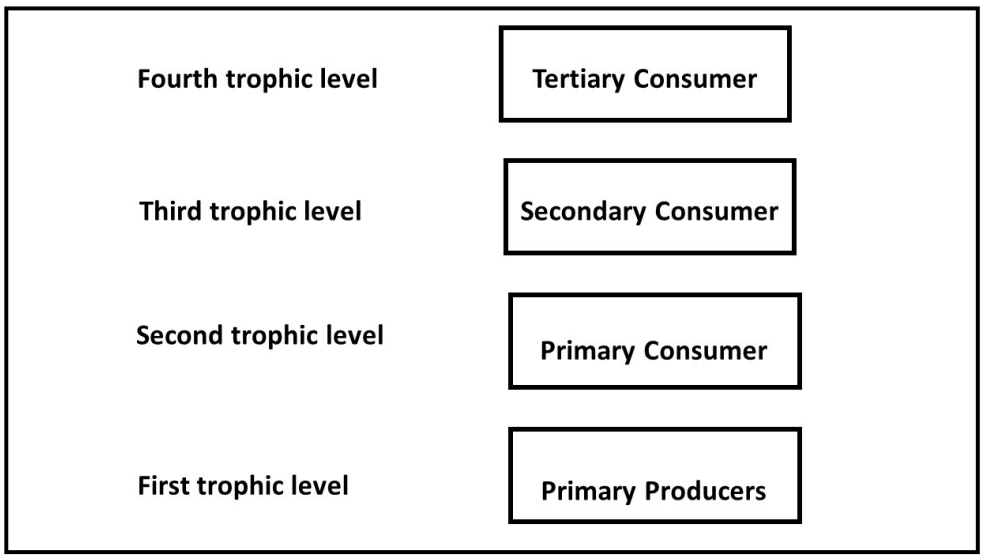

Figure 2.1: *Trophic level refer to the position an organism occupies in a food chain.*

This classification is based on the role that the organisms play in the food chain. Plankton are classified as producers/consumers, and they are important sources of food for many organisms in the marine ecosystem. Phytoplankton play a major role as the first link in the food web. They feed the Zooplankton and the other small animals, and hence the survival of many organisms depends on phytoplankton. Through the photosynthesis process, phytoplankton produce food for the micro-zooplankton and these provide food for the larger zooplankton which may, in turn, provide food for larger fish, etc. [123]. Marine phytoplankton produce a considerable amount of the atmospheric oxygen which is necessary for human and other living beings. This is one of the reasons why they are a very important component of the oceanic food web. The Phytoplankton release oxygen as a by-product of the process by which they synthesise their food with phy-

toplankton highlighted in marine biology as producing up to 70% of the oxygen on earth [30].

There are a diverse range of organisms which are classified as phytoplankton species; these include photosynthetic organisms. The two dominant species of the latter are dinoflagellates and diatoms. The dinoflagellates include the smaller phytoplankton: picoplankton and nanoplankton. Both of these types of organism are very small in size, and the picoplankton group is the one most associated with supporting oxygen production. Diatoms are the other common phytoplankton group. The diatoms come in various different shapes.Picoplankton are also referred to as phytoplankton organisms.
Phytoplankton generally counteract attacks from zooplankton grazers by forming large cells, colonies, complex cell structures, or by producing toxic substances [139]. However, even when phytoplankton is toxic, it doesnt threaten to reduce the zooplankton population to extinction [18].

According to [230], the growth of algae has been observed in both long chains and in single chain cells. Among the algae which have been studied are the green algaes which include the colonial and unicellular flagellates. The green algaes may also come in different forms: e.g., colonial, filamentous, or coccoid. Colonial and unicellular flagellates have both been described as groups of photosynthetic eukaryotes, and there are about 6000 species of these. [70] has stated that a microorganism (or microbe) are living organisms which are too small (as individuals) for the naked eye to see. These come in two forms, single-celled and multi-cellular. Common microorganisms include protozoa, algae and fungi. Plankton, particularly phytoplankton, are key primary producers which form the general foundation of the ocean ecosystem, as shown in Fig. 2.1. Microzooplankton are at the next level in the food chain. They are also key components of marine foodwebs. Their grazing significantly affects the primary producers and they play a key role in shaping the structure of most marine ecosystems as the primary grazers of marine phytoplankton and as intermediaries between the primary producers and the copepods [34]. Microzooplankton provide the only trophic link between the phytoplankton and the copepods. Zooplankton is a category of tiny animal species who depend on the holoplankton [1] while they float with the oceanic currents during their early developmental stages. Among the common microzooplankton species there is the radiolarian; these are one-celled animals with long spines

[1] Holoplankton are organisms that are planktonic (they live in the water column and cannot swim against a current) for their entire life cycle.

radiating from their membranes.

Phytoplankton mortality is predominantly due to grazing by zooplankton. Zooplankton are generally larger than the phytoplankton on which they feed, and some of the largest are cannibalistic and eat other zooplankton. Copepods are extremely important plankton, most are herbivorous, and copepods are the major link in the ocean marine food web. They transfer energy from plant to animal communities. However, not all copepods are planktonic, and many are harpacticoida [2] copepods and are important members of the benthic and interstitial fauna [246]. Females of the Temora longicornis copepods have been used to investigate the chemodetection of dimethyl sulfide (DMS) as it occurs in the interaction between herbivorous copepods and their phytoplankton prey [220], [143].

2.2 Plankton Population Dynamics

In the following, we describe the dynamics of plankton populations, including how planktonic species interact with other marine species. We discuss algal blooms as they occur in both fresh water and seawater in the context of the numerous defense mechanisms that the algae deploy. The prey and predator environment is also presented alongside further information on the types of defense mechanisms used by the different species. As an element of plankton dynamics, examples of the occurrence of allelopathy, a phytoplankton defense mechanism, are discussed as well as the interactions within the marine ecosystem involved.

As noted by [139], algal bloom is the accumulation of an algal population in a marine or freshwater system. Such an accumulation leads to a discoloration of the water. Further examination reveals that the color of algal blooms is determined by the photosynthetic pigments in the algal cells. Common colors include red, yellow and brown. The type of pigmentation involved contributes to the color and is dependent on the species of algae. The defense mechanisms of a number of phytoplankton species can cause a situation called harmful algal bloom (HAB) which can significantly affect marine environments and marine ecosystems; this effect can poison the water, and this results in fish and bird mortalities and illness in humans [105]. Algal blooms are a recurrent problem in both sea water and fresh water environments [139]. These blooms are the

[2] Harpacticoida comes from the Greek noun harpacticon (rapacious predator) and the suffix -oid (akin to) and means reminiscent of a predator, few of these are planktonic or live in association with other organisms.

consequence of an excess of nutrients such as results from the runoff of both phosphorus and nitrogen into waters. High concentrations of these nutrients in water cause increased growth in algae and green plants. As more algae and plants grow, other organisms die [110].

Most organisms have evolved predator-induced defenses in order to protect themselves. Rotifers[3] develop long spines in response to kairmones released into the environment. This development involves either the production of new spines, the elongation of existing ones or a combination of the two as presented in Fig. (2.2) [87]. Different species within the marine ecosystem respond to the physical environment differently, and this defines their place in the food web. This is what marine biology refers to as the trophic interactions [43]. For example, a trophic coupling between some fish populations and the plankton creates a food chain, and studying this food chain helps us to understand productivity issues. The concept of ecological efficiency refers to the situations wherein one trophic level of production governs the next level of production. There are also other concepts within the theory of trophic interaction, including that of assimilation efficiency. Ecological efficiency describes the efficiency with which energy is transferred from one trophic level to the next. It is determined by a combination of efficiencies relating to various organisms efforts at resource acquisition and assimilation. The efficiency with which animals convert the food they ingest into energy for growth and reproduction is called their assimilation efficiency [40]. [65] highlighted that phytoplankton species have highly flexible biochemical compositions. This enhances their ability to defend themselves by producing toxic compounds. This trait represents the basic defense mechanism of most phytoplankton species. These mechanisms can be categorized via their biochemistry: toxins and repellents may be produced; changes in morphology, for instance the formation of thicker cell walls, may be induced; and also changes in life history characteristics and among these would be placed a reduction in the use of infochemicals [147]. Most organisms have developed predator induced defenses in order to protect themselves. Allelopathy is an adaptation technique used by many phytoplankton species with the sole purpose of obtaining an advantage over others [107], [107] and [42].

[156] defined the vertical movement of plankton up and down the water column in response to seasonal changes in marine dynamics as vertical migration. As a way of avoiding predators and protecting themselves,

[3]Rotifers fall prey to many animals, such as copepods, fish (e.g. herring, salmon), bryozoa, comb jellies, jellyfish, starfish, and tardigrades.

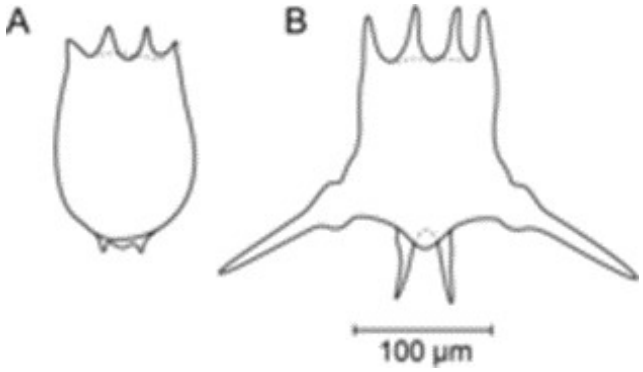

Figure 2.2: *Asplancha-induced defense in Brachionus calyciflorus. (A) Basic or non-induced Morph. (B) Asplancha induced Morph. (Showing elongation of spines). Figure from [87].*

some marine species, including copepods, migrate to some safe area during the night and return to their grazing areas during the day. This is referred to as diel vertical migration. [156] described this type of migration as a behavioral adaptation among copepods whereby they move to the epipelagic zone at night and return to the mesopelagic zones during the day. Research has indicated that phytoplankton and zooplankton communities consist of many different organisms with different rates of nutrient consumption, etc. and different abilities in terms of attacking other organisms in their respective food chains. This allows the organisms to exploit the food availability differentially across the environment. [91] explained that grazing rates across the communities differ based on food concentrations, biomass and taxonomic compositions. [29] stated that the varying compositions of the phytoplankton and zooplankton communities determine the grazing rates within these environments. Evidence discovered by [29] indicated that an increase in zooplankton mass and sizes results in higher grazing activity and that this will then affect the phytoplankton growth rate. Also, a reduction in phytoplankton growth rates reduces the rate of grazing.

[3] wrote that predation has played a crucial role in structuring the various aquatic communities. Defense mechanisms have been researched mainly to address the issue of predation. [249] added that in order to reduce their mortality, zooplankton prey develop predator-resistant morphologies. Such include the production of chemical defenses. There are other species that respond to cues emitted by predators through developmental polymorphisms [3].

[137] shows that one of the major defense mechanism employed by marine organisms is the ability to detect predators from a distance. This latter research indicated that many organisms are able to detect

the hydrodynamic disturbances caused by predator movements. This results in rapid responses by the prey, aimed at escape, and these responses can be referred to as anti-predation adaptations. A coupling of biological and physical dynamics has been used to explain the ecology of some species of plankton [185]. The process described is one that explains plankton spatial dynamics, including the interaction of plankton and other organisms within their environment. [50] further observed that planktonic processes and spatial patterns within the marine ecosystems drive plankton behavior. However, that author also indicated that the ocean food web can be affected by changes in plankton behavior. An understanding of the plankton ecology requires an understanding of the various different scales involved, including, for instance, the effect on plankton growth of micro-scale turbulence. The larger-scale distribution of plankton can also be shaped by local features such as eddies and fronts [185]. Such interactions between the plankton and the environment are elements in a vast biological and physical dynamical system. Advances in technology have made it possible, in marine ecological studies, to highlight these dynamics, and this in turn has made it possible to observe the planktons behavior within the marine environment. It has been observed, for instance, that as a result of fluid flow interacting with planktonic behavior, spatial patterns are formed. Among the processes which drive the plankton-environmental interactions is microscale turbulence [57], which effects plankton and changes its distribution. This research also indicated that the chain-forming diatom life-forms which dominate (Leptocylindrus, Chaetoceros and Skeletonema) were able to thrive in the growth pulses caused by the increases in nitrogen which occur in late-winter. The prevailing turbulence intensities observed, associated with the wind speed, were such that the Batchelor scale was smaller than the length of the diatom chains (100–300μm), implying that these diatoms could experience microscale nutrient gradients.

2.3 Marine Infochemistry

Chemical signaling is a way by which species coordinate their behavior via the passage of chemicals between individuals. In the following, we discuss the different types of chemical released and the roles of these chemicals within the marine ecosystem Infochemistry is used to describe the generation of environmental chemical signals, chemical defenses and the other chemical agents that constitute the driving forces in the ecology and evolution of marine systems [257]. Infochemicals such as kairomones, allelochemicals and pheromones play

a vital role in predator prey interactions and strongly influence the ecological structure and population dynamics of an ecosystem [142], [107]. Infochemicals exuded from marine phytoplankton influence the feeding behavior and selectivity of predators and so play important roles in food web interactions [142], including being utilized as grazing cues. Such evidence has resulted in increased research into the areas of establishing the chemical production principles and interpreting the biological responses to the respective stimuli within the ecosystem. [73] indicated that dimethyl sulfide (DMS) is a biologically produced sulfur compound. The production process supports natural trophic interactions between the plankton and the environment. DMS has also been documented as being released in large quantities by coral reefs in order to support larval orientation [40].

Both [243] and [72] describe prey predator relationships as mediated by chemical signaling. Many organisms in the marine environment release chemical substances into the water in order to locate their prey, as noted by [220]; find desired mates; mate and reproduce [130], [107]; and to detect and protect themselves against predators. This is illustrated in Fig.2.3 where stimulus production is shown to induce the physical movements that contribute to the delivery of a behavioral or psychological response [107], [240]. Infochemicals strongly influence the population structure of plankton in that the infochemicals released by phytoplankton greatly affects their likelihood of predation and competitive interactions [143]. Infochemicals can affect the scavenging and selectivity behaviours of zooplanktonic predators by acting as defense mechanisms, or by enhancing the ability of a zooplankton species to locate its prey [243], [25]. For example, as described by [257], small peptides with arginine or lysine at their carboxy termini induce ovigerous mud crabs to release and further disperse their brooded embryos and also induce oyster larvae to settle near conspecific [4] adults. A study was carried out by [69], to determine whether P.dubias, an organism that feeds on filamentous cyanobacteria, can detect the bacteria by the use of only chemical cues and without any direct contact. Before commencing the experiment the test organisms were starved for 24 hours. They found that the starved ciliates obtained enough food without difficulty. It was evident that a waterborne chemical factor originated from the grazers, thus limiting the dispersion of cyanobacteria trichomes. Another example, given in [126], illustrates how copepod use chemoreceptors to detect food and use coordinated movements to draw

[4] An organism belonging to the same species as another

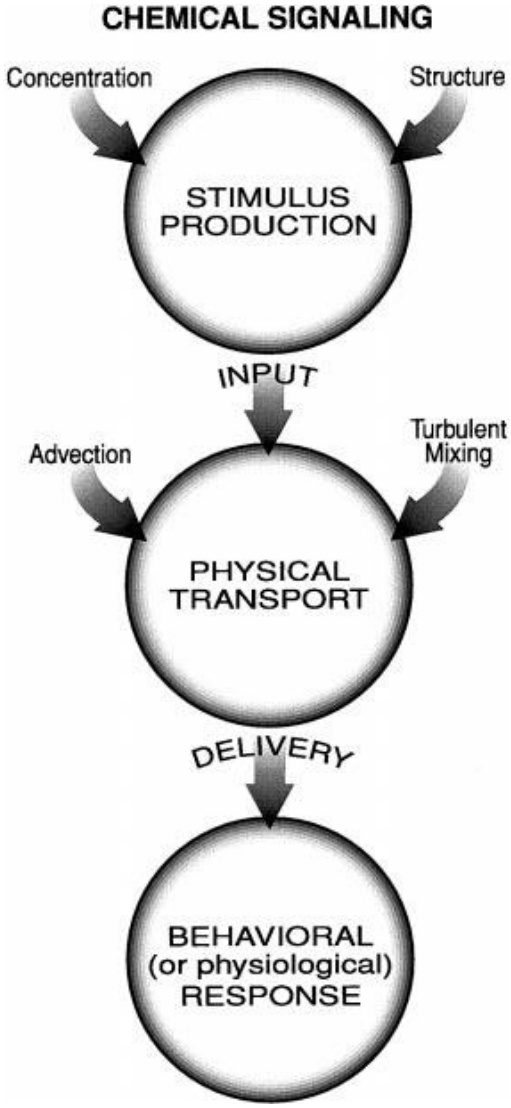

Figure 2.3: *Figure illustrating the factors that determine the production, transportation and perception of chemical cues by macroscopic organisms. Figure from [257].*

the food particles to desirable capture areas. Kairomones are known to be very commonly used as chemical signals, and they can also be responsible for transferring information between species to the benefit of the receiving organism and to the disadvantage of the producer. Kairomones are solely used, by their producers, to locate food and detect or fend off predators [183].

Volatile organic compounds (VOCs) are also considered, in marine biology, to be another family of crucial infochemicals. They are defined as low molecular weight compounds with low to moderate hydrophilicity which can easily dissolve in water and also dissipate into the gas phase at air water interfaces. Dimethylysulphide (DMS) is a volatile sulfur compound produced from the algal secondary metabolite, dimethlyesulfo-

niopropionate (DMSP), via complex biotic interactions [217], [220], [55]. The conversion (from the metabolite) is governed by the chemical equation in Fig.2.4 which depicts the conversion of DMSP to DMS using DMSP lyase as described by [239].

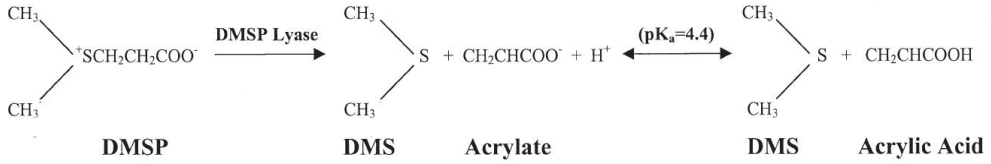

Figure 2.4: *Conversion of DMSP to DMS, Figure from [239]*

Allelopathy is an adaptation technique, used by many phytoplankton species, which has the sole purpose, for the producer, of obtaining an advantage over other species [107], [107] and [42]. Allelopathy may be considered as a defense mechanism since it involves the release of allelochemicals; these contribute to the success of the species through: leaching, exudation, volatisation, and decomposition. Phytoplankton produce numerous chemical products [6], the most common being dimethylsulphide (DMS), which is released when zooplankton attack a bloom of phytoplankton [107]. DMS is produced by the breakdown of Dimethylsulphoniopropionate (DMSP) via two processes, the DMSP lyase pathway described above and directly by the algae [42, 221]. The DMS acts as a feeding beacon for sea birds, reef fishes and whale sharks [53].

The DMS produced by marine algae is released into the atmosphere and oxidised to sulphate [72]. DMS accounts for up to 60 percent of the total natural sulfur released into the atmosphere, and the oceans are the main source of DMS since they provide up to 95 percent of atmospheric DMS [217]. DMS has attracted much research attention recently because of its role in marine ecology, in cloud formation and in climate processes. It is released in vast amounts and it is believed to have large scale meteorological impacts [8]. In relation to marine ecology, DMS is responsible for initializing the defenses of marine algae aimed at counteracting herbivore attacks; DMS has the effect of providing prey related chemical cues to predators, [183]. Thus, DMS release can be included as a survival mechanism of the phytoplankton since it attracts copepods which prey on microzooplankton into the ecosystem. Copepods are small crustaceans, some of them planktonic, that mostly drift in ocean waters or live on the ocean floor (these latter are referred to as benthic). [220] observed that copepods have a larval form and that the larva moults several times. The more a larva has moulted, the further it is towards achieving adult development. Copepods respond positively to DMS, which increases

the tail flapping behavior necessary to assist the copepod in detecting patches of DMS releasing algal prey, as illustrated in Fig 2.5 [220]. DMS affects predator-prey interactions by effecting directional foraging in seabirds and marine mammals who are enabled to locate areas with high biological productivity [170], [135], and by encouraging behavioral changes in copepods which are searching for prey [220]. The copepod reaction to DMS results in multi-trophic interactions between phytoplankton, zooplankton and copepods thus enhancing predation on microzooplankton which in turn releases the grazing pressure on phytoplankton [220].

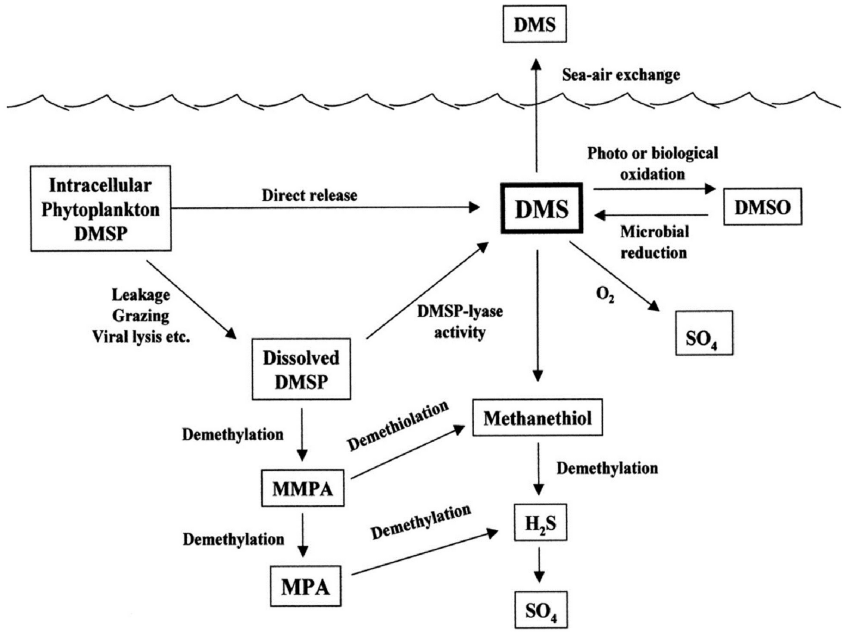

Figure 2.5: *Environmental constraints on the production and removal of DMSP and DMS [183].*

2.4 Climate Change and the CLAW Hypothesis

The marine environment, as is described in [64], has been affected for very many years by changes in the climate. One major observation is that human activities including the creation of pollution, the introduction of new species and coastal developments have resulted in alteration in marine ecologies. Climate changes have been among the major factors that have resulted in a number of impacts on the ecosystem. Greenhouse gas emissions, which have altered the climate, have led to a variety of different responses from marine ecological systems. The CLAW hypothesis has been used to explain the relationships between the Earth's climate and the changes in the ocean ecosystems. Below, we describe the CLAW hypothesis and we present

information about oceanic acidification and how changes in DMS production affect climate change.

The CLAW[5] hypothesis was published over 20 years ago and has stimulated a great deal of research since [181]. The CLAW hypothesis, which derived its name from the initials of the authors surnames [41], proposes that a climate feedback loop exists between phytoplankton, DMS, cloud condensation nuclei (CCN), and cloudiness [138]. Fig.(2.6) illustrates the steps of this feedback loop as outlined in the CLAW hypothesis. DMSP plays a vital role in climate regulation and in the formation of cloud condensation nuclei (CCN) in the atmosphere [41]. CCN are largely caused by the DMS produced by marine algae; the DMS oxidizes in the atmosphere to form sulfate aerosols. DMS is a product of DMSP, as shown in Fig. (2.4). The latter is produced by marine algae as a result of them encountering increased osmoregulatory demands [56]. This production is affected by the temperature, salinity and the light surrounding the ecosystem. Research has indicated that the most illuminated, warmest, and most saline environments support the most DMS production. Based on the CLAW hypothesis, it can be inferred that phytoplankton have the ability to regulate their own population. This is made possible through the regulation of DMS emissions; this, in turn, leads to increases or decreases in the solar energy input. Therefore, this process regulates temperature, salinity and light which are the major determinants of DMS production; hence the feedback loop is formed.

[41], argues that as a result of the emission of DMS into the atmosphere, a homeostatic feedback loop may exist between the oceanic phytoplankton and the climate. Further observational studies carried out by [48], [163], indicate a correlation between cloudiness, atmospheric aerosol concentration and phytoplankton. These findings, however, lack the spatial and temporal coverage that is crucial in order to investigate whether *DMS* and *CCN* coupling is solely relevant for global climate processes. [238] carried out an experiment to investigate the timescales at which the DMS-CCN coupling operates and whether DMS could alleviate the effects of global warming. They found that DMS affects global temperatures indirectly through the associated shoaling of the upper mixed layer, which causes in turn an increase in surface DMS concentrations; this indicates that a small increase in DMS is negligible in terms of counteracting the effects of global warming. Ecosystem studies have also been utilized to investigate the ecosystem production of DMS. *DMS* production has been strongly promoted as a candidate solution to global warming and climate change, although such a

[5]R. J. Charlson , J. E. Lovelock , M. O. Andreae , S. G. Warren.

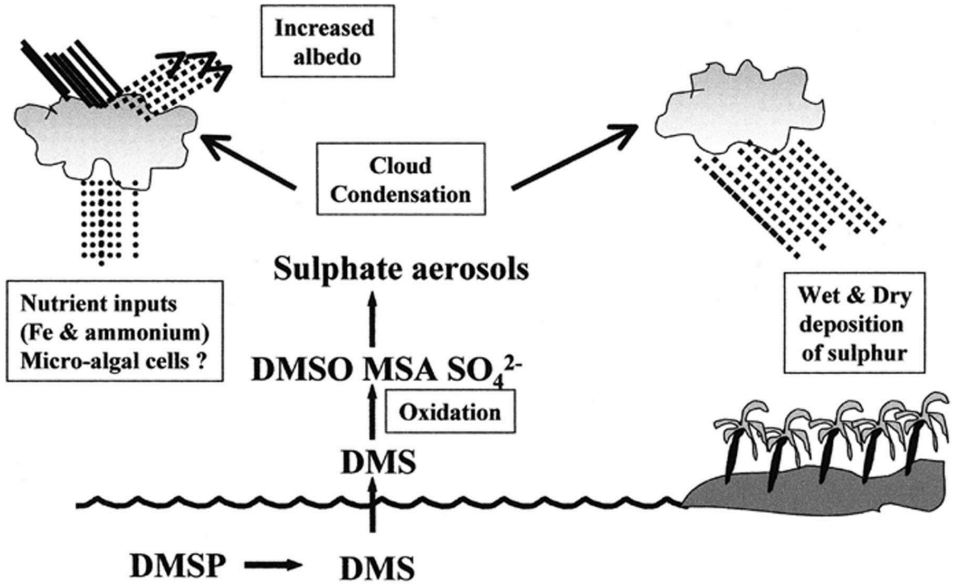

Figure 2.6: *The CLAW Hypothesis – Figure showing the steps involved in the CLAW hypothesis whereby* (1)*DMS emits fluxes into the atmosphere which then produce CCN.* (2) *The process increases the reflective properties of the clouds albedos.*(3) *Large amounts of solar radiation are reflected back into space, thus reducing global temperatures and received radiation. Figure from [12].*

possibility is subject to further study and research. The role of DMS in plankton physiology is still unclear. Thus it is difficult to determine how the emission of DMS in relation to phytoplankton may change as the surface water changes in response to climate change [32]. DMS emission has been associated with the formation of sulfuric and methanesulfonic acids in the atmosphere [143]. The main cause of such changes in the atmosphere is the oxidation of DMS. It is also argued that significant numbers of cloud condensation nuclei (CCN) are formed through the oxidization of DNS. This results in cloudiness in the atmosphere. Further observation highlights that global climate change has been significantly affected by the increased production of DMS. [71] observed that increased DMS production is associated with a cooling effect in the atmosphere. DMS production has also been associated with an offset effect with regard to the greenhouse warming of the atmosphere. The major observation is that algal production has featured in some major marine biology experiments as of use in regulating the Earths climate. The 1987 findings from James Lovelock also emphasized that DMS, which persists in the atmosphere, is converted to sulfur compounds [181]. These include a variety of aerosols that cause the condensation of water vapor in the atmosphere, leading to the formation of clouds. As further indicated by [56], clouds serve a major purpose in terms of the regulation of the climate. They are known to reflect solar radiation back into space thus preventing overheating that may

affect the earths surface. Therefore, they are important in that they have a cooling effect on the earths surface. Associating this with DMS, the more the oxidization process occurs, the more clouds are formed.However, a major contention is whether the oceanic ecosystems have enough algae to produce enough DMS to produce good cloud cover. This is a major issue that modern researchers are aiming to understand from the perspective of the CLAW hypothesis. A broader conclusion from marine biology research is that DMS has a major role to play in providing a stability mechanism which may combat climate change. In fact, in relation to the concept of DMS emissions, researchers have indicated that releasing sulfur into the atmosphere could be a more effective antidote to global warming than other efforts targeted at removing carbon dioxide from the atmosphere [143].

The concept of ocean acidification has also been associated with human interference in the marine environment. An increase in the amount of carbon dioxide has been recorded within the ecosystem as a whole, as a result of increased human activities [143] and this acidifies the ocean. The findings indicate that human activities, such as the disposal of waste in the sea, have resulted in an increase in carbon dioxide. Statistics further indicate that the amount of carbon in the atmosphere has indeed increased and this has led to a huge amount (of carbon) being absorbed into the marine environment. In fact, over one-third of all CO_2 emissions released into the atmosphere as a result of human activity end up being absorbed by the marine environment. The result is an increase in acidity that affects phytoplankton dynamics [187]. The pH (power of Hydrogen) is simply a measure of the acidity of a solution and this has been recorded as decreasing (indicating increased acidity)in the marine environment, resulting from the increased absorption of CO_2. This leads to major negative impacts on the marine ecosystem.

2.5 Human Interaction and the Plankton Cycle

Human interaction with the marine ecosystem has been viewed as having a major impact on plankton dynamics. Here, we provide information about the human cycle including its effect on fisheries, non-toxic algal bloom and on toxic bloom formation. We also illustrate that DMS has an effect on global warming and climate change. Research by [94] has indicated that human activities have been central to pollution, the introduction of new species and the over-fishing that severely affects the fisheries and the entire life of the

sea. The research indicated that acidification has affected the productivity of phytoplankton. [244] added that, in relation to human activities there have been major changes in the marine ecosystem over the years.

Human activities impacting ecological communities have produced pervasive and accelerating changes to these ecosystems and remain major sources of uncertainty when predicting the structure and dynamics of ecological communities [136]. There is increasing recognition of the significance of altered trophic interactions and energy flows in ecosystems being degraded by human activities [253]. The major observation is that the human activities within these environments have an impact on the marine ecology. Recent substantial technological developments have meant that there have been increases in the production of waste, increases in over-fishing, the introduction of new species and other forms of pollution that affect the coastal ecology. Such human activities which impact on ecological communities are becoming pervasive. They are accelerating changes to ecosystems and remain major sources of uncertainty when attempting to predict the structure and dynamics of ecological communities [136]. The strength of the interactions within plankton networks and their changed nature in human altered ecosystems remain poorly understood and there is increasing recognition of the importance of altered trophic interactions and energy flows in ecosystems degraded by human activities.

One of the many changes in the ecosystems has been eutrophication. This is a pollution that results from excess nutrient release into the sea. [94] observed that the over use of fertilizers means that the excess nutrients end up in the sea and lead to excessive phytoplankton growth. Oxygen levels are then depleted, leading to the death of other species, such as fish. Additionally, a significant loss of biodiversity has been documented on the sea bed as a result of new species being introduced into an ecosystem. In relation to eutrophication, the research indicated that huge competition for nutrients affects the growth of phytoplankton and this leads to the death of other species, further along the food web, that depend on some aspects of this growth. Eutrophication is used in marine biology to explain the damage induced by human activities within the coastal environments [143]. The excess nutrients in the coastal streams lead to excessive growth of the phytoplankton resulting in blooms. The blooms result from the increased decomposition of dead organisms. The increased rate of death of these organisms is caused by the depleted levels of oxygen supply within the marine ecosystem. When this depletion reaches a certain level, some large species may also die as a result of the lack of oxygen in the environment. New species introduced within an ecosystem can threaten the existence

of phytoplankton within the marine environment, though it can also be said that not all new species survive within such environments. However, there are some species, introduced into ecosystems, which become difficult to remove. Research has highlighted wakame undaria pinnatifida, a Japanese seaweed as being one of the most difficult species to remove from an ecosystem [181]. This seaweed has had major impacts on the survival of native marine organisms along the coastline it was introduced to.

2.6 Observing and Monitoring Plankton Population

Advanced technologies have been used in the research which attempts to understand the marine ecology. Different approaches have been used to observe and monitor the plankton population. In the following, we present information concerning plankton spatial dynamics. We further discuss the remote sensing of plankton species. An outline of the standard methods for remote sensing is presented; this outline includes a discussion of the different types of satellite sensing. We study organisms in terms of their spatial dynamics because the study of non-local interactions is helpful to biologists as such describes biological systems on scales which are convenient in terms of observation, data collection, and insight [140]. We examine how the movement, spreading and interaction of plankton can be mapped via remote sensing algorithms [71]. This mapping helps biologists to monitor non-local phenomena. For determining effective management approaches in relation to plankton dynamics within the ecosystem [196] used the Plankton Survey System (PSS). This is a system which carries out an analysis of the health and productivity of marine ecosystems. [196] further observed that the survey system collects spatial and temporal related environmental data from the ecosystem. This data can be used to understand plankton dynamics with a focus on the spatial interactions within the ecosystem. An optical plankton counter measures the size and distribution of zooplankton. This counter involves the use of an LED array and LIDAR photodiode receivers in order to collect adequate data for the measurements. The algorithms which perform remote sensing are based on the ocean color being expressed as a function of the inherent optical properties of seawater, such as the absorption coefficient [205]. Phytoplankton and non-chlorophyllous particles are the most easy to detect, while dissolved organisms are a much more difficult matter. The effect of chlorophyll color on the ocean color is mediated by the phytoplankton concentration [9].

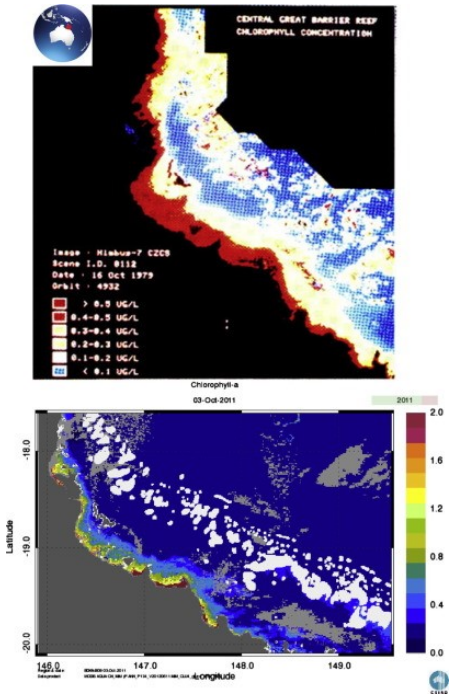

(a)

Figure 2.7: *Satellite images from ocean color sensors from [21]*

2.6.1 Model for the remote sensing of plankton (plankton interactions in a terrestrial context).

Remote sensing has been used as a technique for synoptically mapping aquatic systems. This technique uses Climate Data Records that have been made over long periods of time and so the results are driven by global trends [71]. Spatial and spectral resolution is the newest of the technologies which have been applied in remote sensing. The monitoring of Algal blooms has been indicated as critical, given that blooms are indicators and measures of the health of an ecosystem. Novel algorithms for mapping plankton were introduced way back in the 1970*s*. The technologies have advanced over the years, leading to major improvements in the algorithms related to coastal waters – see Fig. 2.7 from [252]. Scientists have successfully managed to produce novel algorithms for the mapping of plankton of different functional types. Advances in satellite ocean color technologies have been cited in research studies as critical to such algorithmic research. The mapping of phytoplankton blooms has been made possible by the provision of a synoptic view of the ocean [96]. Investigations into the abundance, attributes and distribution of phytoplankton over the seasons, including the differences in physico-chemical characteristics which become apparent, have been

successfully conducted using a number of different qualitative and quantitative estimates. [4] stated that these estimates have been used to understand the growth cycles of phytoplankton across the ecosystem. In deriving these estimates, [4] observed that plankton samples must be collected from different locations within the ecosystem. These estimates are made possible by the variations in light backscattering and algal pigment absorption. The use of ocean color remote sensing provides near-real-time synoptic measurements which generate both qualitative and quantitative estimates of the global phytoplankton biomass [142]. This makes it fairly straightforward to collect data cheaply for mass analysis. The presence of Turing patterns, as described in Appendix A.6, can be verified for the analysis of the reaction chain from the genomic structure of the plankton. Also, an understanding of the mechanism that generates DMS may facilitate the genetic engineering of phytoplankton / algae for the production of higher amounts of DMS. Near exascale climate modeling of atmospheric distribution by SOLAS means that we can do very precise modeling of atmospheric processes. Results from robot ocean sensors can verify the production rates of DMS from phytoplankton and the dispersion in the ocean, as measured.

2.6.2 Standard methods in remote sensing

Among the remote sensing technologies are the satellite sensors. Satellites provide a high level of spatial analysis and this enables the mapping of plankton groups. As indicated in the literature, regional differences in plankton group composition have led to huge diversity within the ocean ecology. The use of satellite sensors provides a mechanism whereby phytoplankton groups may be distinguished from each other. The technique identifies variations in cell structure and pigment complexes in order to categorize the different phytoplankton groups (see Fig.2.8).

The MERIS satellite is one of the sensor systems; it has been operational, and mapping phytoplankton, since the year 2000 [142]. The Airborne Visible/Infrared Imaging Spectrometer (AVIRIS) is another remote sensing device used for imaging phytoplankton groups [252]. The device is used to discern between phytoplankton pigments in inland water bodies. Phytoplankton pigments are used in determining the state of phytoplankton. In marine biology, these pigments are associated with biogeochemical cycles in the ocean ecosystem. Through the pigments, assessments of the physiological condition of a phytoplankton can be made. The central thesis is that the phytoplankton pigments are affected by the trophic conditions –

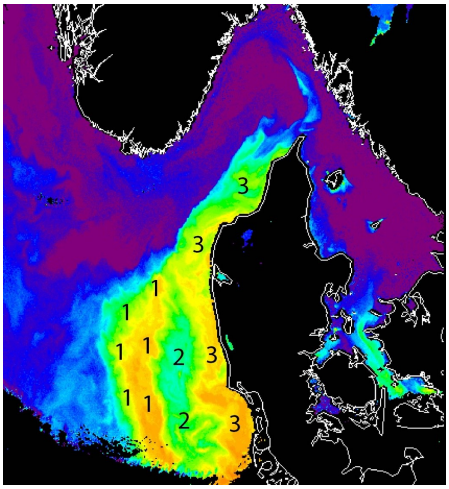

(a)

Figure 2.8: *Satellite sensor images of different phytoplankton assemblages [200]*

with photoprotective carotenoids (PPCs) being associated with low productivity waters, and photosynthetic carotenoids (PSCs) [6] being dominant in high productivity waters [142].

[6] serve two key roles in plants and algae: they absorb light energy for use in photosynthesis, and they protect chlorophyll from photodamage (PSCs)

Chapter 3

Plankton Mathematical Modeling

3.1 Introduction

Models of planktonic processes have been of major relevance to oceanographers for many years. They are especially important for the understanding of the different functions which exist within planktonic ecosystems. [176] wrote that plankton models have been of relevance in studying the distribution of copepods, in studying global carbon balances and in understanding chlorophyll layer dynamics. However, the uses to which different models can be put are dependent on their different formulations. The main purpose of understanding plankton models is the development of tools for the understanding of biodiversity and global marine production –which affect climate change. This chapter presents the mathematical plankton modeling dynamics. Besides the climate models, modeling in marine ecology has also focused on the modeling of autumn plankton bloom dynamics. But research in that field as well has highlighted the fact that climatic conditions have been of major influence on the production of plankton bloom. The major observation by [37] was that the responses from the system following changes in the climate have resulted in disturbances of the ecosystem. The findings have been further underscored by other publications in this field. [215] focused on understanding the dynamics of plankton blooms by analyzing the remotely sensed ocean colour. In their study, these authors highlighted that a general pattern in terms of the oceans colour can be identified as

being caused by an eastward progression of the FPB[1]. This was mostly found to be evident in the NSSGoM[2] region where data has indicated a change in the spatial pattern of chlorophyll concentrations. In this chapter we present plankton population dynamics, both the non-spatial interactions and the local interactions are presented. Detailed information concerning spatial plankton dynamics and the Turing mechanisms found in a prey predator model has been documented. The chapter also provides data and information on chemical models relating to plankton dynamics. The last section of the chapter discusses climate change models with a focus on plankton modeling dynamics.

3.2 Plankton Population Dynamics (Non-spatial Interactions).

This section is concerned with plankton population dynamics. This discussion is based on an understanding of the non-spatial interactions (or local interactions) that exist within marine ecosystems. Here we investigate, using a number of different models, the multitrophic interactions which occur in aquatic environments. Among these models are a simple population model, a three species model and a four species prey predator model. The Malthus model described in Appendix A.1 has been used in marine biology to explain population theory dynamics. This model was formulated in the early nineteenth century to predict the problems which might be caused by the exponential growth of a population in relation to the available resources –an example would be the exponential growth of bacteria [151]. Population theory made use of a basic logistic equation, described in Appendix A.2, to explain population dynamics. The model has been used in mathematical biology to analyse population trends and interactions among species. It has been the main ground for many scientific biological interpretations, including the understanding of the carrying capacity of the marine ecosystem. For the last half–century, researchers have been using mathematical models in order to assist in their studies of marine ecosystems [176]. The complex nature of aquatic environments and the cost of experiments has driven researchers and pioneers to formulate mathematical equations that are used to model the various different behaviours which manifest within plankton communities [176]. These models are generally constructed in order to study a particular group and/or in a particular area to study specific

[1]Fall Phytoplankton Blooms
[2]Nova Scotian Shelf (NSS)Gulf of Maine (GoM) region

phenomena. The different approaches to marine ecosystem modeling include [176]:

1. Models based on the mathematical techniques involved:
    - Models based on ordinary differential equations (homogeneous or space discrete).
    - Models based on partial differential equations (space-continuous).
2. Models based on the problems that they are applied to:
    - Models developed to analyze the vertical or horizontal dynamics of an ecosystem.
    - Models developed to analyze the temporal dynamics of a community.

Predator prey models have been developed from those focusing on just one species, to those focusing on two, three and four species, although there has been little research on the latter kind of model. The modeling methodology which uses mathematical equations is based on the pioneering work of Lotka and Volterra, described in Appendix A.3 [236], [194], [88]and [58]. Predator versus prey density graphs have been use to explain the nature of predator-prey interactions [194]. The research has also indicated that there are major effects from natural selection that may affect predator-prey interactions. It is concluded in [194] that to establish stability in predator-prey interactions researchers should focus on the understanding of equilibrium densities and consider the predator-limiting resource.

The differential approximations in Eq. (3.1) can be written as:

$$\begin{aligned} \frac{dP}{dt} &= \alpha(k_1 P - M), \\ \frac{dM}{dt} &= \beta(P - \frac{M}{k_2}). \end{aligned} \tag{3.1}$$

The predator-prey interactions given in Eqs. (3.1), are shown here [194]. What is normally highlighted is the comparison between the prey and the predator densities. This seems, usually, to be understood as the major determinant of conditions within the ecosystem. The observation is that stability can be achieved from unstable interactions through the management of predation pressure. The limitation of the predator at its equilibrium density results in a stable condition. Eqs.(3.1) show that if the predator nullcline lies to the right of the peak of the prey nullcline, then the system is stable, and if the predator nullcline lies to the left

of the peak of the prey nullcline, the system will exhibit instability [134]. A recent analysis by [143] proved that, for $\lambda = 0$, the microzooplankton nullcline lies to the left of the peak of the phytoplankton nullcline [3], and thus the system is unstable in the absence of DMS. In this situation, solutions will oscillate over time and not reach a stable steady state [168]. It can also be observed that the mathematically-continuous model explains in detail the interactions close to the equilibrium. However, there is no clear-cut explanation of how the isoclines are affected by natural selection. The model also lacks adequate explanation of how interactions can be stabilized.

The simple population model developed by [143] illustrates phytoplankton that produce DMS in small quantities as a one species model, grazed by microzooplanktons developing the two species model and thereafter, the microzooplanktons are consumed by mesozooplankton. The study [143] was based on an initial assumption that microzooplankton act as a trophic link between plankton and copepods. The assumption was made that an increase in the background concentrations of DMS enhances the grazing rates of microzooplanktons. The equations showed that as the value for prey carrying capacity increased, the stability of the system was compromised via Hopf bifurcation in Appendix A.5[4], and this process is referred to as the Paradox of enrichment as established by [194]. The model, as formulated, provides a system which generates stability by implementing a predominant route for the mortality of small phytoplankton whilst excluding the grazing of copepods. The sole purpose of the study was to examine the idea that infochemicals can play a vital role in influencing multi trophic interactions –i.e., those between phytoplankton, microzooplankton, and copepods–and promoting the formation of phytoplankton blooms. [193] Rosenzweig carried out a study on the destabilization of exploitation ecosystems over ecological time. Six reasonably accurate models of trophic exploitation in a two species ecosystem–where exploiters compete by depleting each others resources, were examined. The study found that the more the nutrients or energy were available, the more the steady state was destroyed. The study agreed with that of [114], who carried out similar research and established that a stable ecosystem was destabilized in these circumstances, resulting in the extinction of both the exploiter and its victim. Earlier models have proved that sufficient enrichment of the prey population will result in limit cycle oscillations that will rapidly grow, resulting in the amplification of enrichment a circumstance

[3] See Fig. 4.1 in chapter 4

[4] The types of bifurcation relevant to this thesis results.

that became known as the Paradox of Enrichment, as modeled by May (1972) in [158], Gilpin (1975) [88] and [254] Yodzis (1992), among others. Abram (1996) in [2], carried out a study on the stability of predator prey models whereby they found that increase in carrying capacity decreased the density dependence felt by the prey population thus destabilizing this population.

[168] demonstrated that in conditions of persistent phytoplankton bloom there should be a deficiency of nutrients in the system. Phytoplankton abundance is largely dependent on the bottom-up factors that affect growth, such as light intensity and the availability of a wide range of macro- and micro-nutrients [127]. In the mixed layer, phytoplankton receive an adequate amount of light, but they remove nutrients from the environment, making these unavailable to other cells [164], [127]. This important phenomenon has not been explored in detail in previous models of this infochemical mediated tritrophic system.

Nutrient-Phytoplankton-Zooplankton (NPZ) models examine the quantities of nutrient and assimilated nutrient (plant and herbivore biomass) in a system and are a common tool used to model plankton interactions in the nutrient-limited marine environment [74], [127]. NPZ models have the most important attribute that they yield to a reliable parameterized analysis which allows for analytical solutions relative to the limited number of state variables. NPZ models are simpler to initialise and explore than other, more complex models. While some aspects may render them less realistic, they still allow for a different range of model behaviors which are sufficient in terms of providing realistic simulations of some ecosystem dynamics [174].

A study carried out by Stone (1990) in [222], investigated phytoplankton-bacteria-protozoa interactions in order to understand the paradoxical behavior of phytoplankton under stress. The study made use of matrices, in particular it made use of inverse and loop matrix manipulations in order to derive the community effects which occur between microbial organisms and phytoplankton. The study found that by including protozoa and by allowing them to graze on bacteria and recycle nutrients, many aspects of the paradoxical behaviour of such systems could be resolved. The main reason for this analysis was to develop a comprehensive framework that would explain the 'lengths' and 'levels', within the interaction matrix. Such are evident because the protozoa induce a number of indirect interactions that are advantageous to phytoplankton. The protozoa also supply the much needed nutrients to phytoplankton by indirectly alleviating the competitive pressure of bacteria on phytoplankton.

[189], carried out a mathematical analysis of a nutrient plankton system which had a delay mechanism.

They introduced a discrete delay to account for the time needed for the phytoplankton to mature–after which they can release toxins. A system of delay related differential equation describing nutrient-plankton interactions were used and then different theorems regarding the positivity and boundedness of the solutions were applied. The study concluded that without discrete time delays the conversion rates from nutrients to phytoplankton and phytoplankton to zooplankton would be lower and insufficient to reach a threshold value. This threshold value is such that if it is not met the plankton will become extinct. The introduction of a discrete time value ensures that as soon as the threshold is achieved, the delayed nutrient plankton system enters into Hopf bifurcation (see Appendix A.5). Thus, a periodic orbit is created whereby a switching of stability is created. [95] explored the seasonal plankton dynamics in the Dars Zingst Bodden Chain (DZBC); this is a body of water on the Baltic Sea coast, in the northeast of Germany. DZBC consists of lagoons arranged in an east-west direction that stretch over $197km^2$ and have about a two metre average water depth [228]. [95] implemented the Lotka-Voltera competition model which portrays the coexistence of algae and cryptopyhtes. They found that both allelopathy and mixotrophy related substances are vital for the stabilizing of the environments in the DZBC.

[222] carried out an investigation into a three species prey predator model describing the interactions between microbial organisms and phytoplankton in the context of a plankton community. The study found that such interactions are highly stable and that the presence of the microbial organisms provides the phytoplankton with added advantages [222]. Stone's study was recently reviewed by Hardly and Forbes where they found, using a dynamical systems approach, that there were no limit cycles arising from a Hopf bifurcation [92]. The three species model, as developed in Stone's (1990) was further developed into a five species model by the use of dynamical systems theory [7]. Most recently, numerous models have been formulated to determine the nature of prey predator interactions. [245] carried out a study on a Hopf-transcritical bifurcation in a toxic phytoplankton-zooplankton model with time delay. By analyzing the equations, [245] addressed the local stability of the Hopf bifurcation at the coexistence equilibrium. The authors discussed the issue of global stability via significant illustrations using numerical simulations. From this discussion, a feasible equilibrium of the model was illustrated. They presented the inner equilibrium and direction and stability of the Hopf bifurcation, established the norm form for the Hopf-transcritical bifurcation, and performed a bifurcation analysis using numerical solutions. Their study yielded important results with re-

spect to dynamical behaviours such as stable periodic solutions and attractive quasi-periodic solutions. The study illustrated the reasons behind the presence of approximately periodic or quasi periodic motions with respect to the changes in time of plankton populations. The model developed portrayed interactions between phytoplankton, bacteria, protozoa, zooplankton, and nutrients. The focus of the study was to determine the stability of the steady state populations and of the possible self-sustained oscillations. The study found that if nutrients are allowed to vary it was possible for the degeneration to be counteracted and perhaps for Hopf bifurcations to occur, instead of a central behaviour [92].

Turing patterns in Appendix A.6 may be developed by using a systematic approach to the design reaction diffusion patterns–by utilizing the fact that the reversible complexities of an activator species forms a nonreactive immobile complex that reduces the effective diffusion constant of the activator [141]. The study of chaotic motions was first formulated by a French mathematician in the early 1890; it was based on the stabilities discovered via solar studies. This study was later picked up by Kalmogorov, Arnold, and Moser who then formulated the KAM theory (named from their surnames). This theory covered the conditions resulting in weak chaotic motions in conservatives systems. James Yorke, in the 1970*s*, carried out a study of random looking dynamics in deterministic systems, the term Chaos itself was coined in the course of this study. The study was further enhanced by Feigenbaum where he proved the existence of the situation whereby a system can be independent of possible routes towards chaos [227]. The four species model developed in the current study will describe interactions in a plankton closed system between infochemical producing phytoplankton, microzooplankton and copepods; it has been developed from [143]. The layout of this chapter is as follows. The first sections of this chapter will concentrate on models of single species, such as the exponential growth, and the logistic growth models (Verhulst). The second section presents the different types of bifurcation which will be investigated in this thesis. Section three will describe the two species model (prey predator) and Holling functional response types. Section four will show the diffusion equation and its different applications in a variety of fields. Section five presents diffusion equations and their application via some famous equations. Section six introduces the meaning of Turing instability. Finally, in section seven, we provide a brief overview of the thesis as a whole.

The models discussed in the current section are important in exploring the spatial movements and interactions among phytoplankton and zooplankton species. As explained by [142], the introduction of

reaction-diffusion equations is critical for the understanding of the non-spatial interactions. The use of the spatial models helps in exploring the spatial movements of planktonic systems. It is from this that the sustainability of biodiversity can be explained.

3.3 Spatial Plankton Dynamics and Turing Mechanisms in Prey Predator Models.

This section provides an intensive investigation into spatiotemporal dynamics. It discusses prey predator models with a focus on a phytoplanktontoxic phytoplankton zooplankton model and the reaction-diffusion processes in predator prey models. This focus is based on the argument that there is a need for models which advance the understanding of predator prey interaction in marine ecosystems. The non-linear evolution equations or reaction diffusion equations presented in Eq. (A.6.30) and their linear stability analysis will be discussed in detail in Appendix A.6. Chemicals can react and diffuse under certain conditions in order to produce steady state heterogeneous spatial patterns of chemical or morphogen concentrations, as Turing suggested [49],

$$\frac{\partial U}{\partial t} = f(U) + D\nabla^2 U, \tag{3.2}$$

In Eq's A.6.30, U is the vector of morphogen concentration, f represent the reaction kinetic, while D is the diagonal matrix of positive constant diffusion coefficients [121]. Reaction diffusion systems are perhaps the easiest to study mathematically of the many experimental systems considered [15]. Reaction diffusion systems are a broad and important class of non-equilibrium systems which are present in biology, chemistry ecology, and engineering. Turing instability analysis examines analytically, see Appendix A.6, the linear stability of the simplest possible reaction-diffusion system. The analysis leads to several insights into what forms a uniform state, some are unexpected [49].

- One insight is that at least two interacting chemicals are needed to form a pattern.
- Diffusion can be a destabilizing influence in reacting chemical systems.

- The instability caused by diffusion can cause the growth of structures at particular wave lengths, such as the segmentation patterns in the developing fly embryo or the zebras stripes or spatial population density. The latter is the main effect studied.

- Pattern formation in a chemical system will not occur unless the diffusion coefficient of at least two reagents differ substantially.

Prey predator relationships are hugely affected by chemical signals and cues released by both prey and predators which result in changes in their of behavior and morphology which are crucial for their survival and well-being [247]. Plankton in food webs are considered as the dominating factors in the understanding of the ecology of marine environments. Phytoplankton, microzooplankton and copepods interact with each other via infochemicals in a prey and predator relationship. as illustrated in Fig 3.2. r, depicts the rate of growth of prey in the absence of predators; the predators capture prey at the rate, g, where the rate of consumption is denoted by γ. The predators will be affected and eventually die with lack of prey at a rate of m. The Lotka and Volterra model has been proven unrealistic by many researchers [121], [134], since the introduction of a small perturbation will shift the trajectory into a state that it is completely different from the original one. The model is also shifted to instability with the introduction of a small perturbation in favor of either the prey or predator. [18] carried out a study to investigate the interaction between phytoplankton, toxic phytoplankton and zooplankton. They formulated a mathematical model using a Monod Haldane[5] response function as described in Appendix A.4–to model the grazing of toxic phytoplankton by a zooplankton population that takes care of the fact that the consumption rate of the toxic population decreases with increases in its biomass. This shows that the presence of toxic phytoplankton induces a reaction in the zooplankton. Its presence reduces consumption up to the point where the microzooplankton starve. However, the mechanism will not drive the zooplankton population to extinction due to, the presence of spatial movements in the planktonic system. Further investigation of the multitrophic interactions in aquatic environments were undertaken by [142] using a 1D spatial reaction diffusion system to simulate a three species prey predator model and comparing the cases where copepods forage randomly to the cases where they adjust their positions to follow

[5]Holling functional response.

distributions of infochemicals that are produced by grazing. [168] investigated the role of nutrient limitation and infochemicals in a plankton food web model. They created a full four species model that employed the use of a NPMZ model for which the parameters were non-negative and constant in time. This was in order to investigate the top down role of infochemical-mediated predation and the bottom up effects of nutrient limitation. They found that the chemicals released due to microzooplankton grazing on phytoplankton elicit a behavioral foraging response in carnivorous copepods, thus increasing their efficiency in their search for suitable prey. In explaining the Turing mechanism [14] focused on explaining the Turing instabilities and spatio–temporal chaos within the marine ecosystem. These phenomena are also explained by [177] who highlighted the role of spatial diffusion as in Eq.(3.3).

$$\begin{aligned} \frac{\partial u}{\partial t} &= \frac{\partial^2 u}{\partial x^2} + u(1-u) - \frac{uv}{u+h}, \\ \frac{\partial v}{\partial t} &= \frac{\partial^2 v}{\partial x^2} + k\frac{uv}{u+h} - mv. \end{aligned} \tag{3.3}$$

The system in Eq. 3.3,first, has a reaction term which describes the prey growth by using the logistic equation, which is a common realistic model in a resource limited environment, with an intrinsic growth rate of $r = 1$ and a carrying capacity of $k = 1$. The second term is a Holling type-II functional response here-–e.g Appendix A.4. The spatial diffusion implemented in Eq. 3.3 explains that sufficiently low nutrient levels results in a collapse of the zooplankton population, and that this leads to the phytoplankton population reaching its carrying capacity. Solving the spatiotemporal dynamics requires the use of the explicit method of [23] finite difference and requires the setting of the perturbed initial distribution of the species, in order to obtain non-trivial spatiotemporal dynamics. The initial condition could have the following form:

$$u(x,0) = \overline{u}, \tag{3.4}$$

$$v(x,0) = \overline{v} + \epsilon x + \delta, \tag{3.5}$$

In Eq's 3.5, ϵ and δ are constant values [151]. This type of system depends significantly on the values of ϵ and δ. In cases where ϵ is small and δ is positive, the initial conditions gradually will vary in time and the local

temporal behavior of the dynamical variables u and v will be strictly periodical following the limit cycle of the non-spatial system [120], as is shown in figure 3.1.

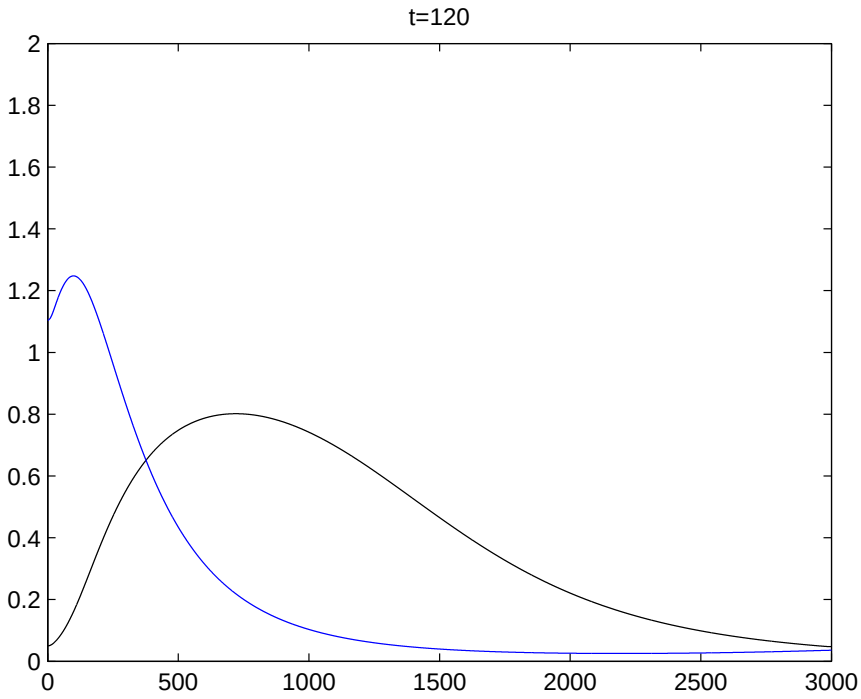

Figure 3.1: *Matlab has been used to solve the spatial distribution of the prey-predator model with initial distribution as per 3.5 and no flux Neumann boundary conditions [151], [120]*

A two species diffusion reaction system has been considered to be too simple to produce anything more complicated than regular patterns with regular dynamics and this conclusion leads us to the work in the following section [151].

The authors in [120] and [151] used a modified spatiotemporal ecological system to study the stability of coexisting homogeneous interactions among prey and predator populations. In this study, an investigation of a modified PDE system was conducted to examine Turing and non-Turing patterns. It was discovered from this study that there is no observable convergence of prey or predator population in any stationary state. The results further indicated that spatiotemporal chaos is exhibited by prey and predator populations as a result of a Turing–Hopf domain. The study by [14] concluded that to understand such spatio–temporal chaos, it is important to evaluate the Turing-Hopf bifurcation domain. The author [14] provided adequate information relating to how future researchers can integrate the relevant parameters for measuring the spatial plankton dynamics in prey predator relations. When presenting literature related to spatial dynamics and

prey predator models the work of [80] should also be introduced into the discussion. The authors in [120] and [151] were of the view that linear cross-diffusion explains the destabilization of the constant state in the marine ecosystem. In that study, they integrated chemical reaction modeling into their system in order to explain the Turing pattern formation mechanism. These authors performed an analysis of Turing patterns in order to evaluate the influence that these patterns have on the occurrence of sub-critical bifurcations. From the study, it could be seen that cross-diffusion coefficients influence the existence of multistable stationary solutions. The study is of huge relevance in marine biology having concluded that the reaction-diffusion Schnakenberg model should be investigated further in order to understand spatial plankton dynamics. Future researchers may use this model to explain prey predator relations.

However, a different dimension is presented by [14] who indicated that the three species spatial model is the main equation that elucidates and explains spatial plankton dynamics and Turing mechanisms. In their study, [14] described how they used Hollings type III functional responses to construct the model. In this study, the authors found out that there is the possibility of stable oscillations forming following the coexistence of the three interacting species. However, it was also indicated that the species may be destroyed through damped oscillations. The conclusion from this study was that understanding the cross-diffusion[6] of the top predator is important in terms of understanding the spatial plankton dynamics. The authors emphasized that the three species model is very relevant for analyzing habitat segregation within ecosystems.

Advancing the Turing mechanism discussion, [14] and [17] focus on explaining the Turing instabilities and spatio temporal chaos within the marine ecosystem. [17] used a modified spatiotemporal ecological system to study the stability of a coexisting equilibrium point. In this study, an investigation of a modified PDE system was conducted in order to investigate Turing and non-Turing patterns. It was discovered from this study that there is no observable convergence of prey or predator populations in any stationary state. The results further indicated that spatiotemporal chaos has been exhibited by prey and predator populations as a result of Turing-Hopf domains. Thus, the study concluded that to understand spatiotemporal chaos, it is important to evaluate the Turing-Hopf bifurcation domain [7]. The study provides useful information relating to how future researchers can work with the relevant parameters in order to measure the spatial plankton

[6] A nonlinear diffusion which links multiple diffusing communities and which add to the standard Laplacian terms.
[7] All related details in chapter 5.

dynamics of prey predator relations.

The discussion concerning the prey predator model was also continued in the study by [180] who focused on intratrophic predation. In this study, the researchers consider a terrestrial ecosystem as the main foundation for an explanation of spatial plankton dynamics. [180] argued that in such an ecosystem, flora and fauna can be considered as the two main species in play. Their argument was that modelling the relations between these species requires the use of a predator–prey system. The research indicated that the inclusion of a predator–prey model for modelling intratrophic predation results in intuitively plausible features. These features are important for understanding the predation since they affect the position and stability of the equilibria within the ecosystem.

Advancing to another discussion of prey predator models, [96] studied mixotrophy as the phenomenon used to explain the effects of low light–or nutrient–limitation within aquatic ecosystems. This study argued that different types of mixotrophy have been used in developing the predator–prey model and explaining the productivity of plankton blooms. The researchers demonstrated that significant effects on a system's equilibrium structure is felt when small levels of type III mixotrophy are introduced. The final results of the study indicated that the productivity of phytoplankton–zooplankton systems increase in the presence of different types of mixotrophy. This is a study which has been applied in marine biology research to understand the production of phytoplankton–zooplankton systems and how these relate to the other spatial plankton dynamics.

From another direction, [71] used a set of simple differential equations to model autumn phytoplankton bloom. This study was carried out in temperate oceans through an advanced mechanism. The researchers, in their model, made the upper mixed layer deeper, in order to trigger blooms, and provided increased sunlight to enhance the phytoplankton growth rate. The authors further argued that rapid deepening affects the production of blooms, given that it deteriorates the phytoplankton growth. In this study, it was observed that there is a need for alternative grazing and deepening regimes in order to avoid the extinction of phytoplankton.

3.4 Chemical Models.

Chemical models have been used for the understanding of plankton dynamics. Issues concerning plankton populations are raised in many scholarly works on marine biology. In this section, we demonstrate a variety of chemical models for use in relation to plankton dynamics. The works of [143] have been reviewed in this section to highlight the model equations used in the chemical modeling of plankton dynamics.

$$\begin{aligned} \frac{dP}{dt} &= rP\left(1-\frac{P}{K}\right)-\frac{aPM}{1+bP}, \\ \frac{dM}{dt} &= \frac{\gamma aPM}{1+bP}-mM-\lambda\frac{aPM^2}{1+bP}, \end{aligned} \tag{3.6}$$

In Eq's 3.6, P and M are the densities of the phytoplankton and microzooplankton in the closed homogeneous system, respectively. It is assumed that phytoplankton grows logistically with intrinsic rate of growth, r, and carrying capacity K, where the carrying capacity corresponds to nutrient limitation and self-shading. The microzooplankton graze on the phytoplankton according to a Holling type II functional response, as described in in Appendix A.4; the rate of grazing saturates at high densities of phytoplankton. The conversion of phytoplankton biomass to microzooplankton biomass is performed with efficiency, γ. The parameter m corresponds to the total microzooplankton mortality that would occur in the absence of DMS; microzooplankton mortality is assumed to be mainly caused by copepods, but this term also accounts for a background mortality due to processes such as sinking and additional predation by other zooplankton or by species at higher trophic levels. The parameter λ corresponds to an increase in the background concentration of DMS which would allow copepods to improve the efficiency of their search through chemodetection. In the subsequent analysis we consider λ as an exploratory parameter that we vary in order to consider different scenarios in relation to the possible effects of DMS. The analysis and further developed model of Eq.(3.6) are in Chapter 4 and Chapter 5 respectively. [143] presents a multitrophic plankton model which describes the plankton interactions across three trophic levels. These levels are represented by grazing microzooplankton, phytoplankton, and predatory mesozooplankton. In this model, the complexity of these interactions is explained. The authors show that in relation to stabilizing the system dynamics, the inclusion of grazing-induced DMS production increases mesozooplankton predation. The grazing rate of microzooplankton is

also increased, demonstrating that a potential lead in the formation of phytoplankton bloom. Through the works of [143], an understanding of the role of DMS beyond it being a cooling gas can be developed. The multitrophic plankton model emphasizes the role that DMS plays in the ecology of marine food webs. This is further reviewed by [144] who affirmed that the multitrophic plankton model is critical to the further understanding of the effects and feedbacks of host interactions within the marine ecosystem. In the discussion by [143], infochemicals are underscored as being critical in stabilizing the marine food web. The role of DMS in trophic interactions is emphasized by the author in their efforts to elucidate the interactions among the phytoplankton and zooplankton populations Fig. (3.2) illustrated the interactions between phytoplankton, microzooplankton, and copepods via Eqs. (3.6). The findings from [143] indicate that in relation to stabilizing the phytoplankton population, the release of grazing-induced infochemicals is critical to the formation of phytoplankton blooms. The explanation is that the impact of a loophole in the microzooplankton grazing mechanism is the formation of these blooms. Therefore, from these studies, we can develop an understanding of the role of infochemicals in the dynamics of marine systems.

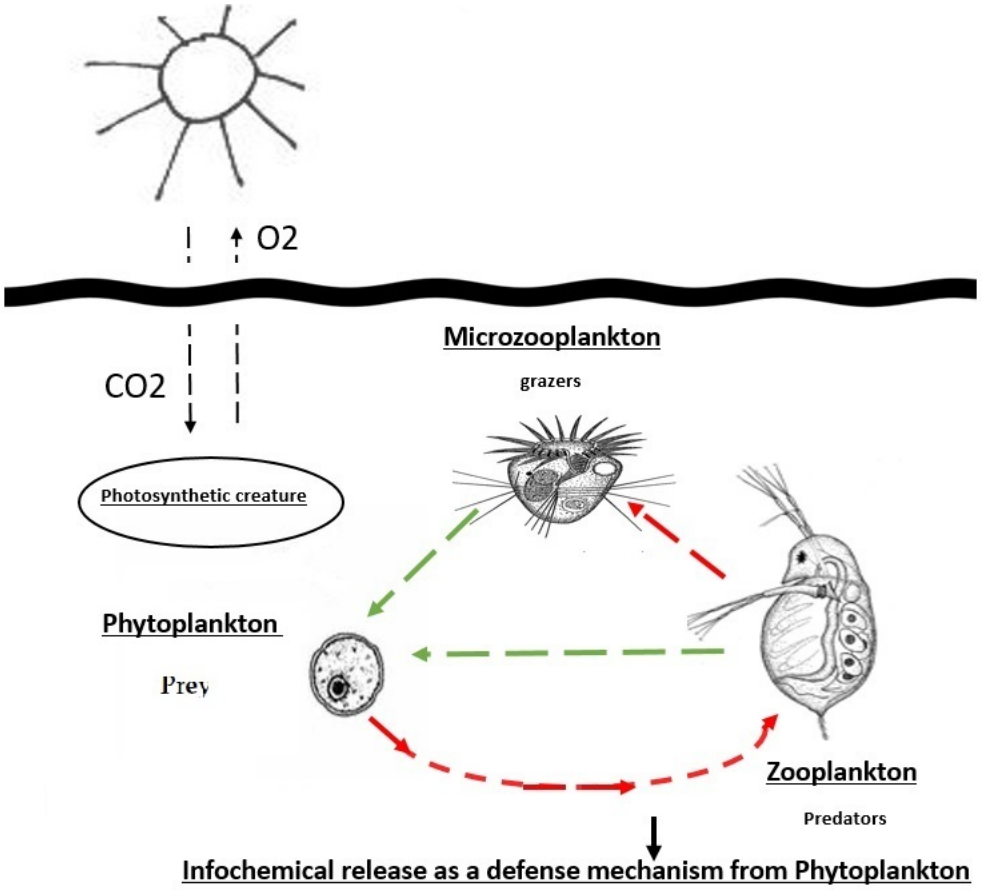

Figure 3.2: *Prey predator Interactions: Interactions between phytoplankton, microzooplankton, and copepods in a prey predator relationship.*

In furthering the discussion on plankton population dynamics, [142] underscored the need to understand the phytoplankton competition model presented in Eqs. (3.7); these are based on the role of infochemical mediated zooplankton grazing.

$$\begin{aligned}
\frac{dP_1}{dt} &= r_1 P_1\left(1-\frac{P_1+\alpha_{12}P_2}{K_1}\right)-\frac{g_1P_1M}{k+P_1+P_2}\\
\frac{dP_2}{dt} &= r_2 P_2\left(1-\frac{P_2+\alpha_{21}P_1}{K_2}\right)-\frac{g_2P_2M}{k+P_1+P_2}\\
\frac{dP_3}{dt} &= \frac{(\gamma_1-\lambda)g_1P_1M+\gamma_2g_2P_2M}{k+P_1+P_2}-mM.
\end{aligned} \tag{3.7}$$

In Eq's 3.7, P_1, P_2 and P_3 and all other parameter values are nonnegative and constant in time. From these author perspectives, the competition for light and nutrients is enabled through a vertically heterogeneous

environment, and this support the survival of the plankton population. The authors explain in detail that the investigation of infochemical mediated zooplankton grazing plays a critical role in the understanding of the phytoplankton competition model. [142] were of the view that the interactions in food webs is enabled through the release of infochemicals among the marine phytoplankton. This process influences the feeding behaviour of the phytoplankton. The selectivity of zooplanktonic predators is also influenced by the infochemical mediated zooplankton grazing [63]. In the context of this discussion, [142] observed that infochemicals play a role as toxic grazing deterrents, thereby supporting the phytoplanktons competition amongst themselves. It is further discussed that the predators also benefit from the process given that these infochemicals may also play a critical role as grazing cues. The authors introduced a standard 3-species phytoplankton competition model to explain the infochemical dynamics. Through this model, the study found that the grazing susceptibility of the producer is increased as a result of infochemical release. But this also provides a refuge for phytoplankton given that carnivorous copepods are attracted by the infochemicals, leading to the consumption of microzooplankton grazers. This is what [142] refers to as the multi-trophic interaction.

Via a different study, by [237], it is possible to achieve a better understanding of the impacts of climate on the ecosystem. That study made use of a dynamic model of oceanic sulphur (DMOS) in order to understand the Dimethylsulphide (DMS) summer paradox. In this study, it was observed that in the Sargasso Sea, the DMS paradox has challenged marine ecologists in terms of explaining the changes in plankton dynamics. A one-dimensional model of DMSP/DMS dynamics (DMOS) was used to explain the concentrations of DMS and the changes in the phytoplankton biomass. In this study, it was explained that there is a major mismatch between the DMS production and the phytoplankton population. This is particularly so during the summer season. The study results indicated that during summer, ultraviolet radiation (UVR) inhibit bacterial DMS consumption, resulting in an effect on phytoplankton production. The study indicated that UVR-induced oxidative stress can be highlighted as a major cause of the changing dynamics in phytoplankton production.

And other researchers have supported [142] by highlighting the idea that infochemicals play a critical role in the dynamics of marine food webs. [63] noted from their study that the formation of phytoplankton bloom is a result of the utilization of infochemicals to stabilize the system. From their findings, it can be stated that infochemical mediated zooplankton grazing plays a critical role in stabilizing the phytoplankton. Therefore much can be sought from these authors which furthers discussion about plankton population dynamics,

especially in terms of the different chemical models.

It is further discussed by [176] that dynamics in biological and chemical systems need to be understood in order to explore the issue of chemical modeling, and so further understand plankton dynamics. This study gathered some significant data in order to review the plankton dynamical system. In this study, biological science is the main discipline, and the emphasis is on the formation of irregular spatial patterns within the marine ecosystem. The authors argue that there is a need to quantify the spatial aspect in terms of the correlation length. [176] further discussed how an understanding of system stability has been achieved using the reaction diffusion model of population dynamics, see details in Appendix A.6. The research findings indicated that analytical formula for an intrinsic length needs to be considered when analyzing the correlation of the system parameters. This article is of huge relevance in biological science given that it presents relevant information on the formation of irregular spatial patterns that supports the understanding of plankton modeling dynamics. Other research has further highlighted the relevance of results from chemical modelling in relation to biological science. [176] clearly illustrated the spatio–temporal variability mechanisms that explain the dynamics of natural plankton populations. In this study, the researchers explained the biological processes that govern the chemical dynamics of plankton. It was found that the use of conceptual minimal models in biological science to understand pattern formation has made the study of patchiness and phytoplankton blooms easier. These models have been based on reaction –diffusion equations, see details in Appendix A.6, and these equations explain the interaction and transport of plankton in the ecosystem. Indeed, further review has indicated that patterns in spatio–temporal plankton populations can best be modelled using these equations. Therefore, this article is very well suited to advancing our understanding of the relationship between chemical modelling and the plankton population. The purpose of the above models is to further elucidate infochemical–mediatedplankton interactions and their role in phytoplankton bloom formation. These models aimed to provide details of predator–prey interactions, via the exploration of the dynamics of the models across the full range of the few parameters of interest.

3.5 Climate Change and Human Interaction in Relation to Marine Ecology Models

We begin by reviewing the appropriate academic literature concerning the understanding and managing of human threats to the coastal marine environment. [207] conducted a study on marine ecosystems and observed that there has been a slight reduction in the production of marine species following the changes in climatic conditions. The difference in climate has created regional differences in the composition of marine species. [207] were of the view that the dynamics of the phytoplankton group have been affected. As noted in the study, climatic changes have resulted in reduced ice cover and increased water temperature. This has resulted in algal abundance and productivity along the tropical coasts thus influencing the survival of plankton in that region. In marine biology, to better understand the effects of climate changes on ecosystems, various climate models have been advanced. A study by [251] contains an example of the models used in understanding this topic. [251] used species distribution modeling to predict the impact of climate on marine ecosystems. In their study, the authors revealed that natural and human-managed ecosystems have been severely affected by the changing climate. It was revealed that the species distributions can be explained using biogeographic modeling. This is the modeling that focuses on the distribution of species in terms of the different climates along the coast lines. The research revealed that a number of different species have established new regions as new habitats have emerged as a result of the environmental alterations. [64] further noted that physiological ecologists and biogeographic modelers have predicted that changes in habitat among different marine species will continue to occur due to the continuing changes in the climate. A further discussion of the spatial patterns of plankton blooms can be found in a study by [79] who analyzed the mean chlorophyll concentrations in marine ecosystem. The study modeled these concentrations in relation to the changes in sea surface salinity (SSS). The major findings were that a change in sea surface salinity (SSS) has resulted in the continuing changes in the ocean color. The authors correlated the sea surface salinity (SSS) with the changes in sea surface temperature, and argued that the salinity changes affect the survival of plankton blooms. [190] used a process-oriented numerical model to highlight that the production of plankton blooms is influenced by the changes in climatic conditions. The results from the model indicated that bloom timing and magnitude is mainly influenced by salinity. They also found that continued surface heating influences

the variability of blooms. Other results showed that the magnitude of blooms has also been affected by the nutrient level changes; these have led to changes in bloom timing and production. The conclusion from these studies was that the marine ecosystems were experiencing phytoplankton phenological shifts as a result of climate changes. The changes in phytoplankton biomass production have also been emphasised by [79] who used a dynamic model to explain the effects of climate changes on DMS production and thus their effects on the production of phytoplankton. In this study, a new sulfur cycle model was proposed as one which is better for use in understanding these dynamics. It was observed that bacteria have a major role to play in DMS production and consumption. The authors discussed that because of the susceptibility of bacteria to solar-radiation inhibition, the phytoplankton are exposed to solar-radiation-induced stress. This is a similar argument to that which [237] put forward in relation to the Sargasso Sea study. The study emphasized that changes in climate affect how DMSP is dissolved by phytoplankton. Therefore, the study concluded that for understanding phytoplankton compositions in the ecosystem, it is important to analyze the DMS and reproduction simulations with a focus on how they are affected by changing climate. These studies are critical in explaining the DMS summer paradox and furthering our understanding of the effects of climate changes in relation to marine ecologies. Research in marine ecology has furthered discussion concerning other human factors that could threaten marine ecology besides climatic changes [190]. Models and analysis have been used to explain human impacts on plankton dynamics. Multivariate auto regressive models are among the models that are being used to develop an understanding of biotic interactions within natural multitrophic communities [124]. The models explain the effect of invasions of non-native species. Among the noted human impacts include atmosphere modification and the degradation of marine habitats through the introduction of non-native species.

In relation to understanding the impacts of climate on the marine ecosystem [104] further highlighted the importance of interactions between trophic components. However, it is rare to find studies concerning integrative end-to-end ecosystems. Therefore, there is an under representation of the role that zooplankton communities play within ecosystems. The link between phytoplankton and fish communities is not well understood. However, [171] observed that some fisheries models, including the stock-recruitment (S/R) relationship, have been important in understanding these relationships and managing the fisheries. The established nature of this relationship is an indication of how important it is for understanding the level at

which human fishing should be controlled in order to manage the fish population. It is also emphasised in the study that the human interactions which involve the commercial harvesting of fish affect the fish populations. Using the ecosystem-based management model, [104] explained that the full array of interactions should be established in order to consider the management of even single fisheries species. Supporting these findings, [171] also used the food web model for the Baltic sea in order to engage with multispecies virtual population analysis (MSVPA) in order to evaluate the vulnerability to predation of specific species. The conclusion from this study was that there is a need for effective management of fishing since it is the chief source of mortality within fisheries. As reviewed by [46], human activities threaten coastal marine habitats. However, the challenge has been the quantification of these threats in terms of the damage which will be caused to the ecosystem. It is not adequately understood that there are different ecosystem-level impacts that need to be managed to avoid the extinction of marine species. [79] conducted a threat analysis to better evaluate the most appropriate conservation targets for marine ecologists. The main objective was to highlight the vulnerabilities of different species which have resulted from the changes that have come about. The study also utilised spatial analysis in order to help make predictions about these threats. In this study, the major findings were that human factors can be considered as causing multiple-stressor effects on the ecosystem. This results in different responses by the species. The study concluded that there is a need for ecosystem-based management (EBM) to conserve the ecosystem. These findings are also supported by other studies, for instance by [190] who found that comprehensive spatial management is best suited to address the impacts of human activities on the ecosystem. The main objective here is to establish regulatory mechanisms for human activities and create awareness of ecological changes that may be caused by human activities. Presenting an ecosystem model of food web and fisheries interactions [104] conducted a study of the Baltic Sea. The researchers argued that there is an array of species interactions that affect the fisheries populations there. In the study, the researchers used Ecopath with Ecosim software to create the Baltic Sea model. The study found that the structuring forces of the trophic relationships of the Baltic Sea included fishing, which is highlighted as causing mortality in cod and herring. The researchers developed different hypotheses to explain the relationships within the Baltic Sea food web. This study was effective in helping to develop community responses that would be proficient in managing human actions that affect species interactions within the fisheries populations. The oceans biogeochemistry is mainly determined by the ecosystem processes, and

among these can be included climatic changes [186]. The research by [155] indicated that there are models of the oceans as a whole that highlight these processes and link geochemical tracers to ocean physics. IPCC[8] reports indicate that there are ecosystems that are resilient to warming, and other research studies by [241] indicate that climatic variability is inevitable within the ecosystem. However, the argument is that climatic changes have major impacts on the behavior of decadal-scale oscillations within the ecosystem. [155] further observed that the ecological changes are dependent on the oceanic uptake of $CO2$, and that this affects the climatic conditions including the temperature of the ecosystem. Therefore, the IPCC report also draws the conclusion that to manage the marine ecosystem, it is critical to understand the different environmental factors that affect the ecosystem. [186] utilised the Dynamic Green Ocean Model (DGOM) to better explore the factors that control the marine ecosystem. The study found out that different plankton functional types affect the biogeochemical process of the ocean. This in turn affects the growth and mortality of these functional types.

In another study by [182] the purpose was to quantify the effect of environmental variability on fish recruitment. The study used recent findings from authors to discuss the recruitment issue. In this study, linear growth models were used to analyze these effects. The findings indicated that the probability of fish recruitment increases with an increase in environmental variance. The variance is also responsible for the differences in growth rates of the recruited fish thus affecting the overall population growth. Other research studies, including [96], have discussed fisheries models with a focus on Mixotrophy[9].How plankton blooms affects the hatching of fish larvae, and recruitment has also been discussed in other studies by [123]. In this study, prey population dynamics are described using models of fish recruitment. The researchers model which describes the growth of haddock larvae is explained. The study found that there is a non-trivial interaction between the planktonic populations and the larval populations. The findings indicated that in order to influence the date of phytoplankton bloom, fish spawning can be used as a reproductive strategy.

[8] the Intergovernmental Panel on Climate Change is a scientific and intergovernmental body which operates under the auspices of the United Nations.

[9] Heterotrophy and photosynthesis by a single species [96].

Chapter 4

Bloom Formation and the Hydra Effect in the non-Spatial Infochemical-Mediated Plankton Model

4.1 Introduction

In this chapter, we consider a simple food-chain model that was first studied in [143]. This model included the key interactions between the small phytoplankton, and the microzooplankton and copepods foraging under the influence of grazing-induced infochemicals. An example of such an infochemical is Dimethylsulphide (DMS) which is derived from the algal secondary metabolite dimethylsulphoniopropionate (DMSP) and is a climate-relevant trace gas [35]. Small DMS-producing phytoplankton (P), which may grow in great abundance [159], form the first trophic level of the model. Phytoplankton[1] are grazed by microzooplankton (M, the second trophic level), which are in turn consumed by mesozooplankton such as copepods (copepods population is represented by$v$). Microzooplankton grazers play an important role in this plankton model because DMS production will accelerate following microzooplankton grazing and this trace gas may act as

[1]Emiliania huxleyi represent the first trophic level

an infochemical cue, assisting copepods to locate prey-rich patches. This is termed 'trophic upgrading', [26] and [226]. One of the key assumptions of this model is that microzooplankton provide the only trophic link between phytoplankton and copepods. Microzooplankton grazing is generally accepted as being the main predatory pressure on planktonic primary production, consuming 60-70% [35], whereas mesozooplankton, and in particular copepods, consume in general 10 - 40% of microzooplankton [33]. The sum of all interactions between single predators and single potential prey animals can be considered predation in an ecosystem. Interaction can result in success or failure for the predator, corresponding to death or escape for the prey

Chemically-mediated interactions have a strong effect on the structure, functioning and population dynamics of an ecosystem [107], [145]. Studies initially focussed on the possible role of dimethylsulphide (DMS) before examinations of other infochemicals and their effects on foraging took place [25] and [183]. Infochemicals have been shown to elicit a behavioural foraging response in the copepod Temora longicornis [183] suggesting that copepods may use infochemicals when searching for prey. According to [258], infochemicals are rapidly released when microzooplankton graze on phytoplankton. In the above plankton model, grazing by microzooplankton induces the release of infochemicals that promote interactions between the species due to the fact that copepods can detect DMS and modify their trophic behaviour in response to it [218]. It is known that microzooplankton are prey items for mesozooplankton [117]and [118]. Mesozooplankton, especially copepods, which benefit from the general increase in food concentrations during blooms, will also increase predation pressure on microzooplankton in these circumstances [116]. The ability of copepods to react to infochemicals suggests that, in principle, the grazing-induced release of infochemicals can promote multi-trophic interactions between phytoplankton, microzooplankton and copepods by providing an infochemical cue for foraging copepods. In addition, there are some models of grazing wherein marine tritrophic-induced toxin chemicals are released that attract the natural enemies of herbivores [191], [234] and [26].

Following [143] we investigate the complexity and stability of a two species plankton model. The dynamic interactions between these biological communities involve the production of infochemicals. This leads to the relief of grazing pressure on the phytoplankton, and this in turn can lead to a stabilizing of the food-web species, allowing the phytoplankton to reach an equilibrium density in the formation of a phytoplankton bloom [218], [143] and [25]. [142] highlighted that there are a number of different chemicals,

including the allelochemicals and kairomones that play critical roles in conveying information relating to food–web interactions. The argument of that research was that chemical communications affect predator relations. Individual species exploit these communications in order to find or avoid prey. [143] also wrote that the community structure, including the population dynamics of the different species, is affected by these chemically mediated interactions. This is also argued by [11] who noted that in the marine food–web, the foraging behaviours of some species are affected by infochemicals. These can affect the selectivity of zooplanktonic predators. [97] has also indicated that, with competition being on the high side in the nutrient-dilute marine environment, chemical communications enable species to select alternative prey. This behaviour facilitates the grazing of phytoplankton species. Based on the two species plankton model, [20] argued that the infochemicals are critical for Microzooplankton (M) grazing. They communicate about the availability of the infochemical producing phytoplankton, thus enabling grazing.

The mathematical behaviour of the plankton model is obtained by carrying out a phase plane analysis and a bifurcation analysis, both relating to two control parameters. This is a standard technique used for determining the behaviour of an ecological system and has been employed by many authors [134], [86]. The main aim of this chapter is to provide a mathematical explanation of the numerical results shown in [143]; these results were obtained by considering only one control parameter, v. Here, we aim to explore the set of model parameter values and to study and analyse the stability and bifurcation of the model by changing three control parameters: K, the phytoplankton carrying capacity, v; the infochemical release; and r, the growth rate. We focus our efforts on how to change the main phytoplankton parameters in order to gain more insight into the general bifurcation of the system and the systems stability.

4.2 Mathematical model

Here we analyze the qualitative behaviour of a model of the interaction between the 3-trophic levels of plankton: phytoplankton, P; grazing microzooplankton, M; and predatory mesozooplankton (copepods). The following model was first studied in [143].

$$\frac{dP}{dt} = rP\left(1 - \frac{P}{K}\right) - \frac{aPM}{1 + bP} \tag{4.1}$$

$$\frac{dM}{dt} = \frac{\gamma aPM}{1+bP} - mM - \frac{vaPM^2}{1+bP}. \tag{4.2}$$

In Eq. (4.1), the prey (i.e., the phytoplankton) growth is modeled using a logistic model – utilising an intrinsic growth rate of r and a carrying capacity of K – wherein the carrying capacity is assumed to correspond to nutrient limitation and self-shading [143]. The second term is a Holling type-II functional response [112], used to describe the effects of the predatory microzooplankton on the prey. The Holling type-II functional response is a hyperbolic function and represents the fact that predation saturates at high prey densities because of the time it takes to handle the prey. In Eq. (4.2), the first term on the RHS represents the predatory growth rate described by the Holling type-II function whereby phytoplankton biomass is converted with an efficiency of γ. Next is the first microzooplankton mortality term, which is assumed to be in effect in the absence of the infochemicals: i.e., the mortality resulting from predation via non-infochemical cues or from natural death, etc. Although a term directly related to copepods is not included in the model, the effects of copepod predation are accounted for by the third term in Eq. (4.2), which has an exploratory parameter, v, that represents the effects of info-chemical mediated predation by copepods on microzooplankton.

4.2.1 An analysis of the location of the equilibrium

Linearisation about the equilibrium points determines the type of singularity present and the stability of the steady states. The first steady state is the trivial (biologically irrelevant) case at point $(0, 0)$ and the second equilibrium (one that is biologically relevant) is at $(K, 0)$, where K is the carrying capacity of the phytoplankton. The other biologically relevant equilibria are co-existent states given by a cubic; all these steady states are obtained by setting the LHSs of Eqs. (4.1) and (4.2) to zero:

$$F(P_e) = rbvP_e^3 + (-vrKb + rv)P_e^2 + (\gamma aK - mbK - vrK)P_e - mK = 0, \tag{4.3}$$

and M is given by:

$$M(P_e) = \frac{-r(P_e^2 b - P_e K + P_e - K)}{aK}, \tag{4.4}$$

where, P_e and M_e are the biologically relevant equilibria (the co-existence points). Note that 4.3 is a cubic polynomial, and all its roots can be found using **Cardan's method** [197]. Cardan's method depends on

finding the reduced cubic polynomial, y_N, and another polynomial h. Since the relationship between y_N and h will help us to determine the nature of the roots of the original cubic and N, the number of inflections, we can consider y_N as the local maximum of the polynomial and h as a local minimum.

To define y_N, we follow the same steps as in [197]. To find the roots of the first species polynomial in 4.3 we obtain:

$$y_N = \frac{1}{27}\frac{\nu(Kb-1)^2)r}{b^2} + \frac{1}{9}\frac{(-\nu rKb + r\nu)(Kb-1)^2}{b^2} + \frac{1}{3}\frac{(\gamma aK - mbK - \nu rK)(Kb-1)}{b} - mK,$$

and to find h, start by substituting $Z = -\frac{(-\nu rKb+r\nu)}{3(\nu rb)}$ in y_N so that

$$h = \frac{2}{27}\nu rb\left(\frac{(-\nu rKb + r\nu)^2 - 3\nu rb(\gamma aK - mbK - \nu rK)}{\nu^2 r^2 b^2}\right)^{\frac{3}{2}}. \tag{4.5}$$

To specify the number and the types of the roots of the cubic polynomial in the system for the two species Eqs. (4.1) and (4.2), we can rely on the relation between y_N and h – this was the main idea introduced by [78]. The following analysis shows the type of each root of Eqs. (4.2) and (4.1).

- If $y_N^2 > h^2$ the system will have one real root.

$$\alpha = x_N + \sqrt{\frac{1}{2a}(-y_N + \sqrt{y_N^2 - h^2})} + \sqrt{\frac{1}{2a}(-y_N - \sqrt{y_N^2 - h^2})}. \tag{4.6}$$

The remaining two complex roots are given by:

$$\beta, \gamma = -\frac{\alpha}{2} \pm j\frac{\sqrt{3}}{2}\sqrt{\alpha^2 - 4\delta^2}. \tag{4.7}$$

where δ is the crucial parameter which helps to find the roots and h.

$$\delta^2 = \frac{1}{9}\frac{(-\nu rKb + r\nu)^2 - 3\nu rb(\gamma aK - mbK - \nu rK)}{\nu^2 r^2 b^2}.$$

- If $y_N^2 < h^2$ the system will have three distinct real roots.

$$\alpha = \frac{Kb-1}{3b} + \frac{2}{3}\sqrt{\frac{(-vrKb+rv)^2 - 3(vrb)(\gamma aK - mbK - vrK)}{v^2r^2b^2}}\cos\left(\frac{\theta}{3}\right), \tag{4.8}$$

$$\beta = \frac{Kb-1}{3b} + \frac{2}{3}\sqrt{\frac{(-vrKb+rv)^2 - 3(varb)(\gamma aK - mbK - vrK)}{v^2r^2b^2}}\cos\left(\frac{\theta+2\pi}{3}\right), \tag{4.9}$$

and

$$\widehat{\gamma} = \frac{Kb-1}{3b} + \frac{2}{3}\sqrt{\frac{(-vrKb+rv)^2 - 3(vrb)(\gamma aK - mbK - vrK)}{v^2r^2b^2}}\cos\left(\frac{\theta+4\pi}{3}\right). \tag{4.10}$$

where $\theta = \cos^{-1}\left(\frac{Y_N}{h}\right)$.

We can therefore summarize all of the above results by means of the following three conditions:

- $y_N^2 > h^2$, the cubic will have one real root.
- $y_N^2 = h^2$, the cubic will have three roots (two or three equal roots).
- $y_N^2 < h^2$, the cubic will have three distinct real roots.

4.2.2 The stability of the equilibrium

Consider the two-species Jacobian matrix, as follows:

$$J = \begin{pmatrix} a_{11} & a_{12} \\ a_{21} & a_{22} \end{pmatrix} \tag{4.11}$$

The elements of the Jacobian matrix, a_{ij}, are represented by partial derivatives of Eqs. (4.1) and (4.2)

$$\begin{aligned} a_{11} &= r - \frac{2rP_e}{K} - \frac{aM_e}{(1+bP_e)} + \frac{abP_eM_e}{(1+bP_e)^2}, \\ a_{12} &= -\frac{aP_e}{1+bP_e}, \\ a_{21} &= -\frac{aM_e\left(vM_e - \gamma\right)}{(1+bP_e)^2}, \\ a_{22} &= -m - \frac{aP_e\left(2M_ev - \gamma\right)}{1+bP_e}. \end{aligned} \tag{4.12}$$

where the system equilibrium is represented by (P_e, M_e). The Jacobian at $(0, 0)$ is:

$$J = \begin{pmatrix} r & 0 \\ 0 & -m \end{pmatrix} \tag{4.13}$$

And the Jacobian at $(K, 0)$ is:

$$J = \begin{pmatrix} -r & \frac{-aK}{(1+bK)} \\ 0 & \frac{\gamma aK}{(1+bK)^2} - m \end{pmatrix} \tag{4.14}$$

The eigenvalue analysis of the plankton dynamics therefore leads to the following conclusions: the model's trivial steady state is an unstable saddle as $\lambda_1 = r$ and $\lambda_2 = -m$ are the eigenvalues. The second steady state (and this is a biologically relevant one) is also unstable when $\gamma aK > bKm - m > 0$ as the eigenvalues are $\lambda_1 = -r$ and

$$\lambda_2 = \frac{\gamma aK - bKm - m}{(1 + bK)}, \tag{4.15}$$

For the numerical parameters that we use in Section 4.3 we have $\lambda_1 > 0$ and $\lambda_2 < 0$, so the equilibrium, $(K, 0)$, is also an unstable saddle which may permit the formation of a phytoplankton bloom [143]. The final set of (three) equilibria, which was found using Cardan's method [197] have the following form for the eigenvalues:

$$\lambda = \frac{1}{A_0}\left(\widehat{\alpha} \pm \sqrt{\widehat{\beta}}\right), \tag{4.16}$$

where

$$A_0 = \frac{1}{K(1 + bP_e)^2}$$

and $\widehat{\alpha}$ represents $Tr(J)$ and $\widehat{\beta}$ is $Det(J)$.

The following two equations represent the real and imaginary parts of the eigenvalue of the third steady state:

$$\widehat{\alpha} = (-2rb^2)P_e^3 + (rKb^2 - Kb^2m + Kb\gamma a - 4rb - 2KbvaM)P_e^2 + (-2Kmb + 2rKb + 2r + K\gamma a - 2KvaM)P_e - (aM + r - m)K,$$

and $\widehat{\beta}$ is $Det(J)$, which is as follows:

$$\widehat{\beta} = C_1 P_e^6 + C_2 P_e^5 + C_3 P_e^4 + C_4 P_e^3 + C_5 P_e^2 + C_6 P_e + C_7 P_e \tag{4.17}$$

where $C_i, i = 1, 2, 3, 4, 5, 6$ are cascading parameters that have a hierarchical relationship [248], as shown in Appendix B.1. As $\widehat{\alpha}$ in Eq. (4.17) is the real part of the eigenvalue of the coexistence equilibrium point, it is readily seen that it is a cubic polynomial in P_e . To determine its roots we need to solve Eq.(4.18) using Cardan's method. However, we need first to find a general formula for M, as in Eq. (4.4), and for the control parameter ν as follows:

$$f(\nu) = A\nu^3 + B\nu^2 + C\nu + D, \tag{4.18}$$

The above will allow us to construct the general stability diagram in the next section. Evaluating Eq. (4.18) using Cardan's method will give us the roots for the saddle node bifurcation, see Appendix B.2, and will locate where this type of bifurcation takes place. However, it should be noted that the region between the two curves of the saddle node contains another two curves, one related to the Hopf bifurcation curve [2] and the other directly related to the saddle node (this curve separates the area between the two saddle curves). To find these two curves we need to calculate the eigenvalue of the model in Eq. (4.16) by setting $\widehat{\alpha}$ to obtain the Hopf curve and $\widehat{\beta}$ to obtain the saddle node curves; this will separate the area which has three real roots from the area with one real root as in Fig.4.3(b).

4.2.3 The variational approximation (VA) method for the Orbit

This section aims to find an analytical representation for the limit cycle or bifurcation curve in the model equations Eqs. (4.1) and (4.2). The limit cycle results in a large oscillation in the system dynamics, meaning that both predator and prey may come close to local extinction as their phase plane trajectories draw close to the axes [134]. The large oscillation in the prey (phytoplankton) density for a certain parameter range has already been presented in [143]. The Variational method [150] is used in a wide variety of physical

[2] For more details on bifurcation theory see Appendix A.5.

applications, ranging from chemical reaction theory to radiative heat transfer [44, 122], and is one of the most popular tools for nonlinear analysis as compared to other approximate analytical methods. It helps to verify numerical simulations. However, there is a variety of other methods that have been used in the past to calculate the limit cycle, [150] and [146]. Below are the full details of the analytical approximation that we have followed in order to represent the curve of the periodic orbit, analytically.

4.2.4 Periodic orbit

The Hopf bifurcation which exists in the multitrophic plankton model, Eqs. (4.1) and (4.2), has potentially a periodic orbit which leads to a limit cycle solution. We can obtain the limit cycle by scaling the time into $t = [0, 1]$ for a one period solution. So, we have

$$\begin{aligned} \frac{1}{T}\frac{dP}{dt} &= rP\left(1-\frac{P}{K}\right)-\frac{aPM}{1+bP}, \\ \frac{1}{T}\frac{dM}{dt} &= \frac{\gamma aPM}{1+bP}-mM-\nu\frac{aPM^2}{1+bP}, \end{aligned} \tag{4.19}$$

$$P(t_0) = P_e \quad \text{or} \quad M(t_0) = M_e \tag{4.20}$$

and $T \in [0, 2\pi]$ is the period of a single cycle. We have the approximation: $P(t_0) = P_e$ or $M(t_0) = M_e$ is a constraint for the system. We can use a periodic function as an initial guess to solve Eq. (4.19) near the Hopf point: i.e.,

$$\begin{pmatrix} P^{(0)}(t) \\ M^{(0)}(t) \end{pmatrix} = \begin{pmatrix} P_H \\ M_H \end{pmatrix} + \epsilon \begin{pmatrix} 1 \\ 1 \end{pmatrix} \sin(2\pi t) \tag{4.21}$$

where $0 \leq t \leq 1$ and $\epsilon \ll 1$. Another option for obtaining the periodic orbit is that of performing numerical integration for the system Eqs. (4.1) and (4.2) for a very large period, T, and using Eq. (4.21) as an initial condition. We also perform variational approximation, as in [52], to approximate the periodic orbit and

choose ν = Hp as the centre for this approximation. We write

$$\begin{pmatrix} \tilde{P}(t) \\ \tilde{M}(t) \end{pmatrix} = \begin{pmatrix} P_H \\ M_H \end{pmatrix} + \frac{\epsilon}{2} \begin{pmatrix} P \cdot ev_P \\ M \cdot ev_M \end{pmatrix} e^{\lambda(t)} + c.c. \tag{4.22}$$

where $\begin{pmatrix} P \\ M \end{pmatrix}$ is the variable of VA, λ and $\begin{pmatrix} ev_P \\ ev_M \end{pmatrix}$ are eigenvalue and eigenvector at ν = Hp where λ is purely imaginary or $Re(\lambda) = 0$, and $c.c.$ is a complex conjugation. By substituting the ansatz Eq. (4.22) into Eq. (4.1) and Eq. (4.2), performing a Taylor expansion and linearising about $\epsilon = 0$, and then integrating in their domain, we can obtain the limit cycle curve and repeat this method for different values of K.

$$\begin{aligned} F_{va}(P,M) &= \int_0^{\frac{2\pi}{\lambda}} \frac{\partial \tilde{P}}{\partial t}\, dt - \int_0^{\frac{2\pi}{\lambda}} F(\tilde{P},\tilde{M})\, dt = 0 \\ G_{va}(P,M) &= \int_0^{\frac{2\pi}{\lambda}} \frac{\partial \tilde{M}}{\partial t}\, dt - \int_0^{\frac{2\pi}{\lambda}} G(\tilde{P},\tilde{M})\, dt = 0. \end{aligned} \tag{4.23}$$

After one step of solving the system in Eq. (4.23), we will obtain Eq. (4.24), which represents the approximation solution of the limit cycle for any value of K.

$$A(\nu) = \frac{\psi_1 \cdot \sqrt{\psi_2 + \psi_3 \nu - \psi_4 + \psi_5}}{\psi_6 + \psi_7 \nu}. \tag{4.24}$$

where all the values of ψ_i are cascading parameters, and will be determined numerically. Solving Eq. (4.23) numerically using Newton-Raphson gives an approximate limit cycle for the various different values of the system carrying capacity, K, as in Eq. (4.24). Plotting the obtained equation with respect to ν, could give us an approximate solution for the periodic orbit, or the limit cycle, that exists for different values of K. All the required details are presented in the numerical section .

4.3 Numerical Exploration of the Model

In this section we explore the effects of changing K, ν and r on the systems stability. We introduce the related parameters in the next subsection to clarify the specific ranges and values of these which may lead to different behaviours – as explained separately in the bifurcation and stability analysis section.

4.3.1 Parameter values

A table of parameter values is given in this section; the biological meaning of each one is given in [143]. This gives the parameter values used in the numerical analysis of the model given by Eqs. (4.1) and (4.2). Each term in the model contains several parameters which were fixed for the purposes of simulation; these can be changed to different values when conducting a sensitivity analysis.

Table 4.1: *Outlines, default values and the ranges of the parameters. The ranges cover values used by a variety of authors with different models [59], [61], [202] and [143].*

Parameters	Definition	Value	Unit	Range	Source
P	Phytoplankton density	-	$\mu g\, C\, l^{-1}$	-	
M	Microzooplankton density	-	$\mu g\, C\, l^{-1}$	-	
r	Phytoplankton intrinsic growth rate	1.5	$days^{-1}$	0.5, 1.5, 5	[59]
K	Phytoplankton Carrying capacity	120	$\mu g\, C\, l^{-1}$	0 – 1000	[174] and [165]
a	Clearance rate of microzooplankton at low food densities	0.3	$\mu g\, Cl^{-1}\, days^{-1}$	[202] and [13]	
b	Half saturation density of microzooplankton	0.05	$\mu g\, C\, l^{-1}$	–	[202] and [13]
γ	Microzooplankton grazing efficiency	0.5	$days^{-1}$	–	[61]
m	Microzooplankton mortality in the absence of DMS	0.3	$days^{-1}$	–	
ν	Chemical evaporation or flux to the atmospheres	-	$days^{-1}$	0 – 0.2	

The units of the main variables, P and M, are $\mu g\, C\, L^{-1}$, which refer to a typical oceanic range per unit area (unit volume) and the time unit is one 'day'. The cell unit is μg and the units for the mortality term are $\mu g\, C\, L^{-1}\, day^{-1}$.

4.3.2 Phase portrait and system dynamics

In this section, we show the system phase portrait and the value of the equilibrium for each intersection of the nullclines. The plane is naturally divided, by a number of nullclines, into regions in relation to which we place information regarding the system. These regions/descriptions provide a bulk picture of how things change at different points in the plane [67]. Figs 4.1 and 4.2 illustrate the five qualitatively different types of system dynamics that the model described in Eqs. (4.1) and (4.2) has; each symbol (star, cross or circle) acts as in Fig. 4.3. The intersections of the two solid lines, representing the phytoplankton and microzooplankton nullclines, in Figs. 4.1 and 4.2, indicate different types of stability. For instance, Fig.4.1(a) shows the region where we have a stable state along the ν range, as shown by the filled black circle. Figs.4.1(b)- 4.1(d) illustrate the area wherein $K = 71.973$; this is where the two saddle-node curves collide and disappear. We call this a cusp bifurcation. This case is presented by switching between two symbols, from empty to filled circle, in Fig. 4.2(a)-4.2(d), to show the different cases for $K = 120$ with different values of ν. We show the Hopf

bifurcation by switching between two symbols, from empty to filled circle as in Fig. 4.2(b), and we show the bistability region where the saddle node bifurcation takes place, as in Fig. 4.2(c), by cross symbols and stars in Fig. 4.3(b).

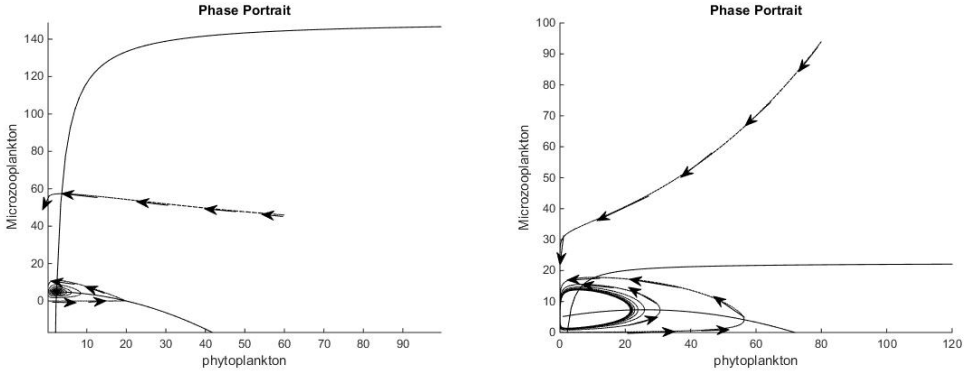

(a) $K = 24$ and $\nu = 0.043$

(b) $K = 71.973$ and $\nu = 0.020$

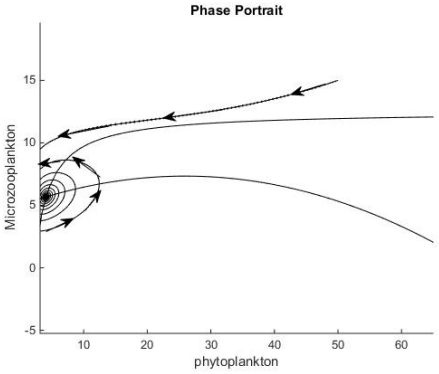

(c) $K = 71.973$ and $\nu = 0.036$

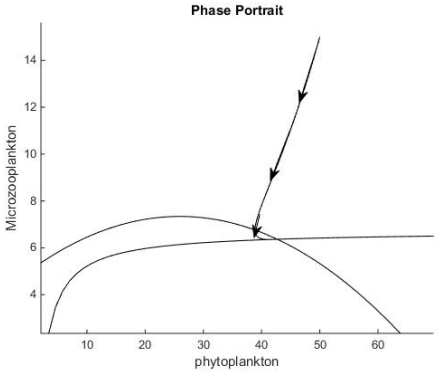

(d) $K = 71.973$ and $\nu = 0.067$

Figure 4.1: *The phase portraits of the system corresponding to different values of ν when $\nu = 0.043$ and $K = 71.973$. The two solid lines show the phytoplankton and microzooplankton nullclines while the dashed lines are solution trajectories. The intersections of the nullclines give the equilibrium points of the system. In 4.1(a), where $K = 24$ and $\nu = 0.043$, the point $(30, 14)$ is a stable focus. In 4.1(b), where $K = 71.973$ and $\nu = 0.020$, the point $(80, 94)$ is an unstable focus; solution trajectories are drawn to a stable limit cycle around this point [134]. In 4.1(c), $\nu = 0.036$ and the point $(50, 15)$ is a stable focus. In 4.1(d), $\nu = 0.067$ and the point $(50, 15)$ is a stable sink (node); all the solution trajectories tend towards this point [143].*

4.3.3 Bifurcation and stability analysis

A bifurcation is a qualitative change in the system dynamics produced by varying the parameters [109, 157]. To study the effect of ν and K on the system, numerically, we experiment with both of these parameters using the polynomial that we deduced by satisfying Cardan's second condition: i.e., when $\Upsilon_N^2 = h^2$ as in Eq. (4.18). In the following, we present different cases of the carrying capacity *w.r.t* the infochemical load, ν. As the model represented by Eqs. (4.1) and (4.2) provides a suitable framework for further exploration, we

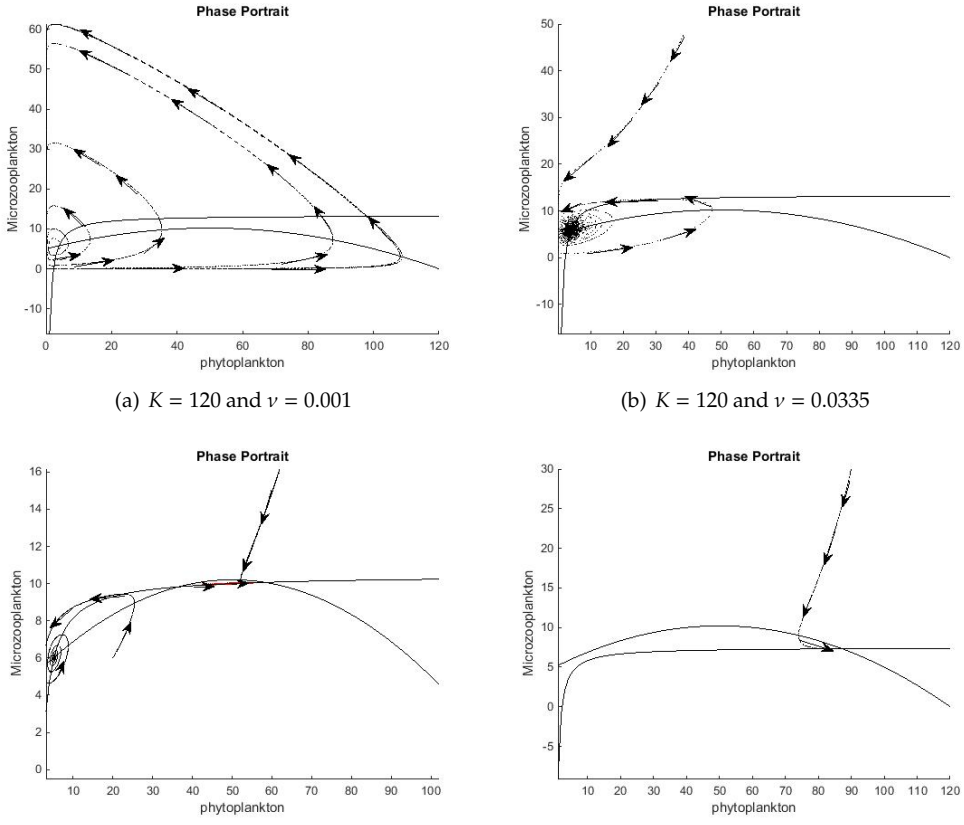

(a) $K = 120$ and $\nu = 0.001$

(b) $K = 120$ and $\nu = 0.0335$

(c) $K = 120$ and $\nu = 0.0431$

(d) $K = 120$ and $\nu = 0.061$

Figure 4.2: *The nullclines of the system corresponding to different values of ν when $K = 120$. The two solid lines show the phytoplankton and microzooplankton nullclines while the dashed lines are solution trajectories. The intersections of the nullclines give the equilibrium points of the system. In 4.2(a), when $\nu = 0.001$ we have an unstable focus point and the solution trajectories are drawn to a stable limit cycle around this point. In 4.2(b), when $\nu = 0.0335$, the point $(3.94, 5.765)$ is a stable focus and the trajectories are all drawn to this point. In 4.2(c), when $K = 120$ and $\nu = 0.0431$, the points are $(5.251, 6.036)$ and $(58.265, 10.66)$; the first one is a stable focus and the other one is a stable sink, this figure is used to show the bistability in the system when $K = 120$. In 4.2(d), when $\nu = 0.061$ the point $(88.06, 7.191)$ is a stable sink.*

undertake to find the value of the cusp bifurcation of K, where the two saddle-node bifurcation curves collide and disappear, and by solving the two curves for the saddle node, presented in Eqs. (B.2.10) and (B.2.11), we determine an accurate value for K, which is $K = 71.973$. In fig 4.3, we have two bifurcation parameters, used to specify at which value of K Hopf bifurcation will be experienced –which is when $K = 71.973$, and under what circumstance the bifurcation will vanish completely. It can readily be seen that the carrying capacity is a very important parameter in relation to each model as it specifies the maximum value of the population density for plankton, P and Microzooplankton, M, and determines the different stability conditions corresponding to each (K, v) [143]. As we mentioned in the analytical section of this chapter, we found an interesting result which connects the carrying capacity with the infochemicals – via the polynomial Eq. (4.18). The relation between these two control parameters should be mentioned. As K is very small, the type of the equilibrium (P_e, M_e) will only be that of a stable stationary state (stable focus) over the region which corresponds to low densities of phytoplankton and microzooplankton, as shown in Fig 4.4. As $K \geq 71.973$ the system will have three different stationary states as shown in Fig. 4.4. First, the system will exhibit no bifurcation when $0 < K < 24.99$, as the Hopf bifurcation curve (the first dashed curve on the left) ends in the second quadrant. When $24.99 < K < 71.973$, there will be one bifurcation (a Hopf bifurcation), because increasing the value of the prey-carrying capacity acts to destabilize what would otherwise be a stable system, via a Hopf bifurcation. When $K > 71.973$ the system will exhibit two types of bifurcation: a Hopf bifurcation and a saddle node bifurcation.

At the beginning of the curve shown in Fig. 4.3(a), the steady state is unstable. This situation results in the infochemicals having no effect (i.e., there is no change in the systems stability) until Hopf bifurcation occurs at $v = 0.02810$. From this point on, the system is stable, which means that the solution trajectory will reach a stable steady state. These two areas are separated by the curve generated by Eq. (4.17). The stable state (node) corresponds to high densities of phytoplankton and similarly high microzooplankton densities.

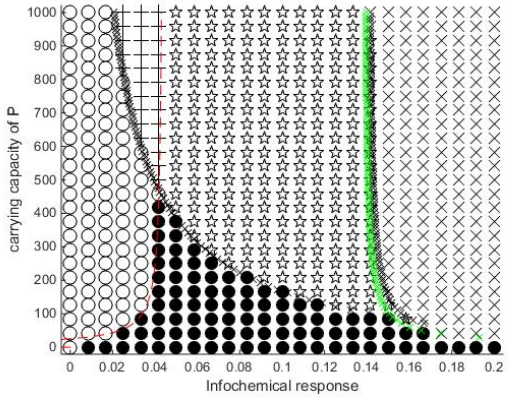

(a) $r = 0.5$

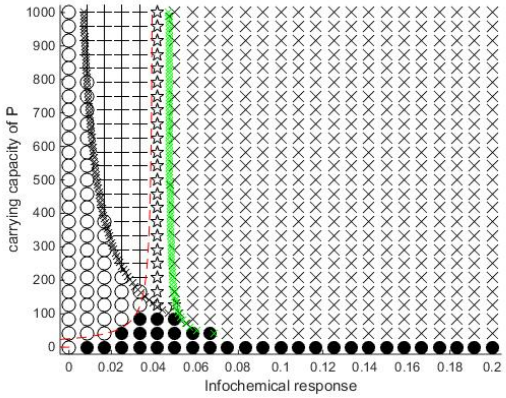

(b) $r = 1.5$

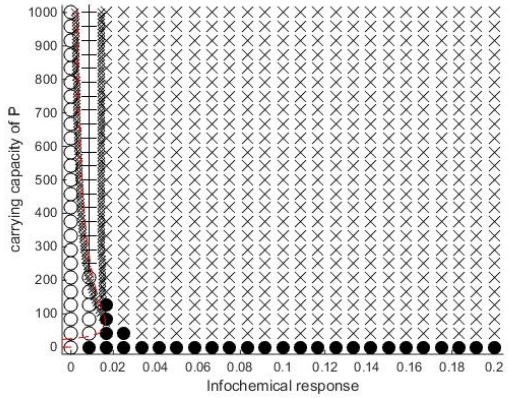

(c) $r = 5$

Figure 4.3: *Two-parameter bifurcation maps for the prey-predator model. In 4.3(a), the area with one positive root and two complex roots has three different cases: the empty circles represent the unstable focus, the filled circles represent the stable focus and the crosses, the stable sink/node. The area between the two curves which create the saddle node bifurcation of the three distinct roots shows bistability. There are two stable roots, a focus and a sink/node respectively and one unstable saddle which is represented by the star symbol. The two unstable roots, a focus and a saddle respectively, and the one stable sink are represented by the plus symbol. In 4.3(b), we have almost the same stability as is shown in 4.3(a), but the region in the middle is a bit narrower than for the case shown in 4.3(a) – i.e., the area that is surrounded by the saddle node bifurcation roots have the same stability analysis but for* $0.0423 < \nu < 0.0.51$. *In 4.3(c), we also have the same stability cases but at different intervals in terms of both ν and K [143].*

The general stability diagram in Fig. 4.3 is based on four main curves; the first two are of Eqs. (B.2.10) and (B.2.11) and the other two curves represent the eigenvalues problem given in Eqs. (4.17) and (4.17). Also, in Fig. 4.3, we attempt to illustrate three different cases related to the system growth rate, r. Each of the figures, 4.3(a), 4.3(b) and 4.3(c), show different stability details: i.e., when $r = 0.5$ the system exhibits 5 different stability regions. It should be noted that in-between the two saddle node curves shown in Eqs. (B.2.10) and (B.2.11) the bistability area is wider than is the case when $r = 1.5$ and when $r = 5$. We still have the two types of bifurcation but for a wider range of ν.

4.3.4 The bifurcation and stability of the prey (phytoplankton)

Examination of the equilibrium densities of each species shows that an increase in the rate of copepod predation on microzooplankton will always cause an increase in the equilibrium density of phytoplankton and a decrease in the equilibrium density of microzooplankton. To show the population dynamics of the two species, P and M, Fig 4.4 is used to represents a special case of Fig.4.3. It shows exactly where the bifurcation starts for different values of K. Also, Fig. 4.4 shows in detail each case of the system's behaviour in relation to different carrying capacities.

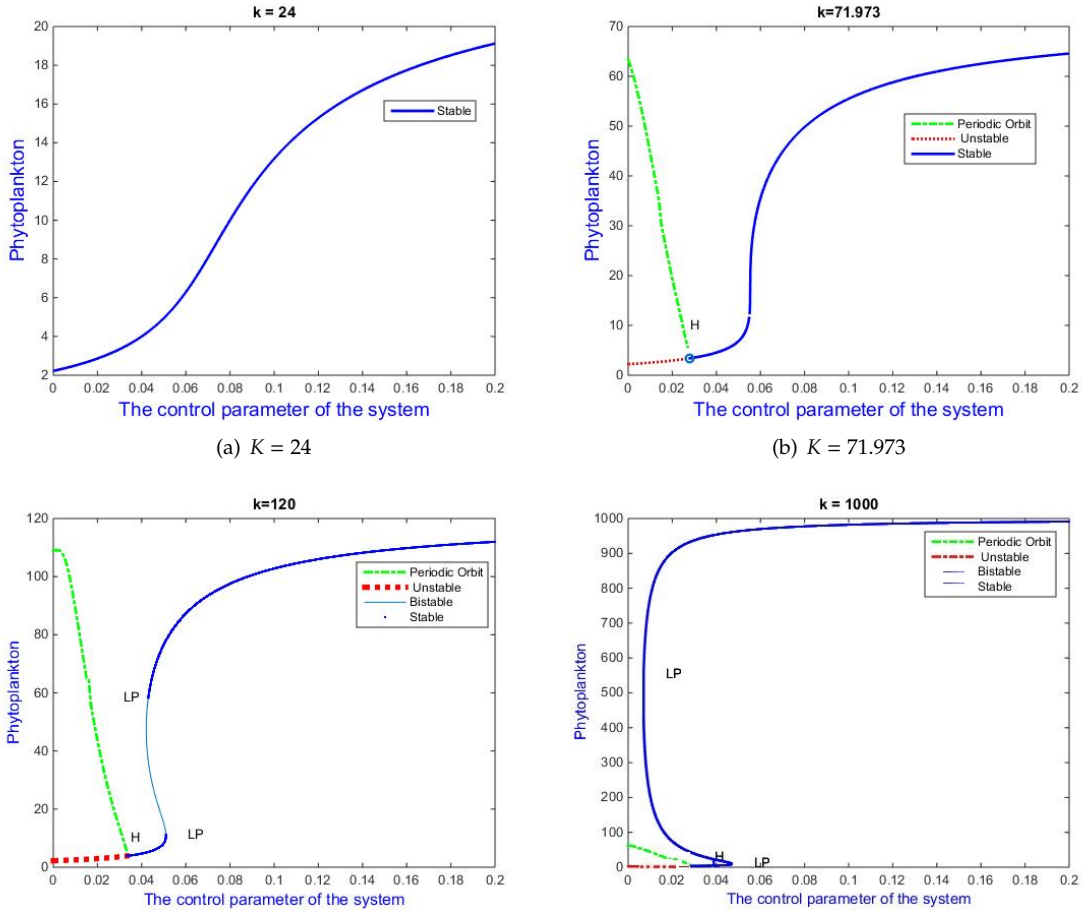

(a) $K = 24$ (b) $K = 71.973$

(c) $K = 120$ (d) $K = 1000$

Figure 4.4: *The behaviour of the system w.r.t. various values of the carrying capacity, K, and the control parameter ν, but with all the other parameters fixed as in table 4.1. In 4.4(a), when $K = 20$, we have only one root of the type stable focus. In 4.4(b), $K = 71.973$, and we have a Hopf bifurcation and after the HB, the system roots are then of type stable sink. We look at this this value of K specifically because it represents a critical value that we have determined by solving the equations for the saddle node bifurcation. This value separates the region of stability, the region with only one bifurcation type, from a region with two bifurcations (one Hopf and one Saddle node bifurcation). In 4.4(c), $K = 120$ as in [143]; here we have a Hopf bifurcation at $(\nu = 0.033512)$ and $P = 3.94$ and also a saddle node bifurcation, (LP_1) and (LP_2); the limit point is in two different places at $(0.042, 58.265)$ and at $(0.051, 11.322)$ respectively. In 4.4(d), $K = 1000$, and we have a Hopf bifurcation when $\nu = 0.039$ and $p = 4.821$, at the earlier points of the bifurcation curve and saddle node bifurcation points are (LP_1) and (LP_2) in two different points, $(0.007, 553.1677)$ and $(0.047, 12.5665)$, respectively [143].*

Fig. 4.4 shows the bifurcation and stability of the phytoplankton for different carrying capacities. This figure can be considered as a special or detailed case of the general stability diagram in Fig.4.3(a). For $K = 24$ we attempt to show that all equilibria are stable – this is so because of the location of each one as yielded by Cardan's conditions and the eigenvalue problem that is given by Eq. 4.16 – and that this leads to no bifurcation in this case. Moreover, for $K = 71.973, K = 120 and K = 1000$ we have a different stability regime. In Fig. 4.4(b), $K = 71.973$, and we have a Hopf bifurcation, and after the Hopf bifurcation the system roots will be of type stable sink. We consider this value of K specifically because it represents a critical value that we have determined to be so by solving the equations. This value separates the region of stability from the region with only one bifurcation type to a region with two bifurcations (Hopf and Saddle node bifurcation). In Fig. 4.4(c), $K = 120$ as first solved and illustrated in [143]; here we have a Hopf bifurcation at ($\nu = 0.033512$) and $P = 3.94$ and a saddle node bifurcation (LP_1) and (LP_2), the limit point is in two different places, at $(0.042, 58.265)$ and at $(0.051, 11.322)$ respectively. In Fig. 4.4(d), $K = 1000$; here we have a Hopf bifurcation at $\nu = 0.039$ and $p = 4.821$ at earlier points in the bifurcation curve, and the saddle node bifurcation points are (LP_1) and (LP_2) at two different points, $(0.007, 553.1677)$ and $(0.047, 12.5665)$ respectively. It should be noted that the solution given in this analysis depends on the parameter values used; these are as shown in Table 4.1. It should also be noted that the analysis in [143] provides an insight, specifically, into the effects of infochemicals, while the analysis in this chapter studies the effect of increasing the carrying capacity and how changing both K and ν affect the system dynamics, even at unlimited nutrient load, as in Fig.4.3.

4.3.5 The bifurcation and stability of the predator (microzooplankton) population

In this section we investigate the stability of the equilibrium density for the microzooplankton and the effects of the control parameters, ν and K, on system behaviour. In Fig.4.5, different cases in terms of the effects of infochemicals on predation by grazers are shown, using the parameter values shown in Fig. 4.4.

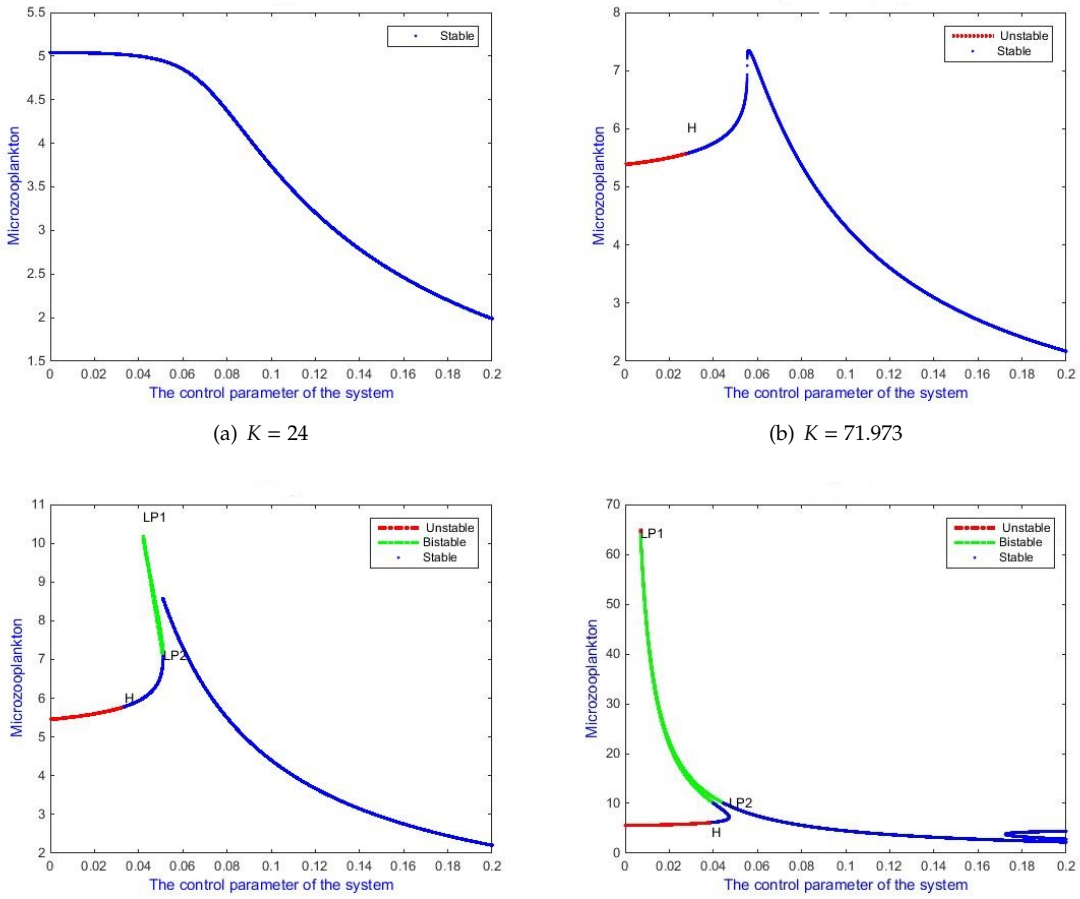

(a) $K = 24$

(b) $K = 71.973$

(c) $K = 120$

(d) $K = 1000$

Figure 4.5: *The behaviour of the predator M w.r.t. various values of K, the carrying capacity and v, the system control parameter, with all the other parameters fixed at the values shown in table 4.1. In 4.5(a),* $K = 24$ *(the effect of DMS on the predation of grazers); here the type of the equilibrium is stable focus for all v− values. In 4.5(b),* $K = 71.973$ *and the system has Hopf -bifurcation at* $v = 0.028$ *and after this Hopf -bifurcation the system roots indicate a stable sink/node. In 4.5(c),* $K = 120$*, and we have a Hopf bifurcation and a saddle node bifurcation,* (LP_1) *and* (LP_2)*; the limit point is in two different places, at* $(0.042, 10.66)$ *and* $(0.051, 7.091)$ *respectively. In 4.5(d),* $K = 1000$*; here we have overlap at the bifurcation, i.e., a Hopf bifurcation at* $v = 0.039$*. After the Hopf bifurcation bifurcation, there is a saddle node bifurcation at two different points* (LP_1) *and* (LP_2) *at* $(0.007, 64.0275)$ *and* $(0.047, 8.0705)$ *respectively*

An increase in the microzooplankton grazing of phytoplankton led to an increase in the microzooplankton mortality rate, via the parameter ν. This is assumed to be as a result of increased predation by copepods. The bifurcation and stability of the microzooplankton is shown in Fig. 4.5 for different cases of the carrying capacity, with $K = 24$, as a special case of the general stability diagram in Fig. 4.3(a). This was constructed in order to show the stability of the model for different values of the model's set carrying capacity such as $K = 71.973, K = 120$ and $K = 1000$. In this analysis we use the parameter values shown in Table 4.1. The case when $K = 24$ is shown in Fig. 4.5(a); here there is no bifurcation and all the equilibria show stable states. Fig. 4.5(b) shows the case when $K = 71.973$, which is the value at which the system starts to exhibit Hopf bifurcation. Due to the change in the stability of the system's equilibrium (from an unstable to a stable state) and when our supercritical limit cycle has occurred, at around $\nu = 0.028$, large oscillations [3] in the system dynamics occur, so that both dynamics may come close to local extinction as their phase plane trajectories draw close to the axes [134]. Fig. 4.5(c) shows the standard case, which has already been studied in [143], of the phytoplanktons behaviour w.r.t the infochemicals. However, here we study the microzooplanktons behaviour w.r.t infochemicals, ν, and this exhibits Hopf bifurcation. Increasing ν leads to multiple stable equilibria. These equilibria are saddle node bifurcations (LP_1) and (LP_2) with limit points at two different places, $(0.042, 10.66)$ and $(0.051, 7.091)$. Microzooplankton behaviour w.r.t infochemicals is shown in Fig. 4.5(d) and the figure also clarifies the nature of the overlapping Hopf and saddle node bifurcations when $K = 1000$: i.e., that there is a Hopf bifurcation with $\nu = 0.039$ and (LP_1) and (LP_2) in two different points, $(0.007, 64.0275)$ and $(0.047, 8.0705)$. This analysis has shown that increasing both the carrying capacity and infochemicals can initially have a stabilizing effect on the system in question.

4.3.6 Plankton blooms and population limitation or the hydra effect in the predator-prey model

A phytoplankton bloom has been defined as a high concentration of phytoplankton in an area caused by increased reproduction under certain environmental conditions, such as when the nutrient source is continuous and conditions remain favorable. Phytoplankton bloom formation is possible in a certain range

[3] Large oscillations represent periodic solutions with big amplitude values in the nonlinear reaction model, i.e. a repetitive variation, typically in time [120].

of parameter combinations, e.g., relating to K and ν. Increased copepod predation on microzooplankton relieves excessive grazing pressure from the phytoplankton, allowing the formation of a bloom. Solving Eq. (4.18) will give the roots of the saddle node bifurcation and can also locate where the bifurcation takes place. However, it should be noted that the region between the area with one root (positive real) and that with three roots (real and distinct) is identified by satisfying Cardan's third condition $y_N^2 = h^2$, i.e., the areas are separated by Eq. (4.18). The results in Fig. 4.6(a) are used to show the maximum value of the population density for the phytoplankton, depending on the level of the carrying capacity. More generally, a bloom can be considered as a phytoplankton population explosion: blooms occur when sunlight and nutrients are readily available to the plants, and so they grow and reproduce to a point where they are so dense that their presence changes the colour of the water in which they live [214]. Fig. 4.6(a) examines two independent parameters, the carrying capacity and the infochemicals determined by using the polynomial in 4.3, and illustrates a potential bloom of phytoplankton. A low population of phytoplankton is represented by a small dark area on the left of the saddle node curves of Eqs. (B.2.10) in Fig. 4.6 (a). The low value of the P_e (the phytoplankton equilibrium point) corresponding to various different values of K and ν, we can readily see in Figs.4.4 in 4.4(a). While the area to the right of the curve shows higher populations of phytoplankton: i.e., potential phytoplankton bloom.

Crossing the first curve in Fig. 4.6(b) will give the same results as (a). However, for a small range of ν, the microzooplankton will also bloom when $0.001 < \nu < 0.02$ and $500 < K < 1000$. Our results show that a hydra effect in relation to microzooplankton populations will typically occur after crossing the saddle node curve of Eq. (B.2.10); this means that an increase in microzooplankton mortality leads to a higher population in M. To connect this result with the microzooplankton bifurcation curve, in Fig. 4.5, when $K = 71.973$, $K = 120$ and $K = 1000$ we can provide a clearer analysis of the illustrated results. The peaks in Fig. 4.5 when $K = 71.973$, $K = 120$ and $K = 1000$ correspond to high population densities of microzooplankton and correspondingly Figs. 4.6 show this peak of bloom formation in the range of $0.001 < \nu < 0.02$ and $500 < K < 1000$. Hydra effects typically occur when the system dynamics are cyclic [213]. The effect refers to the situation where the density of a species increases in response to greater mortality: e.g., when copepod grazing on microzooplankton increases, phytoplankton density will increase as a (counter-intuitive) response to this mechanism. In this situation, the copepod density will remain constant over short timescales. However, the effect does support

our assumption that copepods respond to the concentration of the infochemical signal. The hydra effect also implies seemingly unreasonable responses to changes in immigration and in other parameters affecting population growth [213]. It is also defined as a response to altered mortality [45]. [45] wrote that different levels of copepod predation determine the stabilization of phytoplankton and microzooplankton population densities. From the heat map images, it can be seen that an equilibrium is highlighted which indicates a stable state to the left of the curve of Eq. (B.2.10) in the maximum densities of the equilibria. The results of this are a blooming of both species. The image indicates that after crossing the saddle node curve a stable equilibrium density is reached. This is despite the fact that when the phytoplankton blooms, grazing pressure will affect its population density because of the increased microzooplankton population density and activity [45].

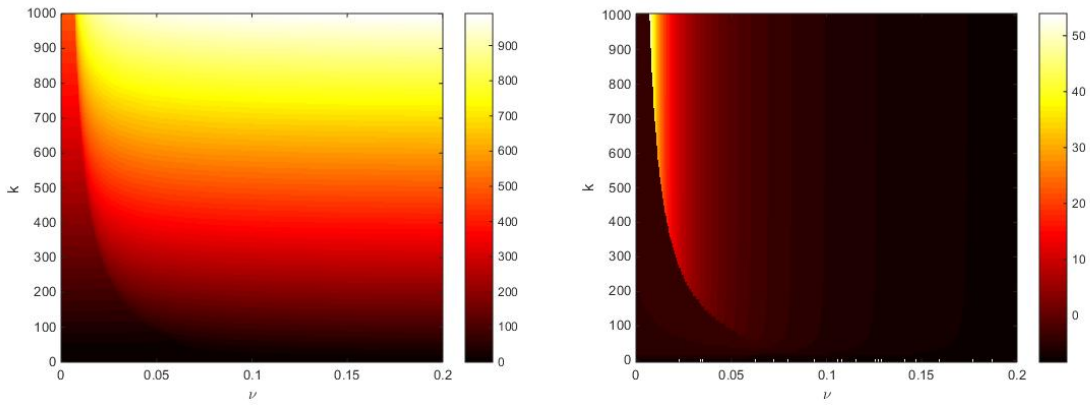

(a) (b)

Figure 4.6: *A graphical representation of the system maximum, P_e and M_e, in relation to the parameters for different values of K and ν. 4.6(a) shows when and how persistent phytoplankton blooms occur given the effect of nutrient limitation on the system, while Fig. 4.6(b) represents the microzooplankton blooming w.r.t the carrying capacity.*

4.3.7 Comparison study of the variational approximation method and numerical analysis

In this section we compare the periodic solution that we represented analytically in Eq. (4.23) with the numerical finding derived from the model Eqs. (4.1) and (4.2). The large oscillations in the prey (phytoplankton) density have already been presented in Figs. 4.4(b) and 4.4(c) – which use the same parameter ranges as are illustrated in Table 4.1. The presence of Hopf bifurcation in the multitrophic plankton model – Eqs. (4.1) and (4.2) – also has a periodic orbit which leads into a limit cycle solution, as shown by Fig. 4.7 and Figs. 4.8.

By using Newton-Raphson to solve Eq. (4.23) and by substituting the results, P and M into Eq. (4.22), we derive the solution profile for the periodic orbit. The numerical results from varying ν are shown in Fig. 4.7 and Fig. 4.8 for $K = 70$ and $K = 120$; these are denoted by the black dot-dash line. The results show that VA is good when ν is near a Hopf point, Hp, see Figs. 4.8(e), 4.8(f), 4.7(c), and 4.7(d).

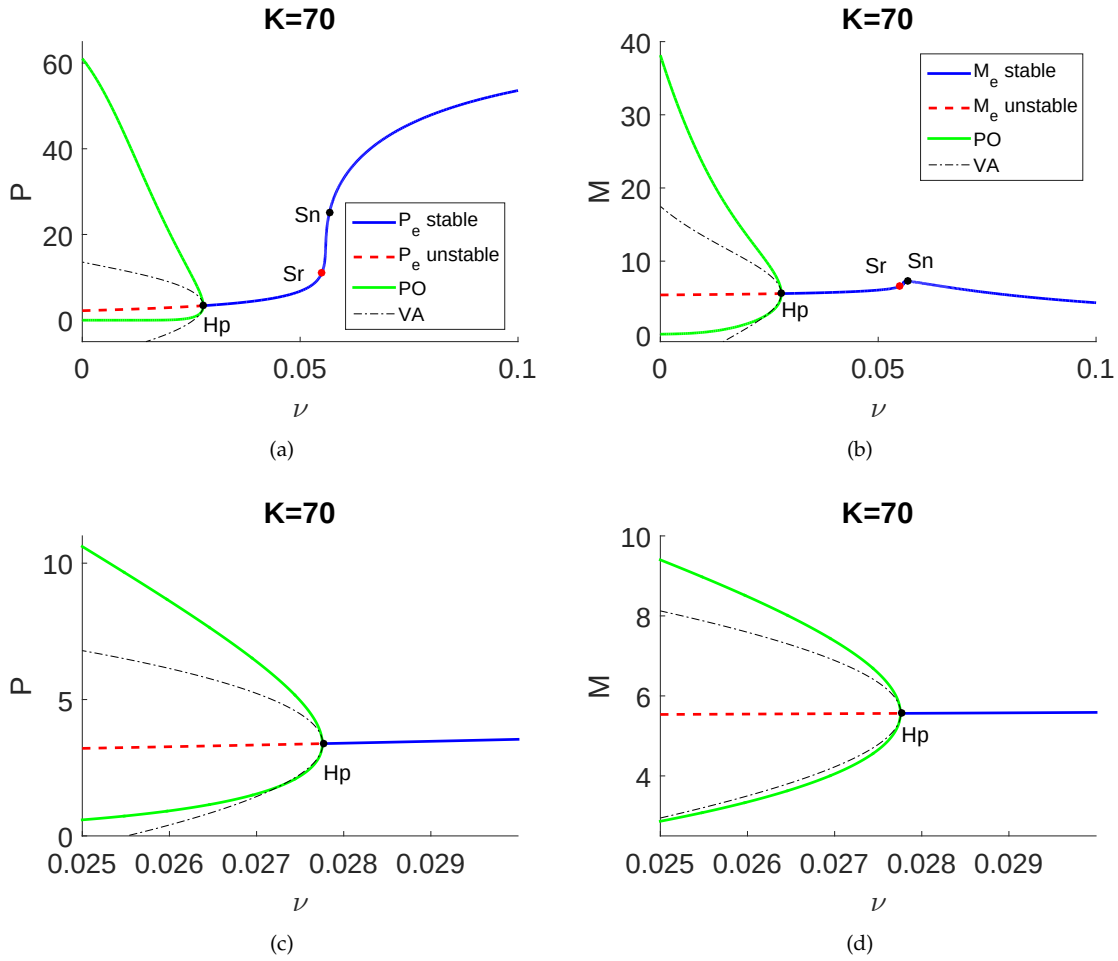

Figure 4.7: *Uniform solutions and periodic orbits for $K = 70$. Hp indicates a Hopf point. Hp indicates a point where the eigenvalues of a uniform solution change from complex to real. Sn indicates a boundary wherein the periodic solutions may exist. Sr indicates a point where the eigenvalues of a uniform solution change from complex to real. The green solid line, PO, indicates the periodic orbit of the system. The black dot-dash line, VA, indicates the Variational Approximation of the periodic orbit.*

Figure 4.7(c) shows a plot of the analytical result of Eq. (4.24), which we obtained after performing the integration in Eq. 4.23 for $K = 70$. All ψ_i, $i = 1..8$ are constants which depend on the parameter values shown in table 4.1. Their values are as follows: $\psi_1 = 3.333$, $\psi_2 = -2.479847343.10^3$, $\psi_3 = 2.349717693.10^2$, $\psi_4 = 3.4161630580$, $\psi_5 = 1.14482461$, $\psi_6 = 4.1630580$, $\psi_7 = 8.2661578100$ and $\psi_8 = 7.83239231$.

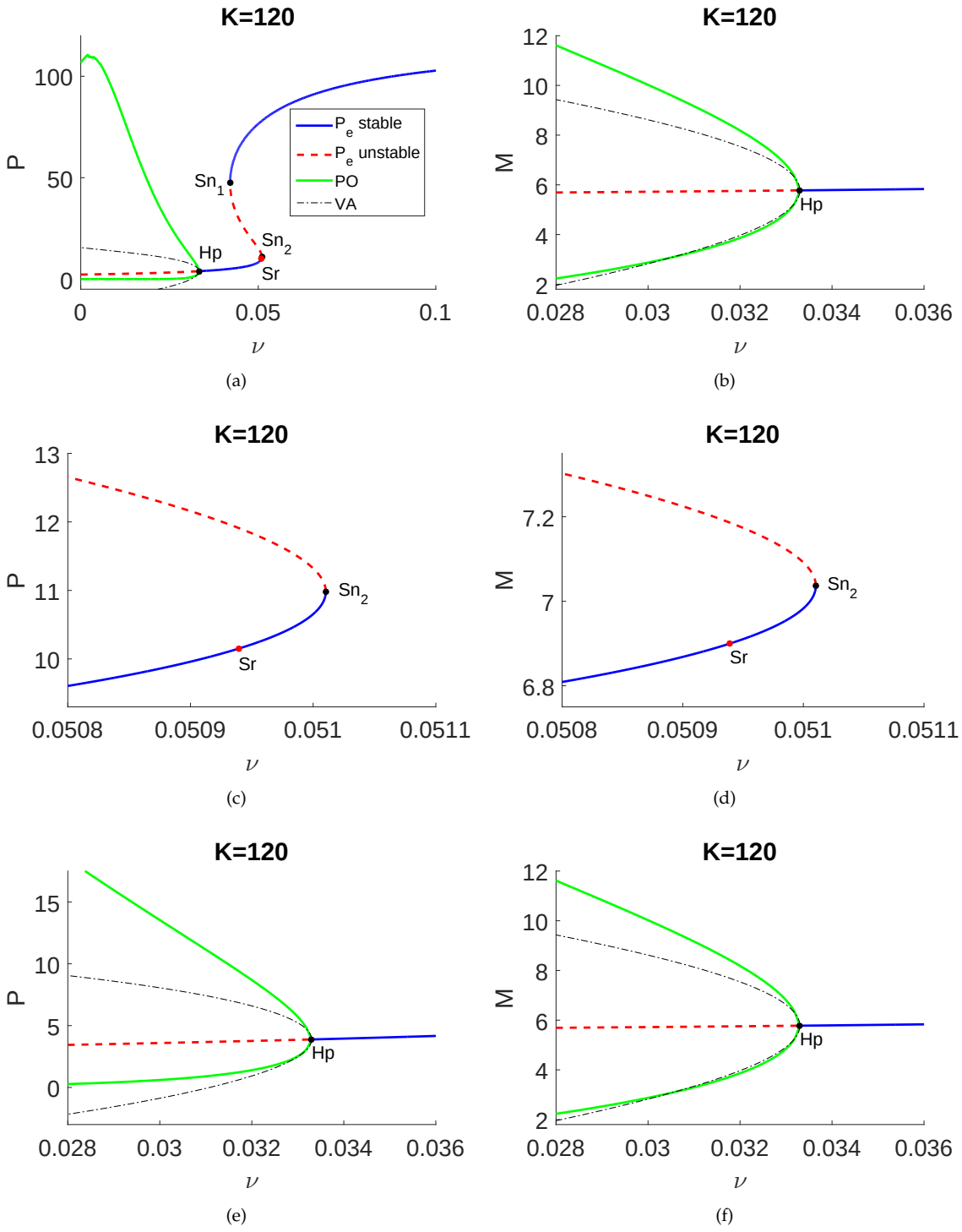

Figure 4.8: *Uniform solutions and periodic orbits for $K = 120$. Hp indicates a Hopf point. Sn_1 and Sn_2 indicate the first and second saddle node. Sr indicates a point where the eigenvalues of a uniform solution change from complex to real. The green solid line, PO, indicates the periodic orbit of the system. The black dot-dash line VA indicates the Variational Approximation of the periodic orbit.*

Fig. 4.8(c) shows the plot of the analytical result of Eq. (4.24), which we obtained after performing the integration in Eq. 4.23 for $K = 120$. All ψ_i, $i = 1..8$ are constants which depend on the parameter values shown in Table 4.1; their values are as follows: $\psi_1 = -5.240303890$, $\psi_2 = 2.0165060.10^2$,$\psi_3 = 4.231355243$, $\psi 4 = 1.5042208.10^2$, $\psi_5 = 0.524030389$ and $\psi_6 = 2.016506160$. It is readily seen that in Figs. 4.7(c) and 4.8(e) the best fit between the numerical and the analytical approach is demonstrated in the curves represented by the minimum values of P – the periodic solution and minimum values of the analytical approach. These two curves are very close to each other, due to the location of their equilibrium points.

After using a numerical simulation tool to solve the model represented by Eqs. (4.1) and (4.2), we want to build trust in its reliability. We can do this by checking whether the simulation tool accurately reproduces the available analytical solutions and that its results match experimental observations. This brings us to two closely related curves for verification and validation. To clarify what these two terms mean in the context of numerical simulations, we can say that both the numerical and the analytical approaches, of finding the limit cycle and of finding the periodic orbit, in terms of Eqs. (4.1) and (4.2) respectively, are close to each other near the Hopf bifurcation point.

4.4 Conclusion

A mathematical understanding of the behaviour of the system described by equations Eqs. (4.1) and (4.2) was obtained by carrying out a phase plane, stability and bifurcation analysis of the model. As a homogeneous environment is assumed, we will utilise only a type II functional response, as a greater range of dynamical behaviours is displayed in this case [143]. This is in agreement with the studies in the literature which favour the use of the Holling type II functional response when considering microzooplankton grazers such as Oxyrrhis marina [51], [192].Our numerical approach helped us to find the effect of the control parameter ν on the system's qualitative behaviour by facilitating an investigation into the stability and the dynamics of the system via the phase plane tool presented in Figs. 4.1 and 4.2. For instance, by having $\nu = 0$, we reduce the system to the Rosenzweig-MacArthur model, [143] and [134], which means that the system will be unstable and will show periodic cycles in terms of the density of microzooplankton and phytoplankton. [2] and [232] considered predator prey interactions between phytoplankton and zooplankton which create a situation

whereby the system possesses a stable equilibrium whose solution trajectories perform large oscillations before returning to that equilibrium.

Increasing the value of the control parameter will result in there being different cases in terms of stability as shown in the stability (bifurcation) diagram Fig. 4.3 and its special cases shown in Figs. 4.4 and 4.5. This explains how infochemical signalling provides a mechanism for increasing copepod predation on microzooplankton. The detailed analyses in this chapter are consistent with the numerical findings in [143] related to the situation where $K = 120$ and $0 < \nu < 0.12$. This chapter has explained in detail the location and the number of the roots and their type; these roots were revealed by using Cardan's method, and this helped us to find the key parameters of the system's behaviour when $K = 71.973$, which is the value of the K parameter when the system exhibits a cusp bifurcation (two equilibrium points coalesce and disappear in a saddle node bifurcation) [103]. We also analysed the model's stability in the (ν, K) plane, and that facilitated the discovery of a microzooplankton hydra effect on the predation by copepods. Besides that, we were able to predict when and where phytoplankton might bloom (according to the model) as shown in Fig. 4.6. We also found another connection between these two parameters, as shown in Fig. 4.3, which shows in a simple manner the stabilizing effect they have on the model. In addition to the results found in [143], analysing Fig. 4.3 shows that the system possesses five different stability states, all the related results are explained in section Fig. 4.3.5. We deduced the effect of changing the growth rate and the phytoplankton carrying capacity on the phytoplankton behaviours, as shown in Figs. 4.3(a), 4.3(b) and 4.3(c); in relation to this, we describe how small values of the growth rate will shift the stability of the model further to its current point, obtained first in Fig. 4.3(b). Furthermore, a relation connecting both K and ν was found, which helped to predict that both species may enjoy a high population density when a rich environment of nutrients is supplied, as is shown in Fig. 4.6. This result demonstrates the hydra effect of the predator-prey model which is mentioned in [45]. The main aim of this chapter, however, was to develop analytical expressions for the curve that describes the bifurcation behaviour discovered earlier by [143], and then to illustrate this using a specific set of parameters. The phase plane technique is a standard method used to produce graphical representations of the dynamics of two component systems (a phase portrait). The technique is described in detail by [134] and [27]. To summarise the results of the study of this model briefly, we can make the following points:

- The eigenvalue problem of the prey-predator model and the second condition of Cardan's method helped significantly in setting up the general stability analysis, as shown in Figs. 4.4 and 4.5. Constructing this diagram helped us to construct the stability analysis for each value of K corresponding to various values of ν. This analysis has led us to the same result as [143] for $K = 120$. However, in addition to [143]'s results, we implemented several cases for the bifurcation in this system depending on different values of K and all cases emphasise that the presence of infochemicals can act to stabilize an otherwise unstable food-web.

- Cardan's method [197] holds for any parameter set. Its conditions helped to solve the polynomial for each species, and solving the polynomial for each species helped in showing the effects of varying the value of infochemicals on each species. Fig. 4.6(b)shows that for large K, M_e is found to initially increase significantly as ν increases past the saddle-node bifurcation, before decreasing as ν increases further. This result is somewhat counter-intuitive, given that an increase in ν corresponds to a higher mortality of microzooplankton due to increased copepod predation. This result can be related to the well-known 'hydra-effect' which is known to exists in predator-prey models [213], but in this case it has a simple explanation: an initial relief of grazing pressure allows P to bloom, and in turn a higher population density of P is able to support a higher population density of M. When the net effect of the infochemical-mediated interactions is large, the only stable equilibrium corresponds to a phytoplankton bloom. Our results in this respect are consistent with [213].

- Analysing the behaviour of the predator, M, by varying the value of K as a second control parameter with respect to infochemicals as the main parameter, we showed the effect of DMS on the predation of grazers, and that the population of both species (phytoplankton and microzooplankton) can increase significantly in parallel, as is shown in Figs. 4.5(a), 4.5(b), 4.5(c) and 4.5(d).

- Exploring the phytoplankton growth rate helped us to discover how having a small growth rate can lead to a small phytoplankton density and the destabilization of the model as shown in Figs. 4.3(a). At the same time, while a high potential growth rate enables hetero-trophic protest to persist during periods of high predation, the system responds rapidly to increases in fast-growing prey, which could be the main reason for there being a limit cycle in the dynamical system.

- The variational approximation method helped us to represents the periodic orbit of the limit cycle [44] by solving Eq. (4.23) using the Newton Raphson method. In Fig. 4.8(e) the best fit between the numerical and the analytical approach is demonstrated by the curves representing the minimum values of P and the minimum values of the analytical approach, as the two curves are very close to each other, due to the location of their equilibrium points. The parameter ranges are those given in Table4.1.

Chapter 5

Transient Turing Patterns in a Spatial Infochemical Mediated Plankton Model

5.1 Introduction

In this chapter, we investigate the phenomena of pattern formation and wave propagation as they relate to the reaction–diffusion system that we studied in chapter four (which was first studied in [143]). We show how variations in the diffusion of predators and prey destabilize the uniform equilibrium and are responsible for the formation of patterns. It is possible to predict the shapes and the amplitudes of these patterns. For the amplitudes, in the supercritical case, we derive the quintic Stuart–Landau equation [31].

The main target of this analysis is the study of the system perturbations and the effects of the spectrum of the spatial model; these depend significantly on the wave number, w, in terms of demonstrating system stability. For instance, if the real part of the spectrum is < 0 then we will have a stable solution and there will be no growth in the wave amplitude and vice versa for the positive real part of the spectrum. After discovering the stability of the perturbed model, we find the spatio-temporal patterns which are both x and t dependent. When the system is stable in a purely temporal pattern (i.e in a non-spatial model), the patterns generated will be restricted by the exact value of the prey diffusivity. There has been increased interest in introducing predator prey dynamics into mathematical biology in such a way as to implement and understand Turing

instability and the formation of patterns. The current chapter will explore Turing instability, as developed by Alan Turing, who suggested that morphogens, a term given to a system of reacting and diffusing chemicals, can generate patterns from a previously uniform state [66].

[81] demonstrates that a steady state can be considered to be Turing unstable, if it is unstable as a solution to the full reaction diffusion system but stable as a solution to the reaction system without diffusion. This situation results in the formation of spatial patterns. Dispersal affects the behaviour of spatial perturbations which do not decay to zero, and this results in Turing instability [169]. There have been important contributions by previous researchers who have developed approaches to pattern formation via (mostly) reaction diffusion equations. Some earlier work carried out by [208] demonstrated the use of reaction diffusion equations in a predator prey context, in terms of the work carried out by Turing. Thereafter numerous studies have been carried out on pattern formation in the behaviours of reaction diffusion models of prey predator interaction. In [5], it was seen that Turing mechanisms can generate patchiness in a homogeneous environment under certain conditions of trophic interaction and predator–prey relative diffusion. Also [19] showed that different patterns can appear at different depths, and by using a model involving nutrients and microorganisms in sediments, they proved that the formation of spatio–temporal patterns can be the consequence of interactions between predation and transport processes. To investigate the key dynamical properties of spatially extended predator–prey interactions [84] presents two finite–difference algorithms for studying these. The analysis of a simple model of phytoplankton–zooplankton dynamics in space and time is presented in [152]. By summarizing the local properties, the emergence of spatial and spatio–temporal patterns can be considered. In [161], reaction diffusion models have been shown to be effective tools for investigating spatiotemporal pattern formation in relation to plankton dynamics. Furthermore, [166]and [242] show, in a time-continuous predator-prey system incorporating the Allee effect, that the temporal population oscillations can become chaotic and the system can exhibit period locking behaviour, which means a small variation in the parameters can lead to alternating–regular and chaotic dynamics.

Reaction diffusion systems are studied by firstly determining the Turing space for a given model. Thereafter, a bifurcation analysis of a specific pattern formation is established [66]. It should also be noted that reactivity is vital for Turing instability; short term transient behaviour indicates that disturbances to a stable equilibrium will eventually diminish. At first the size of such disturbances grows rapidly, and growth

continues for a while, but eventually it decays [169]. Turing instability in relation to pattern formation has also been significantly studied by numerous researchers. Studies have been carried out to investigate the regime shifts whereby cases of sudden extinction of species have occurred –in situations where there were safe numbers initially. The current study is in agreement with previous studies which were carried out to try to explain the reason behind such regime shifts; it has been established mathematically that these are caused by changing from a steady state equilibrium to an unsteady state equilibrium due to saddle node bifurcation [22], [206]. Another reason, as established by [201], is the existence of long living transients. Here we investigate the Turing and Transient Turing instability of nonlinear reaction diffusion systems with different diffusions. Although Turing instability has largely been covered by previous researchers, we demonstrate, in Chapter 3, the possibility of pattern formation in the plankton model first studied by [143] through a linear stability analysis. We show that the coexistence point is stable for reaction only but is unstable for the reaction diffusion system, depending on the choice of ν value. Moreover, a perturbation with a given wave number is also applied to obtain a dispersion relation.

This chapter is arranged as follows. The first section introduces the study by investigating a spatial version of the plankton model looked at in Chapter three, [143]. The second section considers a Turing and Hopf instability analysis of the reaction and diffusion model and the types of the spectra exhibited in one and two dimensions. In the next section we derive an approximate solution using a weakly non-linear analysis and then derive the amplitude equation. In the later sections we analyse the uniform and the non-uniform solutions using a numerical exploration of reaction diffusion models; this helps us to introduce the main finding that there are transient Turing effects exhibited by the reaction diffusion model. We also investigate the type of the spectrum which exists in each area in which these transient Turing effects exist.

5.2 One Dimensional Spatial Distribution

In this section we aim to discuss the possible patterns which may arise in a two component spatial version of the plankton model in chapter three, [143]. Let's introduce the diffusion parameters. The diffusion coefficients are denoted by D_P and D_M, as in Eq.(5.1). This is to include spatial diffusion terms corresponding to the horizontal plane.

$$\begin{aligned}\frac{\partial P}{\partial t} &= F(P,M) + D_P \frac{\partial^2 P}{\partial x^2} \\ \frac{\partial M}{\partial t} &= G(P,M) + D_M \frac{\partial^2 M}{\partial x^2}\end{aligned} \tag{5.1}$$

for $x \in \Omega$, where Ω is a bounded region $[0, L]$ and t $\in [0, \infty)$.

$$\begin{aligned}F(P,M) &= rP\left(1 - \frac{P}{k}\right) - \frac{aPM}{1+bP} \\ G(P,M) &= \frac{\gamma aPM}{1+bP} - mM - \frac{vaPM^2}{1+bP}\end{aligned} \tag{5.2}$$

Note that since we are extending the model from [143] to include horizontal diffusion, we also consider the effects of the diffusion of P and M in the x-direction with the diffusion coefficients D_P and D_M, respectively. For simplicity, and without loss of generality, we fix $D_M = 1$ and undertake a relative exploration concerning how the spatial dynamics change for a range of $D_P < D_M$. To solve the model in Eq. (5.1),numerically, we set the initial conditions as:

$$\begin{aligned}P(x,0) &= P_e + \epsilon \cos(wx) \\ M(x,0) &= M_e + \epsilon \sin(wx)\end{aligned} \tag{5.3}$$

For $x \in [0, L]$.

Note also, however, that there are infinitely many solutions (i.e., eigenfunctions) to the spatial problem. The solution of the mathematical model will always depend on the initial conditions and parameters, because small changes in the initial states (or parameters) of the system produce small changes in the outcome [98]. The initial condition given by Eq. 5.3 is the approximate solution of Eq.5.1. It has the term P_e,M_e as the exact solution of the system (a steady state) and the term $\epsilon \cos(wx)$ as the perturbation. w is the spectrum of (P_e, M_e), with Neumann boundary conditions as periodic boundary conditions, $\nabla P = 0$, $\nabla M = 0$ [1] w.r.t x. This is a periodic function; these are considered to be the periodic boundary conditions that impose the weakest

[1] The derivative of the second term in Eq. 5.3.

influence on pattern formation: i.e., a natural choice is to assume that the boundaries do not influence the interior of the domain and impose zero flux [83] and [47]. The first step in analyzing the model is to determine the equilibria (stationary states) of the non-spatial model obtained by setting the space derivatives to zero, and this has already been done and studied in detail in chapter three, and the results are presented for this context in the next section.

5.3 Turing and Hopf Instability

5.3.1 Turing basic analysis

In this section we investigate the possibility of pattern emergence in Eq. (5.1). Through a linear stability analysis we show that the coexistence point is stable for the reaction system but will become unstable for the reaction diffusion system. In the current work, we will always consider the stability of the equilibrium point defined by $P(t) = P_e$ and $M(t) = M_e$ in relation to Eq.5.1, as corresponding to $dP/dt = dM/dt = 0$, the coexistence equilibria. The other equilibria are linearly unstable so we exclude them from the current analysis. The analysis of each equilibrium can be found in the previous chapter in Secs. 4.2.1.

$$\begin{aligned} P_0 &= \frac{kb-1}{3b} + \frac{2}{3}\sqrt{\frac{(-vrkb+rv)^2 - 3(vrb)(\gamma ak - mbk - vrk)}{v^2r^2b^2}}\cos\left(\frac{\theta}{3}\right) \\ M_0 &= \frac{-r}{(ak)}\left(P_0^2 b - P_0(bk-1) - k\right). \end{aligned} \tag{5.4}$$

Where $\theta = \cos^{-1}\left(\frac{Y_N}{h}\right)$, which is stable if $y_N^2 < h^2$, according to Cardans analysis; this corresponds with it having little effect on the *DMS* and with low predation in the system. Furthermore, for the point (P_0, M_0) to be the coexistence steady state, linear conditions must be imposed. The linearised system in the neighborhood of (P_0, M_0) is:

$$\frac{\partial}{\partial t}\begin{pmatrix} P \\ M \end{pmatrix} = \begin{pmatrix} D_P & 0 \\ 0 & D_M \end{pmatrix}\nabla^2\begin{pmatrix} P \\ M \end{pmatrix} + \begin{pmatrix} F(P,M) \\ G(P,M) \end{pmatrix} \tag{5.5}$$

Let U be a vector of (P,M) and u_e be a constant vector of (P_e, Me), S.t $F(u_e) = 0$. Thus, we can define

$\overline{U} = U - u_e$, and that will lead to the following system:

$$\frac{\partial \overline{U}}{\partial t} = D\nabla^2\overline{U} + F(u_e) + J\overline{U} + H.O.T \tag{5.6}$$

where $F(u_e) = 0$ and J is Jacobian matrix. By neglecting the H.O.T.(High Order Term)[2] of the Taylor series in the above system we obtain the following:

$$\overline{U}_t = D\nabla^2\overline{U} + J\overline{U}, \tag{5.7}$$

where we define:

$$\overline{U} = \begin{pmatrix} P \\ \\ M \end{pmatrix} \tag{5.8}$$

$$D = \begin{pmatrix} D_P & 0 \\ \\ 0 & D_M \end{pmatrix} \tag{5.9}$$

$$J\overline{U} = \overbrace{\begin{pmatrix} a_{11} - D_P w^2 & a_{12} \\ \\ a_{21} & a_{22} - D_M w^2 \end{pmatrix}}^{J(w)} \tag{5.10}$$

Moreover, the first stage of pattern formation can usually be investigated by finding a solution of Eq. (5.7). We can start with the linear stability analysis and linearise about a fixed point, (P_e, M_e); then seeking a solution of the form $\exp^{(\delta t + i(wx))}$ will lead us to the dispersion relation, which gives the spectrum, δ, of eigenvalue as a function of the wavenumber, w. Correspondingly, the local stable homogeneous steady state becomes unstable with respect to a perturbation with a given wavenumber w: i.e., the perturbation will decay with time if and only if all spectrum have negative real parts.

Let the perturbations be:

$$U = u_e + \epsilon e^{\delta t + i(wx)}\widetilde{U}.$$

After deriving the perturbation w.r.t t and x and substituting into Eq. (5.7), we obtain the dispersion

[2]High Order Term

relation. By solving this relation for δ we see how the real part of the spectrum decreases monotonically w.r.t w.

$$\delta^2 - \delta([D_P + D_M]w^2 - [a_{11} + a_{22}]) + ([a_{11} - D_P w^2][a_{22} - D_M w^2]) - a_{12}a_{21} = 0. \tag{5.11}$$

Where,

$$H(w^2) = ([a_{11} - D_P w^2][a_{22} - D_M w^2]) - a_{12}a_{21} \tag{5.12}$$

Requiring that (P_e, M_e) is stable in relation to the spatially homogeneous mode $w = 0$ entails that $tr(J) < 0$ and $det(J) > 0$. In order to have diffusion driven instability, we require $Re(\delta) > 0$ for some $w \neq 0$, and this is equivalent to imposing $H(w^2) < 0$ for some $w \neq 0$. Since $H(w^2)$ is an upward opening parabola, the above condition holds and requires that $D_P a_{11} + D_M a_{22} > 0$. Finally, for diffusively-driven instability to occur, we also require that there exist real w^2 such that $H(w^2) = 0$. It is easily shown this yields to the imposition of $(D_P a_{11} + D_M a_{22})^2 - 4D_P detJ > 0$, whereby diffusion driven instability arises, and spatial patterns can develop; this is given for a particular choice of the other system parameters [121]. In relation to dispersion relations of the form $\delta = \delta(w)$ stemming from Eq. (5.11), the sign of the real part of δ indicates whether the solution will grow or decay in time. If the real part of $\delta(w)$ is negative for all w values, then any superposition of solutions of the form $\exp^{(\delta t + iwx)}$ will also appear to decay. On the other hand, if the real part of $\delta(w)$ is positive for some values of w, then over time some components of a superposition will grow exponentially. The former case is called stable, whereas the latter is termed unstable. If the maximum of the real part of δ is exactly zero, the situation is called marginally stable. It is more difficult to assess the long term behaviour in this case. The basic linear algebra can lead us to derive the stability conditions using the parameter values given in Table 4.1 in the previous chapter. To obtain some conditions we must connect the main parameter ν with the other system parameters [121]. From the Turing first condition, $a_{11} + a_{22} < 0$ where a_{11} and a_{22} are elements of the Jacobian matrix given in Eqs. (4.12), we obtain ν in Eq. (5.13).

$$\nu > \frac{\gamma K P_0^2 ab - K P_0^2 b^2 m + K P_0^2 b^2 r - 2P_0^3 b^2 r + \gamma K P_0 a - 2K P_0 bm + 2K P_0 br - 4P_0^2 br - K M_0 aKm + Kr - 2P_0}{2K(P_0 b + 1)M_0 P_0 a}. \tag{5.13}$$

Also, Turing's second condition, $a_{11}a_{22} - a_{12}a_{21} > 0$, where a_{ij}, are represented by partial derivatives of Eqs. (5.2), gives ν in Eq. (5.14).

$$\nu < \frac{(\gamma K P_0^2 abr - 2\gamma P_0^3 abr - K P_0^2 b^2 mr + 2P_0^3 b^2 mr + \gamma K P_0 ar - 2\gamma P_0^2 ar - 2K P_0 bmr + 4P_0^2 bmr + K M_0 am - Kmr + 2P_0 mr)(P_0 b + 1)}{M_0 P_0 a(-2K P_0^2 b^2 r + 4P_0^3 b^2 r - 4K P_0 br + 8P^2 br + K M_0 a - 2Kr + 4P_0 r)}. \tag{5.14}$$

Consequently, from Eq. (5.11) we can derive a necessary and sufficient condition for stability, whereby the impact of space becomes explicit in the following condition:

$$a_{11}D_M + a_{22}D_P - 2((D_P D_M)^{1/2})(a_{11}a_{22} - a_{12}a_{21})^{1/2} > 0, \tag{5.15}$$

a_{ij} in Eq. (5.15) are Jacobian matrix elements and D_p, D_M are diffusion parameters for prey and predator respectively. Substituting our parameters into Eq. (5.15) can lead us to derive the pattern formation condition as follows:

$$\nu < \frac{A}{M_0 P_0 a(2D_p K P_0^2 b^2 w^2 + 4D_p K P_0 bw^2 - 2K P^2 b^2 r + 4P_0^3 b^2 r + 2D_p K w^2 - 4K P_0 br + 8P^2 br + K M_0 a - 2Kr + 4P_0 r)}, \tag{5.16}$$

$$\begin{aligned} A = -(&D_p K P_0^2 b^2 w^4 + \gamma D_p K P_0^2 abw^2 - D_p K P_0^2 b^2 mw^2 - 2D_p K P_0 bw^4 \\ &+ K P_0^2 b^2 rw^2 - 2P^3 b^2 rw^2 + \gamma D_p K P_0 aw^2 - \gamma K P_0^2 abr + 2\gamma P_0^3 abr - 2D_p K P_0 bmw^2 \\ &+ K P_0^2 b^2 mr - 2P^3 b^2 mr - D_p K w^4 + 2K P_0 brw^2 - 4P_0^2 brw^2 - \gamma K P_0 ar + 2DP_0^2 ar - D_p K mw^2 \\ &- K M_0 aw^2 + 2K P_0 bmr - 4P_0^2 bmr - K M_0 am + Krw^2 - 2P_0 rw^2 + Kmr - 2P_0 mr)(P_0 b + 1). \end{aligned} \tag{5.17}$$

The inequalities in Eqs. (5.13), (5.14) and (5.16) are based on the Jacobian elements a_{11} and a_{22} as given in Eqs. (4.12) of the previous chapter, and they are true if we use the parameter values in Table 4.1. To recap, we have now obtained conditions expressed in terms of the relevant system parameters - for the onset of diffusion-driven instability. A region in the parameter space has hence been identified so that system Eq. (5.1) can exhibit Turing patterns, for convenience we have shown them all as in Eqs. (5.13), (5.14), (5.15).

The derivatives, a_{11} and a_{22}, must be of opposite sign. However, the only restriction on the condition $a_{11}a_{22} > 0$ is that either $a_{11} > 0$ and $a_{22} < 0$ or the other way around. These two possibilities correspond to qualitatively different reactions. All derivatives are given in Eq. (4.12) in the previous chapter.

5.3.2 The spectrum in a 1-dimensional system

We consider the solution stability by analysing the perturbations to the system and in particular by finding out the sign of δ. We can start this analysis by providing some insights into the change of the spectrum, δ, in the dispersion relation of the canonical forms of the linearised system. Spatial patterns can arise in correspondence to those modes, w, for which $Re(\delta) > 0$. Now, since (P_0, M_0) is stable for the reaction system, one has that $tr(w) < 0$. Moreover, one has that $tr(w^2) > 0$. Therefore the only way to have $Re(\delta) > 0$ for some $w \neq 0$ is if $\delta(w^2) < 0$. Thus, the condition for the marginal stability at some $w = w_c$ is:

$$\max \delta(w^2) = 0 \tag{5.18}$$

The maximum of δ is attained when the wavenumber is a function of the prey diffusion. After deriving $\delta(w^2)$ and solving the derivative for w, we obtain the following value for the wave number.

$$w_p = \pm \left(\frac{a_{22} - a_{11}}{D_M - D_P} + \frac{\left(-D_M D_P \left(D_M^2 - D_P^2 \right)^2 a_{12} a_{21} \right)^{\frac{1}{2}}}{D_M D_P \left(D_M - D_P \right)^2} \right)^{\frac{1}{2}} \tag{5.19}$$

From Eq. (5.18), we obtain the values of ν and w. Also, as the dispersion relation gives δ in terms of the wave number it is important to mention that the range of the spectrum is given by $w_1 < \nu < w_2$, depending on the third condition of pattern formation given in Eq. (5.16).

5.4 Weakly Nonlinear Analysis (WNL) in 1D

The aim of studying the weakly non-linear (WNL) behaviour is to properly characterize the shape and amplitude of the patterns close to the Turing bifurcation threshold of the physically relevant equilibria [80].

When the amplitude of the perturbations is just large enough for the nonlinear terms to become relevant we apply the weakly non-linear analysis in order to study the dynamics of the system [128]. This amplitude condition is satisfied when the control parameter, D_P, is close to the critical value D_{P_c}, which indicates the onset of the instability and is the value that we need to look at in order to obtain the amplitude equations near it to describe the dynamics of the system. The critical bifurcation state also means that there are usually very few unstable modes. The idea is to create a reduced set of equations that describes the nonlinear interactions between these few modes [125]. There are a number of ways of constructing weakly nonlinear equations. The steps are not unique, and neither is the output. To obtain the normal equation form governing the amplitude of the patterns, we implement a weakly nonlinear multiple scale analysis. These amplitude equations allow us to construct relevant solutions of the model equations and they reveal the existence of multiple branches of stable solutions arising as the result of supercritical bifurcations. The amplitude equations could help us to describe the modulations of a stripe state near the threshold, because of the spatially periodic solutions of the model described by Eqs.(5.1); this is illustrated later in this chapter.

To start the analysis, we define a linear operator:

$$\mathcal{L} = J_u \overline{U} + D_P \nabla^2 \overline{U} \tag{5.20}$$

where J is the Jacobian matrix, the elements of which are given in Eq. (4.12), and D_P is the diagonal matrix given in Eq. (5.9) but with $D_M = 1$. Let U be a vector of P, M and u_e a constant vector of P_e, M_e, then the solution of the original system is written as a weakly nonlinear expansion in ϵ:

$$U = \epsilon U_1 + \epsilon^2 U_2 + \epsilon^3 U_3 + ... \tag{5.21}$$

Close to the bifurcation, the amplitude of the pattern will develop on a slow temporal scale, because the key idea of WNL analysis is that close to the bifurcation value the pattern evolves on a slow time scale so that, using the method of multiple scales:

$$D_P = D_{Pc} + \epsilon D_{P1} + \epsilon^2 D_{P2} + \epsilon^3 D_{P3} + ... \tag{5.22}$$

Upon substitution of the expansions Eqs., (6.25) and (6.27), into the main system, we collect the terms at each order in ϵ, so obtaining the following sequence of equations for U_i $i = 1..3$.

$O(\epsilon)$:

$$\mathcal{L}^{D_{Pc}} U_1 = S_1 \tag{5.23}$$

where $S_1 = 0$

$O(\epsilon^2)$:

$$\mathcal{L}^{D_{Pc}} U_2 = S_2 \tag{5.24}$$

$$S_2 = \frac{\partial U_2}{\partial T} + \frac{\partial U_1}{\partial T} - JU_2 - \begin{pmatrix} D_{P1} & 0 \\ 0 & 1 \end{pmatrix} \nabla^2 U_2 \tag{5.25}$$

$O(\epsilon^3)$:

$$\mathcal{L}^{D_{Pc}} U_3 = S_3 \tag{5.26}$$

$$S_3 = \frac{\partial U_3}{\partial T} + \frac{\partial U_2}{\partial T} + \frac{\partial U_1}{\partial T} - JU_3 - \begin{pmatrix} D_{P2} & 0 \\ 0 & 1 \end{pmatrix} \nabla^2 U_3 + \begin{pmatrix} D_{P3} & 0 \\ 0 & 1 \end{pmatrix} \nabla^2 U_2 \tag{5.27}$$

The solution to the linear problem, Eq. (5.23), which satisfies the Neumann boundary conditions [3], is:

$$A(T).E.\cos(\omega_c x) \tag{5.28}$$

where E is the corresponding eigenvector, $E \in Ker\left(J - \omega_c^2 D_{Pc}\right)$, [4], where the amplitude of the pattern $A(T)$ is still arbitrary at this level, ω^2 is the first unstable admissible mode and the vector E is as defined in [80]. In the next section we are going to derive the amplitude equation.

[3] A set of periodic boundary conditions $\nabla P = 0$, $\nabla M = 0$

[4] The kernel of the linear operator, $\mathcal{L}^{D_P}$.

5.4.1 Derivation of the amplitude equation

We derive the amplitude equations that govern the evolution of patterns over time and discuss simple solutions of these equations, starting by seeking a Fourier mode as a solution for the linearised model.

$$U(x,t) = U_e + A(t)Ee^{(iwx)} + c.c \tag{5.29}$$

U is a vector of two components, (P, M), we can rewrite our ansatz as follows:

$$\begin{aligned} P(x,t) &= P_e + EA(t)e^{(iwx)} + \overline{EA(t)}e^{(-iwx)} \\ M(x,t) &= M_e + EA(t)e^{(iwx)} + \overline{EA(t)}e^{(-iwx)} \end{aligned} \tag{5.30}$$

where $A(t)$ is the wave amplitude and E is the spatial eigenvector (constant vector) and w is a constant value representing the wave number which we determined, by deriving $Max(\delta(w))$. Substituting the ansatz given by Eq. (5.30) and the given parameter values from our main reference [143] into the linearised model after expanding the reaction term by Taylor, leads us to construct a simple form of the linearised reaction-diffusion model as follows:

$$\begin{pmatrix} F(P,M) - \frac{\partial P}{\partial t} + D_p\nabla^2\overline{P} \\ G(P,M) - \frac{\partial M}{\partial t} + D_M\nabla^2\overline{M} \end{pmatrix}_{(P_e,M_e)} \begin{pmatrix} P' \\ M' \end{pmatrix} = 0 \tag{5.31}$$

We integrate each row in the system Eq. (5.31) w.r.t x in a bounded interval from 0 to $\frac{2\pi}{w}$ which represents a quasi period or a non linear period (maximum displacement of the wave or a nonlinear wave number). After performing the integration we obtain a quintic polynomial, as in Eq.(5.32), called a Stuart-Landau formula [82]. The deduced equation is a first order ODE of $A(t)$. It controls the vertical direction of the wave amplitude. We solve Eq. (5.32) to obtain an accurate value of the amplitude.

$$A^{'}(t) = \epsilon A + \epsilon A^3 - \epsilon A^5 \tag{5.32}$$

Solving the quintic polynomial for A will help us to get an accurate value for the wave amplitude, and this will lead to the discovery of the maximum and minimum analytic solutions which we can then compare with the corresponding values from our numerical approach presented in section Fig. 5.5.1.

5.5 Numerical Exploration of the Reaction Diffusion Model in 1-Dimensions

After we develop the non spatial model by adding the spatial derivative, in Eq. (5.1), we then studied the Turing mechanisms which are in effect in order to specify at what points and under what conditions we obtain Turing patterns. We also performed some numerical simulations in order to understand the behaviour of the reaction diffusion model, using pseudo arclength method computations past the limit points [109], as presented in 5.5.1.

5.5.1 Numerical continuation

We solve for the time independent solution of Eq. (5.1), numerically, using a Newton-Raphson method to obtain the bifurcation curve. However, as the parameter ν is varied, saddle-node bifurcations could emerge. We use the pseudo arclength continuation method in the present section to continue the computations past the limit points [109].

$$U = \begin{pmatrix} P \\ \\ M \end{pmatrix} \tag{5.33}$$

and we add one equation

$$\theta \, ||U^{(i)} - U^{(i-1)}||^2 + (1-\theta) \, ||\nu^{(i)} - \nu^{(i-1)}||^2 = \delta, \quad (i = 3, 4, 5, \ldots). \tag{5.34}$$

where i is the iteration number, $0 < \theta < 1$ is a weighting parameter, and δ is a distance between $\left(\nu^{(i-1)}, \|U^{(i-1)}\|\right)$ and $\left(\nu^{(i)}, \|U^{(i)}\|\right)$.

For $i \geq 1$, as the initial value, we use

$$\begin{aligned} U^{(i+2)} &= 2U^{(i+1)} - U^{(i)} \\ \nu^{(i+2)} &= 2\nu^{(i+1)} - \nu^{(i)}. \end{aligned} \tag{5.35}$$

$\nu^{(1)}$ and $\nu^{(2)}$ as initial points and $U^{(1)}$ and $U^{(2)}$ are the solution for $\nu^{(1)}$ and $\nu^{(2)}$ respectively.

5.5.2 Uniform solutions and linear stability

The multitrophic plankton model, Eq. (5.1), has uniform solutions $P(x,t) = P_e$ and $M(x,t) = M_e$, which are given in Eq. (5.4). The Pseudo arclength method, which computes approximate solutions of a system of parameterized nonlinear equations, is used to solve Eq. (5.1) for $K = 120$ and $K = 70$. To determine the linear stability of the uniform solutions, we use the dispersion relation in Eq. (5.11), for which all partial derivatives are given in Eq. (4.12) in the previous chapter. From Eq. (5.11), a uniform solution is said to be stable when $\delta(w) \leq 0$ for $\forall w \in \mathbb{R}$ and unstable where $\exists w$ such that $\delta(w) > 0$. So, the maximum of the spectrum, Eq. (5.18), is satisfied when:

$$w_0 = 0 \tag{5.36}$$

or as w_P, as in Eq. (5.19). The wave numbers, Eq. (5.36) and Eq. (5.19) are important when studying the bifurcating uniform and periodic solutions which are being carried by them. Fig. 4.8 shows the bifurcation diagrams of the uniform solutions for $K = 120$. The instability occurs for $0 \leq \nu \leq \mathrm{Hp}$ and between two saddle-node bifurcations, $\mathrm{Sn}_1 \leq \nu \leq \mathrm{Sn}_2$. The most interesting dynamics from this model is the existence of Hopf bifurcation, where $\nu = \mathrm{Hp}$ is the Hopf point. So, the largest eigenvalue has a complex value for $0 \leq \nu \leq \mathrm{Sr}$, where Sr stand for a stable regime. Fig. 4.7 shows the bifurcation diagrams of the uniform solutions for $K = 70$. In general, the dynamics are the same as for $K = 120$. The main difference is that the instability interval only occurs at $0 \leq \nu \leq \mathrm{Hp}$, there are no saddle-node (Sn) bifurcations, and Sn is equivalent to Sn_2 in the case of $K = 120$ where periodic solutions may exist for $0 \leq \nu \leq \mathrm{Sn}_1/\mathrm{Sn}$.

5.5.3 Transient Turing and periodic solutions

If the control parameter is increased far above its critical value, it is possible that the pattern itself becomes unstable against itself, causing secondary instabilities, as they are termed. If the control parameter is increased even further, the pattern may become chaotic or turbulent, i.e. disordered in space and time [108]. We obtained this circumstance in between the two stability curves (the uniform and the non-uniform solutions) in Fig.5.1 when $K = 120$. While in Fig. 5.1(b), the two curves were too close to each other and there was no transient area for Turing patterns. Also, Fig. 5.2 shows the detailed numerical results in terms of evolution in time of the phenomena that we observed in the predator prey model when we increased and varied two main parameters in the spatial model: (ν, Dp) when $K = 120$.Where ν is the model highlighting the main parameters, changing the model will show a different stability. In this case, D_p being the prey diffusivity or movement parameter, we found that by increasing ν a bit further on from where Hopf bifurcation occurs, the ν_c solution will travel to another equilibrium. This state represents the stable state of the model. We can explain the phenomena of transient Turing patterns step by step by following the order of the figures. In Figs. 5.2, we started by observing a pattern near the systems perturbed equilibria $(3.920, 5.784)$ and $\nu = 0.037$. These patterns traveled to another perturbed equilibria of type sink/node. The plankton model of Eq. (5.1) possesses a bifurcation in space. In this case, the periodic solution corresponds to a non-zero wave number, w_p in Eq. (5.19). Using the pseudo arclength method described in Section 5.5.1 we obtain the first stability curve, and this is correspondent to the uniform solution of Eq. (5.1) in (ν, D_p); this regime also corresponds to the wave numbers w_0 and w_p, see Figs. 5.3, 5.3(a) and 5.3(b). These figures illustrate the uniform solution curve that separated the system regime into two main areas, a stable area above and an unstable area below the uniform curve. Further elucidation of the transient Turing patterns is presented in Fig.5.1, where we added the non-uniform solution curve. The main function of the non-uniform curve is to separate the unstable area under the uniform curve into two sub areas, an unstable area and a transient Turing area. These two areas start from $\nu \geq 0.033$ and become wider when $0.044 < \nu < 0.06$, where we have the Saddle node bifurcation in the area of the three real roots of the cubic reaction system. Also, there might be another reason behind having transient Turing, and this is the non-linearity in the reaction term, especially in the logistic function of the predator-prey model. This nonlinear equation is intended to capture two effects: first,

that of reproduction when the population increases at a rate proportional to the current population (this is when the population size is small); second, that of starvation (density-dependent mortality), which occurs when the growth rate decreases at a rate proportional to the value obtained by taking the theoretical carrying capacity of the environment less the current population [173].

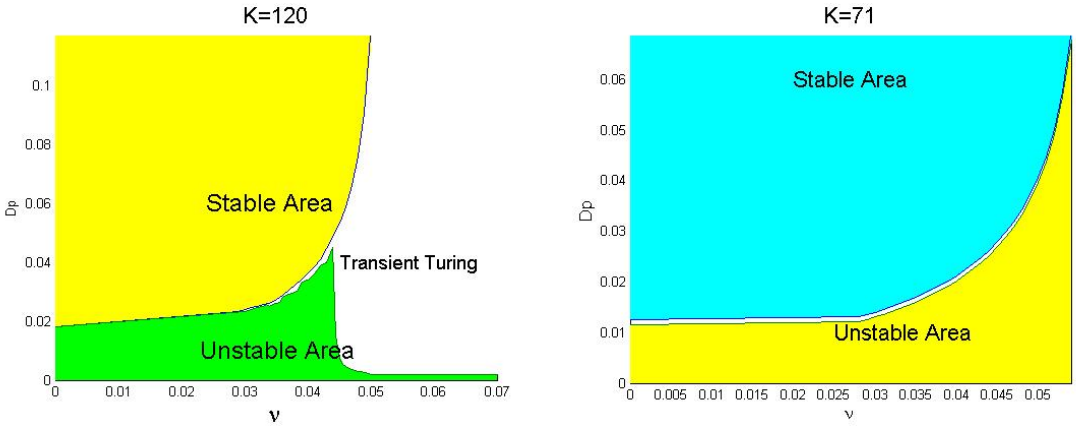

Figure 5.1: *Uniform and non-uniform solutions for* $K = 120$ *and* $K = 71$ *in the* (ν, Dp) *plane for our one dimensional reaction diffusion model*

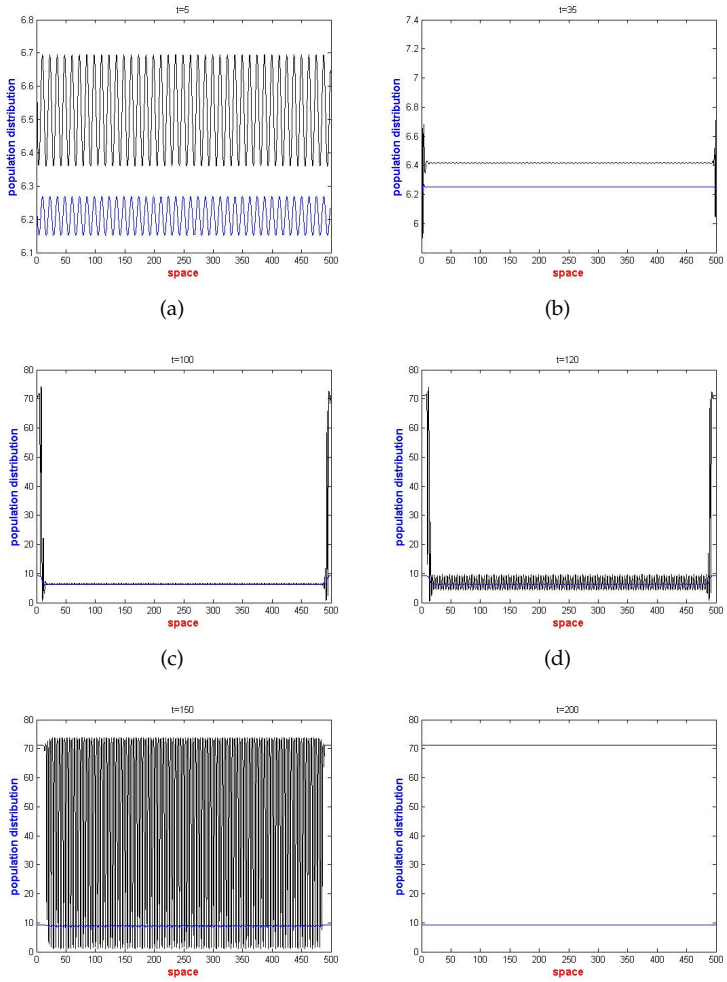

(a) (b) (c) (d) (e) (f)

Figure 5.2: *States of development of a Transient Turing area in one dimension, captured according to different time series, the solution when* $K = 120$*, and* $\nu = 0.037$ *with a stable focus equilibrium point. Choosing* D_p *to beless or greater than* $D_{p_c} = 0.002$ *causes the stable state to become unstable.*

The curve in Fig. 5.3 represents the first part of Fig. 5.1. Fig. 5.3(b) shows the stability regime for $K = 120$. The solid black line, D_{P0}, indicates the boundary between the stable and the unstable regimes which correspond to the periodic solution. The result shows that there are six regimes, and each has different stabilities and solution behaviours. The three main areas are presented in Fig.5.1.

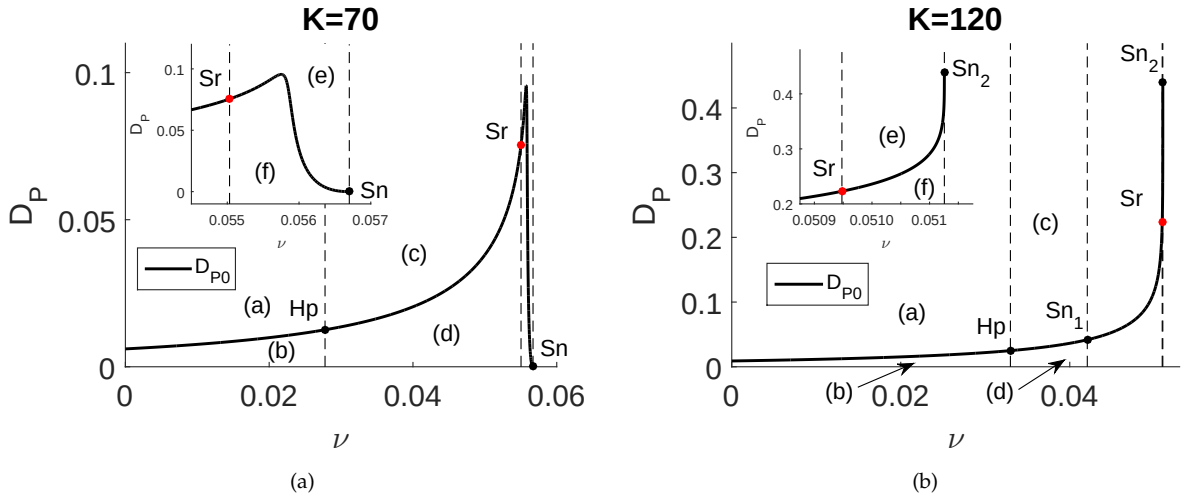

Figure 5.3: *Stability regime curve for $K = 120$ and $K = 70$. This curve separates the uniform from the non-uniform regimes. In each case there exists six individual sub areas which reflect the different stabilities in the spatial model for different values of K the system carrying capacity.*

In regime (a) in Fig. 5.3(b), we have unstable uniform solutions. By perturbing and performing numerical integration, we will obtain uniform solutions that oscillate with period T once a long time has passed, see Figs. 5.4(a) and 5.4(b). One can say that uniform solutions are periodic solutions in time (they have a periodic orbit), as shown in Fig 4.8, and possess a flat state in space. In regime (b) in Fig. 5.3(b), we also have unstable uniform solutions and periodic orbits and we have stable periodic solutions in space once significant time has passed. We can obtain the stable periodic solutions with period $L = \frac{2\pi}{w_p}m$, $m \in \mathbb{Z}^+$. Without loss of generality, we can choose $m = 8$ and by performing perturbations to the unstable uniform solution, we can obtain a periodic solution profile, as shown in Figs. 5.4(c) and 5.4(d). The solution profile in Fig. 5.4(d), we call periodic solution type 1. The most interesting attribute of regime (b) is that it includes pattern-like formations in time and space, as shown in Fig. 5.5. By perturbing the uniform solution in the unstable region and close to D_{P0}, we can obtain Hopf-Turing bifurcation. The existence of Hopf-Turing bifurcation is due to periodic orbits in time and periodic solutions in space.

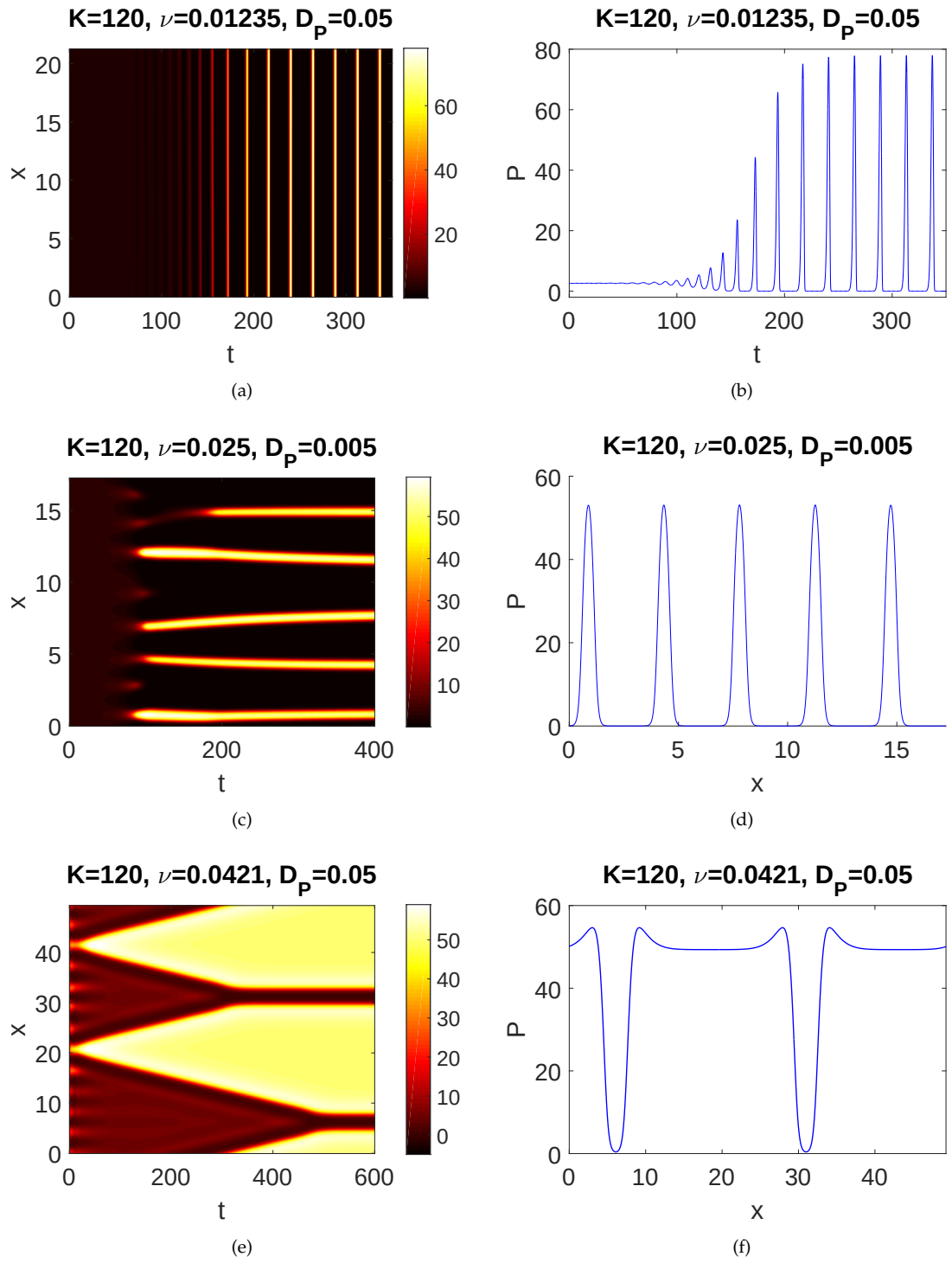

Figure 5.4: *Time dynamics of the uniform solutions in regions (a) and (b) in Fig. 5.3(b) and Table 5.5.3 for different values of D_P. Fig.5.4(e) shows the typical evolution of a Turing instability in region (vi) close to the right saddle-node bifurcation (Sn_2). The left panels show $P(x,t)$, while the right panels show the top view of the dynamics.*

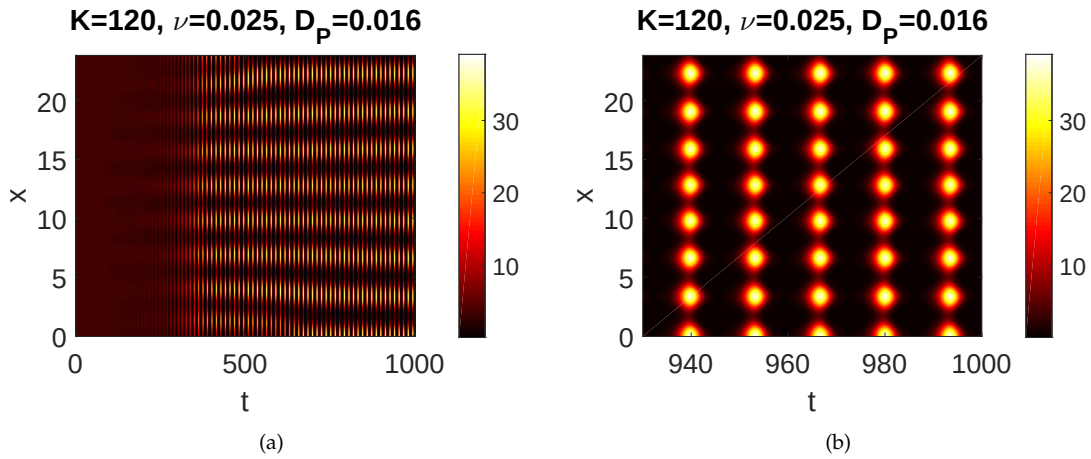

Figure 5.5: *Hopf-Turing pattern for $K = 120$.*

In Fig. 5.5, in regime (c), we have stable, uniform and periodic solutions and no periodic orbit. The stable periodic solutions can be obtained by the same method as they were for regime (b) in Fig. 5.3(b), using the same period $L = \frac{16\pi}{w_p}$. We have no periodic orbit here because $Re(\delta(w_0)) < 0$, and this makes the solution in time to be asymptotic to the uniform solution. The other main difference is that here we obtained a wider solution profile, which we call periodic solution type 2. By performing the same perturbation as for regime (c) in Fig. 5.3(b), we obtain the same results as for regime (d). The difference is that we have unstable uniform solutions.

In regimes (e) and (f), we only have stable and unstable uniform solutions. The absence of a periodic solution is because $Im(\delta(w_0)) = 0$ a non-zero value for which is important for the existence of a periodic solution. The difference between $K = 120$ and $K = 70$ is that if we perform quite a large perturbation for $K = 120$, we can obtain the upper solution state of a uniform solution in a steady state condition, as in Fig. 5.1.

Fig. 5.3(a) shows the stability regime for $K = 70$.The difference in this case is that there is no saddle node bifurcation and no large area for transient Turing patterns to exist in between the uniform and the non-uniform curves.

Region	Uniform Solution			Description
	$\mathrm{Re}(\lambda(0))$	$\mathrm{Im}(\lambda(0))$	$\mathrm{Re}(\lambda(k_p))$	
(a)	> 0	$\neq 0$	< 0	Hopf bifurcation, stable temporally periodic solutions
(b)	> 0	$\neq 0$	> 0	Hopf-Turing bifurcation, spatio-temporally or spatially periodic solutions
(c)	< 0	$\neq 0$	< 0	stable uniform solutions
(d)	< 0	$\neq 0$	> 0	unstable uniform solution, periodic states or bloom in multistability interval
(e)	< 0	$= 0$	< 0	stable uniform solutions
(f)	< 0	$= 0$	> 0	unstable uniform solutions, bloom (equilibrium states)

Table 5.1: *The description of the regions in Fig. 5.3 and their steady states.*

[1] Regime (a) is above $\mathrm{D_{P0}}$ and $\nu \in [0, \mathrm{Hp}]$. [2] Regime (b) is below $\mathrm{D_{P0}}$ and $\nu \in [0, \mathrm{Hp}]$. [3] Regime (c) is above $\mathrm{D_{P0}}$ and $\nu \in [\mathrm{Hp}, \mathrm{Sr}]$.

[4] Regime (d) is below $\mathrm{D_{P0}}$ and $\nu \in [\mathrm{Hp}, \mathrm{Sr}]$. [5] Regime (e) is above $\mathrm{D_{P0}}$ and $\nu \in [\mathrm{Sr}, \mathrm{Sn_2/Sn}]$.

[6] Regime (f) is below $\mathrm{D_{P0}}$ and $\nu \in [\mathrm{Sr}, \mathrm{Sn_2/Sn}]$.

5.5.4 Bifurcation diagrams for the spatial model

After depicting several qualitatively different dynamics within the different regions, it is now instructive to consider the existence and stability of the time-independent spatially periodic solutions. This will explain the observed evolutions. We have solved the time-independent governing Eq. (5.1), numerically using a Newton-Raphson method, in order to obtain the bifurcation diagrams. Here, D_P will be the control parameter. However, as this parameter is varied, there can be a saddle-node bifurcation. We use a pseudo-arclength method, as in Section 5.5.1, to continue the computations past the turning points [109]. Figs. 5.6 show the bifurcation diagrams of the periodic state for $K = 120$.

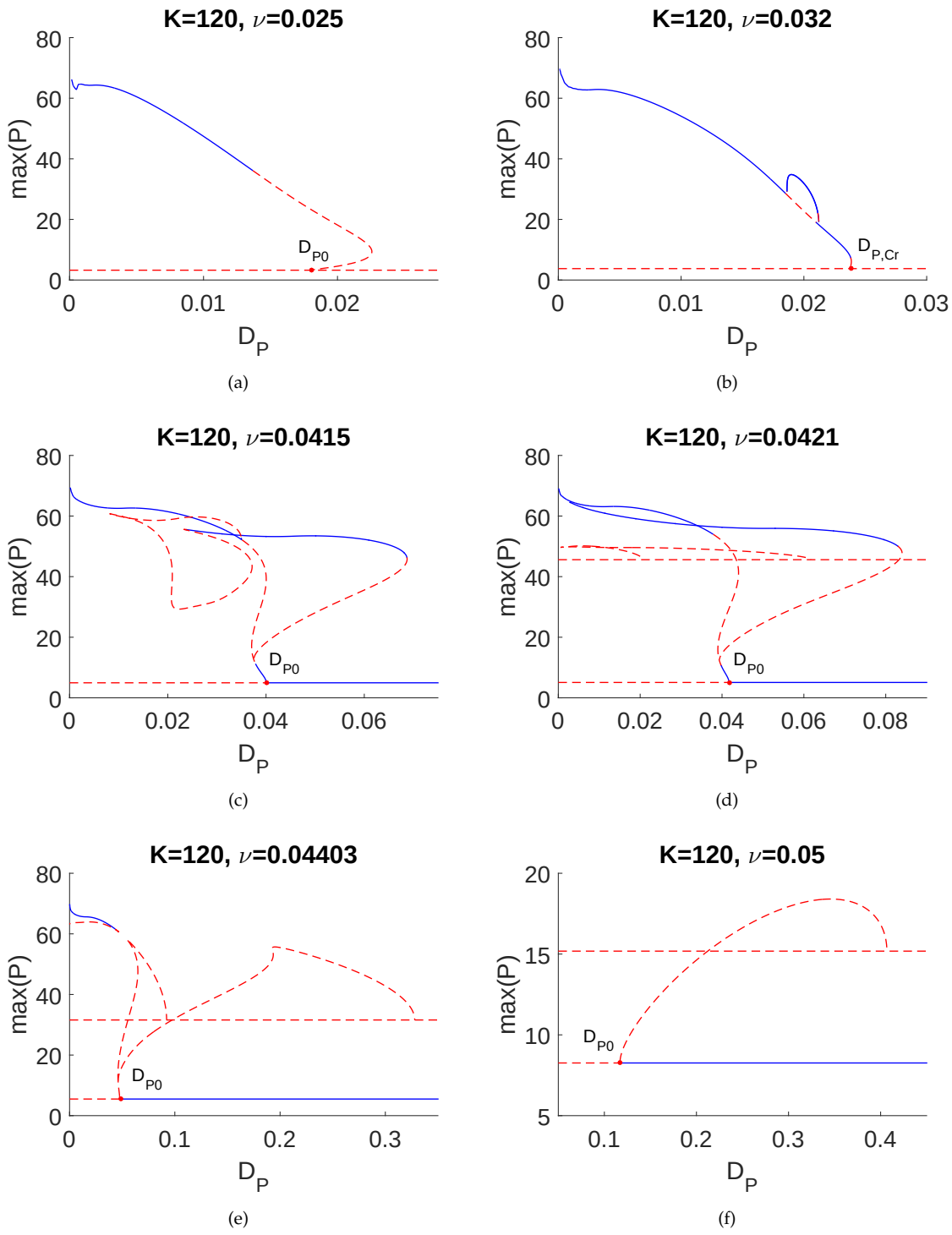

Figure 5.6: *Periodic solutions for* $K = 120$.

Figs. 5.6(a) and 5.6(b) show the bifurcation diagram of $\nu <$ Hp When $K = 120$ in regimes (a) or (b), we always have unstable uniform solutions. At the beginning, we only have one main branch of the solution, but as ν increases, instability occurs, and this leads to another branch of stable periodic solutions which we term branch 2. The difference between the two cases is that for $\nu = 0.025$ we have a Hopf-Turing bifurcation since $D_P < D_{P0}$ and D_P is close to D_{P0}, while for $\nu = 0.032$ these are not close. Heirein, the main branch is considered to be the solution that bifurcates from D_{P0}.

Figs. 5.6(c) -5.6(f) show the bifurcation diagram for Hp $< \nu <$ Sr as presented in regime (c) or (d) in Table 5.5.3. When $\nu = 0.0415$ branch 2 gets larger and admits a longer unstable branch, then for $\nu = 0.0421$ we enter a regime where the uniform solution has three roots. Other unstable branches also appear which bifurcate from the unstable uniform solution, see Fig. 5.6(d). Furthermore, the main branch and branch 2 are connected to the two new branches that bifurcate from the unstable uniform solution for $\nu = 0.044$. The main branch and branch 2 become unstable, as shown in Fig. 5.6(e). For $\nu = 0.05$, we could only obtain an unstable periodic solution which connects the lower stable uniform solution and the unstable uniform solution, see Fig. 5.6(f). Note that for quite large ν, such as $\nu = 0.044$ and $\nu = 0.05$, when we perturb the uniform solution in a regime where a stable periodic solution does not exist, we obtain the upper stable uniform solution.

In general, the bifurcation diagram for $K = 120$ has an unstable main branch and this will only become stable as ν passes a Hopf point going down, i.e., in terms of smaller ν. The main branch will catch another branch for larger ν. A gap containing an unstable region may also appear in both cases. In $K = 120$, the gap may be covered by the upper stable state of the uniform solution. To discover whether the regions above and under the curve are stable or unstable, we need to check numerically by substituting a value of D_p which is less (for under the curve) or greater (for above the curve) than the critical value of D_p; this latter has already been determined by the intersection of $\delta(\varpi_+) = 0$ with the D_P axis. The area under the stability curve depends also on the choice of the value of the control parameter and the corresponding equilibrium point. For example, in Fig. 5.2 we have a stable focus point with $K = 120$, $\nu = 0.037$. The solution of the system becomes unstable by setting the prey diffusivity $D_p = 0.02$, which leads to there being an unstable area under the stability curve. If we choose another value for ν and corresponding equilibrium point, such as $\nu = 0.05$ and its corresponding equilibrium point, this leads to stability; $D_p = 0.12$, which means that the area above the stability curve is stable.

5.5.5 Spectrum in transient Turing

Analysing the coexistence states in their existence regions, we found that only $P_{e,1}, M_{e,1}$, i.e. the lowest equilibrium branch in Figs. 5.7(a),5.7(b),5.7(c),5.7(d),5.7(a) and 5.7(a), can experience a Turing instability. In relation to Fig. 5.3, we plot the critical value of the diffusion coefficient, $D_{P,cr}$, below, by which we obtain bifurcations of spatially periodic states. Figure 5.3 shows the stability region for $K = 120$ and $K = 70$. Our analysis yields six regions (i-vi), which are separated by the vertical dashed lines and the line of $D_{P,cr}$, in which one will obtain different qualitative characteristics. The behaviour of each region is summarised in Table 5.5.3. Note that $\delta(w_p)$ is always real in all regimes.

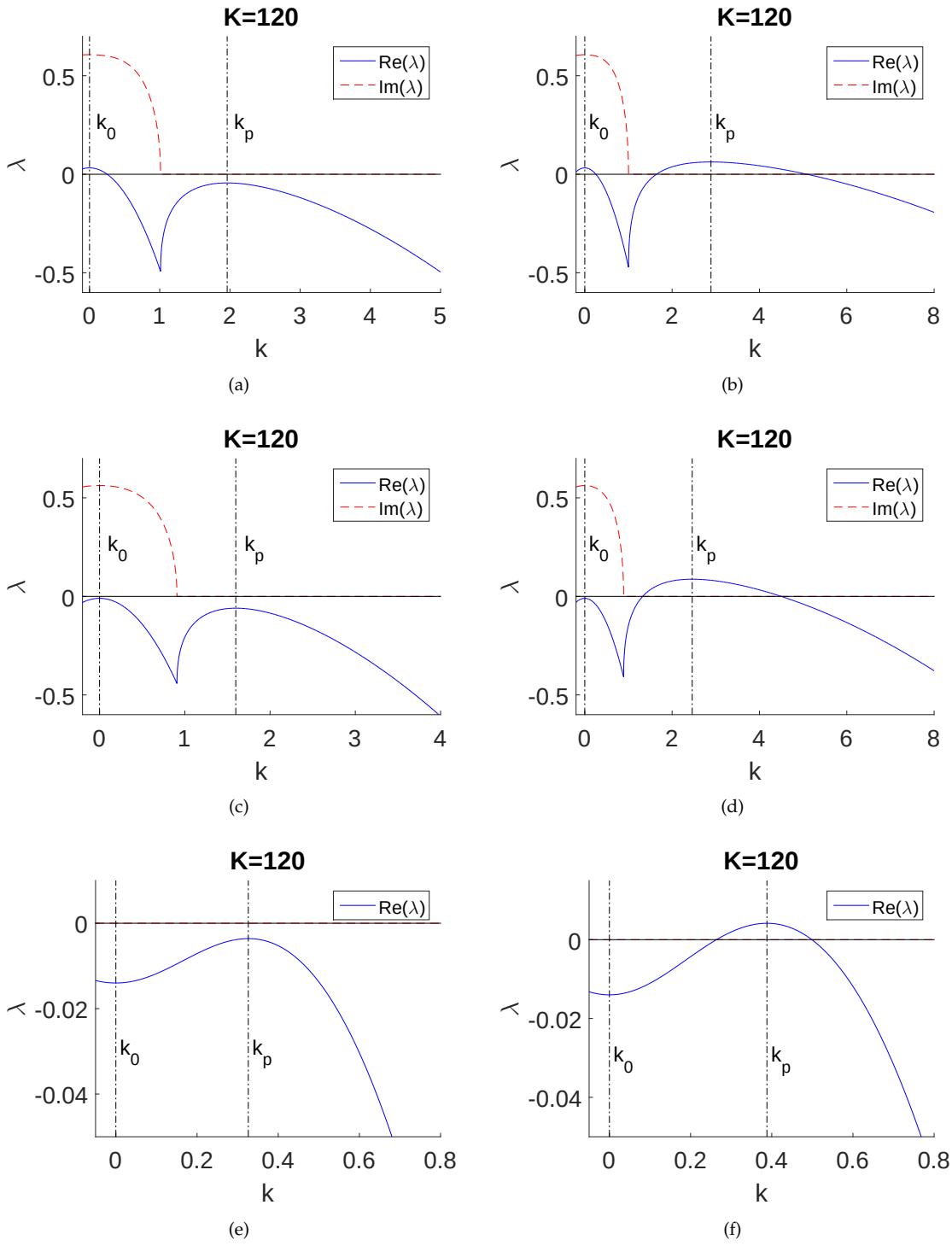

Figure 5.7: *(a)-(f) The corresponding eigenvalue/dispersion relation Eq. (5.11) that mention in each regime (a)-(f) in Fig. 5.3.*

5.6 Two Dimensional Spatial Distribution

In this section we will discuss the possible patterns that may arise in a two dimensional component reaction-diffusion system. We impose the following form on the system:

$$\frac{\partial P}{\partial t} = F(P,M) + D_P\left(\frac{\partial^2 P}{\partial x^2} + \frac{\partial^2 P}{\partial y^2}\right)$$

$$\frac{\partial M}{\partial t} = G(P,M) + D_M\left(\frac{\partial^2 M}{\partial x^2} + \frac{\partial^2 M}{\partial y^2}\right) \tag{5.37}$$

for x, y $\in$ 0, L, t $\in [0,\infty)$ and Ω is a bounded region.

The model in Eq. (5.37) has been solved numerically by using the same numerical simulations as are used in [38], based on finite difference and by using the same parameter values as are shown in Table 4.1. The initial conditions should be clarified in terms of continuous space and time as given in Eq. (5.39), and as follows:

$$P(x,y,0) = P_e(x) + \epsilon\cos(wx)\cos(wy) \tag{5.38}$$

$$M(x,y,0) = M_e(x) + \epsilon\sin(wx)\cos(wy) \tag{5.39}$$

where w is the spectrum of (P_e, M_e) with Neumann boundary conditions, as used in the analysis of the one dimensional model:

$$\nabla P = 0 \tag{5.40}$$

$$\nabla M = 0 \tag{5.41}$$

for $x, y \in \Omega$ is a bounded region..

5.6.1 Turing analysis in two dimensions

In this section we investigate the phenomena of pattern formation and wave propagation for the reaction diffusion model in Eq. (5.1) . We aim to find out where diffusion driven instability occurs in the two dimensional model. Applying the same linear analysis that we used for the one dimensional model will lead us to the required results. There is great consistency between the one and two dimensional models. Let the perturbations be:

$$\begin{aligned} P &= P_e + \epsilon e^{\delta t + i(w_1 x + w_2 y)} \widetilde{P}, \\ M &= M_e + \epsilon e^{\delta t + i(w_1 x + w_2 y)} \widetilde{M}, \end{aligned} \tag{5.42}$$

after following the same procedures that we did in the earlier section, we will determine the following dispersion (characteristic equation):

$$\begin{aligned} \delta^2 - \delta \Big(D_P + D_M] w_1^2 - [D_P + D_M w_2^2 - a_{11} - a_{22} \Big) \\ + D_P D_M (w_1^4 + w_2^4) + 2 D_M D_P a_{11} (w_1^2 w_2^2) + D_P a_{22} (w_1^2 + w_2^2) \\ + D_M a_{11} (w_1^2 + w_2^2) + Det(J) = 0. \end{aligned} \tag{5.43}$$

Solving Eq. (5.43) will give the spectrum of the model in two dimensions; this will help us to determine the system stability and show the consistency between the two spatial model analyses.

5.6.2 The spectrum of a two dimensional system

For the two dimensional model, we use the same techniques that we used in the earlier analysis of the one dimensional model to determine the maximum spectrum, in order to demonstrate the stability curve in Fig. 5.3; this led us to estimate the stability areas under and above that curve. Consequently, we found that the same stability curve could be used for both dimensions. Spatial patterns arise in correspondence to those modes, w_1, w_2, for which $\mathrm{Re}(\delta) > 0$. Since (P_e, M_e) is stable for the kinetics we satisfy the same conditions as

in the one dimensional case. Fig. 5.8 shows the type of the system spectrum when $K = 70$ and $\nu = 0.043$ and all other parameter values are as shown in Table 4.1. Fig. 5.8 reflects the consistency between the 1D and 2D models as plotted in the spectrum of different regimes. Fig. 5.8 gives a number of different ranges of wave numbers which are linearly unstable and, for two–dimensional situations, predicts the final steady state solution. Fig. 5.8(e) shows the mode with the fastest linear growth (positive real part), which is when $\nu = 0.044$ and $(5.478, 6.078)$ for $K = 120$.

5.7 Turing Patterns

The Turing mechanism is a mathematical tool used for highlighting repeating patterns. This includes the identifying of the presence of a periodic solution obscured by chaos. In order to address this issue, we consider the full two dimensional version of equations Eq. (5.1), where $0 < x < L_x$ and $0 < y < L_y$. At the domain boundary, zero flux conditions are imposed and the two species system can be solved numerically using finite differences–the explicit method. The latter is also the case for the one dimensional model, given that the type of the patterns depends mainly on the choice of the initial condition. By slightly perturbing the initial homogeneous population distribution, a smooth pattern arises. In this case, we consider initial conditions which lead to the stripe patterns. Different fields of study define the pattern types in the direction of x and y, depending on the choice of the initial conditions. As a result of this, the population densities fluctuate or oscillate with time. They also show qualitatively similar behaviours in space. Population dynamics, in relation to the spatial aspect, are usually classified in terms of average density. In Figs. 5.9 5.10 and 5.11 we show the types of the patterns that we obtained by applying the initial condition defined by Eq.(5.3). The patterns in both Figs. 5.10 and 5.11 correspond to $K = 120$ and $\nu = 0.044$, $\nu = 0.0335$ respectively. The parameter values shown in Table 4.1 indicate patterns of stripes that are parallel in their long axis during normal development and are parallel to the gradient. Fig.5.9 corresponds to a different value of ν: $\nu = 0.025$ where we have unstable state. A systematic analysis of the different parameter values shows a consistency in the average densities over time and space. Figs. 5.9(c), 5.9(d), 5.10(d), 5.10(c), 5.11(c), 5.11(d) show the consistency in the systematic analysis of the two dimensional spatial model.

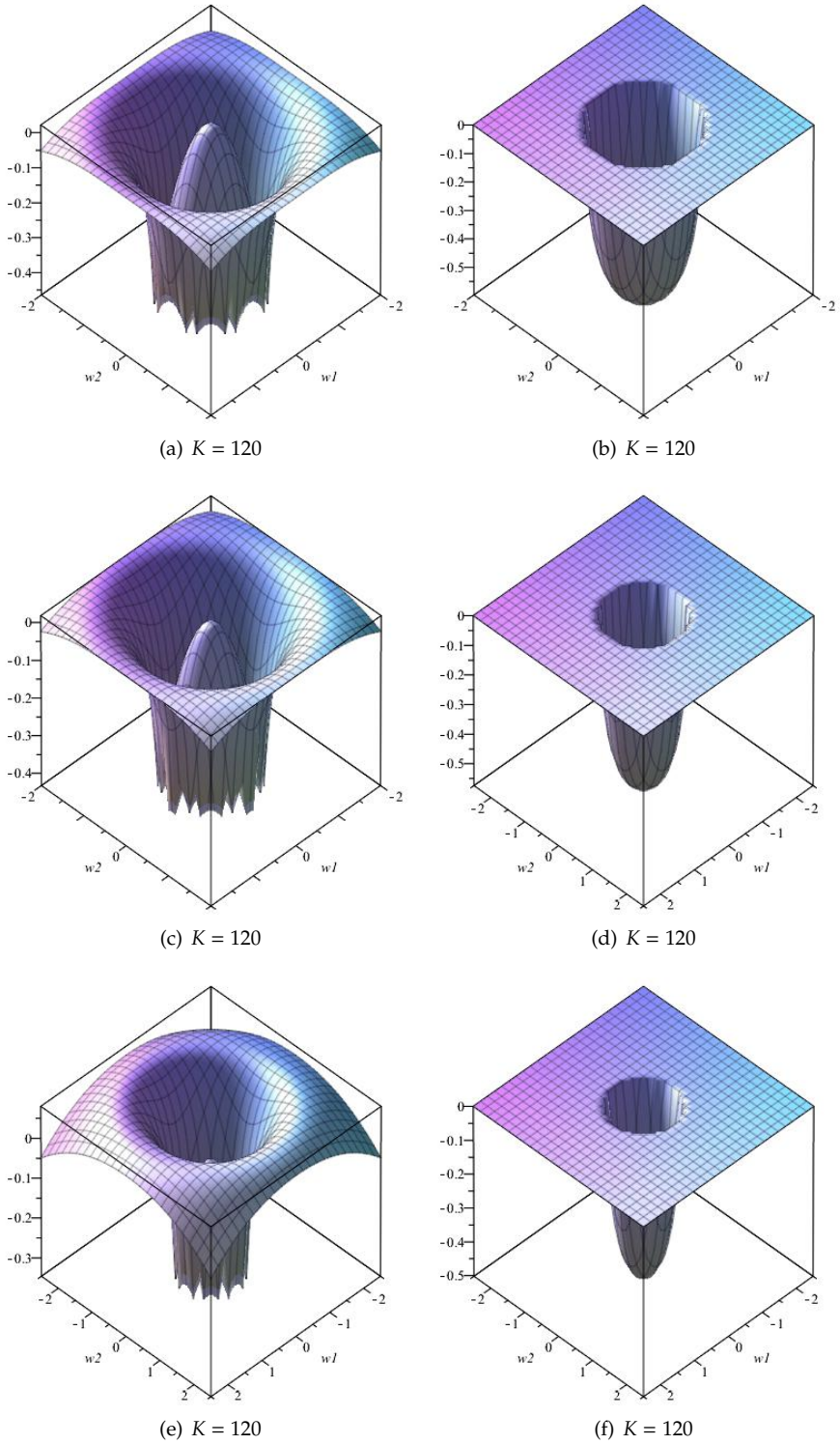

(a) $K = 120$ (b) $K = 120$

(c) $K = 120$ (d) $K = 120$

(e) $K = 120$ (f) $K = 120$

Figure 5.8: *The spatio-temporal spectrum w.r.t* $-2 < w_1 < 2$ *and* $-2 < w_2 < 2$ *for* $K = 120$ *when* $\nu = 0.025, 0.0335, 0.044$. *The left panel corresponds to the real part and right panel corresponds to the imagery part of the spectrum.*

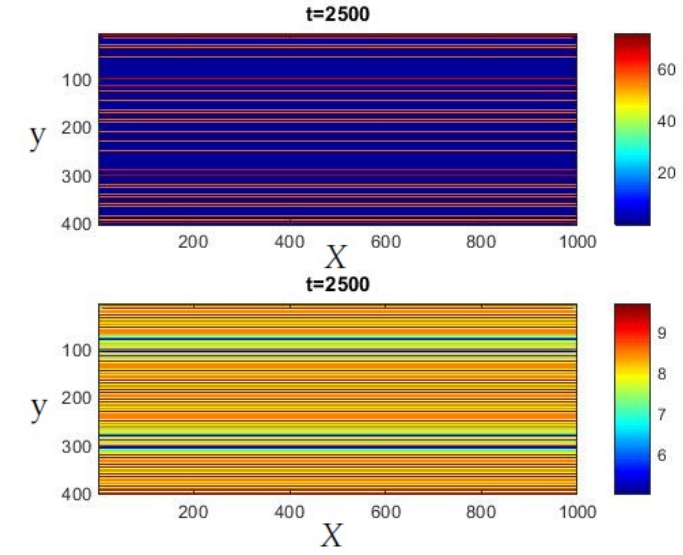

(a)

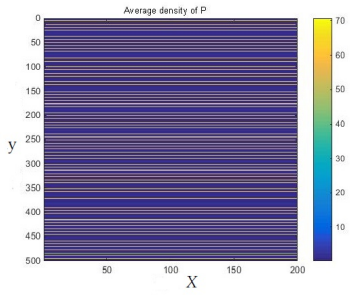

(b)

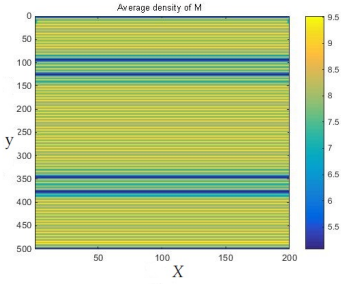

(c)

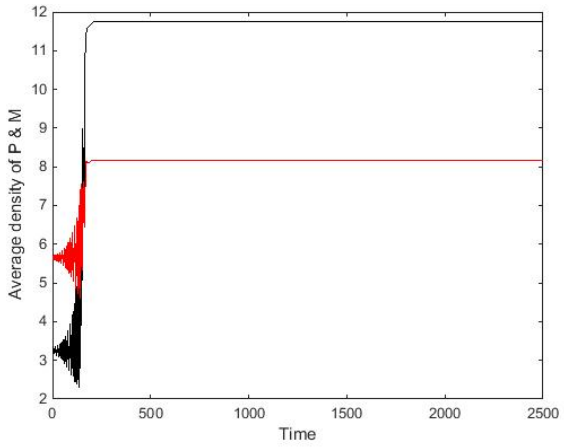

(d)

Figure 5.9: *Snapshots of the prey distribution over two-dimensional space for $t = 2500$ and parameter values given in Table 4.1 and for $\nu = 0.025$, both prey and predator densities shows qualitatively similar behaviour when $\nu > 0.051$ except for very early stages of the system dynamics when the effect of I.C is essential.*

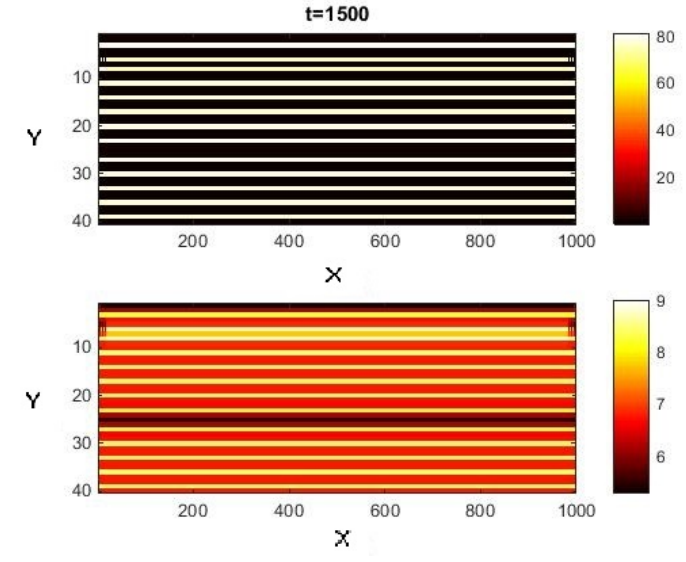

(a)

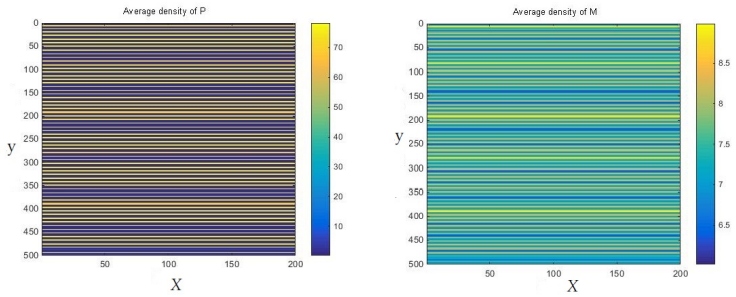

(b) (c)

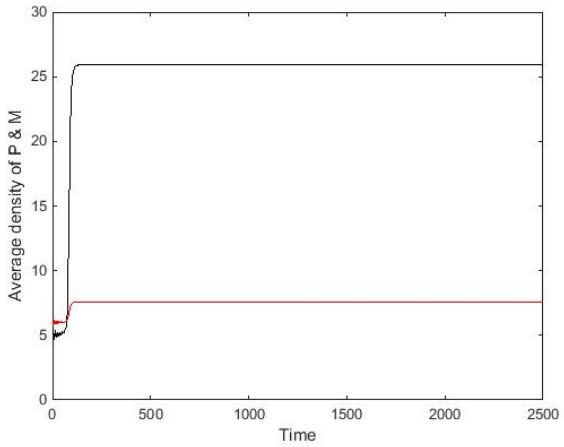

(d)

Figure 5.10: *Snapshots of the prey distribution over two-dimensional space for t = 1500 and parameter values given in Table 4.1and for* $\nu = 0.042$*, both prey and predator densities shows qualitatively similar behaviour when* $\nu > 0.051$ *except for very early stages of the system dynamics when the effect of I.C is essential.*

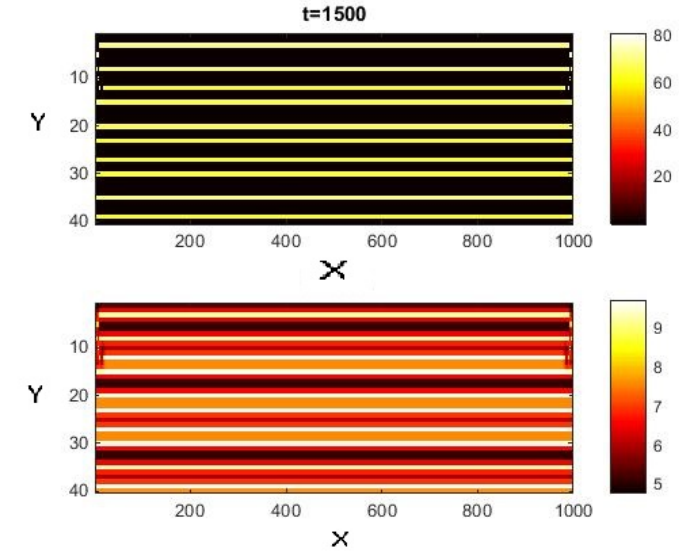

(a)

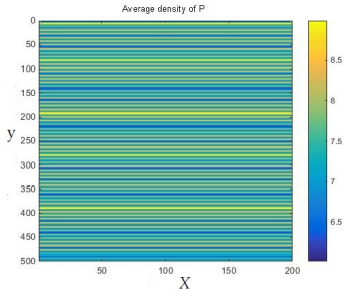

(b)

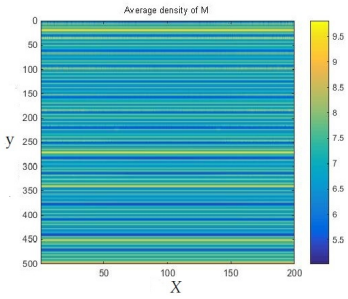

(c)

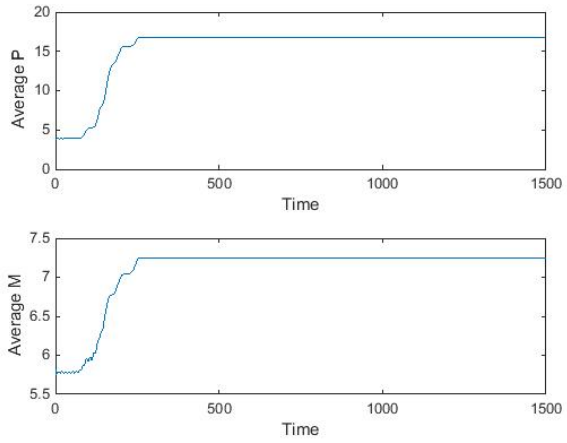

(d)

Figure 5.11: *Snapshots of the prey distribution over two-dimensional space for* $t = 500$*, the parameter values given in Table 4.1 and* $\nu = 0.0335$*, both prey and predator densities show qualitatively similar behaviours when* $\nu > 0.051$ *to each other except in very early stages of the system dynamics when the effect of the I.C. overrides.*

5.8 Conclusion

In this chapter, our prey-predator system with a Holling *II* functional response is considered in relation to its spatial aspects, as in Eq. (5.1). It has already been shown in the previous chapter (4) that there exists Hopf-bifurcation with respect to the mutual interaction of prey and predator. In the qualitative analysis, we studied the dynamical behavior of the spatio temporal system. It is observed that when the rate of interaction, i.e., U_e, crosses its threshold, the value of both species populations start oscillating around the interior equilibrium. These results have been shown numerically in the previous chapter, indicating different values of U_e. We started our spatial analysis by obtaining the amplitude equations in Sec. 5.4.1 and by providing a mathematical description of the reaction–diffusion system close to the onset of instability. The analysis of the amplitude equations [133] guided us to obtain a quintic polynomial leading to the Stuart–Landau in Eq. (5.32) [82]. The deduced equation is a first order ODE of $A(t)$. It controls the wave amplitude. The spatial analysis has shown the occurrence of a number of different phenomena. This includes the stable stripes Turing patterns where all the bifurcations of the periodic states are supercritical and there is no hysteresis observed. This is in agreement with our time-dynamics simulation as indicated in the particular patterns shown in Fig.5.9, 5.10 and 5.11. While many, if not all, of previous works consider vertical motility (see, e.g., [115,209,255,256]), our analysis is innovative in that it proposes horizontal movement. One particularly different result we presented here is the observation of localised solutions that biologically may indicate the presence of hotspots (i.e., that phytoplankton and microzooplankton are abundant in localised areas such as those in Figs. 5.4(c) and 5.4(d)) and 'coldspots' (such as those shown in Figs. 5.4(e). Such observations are possible mainly because the model is considered to be in the infinite domain, as opposed to being a bounded one as the models focusing on vertical motility are. Our study can serve as a significant blueprint for the analytic investigation of dynamics relatively close to bifurcation points; this is addressed as future work. It will be interesting to study the existence and stability of hotspot and coldspot solutions using geometric techniques as employed in, e.g., [101,102].

Spatial patterns can arise in correspondence to the modes, w, for which $Re(\delta) > 0$. Since (U_e) is stable in the reaction system, one has that $tr(w) < 0$ and $Det(J) > 0$ [80]. The solution of the system becomes unstable by setting the prey diffusivity $D_p = 0.02$; this leads to there being an unstable area under the stability curve in

Fig. (5.1). For example, in Fig.(5.2), we have a stable focus point with $K = 120$, $\nu = 0.037$. The solution of the system is made unstable by setting the prey diffusivity $D_p = 0.02$. This leads to an unstable area under the stability curve. When choosing another value for ν and its corresponding equilibrium point, such as $\nu = 0.05$, its corresponding equilibrium point should be stable but $D_p = 0.12$. This means that the area on the upper stability curve is stable. It should be noted that because of the cubic interaction in the temporal system and its corresponding roots, we found that the region can exhibit another stability which can we call the Transient Turing which lies in between the two stability curves as in Fig (5.1). Fig. 5.3(b), clarifies the different stability regimes in the system 5.1. For further elucidation we use Table 5.5.3 to divide the whole region of (ν, D_p). Thus, we divided the region of the spatio-temporal system into three areas. First, the stable area gives flat state $0.025 < D_P < 0.12$ and $0.033 < \nu < 0.044$. Then, the unstable area gives Turing patterns $0 < D_P < 0.025$ and $0.033 < \nu < 0.044$. Finally, there is the Transient Turing area of fig. 5.1; in relation to this area, we studied the effect of having three roots in the cubic reaction systems. Because one of the three roots is a saddle, its trajectory pushed the solution into a stable state where we have a sink, see Fig. 5.2 and the corresponding spectrum fig 5.7. The model in Eq. (5.37) has been solved numerically by using the numerical simulations based on finite differences, the explicit scheme, and by using the same parameter values as shown in Table 4.1. In relation to this approach, the initial conditions should be clarified for continuous space and time, as shown in Eq.(5.39). The numerical analysis of the cubic reaction is explained in detail, along with the location, the number and the types using Cardan's method [109, 197] as presented in chapter three. This helped us to find the key parameters of the system's behavior when $K = 71.973$. Furthermore, the periodic orbit has been determined by scaling the period in time of the model into $t \in [0, 1]$ as in [109]. Hopf-Turing patterns may also appear for both parameter cases due to the complex eigenvalues of the uniform solution (Hopf bifurcation) and the instability region of the periodic state when we introduce a diffusion term. We summarize the uniform and periodic solution behaviours (in terms of time and space) by identifying six regimes, and our main finding, the Transient Turing lies in between regimes (d) and (e). We also simulate several bifurcation diagrams for several parameters of ν for both cases. The results show that the periodic states only exist in regime (a)-(d). For the next chapter, it is important to improve on the mathematical model by introducing more resources into the model defined by Eq. (5.1). The numerical analysis has involved a combination of numerical bifurcation methods, the Pseudo–arclength method of [109] and the

finite difference method of [38], which are used to examine the bifurcations and to produce many of the final graphs [106]. The one dimensional patterns obtained the periodic solution profile as shown in Figs. 5.4(c) and 5.4(d)–the solution profile in– Fig.5.4(d), we call periodic solution type 1. The most interesting observation of regime (b) is that of the existence, there, of Hopf–Turing patterns in time and space, as shown in Fig.5.5. We obtained these patterns by perturbing the uniform solution in the unstable region and close to D_{P0}, when $\nu = 0.025$. The two dimensional patterns in both Figs.5.10 and 5.11 correspond to $K = 120$ and $\nu = 0.044$, $\nu = 0.0335$ respectively. These are also the same parameter values as are shown in Table 4.1. The patterns are stripes parallel in their long axis, during normal development, and parallel to the gradient. Fig.5.9 refers to a different value of ν. This is $\nu = 0.025$ where we have an unstable state, and the patterns change into chaos from the centre of the Fig 5.9. The systematic analysis for the different parameter values shows consistency in terms of the average density in time and space. Figs. 5.9(c), 5.9(d), 5.10(d), 5.10(c), 5.11(c), 5.11(d) show the consistency in the systematic analysis of the two dimensional spatial model. Also, the results of the one and two dimensional model are consistent. Further background information on the spatial analysis and the biological oceanography can be found in [248], [10] and [179]and [113]. It is also important to note that the spatiality in (5.1) was introduced by crudely inserting dispersions into the simple model proposed in [143]. At this stage, we have not analysed the precedence of the dispersion coefficients compared to the other parameter values in terms of being biologically and physically relevant, even though mathematically they can always be scaled out. Also, our model is constructed on the assumption of a stable copepod population. These assumptions and limitations are addressed in relation to future work, which includes, e.g., a more realistic model extension.

5.9 Biological Interpretation

In this section we provide a biological orientated discussion of both the non–spatial and the spatial predator–prey model. In both models, grazing-induced infochemicals have been indicated to have an effect on multitrophic plankton interactions. To derive a biological interpretation for all the mathematical results we obtained in Chapter 4and Chapter 5, we need to clarify that the presence of diffusion does not change the location and stability of the equilibria as discussed for the non-spatial model in the previous sections, but may

change how system perturbations develop. For simplicity, and without loss of generality, we scale the diffusion coefficient of the microzooplankton to the arbitrary value of $D_M = 1$ and consider D_P as an exploratory parameter. We only consider $D_P < D_M$, which is biologically justified since most species of phytoplankton are non-motile and diffuse purely through passive drift due to turbulence and currents; in contrast, many microzooplankton species are highly motile and can swim through the water column, leading to a higher diffusive capacity. Research by [143] used a 1-d reaction-diffusion food web model to investigate this effect by considering vertically migrating copepods in this 1-d model, [144]. Results in Chapter 4and Chapter 5 also incorporate the use of ordinary differential equations and partial differential equations to investigate the copepod dynamics and their role in the multitrophic plankton interactions within the ecosystem. In this investigation, we assume a well-mixed environment to be existent within the biological populations. [119] highlighted that in conducting such an investigation, physical processes, such as turbulent diffusion, are modeled using a system of PDEs, as illustrated in the spatial model equations 5.1. This modeling is facilitated to allow depth-dependent processes, such as light-limitation. From the results of the spatial modeling equations a comparison can be performed to illustrate infochemical–mediated interactions and how much of an effect they have on the formation of phytoplankton blooms through multitrophic plankton interactions, as presented in Fig's 5.6, and proved by the spectrum in each regime as shown in Fig. 5.7 when $\delta(w_p)$ is always real in all regimes. Also, Table 5.5.3summarises all the regimes stabilities. The use of the non-spatial model in 3 illustrates that an increase in the microzooplankton mortality rate is a subsequent effect of an increase in the rates of microzooplankton grazing on phytoplankton. This is also assumed to be as a result of the increased predation by copepods, as shown in the bifurcation figures in Chapter 3, Fig 4.5 and Fig. 4.4. Research by [149] has further indicated that there is a high level of heterogeneity in the distribution of phytoplankton within the ocean. This is caused by the difference in ocean gradients that provide fitness advantages to motile cells. The different depth profiles in the ocean, as explained by [219], highlight the fact that chlorophyll maxima correspond to the demonstrated infochemical concentrations. As a result of this correspondence, the copepods are able to migrate vertically within the ecosystem and to locate prey-rich patches, as explained in Eq's 5.1. Based on the explanation provided by the equation, free distribution allows copepods to respond to distributions of grazing-induced infochemical [143]. Therefore the predation rates can be maintained. This situation also prevents the extinction of the copepods that could not have survived

the high levels of predation and lack of foraging which they would experience if they did not take notice of the distribution of infochemicals. As further illustrated via the spatial modeling by [219], copepods are able to persist under great predation pressure because of their random foraging behaviors. The conversion of predated microzooplankton into new biomass is further explained as a major reason for the increased copepod growth rates, and this is presented in relation to the hydra effect in Fig. 4.6. The total freedom of the copepods allows them to move relatively quickly across different foraging areas across the water columns [165]. The use of diffusion models has been adequate for modeling the copepods. The model in Eqs. 5.1 has been used to explain that copepod infochemical related efficiencies are critical to their survival. The chemically informed copepods are, however, dependent on the foraging density. Results by [194] indicated that the chemodetection used by copepods in their foraging has a significant effect on the stabilization of the system. However, eutrophication can also result to an unstable system, as indicated in Fig.5.9, which corresponds $\nu = 0.025$. Thus we have identified an unstable state while the systematic analysis of the different parameter values proved the consistency between the average densities in time and space. Figs. 5.9(c), 5.9(d), 5.10(d), 5.10(c), 5.11(c), 5.11(d) explain the systematic analysis of the two dimensional spatial model. A stable steady state is established through infochemical-mediated predation and its corespondent results are presented in Fig 5.10. Research by [165] has further indicated that vertical heterogeneity affects the stability of the system dynamics. This also affects the nutrient load within the ecosystem, following a change in the phytoplankton bloom formation. Results by [165] also indicated that phytoplankton concentrations are in the upper euphotic zone where there is an abundance of DMS. These are zones, commonly stated as being between $20m$ and $30m$, where DMS release is stable. It has been discussed that such abundances of DMS in the upper areas must be detected by the copepods. The result is increased biological activity, given that the copepods are able to use such chemical information. The copepods are also able to make use of the cues caused by their increased foraging behavior within these areas. As explained by [28] at least in $4 - 16\%$ of the upper $25m$ water column habitat there are huge concentrations of phytoplankton biomass. Such huge concentrations are important for increasing the prey related cues received by the copepods. The result is increased foraging by the copepods because of chemo detection. The research further indicated that through increased foraging by the copepods, phytoplankton bloom formation occurs, leading to the stabilization of the system, as in Fig. 4.4 and in Fig.4.4(c) when $0.051 > \nu < 0.012$. Both Chapter 3 and 4 emphasize the relevance of grazing-induced DMS

on multitrophic plankton interactions. The results from the two chapters can be summed up as indicating the importance of foraging through chemodetection. The discussion highlights that copepods achieve fitness benefits through the increased use of chemodetection for foraging. The discussion further indicated that copepods are able to resist greater predation pressure through their ability to utilize infochemical cues in their foraging. The less efficient copepod predators are able to avoid extinction by using the chemical cues to forage in layers rich with microzooplankton. It is also concluded from the discussion that an increase in the net microzooplankton mortality is as a result of the infochemical–mediated predation that creates a grazing refuge for phytoplankton. It is further highlighted that 100% efficiency in the distribution of infochemical results in an evolutionarily stable mechanism for the copepods. Therefore, the survival of the copepods is dependent on their ability to sense infochemicals. The conclusion is that in promoting bloom formation, much larger chemical efficiencies have to be realized within the system.

Chapter 6

Infochemical Mediated PMZC- Plankton Model

6.1 Introduction

We investigate a mathematical model that describes the interaction of plankton. This chapter discusses a four trophic model which is derived from the model examined in chapter 4. The latter is based on two components, P and M. We discuss a four trophic rather than a three trophic model because in the two trophic model discussed in Chapter4 and Chapter5, the control parameter, ν, encapsulated the effect of the higher predator population on system stability, as detailed previously in [143]. The following, Eq. (7.1, describes the four trophic model frame:

$$\frac{dU}{dt} = F_i(\overline{U}), \tag{6.1}$$

where $\overline{U} = [P, M, Z, C]$ represents a vector of four components: P denotes the population density of prey phytoplankton, M denotes the predator microzooplankton, Z denotes the top predators (copepods) and finally C denotes the chemical release by phytoplankton. Functions F_i take into account the effects of birth and mortality. In most biologically meaningful situations, the functions F_i are nonlinear with respect to at least some of their parameters. In this chapter we will study the stability and bifurcation analysis of the above four

trophic interaction model and examine the properties of the functions F_i which define the species responses and the types of inter-specific interactions. As highlighted by [180], the ecosystem processes are affected by changes in biodiversity through trophic interactions. This is a major reason why it is important to explore how the stability of the ecosystem and the relationship between biodiversity and processes are affected by the different trophic interactions within an ecosystem. The density functions in the above equation can be termed a functional group'. Most straightforwardly, such a group can be categorized according different trophic levels. A good example is that of phytoplankton and zooplankton [172]. Although in any natural aquatic ecosystem, each of these two groups consists of many different species, in the above equation we are going to study the interaction of four species only –a representative from each category. Furthermore, the functions, F_i, depend not only on the population densities but also on a number of parameters, such as the birth/death rate(s), the population carrying capacity(-ies), etc. These parameters provide an intrinsic scale for each of the variables. The above system creates an appropriate modeling framework for the case of a well-mixed community in a homogeneous environment: i.e., for a community which may in all circumstances be regarded as spatially homogeneous. Obviously, this is not always the case for real communities, and this affects the model choice for a community. For instance, the spatial structure of a given population or community can be predefined by environmental heterogeneity [175]. In the case of small environmental gradients, a relevant mathematical model can still be space-continuous; however, in the extreme cases of large environmental gradients or of a fragmented habitat, a space-discrete approach will sometimes be more insightful. A mathematical model would then consist of a number of systems such as the one above, but where different systems describe the dynamics of different sub-populations which are coupled together due to migration between the habitats [125, 172, 175].

6.2 Mathematical Models

Consider the following model:

$$\frac{dP}{dt} = F_1(P, M, Z, C), \tag{6.2}$$

$$\frac{dM}{dt} = F_2(P, M, Z, C), \tag{6.3}$$

$$\frac{dZ}{dt} = F_3(P, M, Z, C), \tag{6.4}$$

$$\frac{dC}{dt} = F_4(P, M, Z, C). \tag{6.5}$$

Here F_i, $i = 1, 2, 3, 4$, which is the interaction function of the developed model, and has the following format:

$$F_1(P, M, Z, C) = rP\left(1 - \frac{P}{K}\right) - \frac{aPM}{1 + b_1 P}, \tag{6.6}$$

$$F_2(P, M, Z, C) = \frac{\gamma_1 aPM}{1 + b_1 P} - m_1 M - \frac{\beta ZM}{1 + b_2 M}(1 + \frac{\zeta C}{1 + \epsilon C}), \tag{6.7}$$

$$F_3(P, M, Z, C) = \frac{\gamma_2 \beta ZM}{1 + b_2 M}(1 + \frac{\zeta C}{1 + \epsilon C}) - m_2 Z, \tag{6.8}$$

$$F_4(P, M, Z, C) = \frac{\eta aPM}{1 + b_1 P} - m_3 C + \omega P. \tag{6.9}$$

The model describes the interactions between the small infochemical-producing phytoplankton, the microzooplankton and the copepods in a system that is depleted of nutrients. [71], used a system of simple differential equations for modeling autumn phytoplankton bloom and explained that this model indicated that trophic interactions are critical in terms of the interaction functions among the available species, as explained in Chapter 3. The parameter r represents phytoplankton intrinsic growth rates, a is the clearance rate of microzooplankton at low food densities, b_i $i = 1, 2$ are the half saturation constants, β is the copepod linear predation rate, m_i $(i = 1, 2)$ are the predators death rates, m_3 is the chemical evaporation rate, γ_i $i = 1, 2$, is a parameter governing the prey to predator biomass conversion rate. ζ is the rate of change and ϵ is a key parameter which we are going to use to reduce the general four species model to a special case model, the one in [143]. η is the productivity rate for the DMS-infochemical and ω is the amount of chemical given off by each phytoplankton. In Eq. (6.6), we still employ the logistic map to describe the growth rate of

the prey and a Holling II functional response to describe the effects of predator on prey. In Eq. (6.7), we define microzooplankton population growth using the Holling II functional response with γ_1 as a parameter indicating the prey to predator biomass conversion rate. The second term in Eq.(6.7) represents the normal mortality of microzooplankton, while the third term represents the effect of zooplankton on microzooplankton–another cause of microzooplankton death [180]. The third term also represents the increase of predation with β as a linear predation rate [1]. Copepods saturate their behaviour in terms of their ability to handle prey (microzooplankton) with b_2 being the half saturation parameter. The released chemical can also be saturated by the $(1 + C)$ factor and the ζ parameter is used to measure the rate of the chemical increase that affects the increase of predation [2]. In Eq. (6.8), the first term we introduce is the copepod population growth; this connects the predators M and Z. This term also describes how copepods consume microzooplankton following *DMS* release and how copepods saturate because of the time it takes to handle prey. [195] wrote that the spatio-temporal variability of copepods is affected by climate changes within the ecosystem. These include bottom-up and top-down pressures. This can be regarded as an effective concept which is important in explaining the dynamics of the copepod populations. The next term is copepod mortality due to consumption by higher trophic predation. The last equation, (6.9), has three terms. The first term is used to describe the infochemical release following microzooplankton grazing on phytoplankton, with η being the production rate of *DMS*. The second term in F_4 stands for chemical evaporation. The third term represents the chemical released (exuded) by each cell. We can reduce the model in Eqs. (6.6)- (6.9) into a special case model by setting $\epsilon = 0, b_2 = 0, \omega = 0$, i.e.:

$$
\begin{aligned}
F_1(P, M, Z, C) &= rP\left(1 - \frac{P}{K}\right) - \frac{aPM}{1 + b_1 P}, \\
F_2(P, M, Z, C) &= \frac{\gamma_1 aPM}{1 + b_1 P} - m_1 M - \beta ZM(1 + \zeta C), \\
F_3(P, M, Z, C) &= \gamma_2 \beta ZM(1 + \zeta C) - m_2 Z, \\
F_4(P, M, Z, C) &= \frac{\eta aPM}{1 + b_1 P} - m_3 C.
\end{aligned} \tag{6.10}
$$

[1] -β MZ represents the effect of copepod predation on microzooplankton. We changed the form of this term to the Holling II functional response because any species should saturate at some level.

[2] ζ also can be defined as a maximum level for the chemical released, especially if we model this term by $1 + \left(\frac{\zeta C_{max}}{1+C}\right)$.

The main difference between the two set of nonlinearities and the model in Eq. (6.10) is the linear predation function, which describes the linear predation of the copepod on the microzooplankton. It must be assumed that the model is valid over the long term–scales, because we add more resources to the basic food chain of the two species model by modeling the population density of the copepods and also the chemical release. So we must consider the time that both predators, M and Z, take to handle their prey. The model in Eq. (6.10) is considered as a special case model of Eqs. (6.6) - (6.9). When $\epsilon = b_2 = \omega = 0$ the model will be reduced to the two species model shown in Eqs. (4.1) and (4.2) of Chapter 4 and biologically studied in [143] [3]. One goal of the model construction here is to predict the predator–prey kinetic and dynamical properties. Since our model is derived from the two species predator prey model, P and M, which is the model simulated in Chapter 4 and Chapter 5, a basic question to raise here is how can the four species model provide better descriptions than the two species model? As the current model generalizes the behavior of the two species model, P and M, by considering the higher trophic level copepods by introducing Z we can consider the models validity over a longer time scale.

6.3 Qualitative Analysis of The Equilibria

6.3.1 Steady state populations

We now look for the steady-state solutions (P, M, Z, C) which satisfy $(\frac{dp}{dt}, \frac{dM}{dt}, \frac{dZ}{dt}, \frac{dC}{dt}) = 0$. The system described by Eqs. (6.6)-(6.9) possesses five possible nonnegative equilibria, namely the extinction equilibrium E_0, the microzooplankton and copepod eradication equilibrium E_1, the phytoplankton and infochemical eradication equilibrium E_2, the copepod eradication (copepod free) equilibrium E_3 and finally the coexistence equilibrium E_4. Table 7.1 shows the number of equilibria and their type and definition.

The biologically irrelevant equilibrium is given by:

$$E_2 = (0, \frac{m_2}{(\beta\gamma_2)}, \frac{-\gamma_2 m_1}{(\beta\gamma_2)}, 0). \tag{6.11}$$

The fourth equilibrium is given by:

[3] However, we consider a longer time scale as we include higher trophic predation.

Table 6.1: *Biologically relevant and irrelevant possible equilibria of the system given by Eqs. (6.6)-(6.9)*

Equilibrium	Definition	Value in parameterized system	Description	Hyperbolic Eigenvalues
E_0	(P_e, M_e, Z_e, C_e)	$(0, 0, 0, 0)$	Trivial (extinct)	Eq. (6.19)
E_1	$(P_e, 0, 0, C_e)$	$(K, 0, 0, \frac{K\omega}{m_3})$	phytoplankton and infochemical equilibrium	Eq. (6.20)
E_2	$(0, M_e, Z_e, 0)$	$(0, M_e, Z_e, 0)$	Biologically irrelevant equilibrium given in Eq. (6.11)	Eq.(6.21)
E_3	$(P_e, M_e, 0, C_e)$	$(P, M, 0, C)$	Copepod free equilibrium is given by Eq. (6.12)	Eqs. (6.22), (6.23), (6.23)
E_4	(P_e, M_e, Z_e, C_e)	as in Eq. (6.13)	Full Coexistence equilibrium given by Eq. (6.13)	Eqs.(6.13)

$$E_3 = (\frac{m_1}{(a\gamma_1 - b_1 m_1)}, \frac{r\gamma_1(aK\gamma_1 - Kb_1m_1 - m_1)}{K(a\gamma_1 - b_1 m_1^2)}, 0, \\ \frac{(a\eta Kr\gamma_1 - \eta Krb_1m_1 + aK\omega\gamma_1 - K\omega b_1 m_1 - \eta r m_1)}{(K(a\gamma_1 - b_1m_1)^2)}). \tag{6.12}$$

The full co-existence state satisfies a quartic polynomial

$$\sum_{i=0}^{4} A_i P_e^{4-i} = 0, \tag{6.13}$$

where A_i, $i = 0, .., 4$ are cascading parameters given in Appendix C.1. While M, Z and C are given by

$$M(P_e) = \frac{-r}{aK}\left(b_1 P_e^2 - (Kb_1 - 1)P_e - K\right),$$

$$Z(P_e) = A_5(P_e)^2 + B(P_e) + G, \tag{6.14}$$

$$C(P_e) = \frac{(P^2\eta r - P\eta Kr - K\omega)}{(Km_3)}.$$

Where A, B and G in Eq.(6.14) are cascading parameters given in Appendix C.5.

To find the roots of the coexistence polynomial, we need to use Cardans method to find the reduced quartic ($Q(P_e)$), and we can achieve that by finding the turning points (T_1, T_2, T_3) and then eliminating the cubic order in the quartic polynomial, Eq.(6.13) [198]. Cardans method starts by substituting $P_e = -\frac{B}{4A}$ into the P_e –expression of Eq.(6.13) and then choosing some coefficients that make the resulting quartic and P^3

equal to 0, the resultant reduced quartic equation is shown in Eq.(6.15).

$$Q(P_e) = AP_e^4 + BP_e^2 + CP_e + D, \tag{6.15}$$

we can solve any quartic by solving instead a simpler, reduced form of the resolvent cubic, say $T(x) = 0$ in Eq.(6.16); to determine the inflection points in the resolvent cubic, we need to determine some constant multiples such as I, J. Thus each of these invariants has a visible geometric interpretation in relation to Eulers resolvent cubic [198].

$$T(x) = x^3 - 3Ix + J, \tag{6.16}$$

the resolvent cubic constant multiples are given as follows:

$$I = 12AE - 3BC + C^2,$$
$$J = 72ACE + 9BCd - 27Ad^2 - 27EB^2 - 2C^3,$$

by solving Eq.(6.16) we obtain the subroots given in Eq. (6.17)

$$\begin{aligned} R_1 &= \sqrt{\epsilon^2 - (\frac{T_1}{12A})}, \\ R_2 &= \sqrt{\epsilon^2 - (\frac{T_2}{12A})}, \\ R_3 &= \sqrt{\epsilon^2 + (\frac{T_3}{12A})}. \end{aligned} \tag{6.17}$$

using the subroots in Eq.(6.17) will help us to determine the reduced quartic roots given in Eqs. (6.18).

$$\begin{aligned} P_1 &= X_N - R_1 + R_2 - R_3, \\ P_2 &= X_N - R_1 - R_2 + R_3, \\ P_3 &= X_N + R_1 + R_2 + R_3, \\ P_4 &= X_N + R_1 - R_2 - R_3. \end{aligned} \tag{6.18}$$

where P_i, $i = 1, 2, 3, 4$ are all real roots. However only two roots of Eqs. (6.18) are positive; the other two are negative. We can check this by using the parameter values in Table 6.2.

6.4 The Stability of The Steady-States

The Jacobian of the four-species model is given by

$$J = \begin{bmatrix} a_{11} & a_{12} & a_{13} & a_{14} \\ a_{21} & a_{22} & a_{23} & a_{24} \\ a_{31} & a_{32} & a_{33} & a_{34} \\ a_{41} & a_{42} & a_{43} & a_{44} \end{bmatrix},$$

where a_{ij}, $i, j = 1, ...4$ are Jacobian elements and all are given in Appendix C.2. The stability of the four equilibria depends on the eigenvalues of the Jacobian matrix M above. In the next section we investigate the behaviour of each equilibrium point.

6.4.1 System behaviour near the origin E_0

A straightforward calculation shows that the first trivial equilibria (extinction) is an unstable saddle point,

$$\lambda_{E_0} = (r, -m_1, -m_2, -m_3), \tag{6.19}$$

where $\lambda_1 = r$ and $\lambda_i = -m_i$ and $i = 1, 2, 3$ are the four related eigenvalues.

6.4.2 System behaviour near the microzooplankton and copepod extinction equilibrium, E_1

The equilibrium point, E_1, of the system, which represents microzooplankton and copepod eradication, is locally asymptotically stable if $\gamma_1 ak - b_1 km_1 - m_1 \leq 0$. Also if $\gamma_1 ak < b_1 km_1 - m_1$, and $1 + b_1 k > 0$ in the

eigenvalue Eq (6.20), then E_1 is asymptotically stable .

$$\lambda_{E_1} = (-r, \frac{\gamma_1 ak - b_1 km_1 - m_1}{1 + b_1 k}, -m_2, -m_3), \tag{6.20}$$

where $\lambda_1 = -r$, $\lambda_2 = \frac{\gamma_1 ak - b_1 km_1 - m_1}{1+b_1 k}$ and $\lambda_i = -m_i$ $i = 1, 2$ are the four related eigenvalues.

6.4.3 System behaviour near phytoplankton and infochemical eradication equilibrium, E_2

The Jacobian matrix of the system in Eqs. (6.6)-(6.9) around the non- feasible point, the phytoplankton and infochemical release eradication equilibrium point, E_2, gives the following eigenvalues.

$$\lambda_{E_2} = (\frac{\gamma_2 \beta r - b_2 m_2 r - am_2}{\gamma_2 \beta - b_2 m_2}, \frac{1}{2A_0}(\alpha \mp \sqrt{\beta}), -m_3) \tag{6.21}$$

where $A_0 = \gamma_2 \beta$, $\alpha = -m_1 m_2 m_3 b_2$ and $\beta = \sqrt{(4\gamma_2 \beta^2 m_1 m_2 - 4\gamma_2 b_2 \beta m_1 m_2^2 + b_2^2 m_1^2 m_2^2)}$.
Now, this hyperbolic point is an unstable saddle focus, because $\lambda_1 = \frac{\gamma_2 \beta r - b_2 m_2 r - am_2}{\gamma_2 \beta - b_2 m_2}$ and $\lambda_4 = -m_3 < 0$ are unstable saddles and because $\lambda_{2,3} = \frac{1}{2A_0}(-\alpha \mp \sqrt{\beta})$ are stable foci. λ_{E_2} is an unstable saddle–focus.

6.4.4 System behavior near the copepod extinction equilibrium, E_3

The Jacobian matrix of the system in Eqs. (6.6)-(6.9) for the fourth equilibrium, whereby the copepods are eradicated, has the following four eigenvalues:

$$\lambda_1 = \frac{A}{B}, \tag{6.22}$$

$$\lambda_2 = -m_3,$$

$$\lambda_{3,4} = \frac{1}{2A_0}(\alpha \mp \sqrt{\beta}), \tag{6.23}$$

where all the coefficients of Eq's (6.22 and 6.23) are as given in the Appendix C.3.

Now, this hyperbolic point is also an unstable saddle-focus, because λ_1 in Eq. (6.22) is unstable when $A > B > 0$ and because λ_2 in Eq. (6.23) is a stable sink. So $\lambda_{1,2}$ are unstable saddle foci. While $\lambda_{3,4}$ in Eq. (6.23) have negative real parts, they are stable foci. The point, E_3, is an unstable saddle-focus point, because we have four eigenvalues with opposite signs.

6.4.5 System behaviour around the coexistence equilibrium, E_4

Let λ_i, $i = 1, 2, 3, 4$ be the roots of the characteristic polynomial which is given by:

$$\sum_{i=0}^{4} A_i \lambda^{4-i} = 0, \tag{6.24}$$

where A_i are cascading parameters and $A_0 = 1$, and all other coefficients are as shown in Appendix C.4 From the Routh-Hurwitz criteria [184], all the roots of the Jacobian matrix have negative real parts if and only if the determinants of all the Hurts matrices are positive [184]; this implies that E_4, is locally asymptotically stable if and only if $A_1 > 0$, $A_3 > 0$ and $A_1A_2 > A_3 > 0$ and $A_3 > \sqrt{A_1(A_1A_4 - A_2A_3)} > 0$ or $A_1A_2A_3 > A_3^2 + A_1^2A_4 > 0$. Obviously, we have $A_1 > 0$ and $A_3 > 0$, and from the Jacobian element matrix, when $a_{12} < 0$, $a_{21} > 0$, $a_{23} < 0$, $a_{32} > 0$, $a_{33} > 0$ and $a_{44} < 0$, it can readily be seen that $A_1A_2A_3 > A_3^2 + A_1^2A_4 > 0$. Therefore, the coexistence state, E_4, is an unstable equilibrium point. For this purpose, we use the following notation

$a_{11} < 0$ i.e if $r < \frac{aM_e}{(1+b_1P_e)} + \frac{aP_eM_eb_1}{(1+b_1P_e)^2}(\frac{k}{(1-2P_e)}) < 0$ and $a_{12} < 0$ i.e if $\frac{-aP_e}{(1+b_1P_e)} < 0$ and $a_{21} > 0$ i.e. $b_1 < \frac{P_e}{(1+b_1P_e)}$ and $a_{23} < 0$ if $\zeta < \frac{C_e-1}{C_e}$ and $a_{44} < 0$. Hence E_4 is an unstable equilibrium point.

6.5 Asymptotic Expansion Analysis for the Quartic Polynomial

Using an asymptotic approach it is possible to make some limited analytical progress with the general system given in Eq. (6.9). In this analysis, we study how to scale our parameters in order to determine the general stability of the PM-models' roots [52]. We start performing the method by making the following assumption: $k = \widehat{\frac{k}{\epsilon^2}}$, $\widehat{a} = \frac{a}{\epsilon}$, $\widehat{b_1} = \frac{b_1}{\epsilon^2}$, $\widehat{b_2} = \frac{b_2}{\epsilon^2}$, $\widehat{m_1} = \frac{m_1}{\epsilon}$, $\widehat{m_2} = \frac{m_2}{\epsilon}$, $\widehat{m_3} = \frac{m_3}{\epsilon^2}$, $\widehat{\eta} = \frac{\eta}{\epsilon}$, $\widehat{\gamma_1} = \frac{\gamma_1}{\epsilon}$, $\widehat{\gamma_2} = \frac{\gamma_2}{\epsilon}$, $\widehat{\zeta} = \frac{\zeta}{\epsilon^3}$, $\widehat{\omega} = \frac{\omega}{\epsilon^3}$ and by substituting our scaled parameters and the following expansion into the full co-existence persistence state, which is given by Eq. (6.13):

$$P = \frac{P_0}{\epsilon^2} + \frac{P_1}{\epsilon} + P_2 + ..., \tag{6.25}$$

We will obtain an expanded polynomial and by collecting the coefficient of its leading order we can obtain the appropriate value for prey density, P_e, which is:

$$P_0 = \frac{\widehat{k}}{\epsilon^2} \tag{6.26}$$

Also, by substituting the expanded (scaled) value of P into the expanded polynomial of MZC, we can collect the coefficient of the next leading order to obtain a value for $P_1 = 0$. Repeating the same steps to obtain $P_2 = \frac{\widehat{k\omega}}{\widehat{\eta r}}$ will help us find and then compare the numerically yielded value of P with the analytically obtained value from Eq. 6.27.

$$P_{E_4} = \frac{\widehat{k}}{\epsilon^2} + \frac{\widehat{k\omega}}{\widehat{\eta r}} \tag{6.27}$$

and by substituting the analytically derived value of P into the quadratic polynomials of M and C and the fractional polynomial of Z we obtain:

$$\begin{aligned}
M_{E_4} &= \left(\frac{\widehat{kb_1a}}{\widehat{a\zeta}(\widehat{b_1k} + 1)} + \frac{\widehat{m_2a}}{\widehat{a\zeta}(\widehat{b_1k} + 1)} \right) \epsilon \\
Z_{E_4} &= \frac{\widehat{ak}\widehat{m_3}\widehat{\gamma_1}}{(\widehat{b_1k}\widehat{m_3} + \widehat{km_3})\beta} \\
C_{E_4} &= \frac{\widehat{\eta k r}}{\widehat{m_3}}.
\end{aligned}$$

After determining the values of the scaled root, E_4, we can undertake a general stability analysis by following the same procedures. After determining the characteristic polynomial of the model in Eq. 6.5 from the Jacobian matrix, we expand λ as in Eq. 6.28and substitute it back into the characteristic polynomial.

$$\lambda = \frac{\lambda_0}{\epsilon^2} + \frac{\lambda_1}{\epsilon} + \lambda_2 + ... \tag{6.28}$$

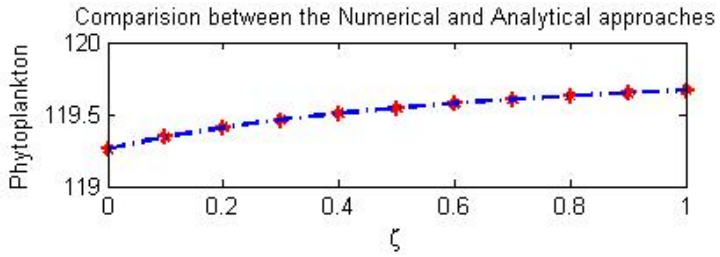

Figure 6.1: *A comparison between the numerical and the analytical approaches used to solve the quantic polynomial of the four species model in Eq.6.5.*

and by collecting the coefficient of the leading order, we will determine four eigenvalues as follows:

$$\lambda_{1,2} = \frac{A}{B},$$
$$\lambda_{3,4} = \frac{1}{2A_0}(\alpha \mp \sqrt{\beta}).$$

Where A, B, α and β are all cascading parameters: the forumula is quite prolix, so it has been moved to the appendix. Comparing the analytical roots and eigenvalues of the system, 6.5, with the numerical results shows that all the results are consistent. Fig. 6.1 illustrates the consistency of the two approaches.

6.6 Numerical Simulation Results

In this section, we investigate the effects of K, ζ, ω and r on the systems stability. We introduce the related parameters in the next subsection to clarify their specifics and their values. Changing these values lead to different behaviours as explained separately in Table 6.3.

6.6.1 Parameter values investigation

A major reason for modeling the dynamics of a population is to understand the principal controlling features and thus to be able to predict the likely pattern of development consequent upon a change in environmental parameters [120]. For the PM model of (6.9) we assume that the parameters for the elementary analysis are similar to their values as described in the two previous chapters [143]. We denote these values as the default values. Oscillatory solutions were present in the two models: i.e., when $\epsilon = b2 = \omega = 0$ and when $\epsilon = 1$, $b_2 = 0.05$, $\omega = 0.1$; this makes the two systems consistent with the results found in the two previous

chapters. However, in this chapter we study a 4 species system. We need to consider carefully the effect of each parameter on the PM food chain, to assist us to gain a valid solution, especially as we are introducing the effects of zooplankton into this system. Following [59], the parameter values used for zooplankton mortality can have a major influence on the dynamics of simple models [61], [59]. They found, for their particular parameter values, limit cycle behaviour (unforced oscillations) which occurred when using a linear mortality term for zooplankton in their four species system and that this limit cycle did not occur when using a quadratic term. In respect of [143] and [165], we will use a maximum growth rate, as these logistic growth models also do, and set it in the range $0.1 < r < 2d^{-1}$. [74] considered the phytoplankton carrying capacity, $K = 50\mu gCl^{-1}$ and [165] considered a much wider range $K = \infty$. Hence, we will use $50 < K < \infty$ [59]. [59], [202] estimated that the half-saturation constant of phytoplankton was in the range $20 < b_1 < 150\mu gCl^{-1}$ and that the zooplankton (copepod) half-saturation constant was in the range $20 < b_2 < 100\mu gCl^{-1}$. This reflects the fact that copepod dynamics develop more slowly than microzooplankton dynamics. However, because we are introducing zooplankton (copepods), and we are going to study the effects of this on this food chain, the accurate values for b_1 and b_2 for use in this model are much smaller than the literature suggests. We will have a very small value for zooplankton (copepod) population density in contrast with microzooplankton, as we are not introducing any higher trophic levels, and because of the fact that our models are not nutrient limited. We have chosen the b_1P and b_2M terms, because these terms may be regarded as reflecting the time it takes for predators to handle their prey [36], and if we choose $\frac{\gamma_1 a}{b_1} - m_1 > 0$, the predator density tends towards zero over time. Therefore, we postulate that $\frac{\gamma_1 a}{b_1} > m_1$ and similarly that $\frac{\gamma_2 \beta}{b_2} > m_2$. Also, we cannot choose $b_2 > b_1$ in this model for the same reason, in order to avoid having predator density tend towards zero over time.

In [223] the microzooplankton conversion efficiency is estimated to be $0.15 < \gamma_1 < 0.64$. [130] states that the conversion efficiency may be higher when considering zooplankton feeding on aeroplankton, hence a higher value of $\gamma_2 = 0.7$ is chosen for the copepod assimilation efficiency. Also, the maximum copepod predation rate was chosen to be $\beta = 1d^{-1}$. In our model, copepods are specified with a normal (as defined in previous chapters) mortality value as we accounted for natural mortality only and not for predation from higher predators. Moreover, if we wish to find the results of choosing these specific values, we can do so, numerically, by substituting the default values from Table 6.2 into the functional responses and then looking at the corresponding population density.

Table 6.2: *The default values and ranges of the parameters. The ranges cover values used by a variety of authors for various different models [59], [61], [202].*

Parameters	Definition	Value	Unit	Range	Source
dP/dt	Rate of change in phytoplankton density	-	$\mu_g\, C\, l^{-1} days^{-1}$		
dM/dt	Rate of change in microzooplankton density	-	$\mu_g\, C\, l^{-1} days^{-1}$		
dZ/dt	Rate of change in microzooplankton density	-	$\mu_g\, C\, l^{-1} days^{-1}$		
dC/dt	Rate of change in chemical productivity	-	-		
P	Phytoplankton density	-	$\mu_g\, C\, l^{-1}$		
M	Microzooplankton density	-	$\mu_g\, C\, l^{-1}$		
Z	Microzooplankton density	-	$\mu_g\, C\, l^{-1}$		
C	Chemical productivity	-	$nM/(\mu_g C l^1)$		
r	Phytoplankton intrinsic growth rate	1.5	$days^{-1}$		[62]
K	Phytoplankton carrying capacity	120	$\mu_g\, C\, l^{-1}$		[74]
a	Clearance rate of microzooplankton at low food densities	0.3	$\mu_g\, C l^{-1}\, days^{-1}$		[166, 202]
b_1	Half saturation density	0.05	$\mu_g\, C\, l^{-1}$	0.01 – 0.05	[13]
b_2	Half saturation density	0.02	$\mu_g\, C\, l^{-1}$	0.01 – 0.05	[13, 202]
γ_1	Microzooplankton grazing efficiency	0.3	$days^{-1}$	0.3 – 0.64	[62]
γ_2	Microzooplankton grazing efficiency	0.7	-	0.3 – 0.7	[61, 62]
m_1	Microzooplankton mortality in the absence of DAMS	0.1	$days^{-1}$	0.015 – 0.15	[62]
m_2	Zooplankton mortality in the absence of DAMS	0.15	$days^{-1}$	0.015 – 0.15	[62]
m_3	Chemical evaporate or flux to the atmosphere	0.03	$days^{-1}$		[13, 202]
η	DAMS production rate	0.1	-		[166]
β	Microzooplankton linear predation term	1	-		-
ζ	Rate of chemical increase	C_P	-		Control parameter
ω	Exudation rate for each phytoplankton cell	0.01	-		-

6.6.2 Time evolution and phase portraits

The main objective of this section is to support the analytical findings by the use of parameter values from the published literature, as reported in Table 6.2. The table is of the 14 parameters of the model 6.9 taken for the same range as the range of parameters shown in Table 4.1–for the analysis in Chapter four. These parameter ranges are also closely related to the value of the main control parameter, ν, or m_3 that helped us to define the initial conditions (ICs) for the numerical analysis. One of the crucial purposes of this section is to verify our analytical findings as shown in Table 7.1. The numerical simulations show important features of the system from a practical point of view. They show that oscillations in all plankton densities are large. This effect, where the stability of a system is lost through the addition of extra resources, is called the 'Paradox of enrichment' [194]. Fig. 6.2 exhibits the local stability of the model around the proposed initial conditions which we set to test the consistency between the two models of Eq. 6.9 and Fig. 6.10–when the parameter values given in Table 6.2 are applied.

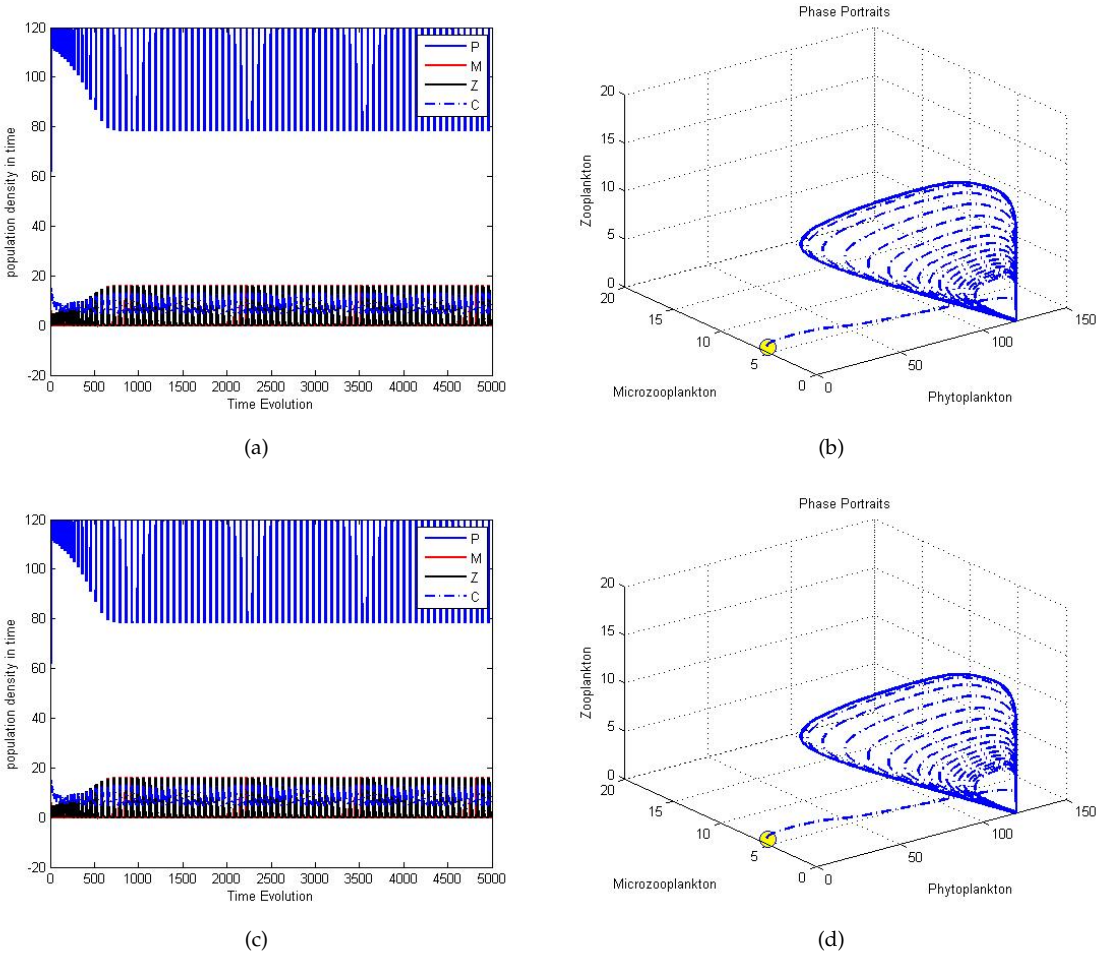

Figure 6.2: *Time Evolution and phase-space trajectory for the two cases of the PMZC system around the proposed initial conditions, other parameters are as shown in Table 6.2 and* $\zeta = 0.001$*. The trajectories in the two cases are attracted to a limit cycle.*

In Figs. 6.2, and 6.2(a), we plot the time evolution and the trajectory in *PMZC* space of the system from the initial conditions $(P, M, Z, C) = (3.942, 5.789, 0.0481, 20.379)$ with $\zeta = 0.001$ and all parameters fixed at their default values. In 6.2(b), the trajectory is attracted onto a limit cycle, with a specific period of roughly 500 days. The trajectory exhibits large-amplitude fluctuations in P.

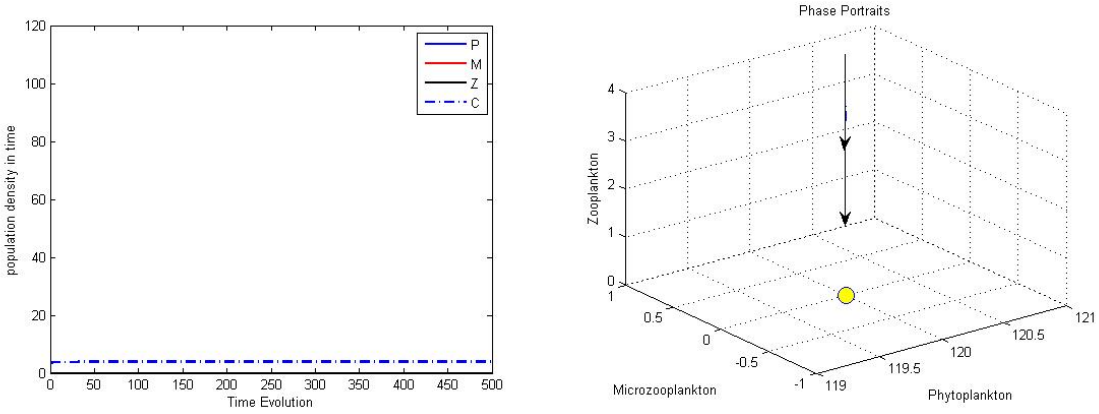

(a) (b)

Figure 6.3: *Time Evolution and phase portraits near microzooplankton and copepod eradicated equilibrium point E_1 and $\zeta = 0.001$. It can readily be seen that the trajectories are attracted onto a stable steady state.*

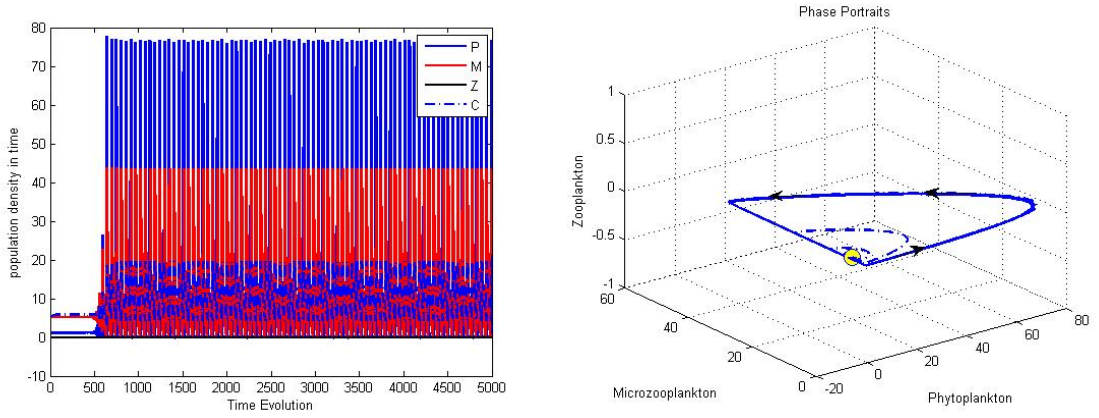

(a) (b)

Figure 6.4: *Time Evolution and phase portraits around the inner equilibrium point, E_3, with parameter values as shown in Table 6.2 and $\zeta = 0.001$. The trajectories are attracted onto a limit cycle*

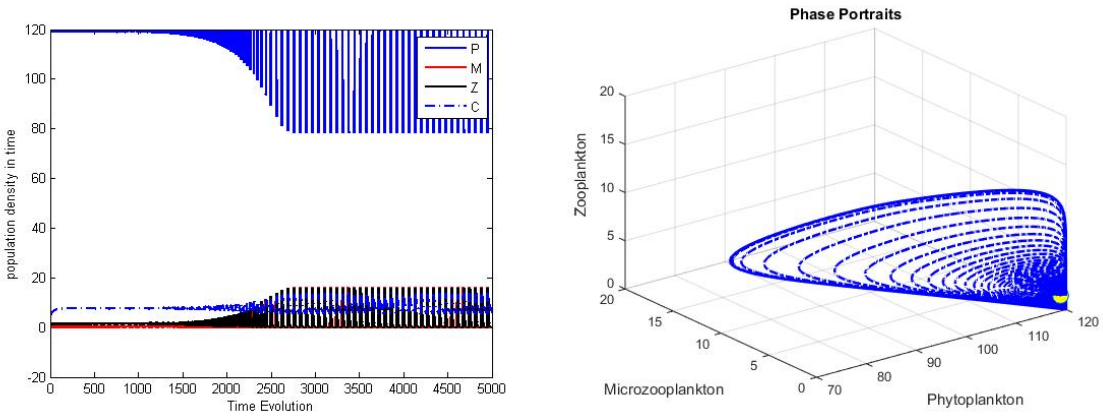

(a) (b)

Figure 6.5: *Time Evolution and phase portraits around the coexistence equilibrium point, E_4, with all of the other parameters fixed at their default values and $\zeta = 0.001$. In Fig. 6.5(a), the time evolution solution shows a limit cycle around the equilibrium E_4 and Fig. 6.5(b) shows that the trajectories are attracted onto a limit cycle.*

The possible dynamics of the prey-dependent model are: stable coexistence, unstable coexistence and extinction of the predator [229]. In the current study, we have an unstable coexistence equilibria. This is because the stability of the two species model in Eq. (4.1) and (4.2) of Chapter four is lost through the addition of extra resources: that is, by adding a population of zooplankton (copepods) and by modeling infochemical release. The above results are shown numerically using ODE45 for different equilibria, as in Figs. 6.2-6.5, we observe that the coexistence equilibrium is unstable when $\zeta = 0.001$.

6.6.3 A one parameter bifurcation diagram

The numerical simulations of the model represented by Eq. (6.9) and Fig. 6.6 can be used to construct a local stability diagram around E_4, with the parameter values given in Table 6.2. It can readily be seen, from 6.6(a), that, with the coexistence equilibria $E_4 < K$, the population of phytoplankton will bloom, specifically, if E_4 is a function of ζ and so reflects a consistency between our previous work and the current model. However, if $E_4 > K$ then the population of prey will decrease significantly. Also, if $E_4 = K$ then the population will remain constant [77].

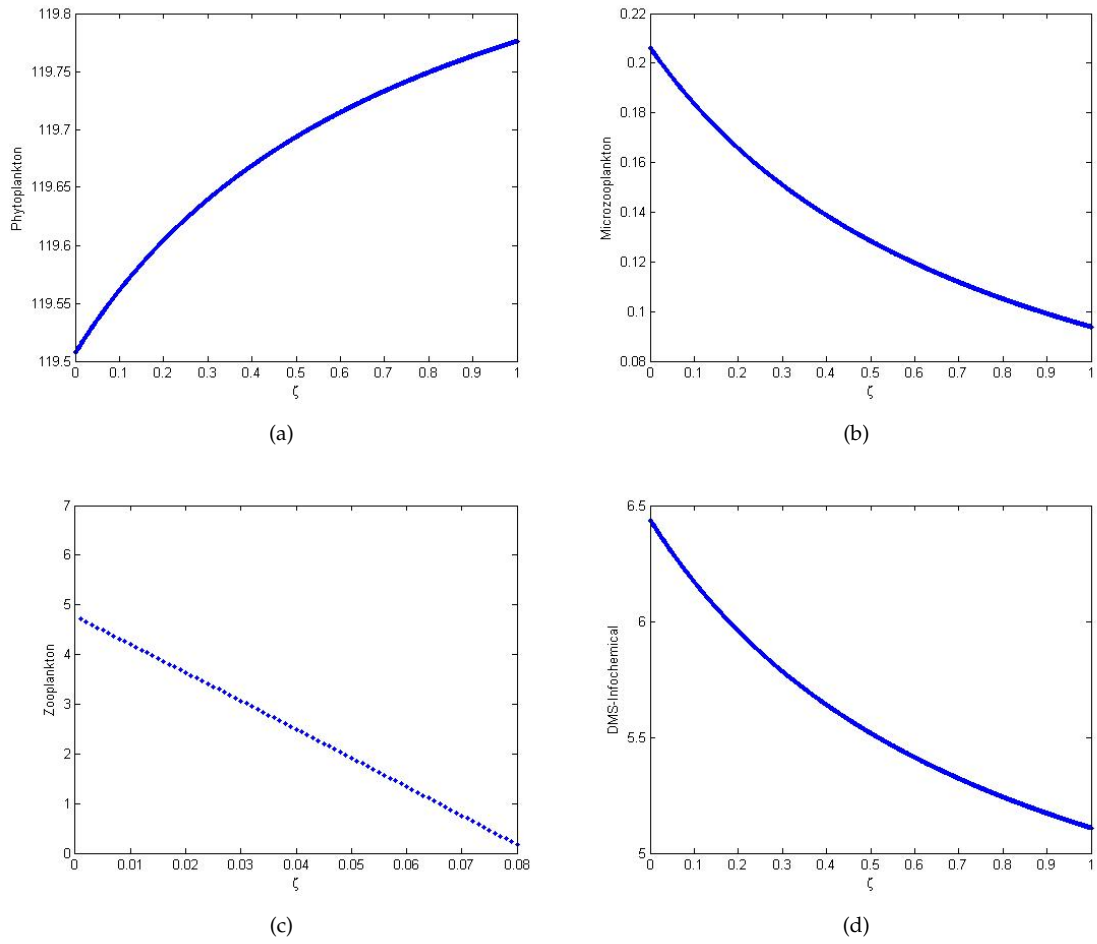

Figure 6.6: *One parameter ζ bifurcation diagram, showing the population density of each species w.r.t the increasing rate of chemical release, ζ.*

For a specific choice of parameters, the prey population increases to extremely high numbers, yet recovers (while the predator population remains sizeable–as at the highest prey density). In real-life situations, however, chance fluctuations in the discrete numbers of individual structures and in the life-cycles of prey might cause the prey to actually go extinct, and as a consequence, the predators as well [39].

To study the effect on the population dynamics of altering the carrying capacity of the prey by varying the value of K, we construct in Fig. 6.7, the stability diagram of the system defined by Eq. (6.9) and Table 6.3.

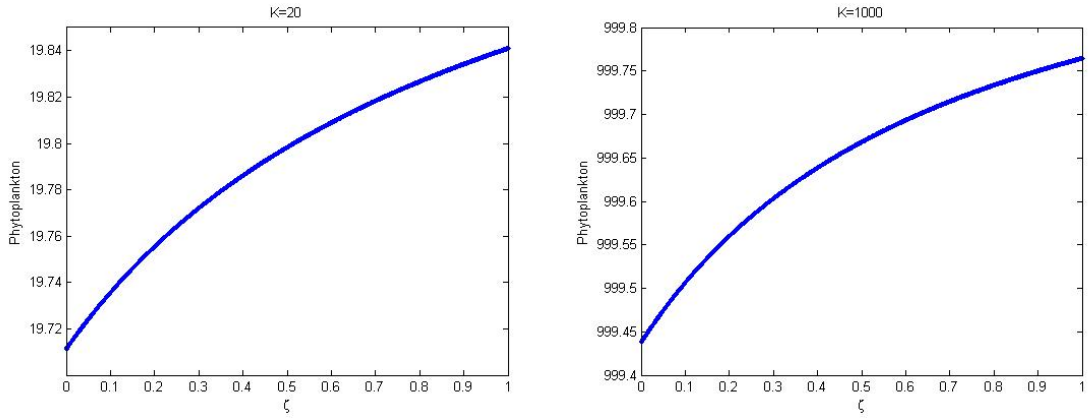

(a) (b)

Figure 6.7: *One parameter ζ bifurcation diagram, showing the population density of each species w.r.t the increasing rate of chemical release.*

Table 6.3: *A summary of the stability and bifurcation analysis of the four species model defined in Eqs. (6.6) - (6.9); this illustrates the system behaviour by varying a number of essential parameter values.*

Nutrient limitation	Chemical release	Exuded rate	Growth rate	System stability
K	ζ	ω	r	–
20	0.001	0.001	1.5	Stable
=	0.001	0.001	0.5	Stable
=	0.001	0.001	5	unstable
20	0.01	0.01	1.5	Stable
=	0.01	0.01	0.5	Stable
=	0.01	0.01	5	unstable
20	0.1	0.1	1.5	Stable
=	0.1	0.1	0.5	Stable
=	0.1	0.1	5	unstable
1000	0.001	0.001	0.5 – 5	unstable
=	0.01	0.01	0.5 – 5	unstable
=	0.1	0.1	0.5 – 5	unstable

6.7 Discussion

Many classical prey-dependent food chain models have been studied by a number of authors since the innovative work of Freedman [160], [77] and [60]; these studies were all aimed at gaining a better insight into the behaviours of such systems. The latest work, [75], studies the existence of periodic solution oscillations and includes an evaluation of how the predator functional response affects these. In the present investigation, an attempt has been made to discuss the directions of the trajectories by solving the model defined by Eq. (6.6) - (6.9). To summarise the analytical findings, we used Table 7.1 to obtain some numerical results generated using *ODE*45 in MALTA. The model in Eq. (6.9) exhibits four hyperbolic, biologically feasible equilibria and one non feasible equilibrium E_2. The first one is E_0 where all populations are extinct, and this is always unstable. This study is similar to the one [143] completed with the aim of understanding the food web. It investigates the stabilization of the food-web dynamics with a focus on DAMS production. The current study also presents an argument from the perspective of predator-prey relations along the marine food-web. The second equilibrium is E_1, where the prey is at its highest population density while the predator microzooplankton and the top predator zooplankton are extinct and the release of infochemicals is limited; this is also unstable as explained in Sec. 6.4.2. The third equilibrium is E_3 where the prey and the predators (microzooplankton) and the infochemical release persist while the top predator zooplankton becomes extinct, Sec. 6.4.4. This is borrowed from [143] who highlighted DAMS production as having an effect on the food-web. That study emphasized the need to understand the role of infochemicals in the food-web structure. The fourth equilibrium is coexistence, E_4, where all species continue to survive, as explained in Sec. 6.4.5. The set of parameters in Table 6.2 allows a wide range of behaviours to be observed in a relatively small ζ parameter space. The stability of the system falls into four categories, based on the predator-prey population, or limit-cycle, graph behavior [76]. An unstable spiral moves away from the initial condition, yielding to population oscillations that grow without bound; we demonstrate the existence of such a region of oscillatory behavior for the four species model and illustrate how this region persists with the set of the parameter values as given in Table 6.2; these results are consistent with [60]. The reason behind the oscillatory behavior in the PMZC model is the challenge of modeling the zooplankton Z functional response, as it is biologically complex and potentially influential on the system [60]. [167] wrote that in terms of understanding the complex dynamics

of plankton, including the oscillatory behavior, the simple reaction-diffusion model can be used to highlight the trophic interactions. In this chapter we employ the simple reaction-diffusion model to show temporal variations in predation by fish within the ecosystem [68]. An Intense focus on the role of infochemicals in the predation process is employed. The limit cycle behaviour that we observed with respect to the linear mortality function for the predator may not occur if we use a quadratic function for predator mortality [216]. We considered the work of [167], which explores the dynamics of a reaction-diffusion predator-prey model. The work of [68] is also critical in this case, in relation to exploring the existence of a Hopf bifurcation as investigated. This is because the stability of the two species model in Eq. (4.1) and (4.2) of Chapter four is lost when extra resources are added. That is, by adding a population density of zooplankton (copepods) and by modeling the infochemical release. This effect is called a "paradox of enrichment" [194]. In the above results shown numerically using ODE45 for different equilibria, as in Figs. 6.2-6.5 we observe that the coexistence equilibrium is unstable when $\zeta = 0.001$. This effect is an example of the "paradox of enrichment" already mentioned [93, 194],and is due to the high value of the carrying capacity of the system. The model in Eqs. (6.6) - (6.9) displays a region of instability near the Hopf bifurcations when $K = 20$, $r = 4.455$, $\zeta = 0.01$ and $\omega = 0.01$ as is shown in Table 6.3. However, this model does not exhibit behaviour in accordance with the enrichment paradox. While increasing the prey carrying capacity does take the system through a region of unstable states, the presence of a higher predator causes the system to be unstable for larger values of K, at least for the parameter values by which Fig. 6.7 was generated. To study, in the next chapter, the effect of the space dimension on the homogeneous steady state, we will investigate the spatial effects in relation to the four species temporal model by using Turing criteria [233]. This captures detailed information on interactions among the three species, the microzooplankton, copepods, and phytoplankton in a similar way to [143]. This investigation highlights that the species range limits are determined by adaptations to environmental variation which exist among the respective species. Relatively, the existence of the irregular distribution of populations over space and the continuous change in these with time depend on the complex interactions which taking place over the spatial and temporal scales. There are no unique criteria for the existence of spatio-temporal chaos [16].

Chapter 7

Non Turing Patterns in a PMZC Plankton Model

7.1 Introduction

Understanding pattern formation in nonlinear complex systems is one of the central problems of the natural, social, and technological sciences [178], [16]. In this chapter a mathematical model describing the interaction of plankton will be investigated. We aim to discuss a four trophic model of the form:

$$\frac{\partial \overline{U}}{\partial t} = D_i \nabla^2 \overline{U} + F_i(\overline{U}), \tag{7.1}$$

where $\overline{U}$ represents a vector of four components. P denotes the population density of the prey phytoplankton, M denotes the microzooplankton (the predator) population density and Z denotes the top predator (copepod) population density. i represents the number of species in the community, C denotes the chemical released as an effect of microzooplankton grazing, and functions F_i take into account the effects of birth and mortality–all relative to time, t. In most biologically meaningful situations, the functions F_i are nonlinear with respect to at least some of their arguments. The first term of the above equation, $D\nabla^2\overline{U}$, is concerned with the diffusion models as being one of the possible mechanisms for generating biological patterns, where D_i is the diffusion

coefficient of the ith species, in order to include spatial diffusion terms ∇^2 corresponding to the horizontal plane (the Laplace operator):

$$\nabla^2 = \frac{\partial^2}{\partial x^2} + \frac{\partial^2}{\partial y^2}. \tag{7.2}$$

Plankton distributions across a limited area and within a specific time scale are homogeneous in contrast with those of the ocean and lakes as a whole which are highly heterogeneous. One of the reasons for this latter heterogeneity lies in the presence of the strong horizontal diffusion which is associated with plankton distribution and this is coupled with the spatial heterogeneity of the nonlinear dynamics of plankton populations.

There are two kinds of physical processes which contribute to mixing: advection and diffusion. In advection, large-scale movements of water occur, and the imbedded organisms are carried with the water, whereas with diffusion, a spatial exchange of organisms takes place without any overall transport of water. As a result of the two processes, the physical mixing of organisms occurs. The term ”diffusion” is sometimes used synonymously with the terms ”mixing” or ”dispersion”. Strictly speaking, ”diffusion” is a form of ”dispersion” in which there is no spatial variation of mean velocity in the field. In a loose sense, however, we shall use ”diffusion” to indicate the result of the mixing of some property–when we wish to stress the process of mixing itself.

The essential features of the diffusive processes in the ocean are as follows. We shall consider the diffusion of a patch of phytoplankton in the sea. Eddies which are significantly larger than the patch size will advect the patch as a whole, while eddies which are smaller than the patch size, such as M and Z, can produce the dispersion of phytoplankton about its center of mass by turbulence diffusion. Eddies of around the same size as the patch will deform the patch and will also contribute to diffusion. All these eddies will produce shears or spatial variations in the velocity field; this velocity heterogeneity will tend to advect one part of the patch relative to another, resulting in the deformation of the patch.

In this chapter, the diffusion terms are a parametrization of the small-scale distribution, and the terms here represent horizontal movement in two dimensions, mainly due to plankton-distributing circulation and flows.

7.2 Turing Analysis of the *PMZC* Model

Several studies have been devoted to the various modes of spatiotemporal organization generated by different models: limit cycles, Turing patterns and, in one dimensional systems, traveling waves [221]. The purpose here is to create a fundamental understanding of the spatial system in 7.1, where U_i and $i = 1, 2, 3, 4$ is a vector of the system state variables P, M, Z, C at position X and time t. It can readily be seen that a corresponding linearized system in the vicinity of a spatially homogeneous steady state (P_e, M_e, Z_e, C_e) will have the following form:

$$\frac{dU_i(t)}{dt} = \sum_{j=1}^{4} a_{ij} U_j, \tag{7.3}$$

where $U_i = P, M, Z, C$, and $i = 1, .., 4$ this is in the case of a spatially homogeneous perturbation, and:

$$\frac{d\overline{U_i}(t,k)}{dt} = \sum_{j=1}^{4} \left(a_{ij} - k^2 D_i \delta_{ij}\right) \overline{U_i}(t,k), \tag{7.4}$$

The above describes the case of a spatially inhomogeneous perturbation with k as the wave number. Here $a_{ij} = \frac{\partial f_i}{\partial U_j}$, δ_{ij} is the Kronecker symbol, and $U_i(t)$ and $\overline{U_i}(t,k)$ are the amplitudes of the perturbation and its Fourier transformation, respectively [152]. It can readily be seen that when $k = 0$, the system in Eq.(7.3) coincides with Eqs. (7.4). The matrix of the linearised system is:

$$A = \begin{pmatrix} a_{11} - D_P k^2 & a_{12} & a_{13} & a_{14} \\ a_{21} & a_{22} - D_M k^2 & a_{23} & a_{24} \\ a_{31} & a_{32} & a_{33} - D_Z k^2 & a_{34} \\ a_{41} & a_{42} & a_{43} & a_{44} - D_C k^2 \end{pmatrix} \begin{pmatrix} P_1 \\ M_1 \\ Z_1 \\ C_1 \end{pmatrix}. \tag{7.5}$$

We obtain the dispersion relation as a quartic polynomial in δ.

$$\sum_{i=0}^{4} P_i \delta^{4-i} = 0, \tag{7.6}$$

where P_i are all cascading parameters. According to the Routh–Hurwitz criterion, all the eigenvalues have negative real parts if and only if the following conditions hold:

- $P_1 > 0$,
- $P_3 > 0$,
- $P_1P_2 > P_3 > 0$,
- $P_3 > \sqrt{P_1(P_1P_4 - P_2P_3)}$ or $P_1P_2P_3 > P_3^2 + P_1^2P_4 > 0$

And according to the analytical analysis presented in table 7.1, E_4 is the coexistence state of the system in Eqs (6.9). This state is an unstable focus node as it has four different types of eigenvalues; the first two are unstable foci and the other two are stable sinks.E_4 does not satisfy the Turing conditions and gave rise to chaos patterns in the spatial system. Spatiotemporal chaos arising from a diffusive coupling system of equations of local limit cycle oscillators [151], and spatiotemporal patterns, depend on the choice of the initial condition.

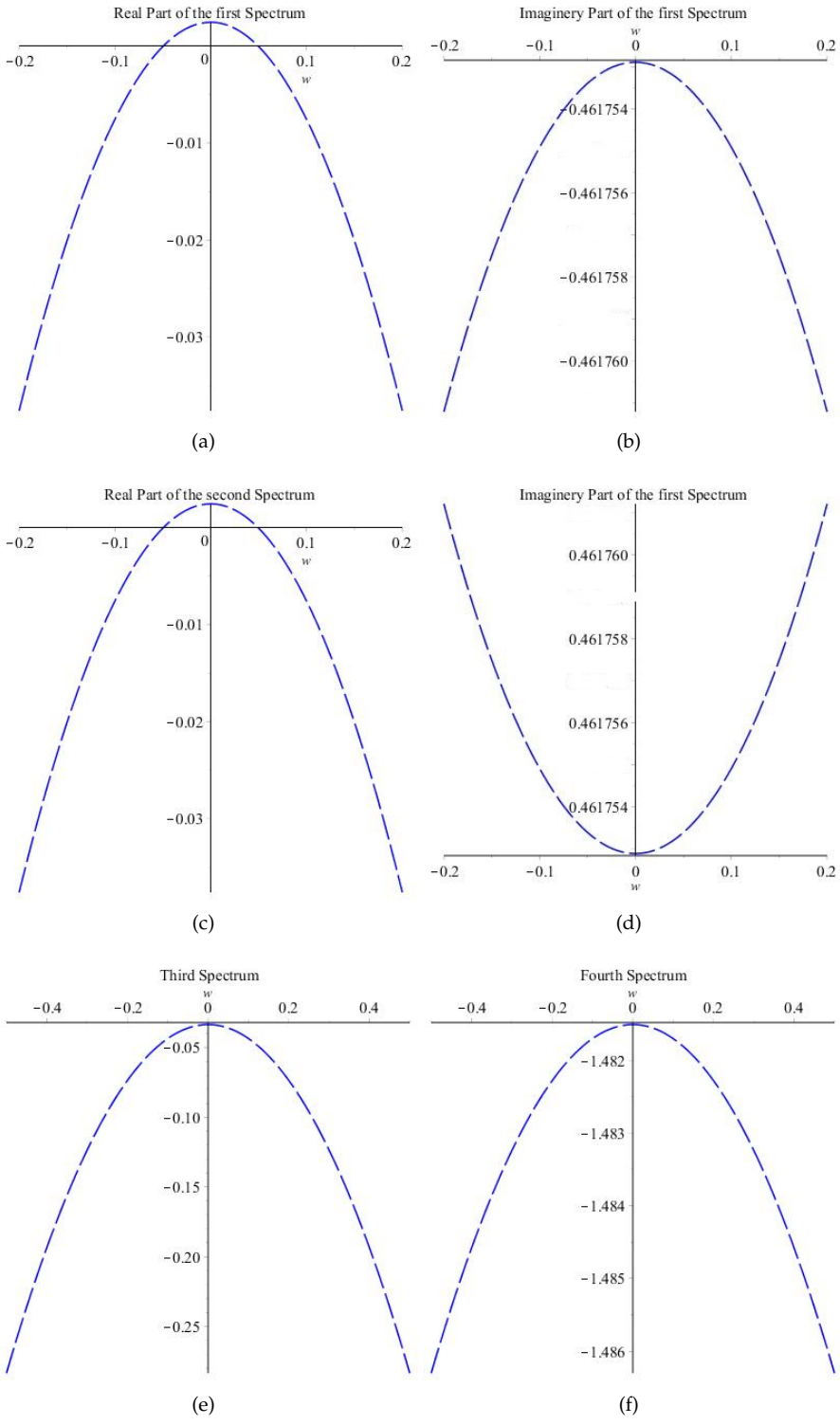

Figure 7.1: *The dispersion relation as a function the of the wave number. Parameter values are in Table 6.2.*

Fig. 7.1 shows the dispersion relation with respect to the wave number. In Figs 7.1(a), 7.1(b), 7.1(e) and 7.1(f), we present the four types of the corresponding spectra; the first two Figs, 7.1(a) and 7.1(b), represent the spectrum, with positive real parts, of an unstable focus type when the wave number is ($-0.002 < w < 0.002$) and in Fig's 7.1(e) and 7.1(f) we have the third and fourth spectra of sink type.

7.3 Spatial Distribution and Limit Cycle

In this section we consider the model in Eq. (7.1) as it exists in continuous time and space. The model is of four interacting species, as explained earlier in Sec. 7.1, and represents an example of a community population with an oscillatory solution. In this section we are interested in the possible emergence of non-Turing, Turing, and limit cycle patterns. First, we assume that the diffusivity is the same for all species, and then we assume that $D_C < D_M < D_Z < D_P$. However, it appears that the type of the choice of the initial condition given by Eq. (7.7) could affect the type of patterns which are generated [120]. Fig's 7.2 and 7.3 show the one dimensional systematic analysis of Eq. (7.1), starting from the type of the patterns and the behaviour of the system in time and space. The PMZC model could generate quite different patterns, depending on the choice of the initial condition.

$$\overline{U(x,0)} = U_e + \epsilon\cos(wx). \tag{7.7}$$

The type of the system dynamics depends significantly on the choice of the initial conditions [151]. The initial conditions in Eq. (7.7) include U_e as the system coexistence point and $\epsilon\cos(xw)$ as the perturbation term which depends on the value of ϵ and the value of w, the wave number. Fig. 7.2 shows how the initial condition evolves to a smooth spatial distribution of prey and predator. The spatial distribution gradually varies over time: the local temporal behaviours of the dynamic variables, *PMZC*, are strictly periodic and depend on the limit cycle of the non-spatial system. Another type of initial condition, as presented in Eq. (7.8), gives chaotic non-Turing patterns when the zero-flux boundary condition is imposed. Non-Turing patterns result when we perturb the initial distribution by adding some terms like ϵ and δ into the two dimensional initial distribution below:

$$\begin{aligned}
\overline{P}(x,y,0) &= P_e + \epsilon_1(x-0.2L_x)(x-0.8L_x) + \epsilon_2(y-0.3L_y)(y-0.7L_y),\\
\overline{M}(x,y,0) &= M_e + \epsilon_3(x-0.5L_x) + \epsilon_4(y-0.45L_y),\\
\overline{Z}(x,y,0) &= Z_e + \epsilon_1(x-0.2L_x)(x-0.8L_x) + \epsilon_2(y-0.3L_y)(y-0.7L_y),\\
\overline{C}(x,y,0) &= C_e + \epsilon_3(x-0.5L_x) + \epsilon_4(y-0.45L_y),
\end{aligned} \tag{7.8}$$

where the values for the important terms, ϵ and δ in Eqs. (7.8) are given as follows

$$\epsilon_1 = -2.10^{-7}, \epsilon_2 = -6.10^{-7}, \epsilon_3 = -3.10^{-5}, \epsilon_4 = -6.10^{-5}$$

[151].

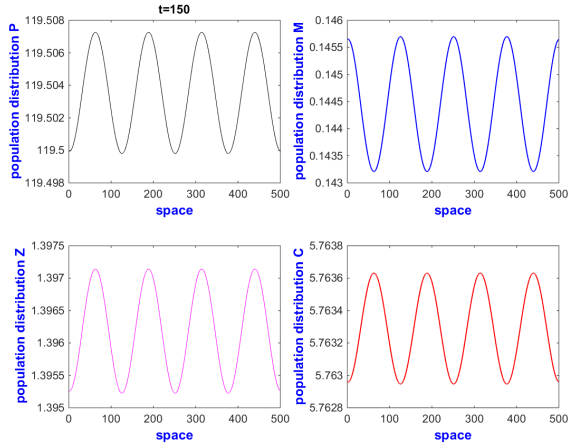

(a)

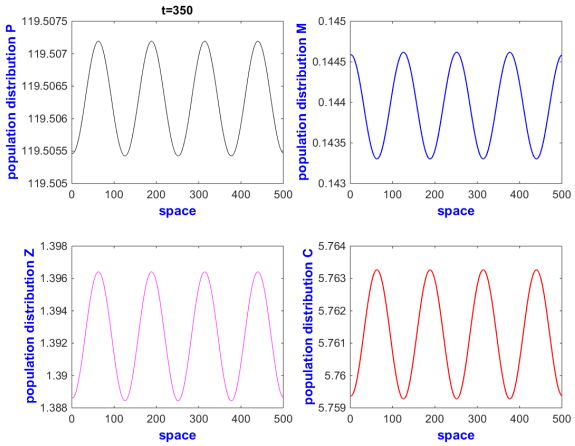

(b)

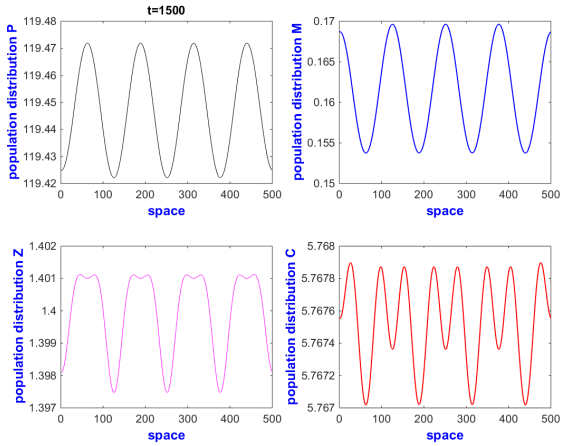

(c)

Figure 7.2: *Population distribution over the one dimensional space at* $t = 150$, $t = 350$ *and* $t = 1500$ *using Eqs. (7.7) as the initial condition and* $U_e = E_4$ *with parameters as shown in Table 6.2.*

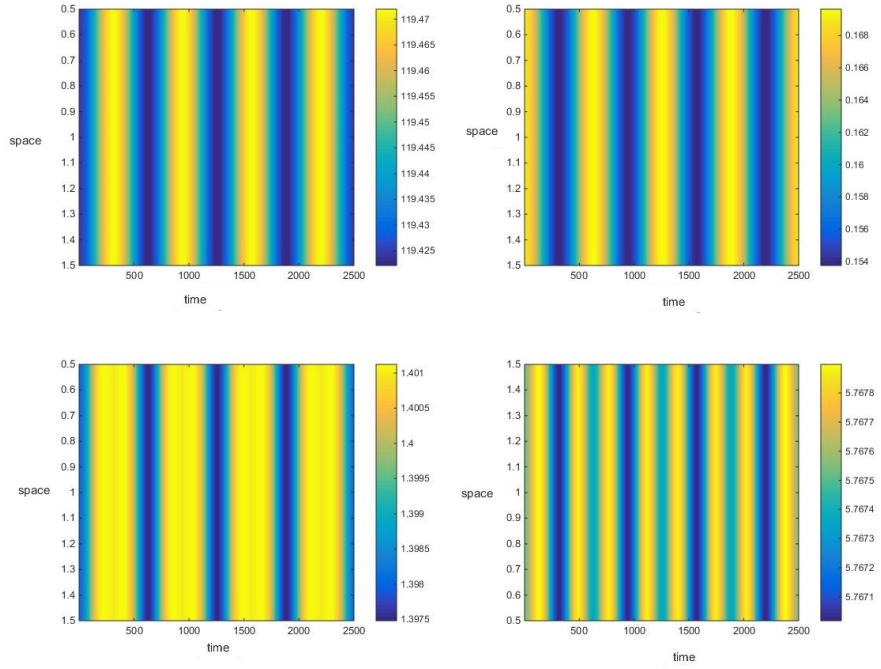

(a)

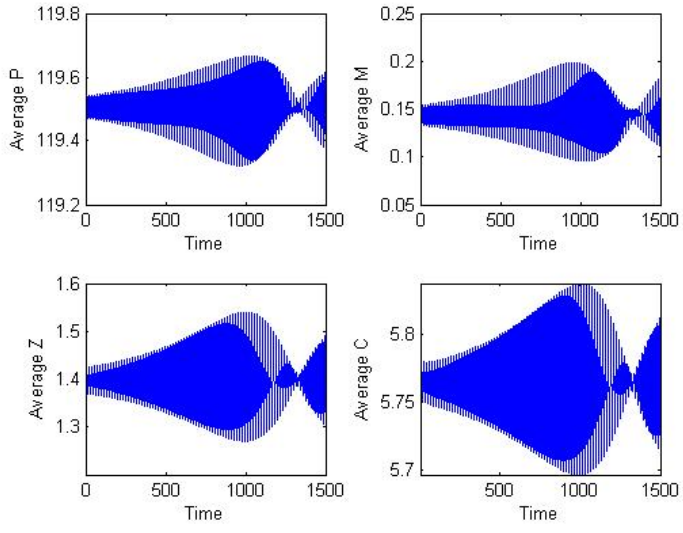

(b)

Figure 7.3: *Schematic analysis with respect to space and time Eqs. (6.9) and the average density of PMZC in time, using Eqs. (7.7) as the initial condition and $U_e = E_4$ with parameters as shown in Table 6.2.*

Figures 7.2(a), 7.2(b) and 7.2(c) show the population density generated by the dynamics variables at times t = 150, 350 and 1500, using $U_e = E_4$. Fig. 7.2(c) shows the regularity of the oscillatory solution of the population density of the dynamics variables in time and space. Both figures 7.3(a) and 7.3(b) in 7.3 show regular spatiotemporal oscillations over the whole domain. Furthermore, we decided to analyse each equilibrium point of the four species model and we present the results of this in Fig. 7.4 and Fig. 7.5, for $U_e = E_3$ and $U_e = E_1$ respectively.

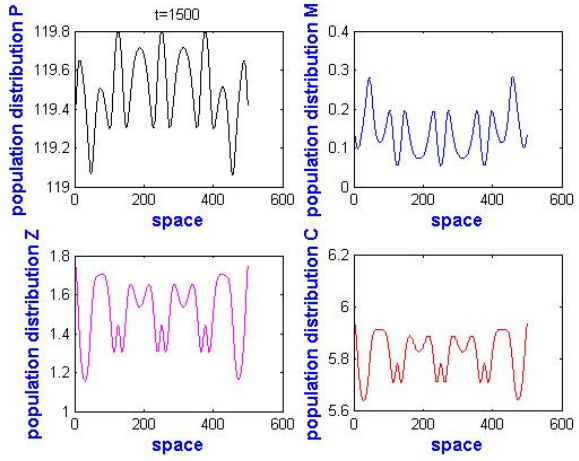

(a)

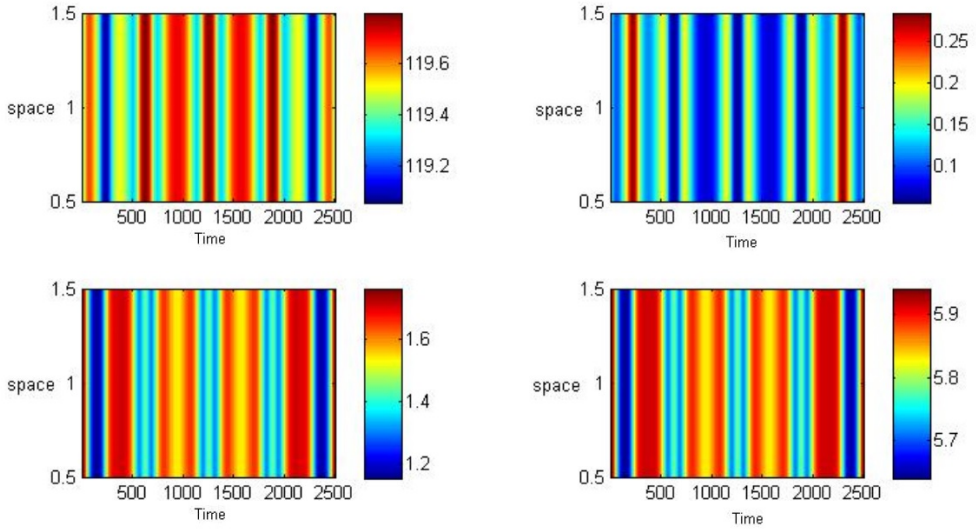

(b)

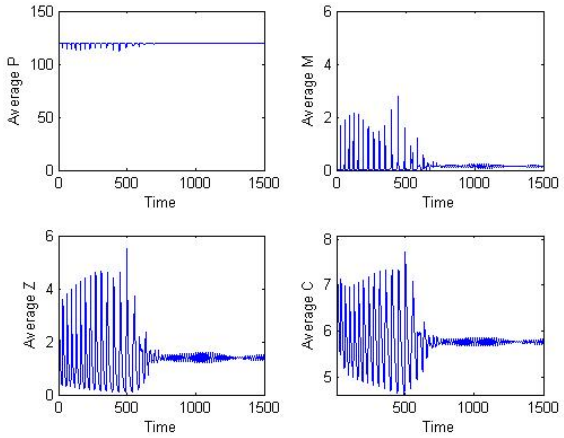

(c)

Figure 7.4: *The population distribution over the one dimensional space at* $t = 1500$*, plus the correspondent schematics analysis across space and time Eqs. (6.9) and the average density of PMZC over time, using Eqs. (7.7) as the initial condition and* E_3 *for* $\zeta = 0.001$ *other parameters are as shown in 6.2.*

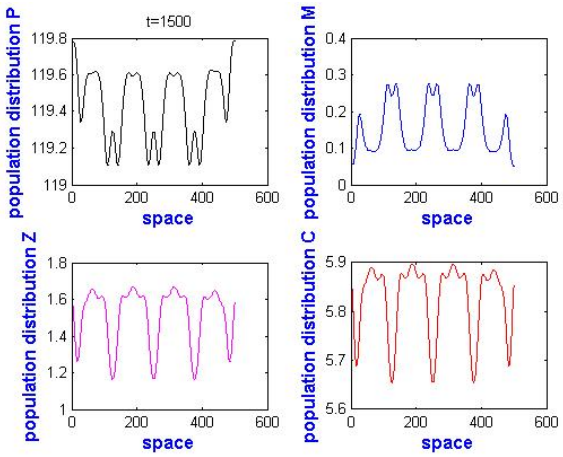

(a)

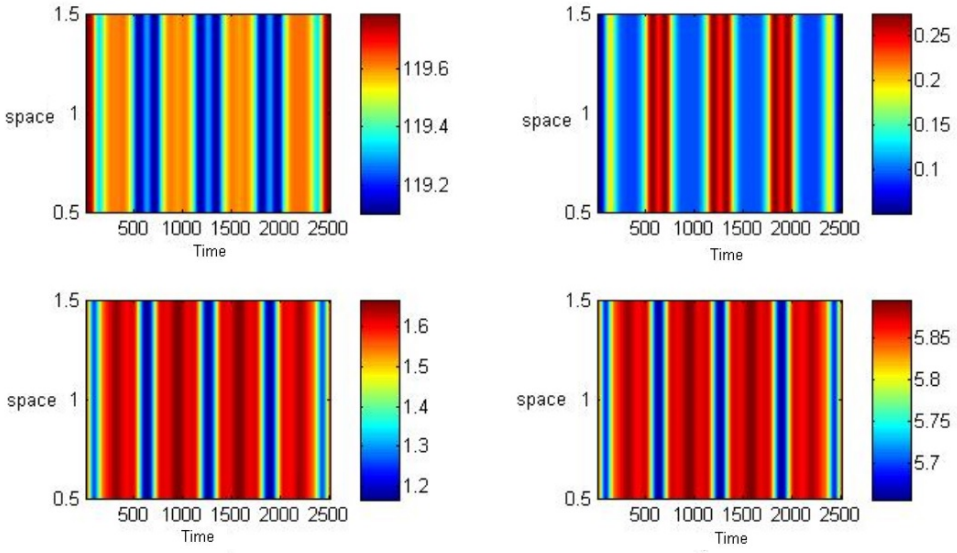

(b)

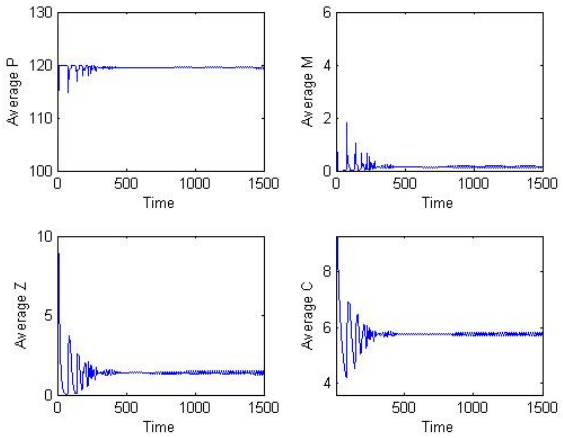

(c)

Figure 7.5: *Population distribution over the one dimensional space at* $t = 1500$ *plus the correspondent schematics analysis across space and time Eqs. (6.9); also the average density of PMZC in time using Eqs. (7.7) as the initial condition and* E_1 *for* $\zeta = 0.001$*; other parameters are as in 6.2.*

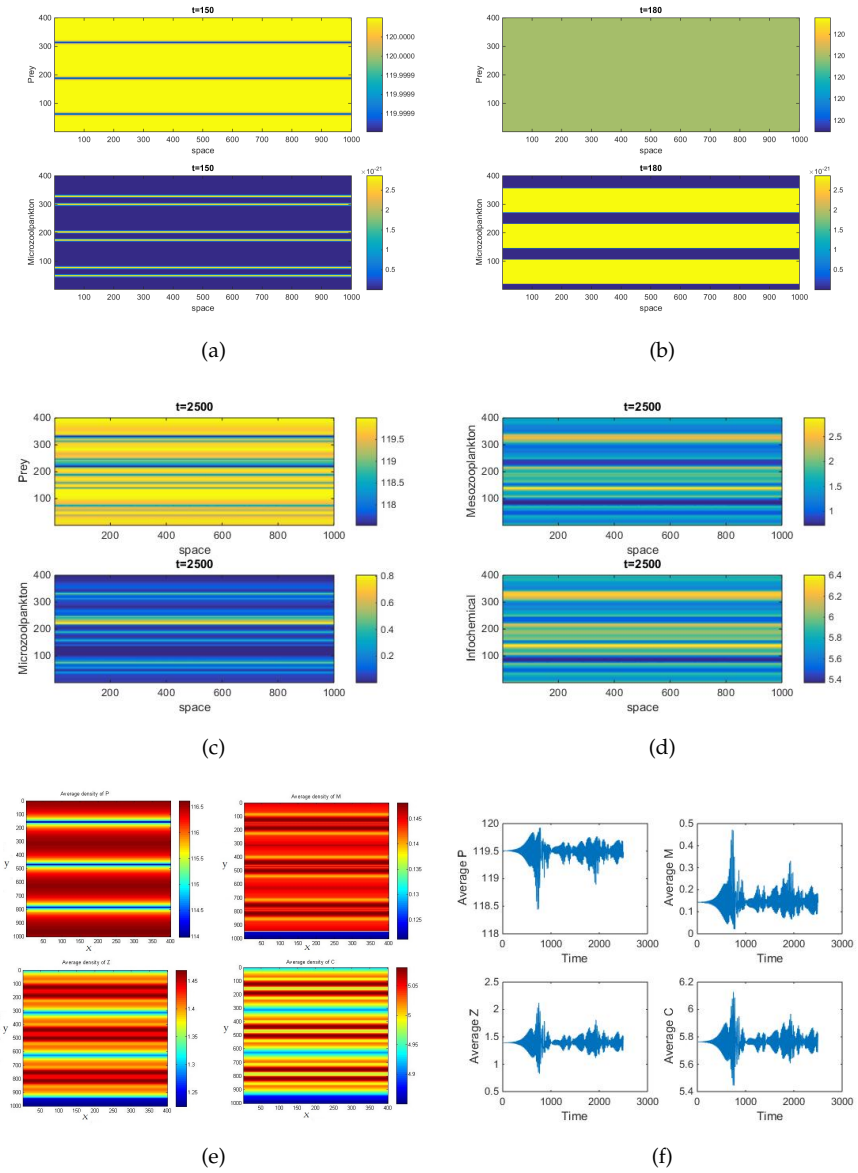

Figure 7.6: *Non-Turing patterns in a predator-prey distribution over two dimensional space for* $t = 150$, $t = 180$ *and* $t = 1500$, *using Eq. (7.7) as the initial condition and* $U_e = E_4$ *with parameters as shown in Table 6.2.*

In Fig .7.6, the spatial distributions of prey species at different times is presented to show the continuous changes in the distribution of species. Patterns are presented here which were generated within the time span $t = 10$ to $t = 1500$, but the existence of similar patterns was verified for longer duration simulations. This type of pattern is classified as a stripes patterns and it is a non-Turing pattern, because not all the Turing conditions hold.

In Fig. 7.7, we find another non-Turing pattern, generated by the PMZC model when $\zeta = 0.001$ and when a suitable choice of the parameter with $D_C < D_M < D_Z < D_P$ was made, to include horizontal diffusion, we also consider the effects of the diffusion of P, M, Z and C in the x-direction. We have observed that the stationary non-Turing patterns are cold spot patterns which exhibit circular patches which have lower concentrations of prey and predators. The non-Turing patterns observed for the classical Holling-functional response are of two types: hot spot patterns and cold spot patterns. Hot spots consist of localized circular patches with high population densities. Our stationary cold spot pattern changed to a chaos pattern due to the coalescence of nearby circular patches with low population densities. The stationary patterns obtained for the PMZC model are completely independent of the initial condition. We have checked this independence numerically, by using E_4 as an initial guess, without perturbing it; we obtained a flat state. This unstable steady-state property of the non-stationary patterns is illustrated in Fig.7.6 and 7.7, where the spatial averages of the population densities are plotted against the space dimension, as in 7.6(e), and against the time dimension, as in 7.6(f). It is important to note here that the temporal steady-state is unstable and oscillates for $\zeta \geq 0.001$. Further analysis is performed in order to investigate other biologically relevant equilibria which have been implemented in order to obtain some specific patterns; the patterns yielded vary according to the choice of the initial condition and the type of the equilibria. See Fig. (7.8).

Table 7.1: *Spatial Analysis of the four species model presented in Eq. (7.1).*

Equilibrium	Description	Turing conditions	Routh–Hurwitz criterion	Type of patterns
E_0	Trivial (extinct)	$\lambda(k^2) > 0$ and $H(k^2)$	$P_1 > 0$,	
E_1	phytoplankton and infochemical equilibrium	$\lambda(k^2) > 0$ and $H(k^2) < 0$	$P_1 > 0$,	Strips patterns using Eq.7.7 as I.C and spot using Eq.7.8 as I.C.
E_2	Biologically irrelevant equilibrium given in Eq. (6.11)	$\lambda(k^2) > 0$ and $H(k^2) > 0$	$P_1 > 0$,	Strips patterns using Eq.7.7 as I.C and spot using Eq.7.8 as I.C.
E_3	Copepod free equilibrium given by Eq. (6.12)	$\lambda(k^2) > 0$ and $H(k^2) > 0$	$P_1 > 0$,	Strips patterns using Eq.7.7 as I.C and spot using Eq.7.8 as I.C.
E_4	Full Coexistence equilibrium given by Eq. (6.13)	$\lambda(k^2) > 0$ and $H(k^2) > 0$	$P_1 > 0$,	Strips patterns using Eq.7.7 as I.C and spot using Eq.7.8 as I.C.

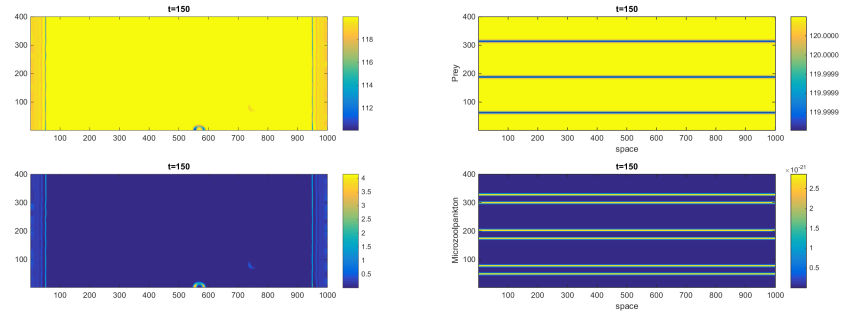

(a) (b)

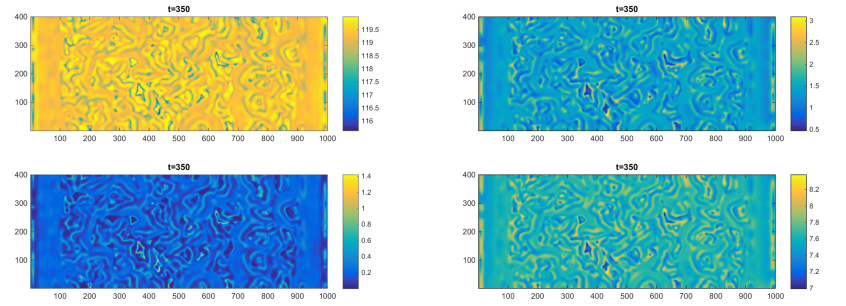

(c) (d)

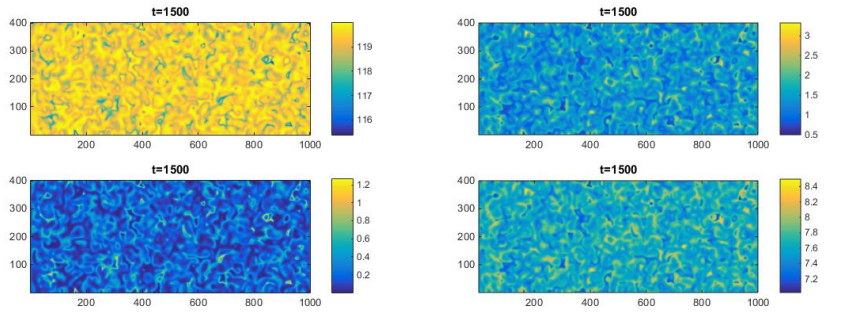

(e) (f)

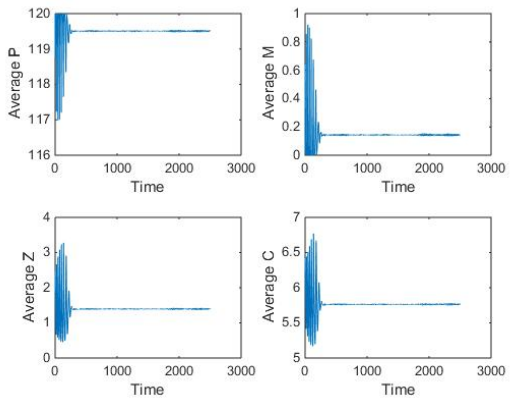

(g)

Figure 7.7: *Non -Turing patterns for predator-prey distribution over a two dimensional space representing prey and predator for* $t = 150, 350$ *and* $t = 1500$*, using Eq.7.8 as I.C. with* $U_e = E_4$ *and* $\zeta = 0.001$*; all other parameters are as shown in Table 6.2.*

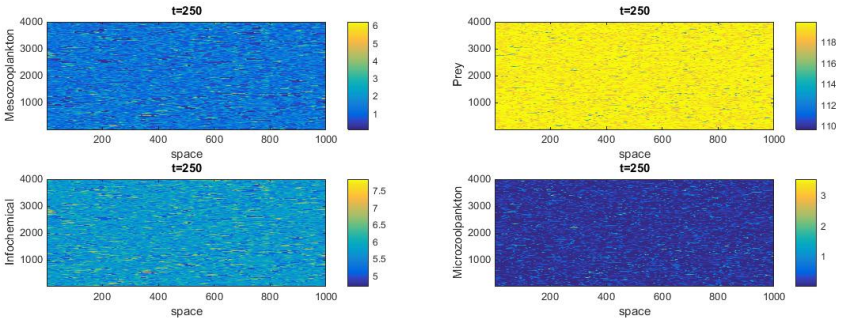

(a)

(b)

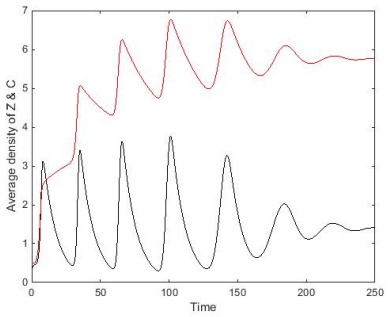

(c)

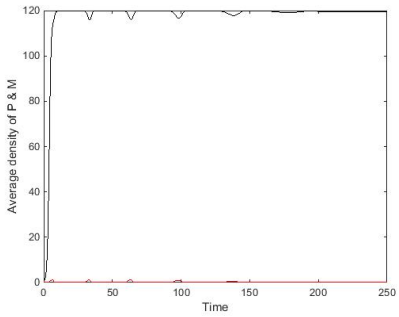

(d)

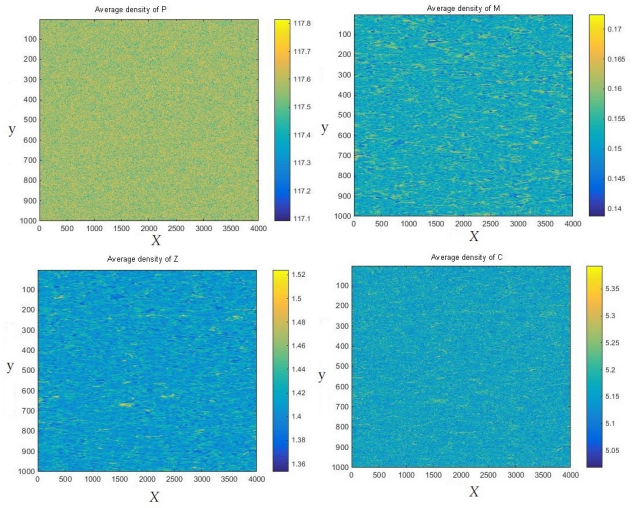

(e)

Figure 7.8: *Non-Turing patterns generated by Eq. (7.1) using the initial conditions from Eq. (7.8) with* $U_e = E_1$ *and* $\zeta = 0.001$*; other parameters are as shown in 6.2.*

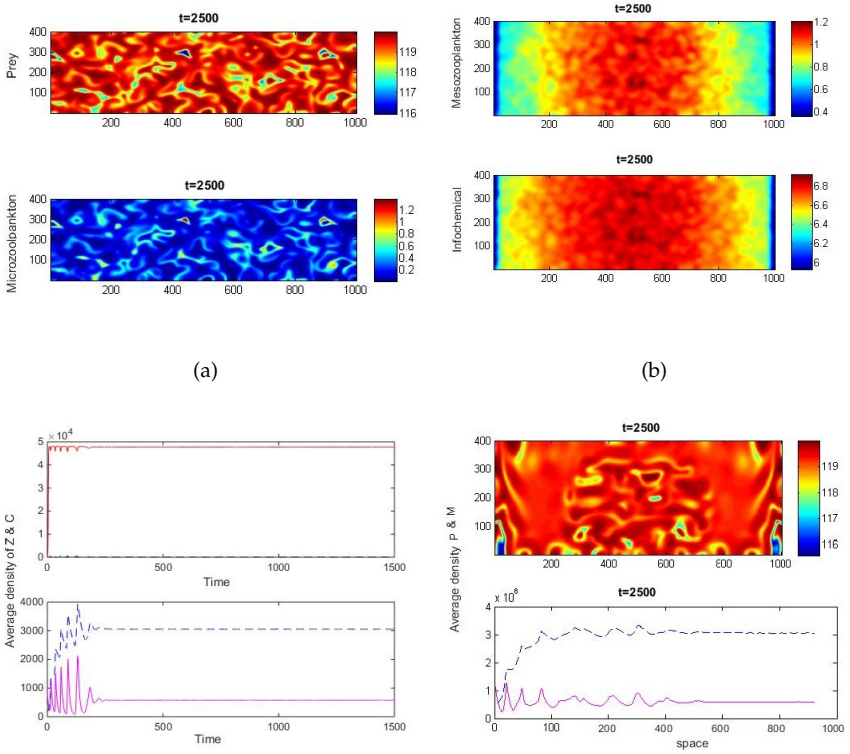

Figure 7.9: *Non-Turing patterns for Eq. (7.1) using the initial conditions from Eq. (7.8) with* $U_e = E_3$ *and* $\zeta = 0.001$*; other parameters are as shown in 6.2.*

Patterns produced by the PMZC model 7.1 can be in the form of a stripe-like arrangement of activated cells (in terms of phytoplankton concentrations)[1]; alternatively the active spots can lead to chaos. E_1, E_3 and E_4 are unstable equilibriums of the non-spatial model: Eqs.6.6–, 6.9, $\Rightarrow \Re(\lambda) > 0$. The Turing conditions are not satisfied and this gives rise to chaos patterns in the spatial system because $\Rightarrow \lambda(k^2) > 0$. Spatiotemporal chaos arising from a diffusive coupling system of equations with local limit cycle oscillators [151] and spatiotemporal patterns depend on the choice of the initial conditions. Infochemical mediated interaction can have a strong effect on the structuring, functioning and composition of marine ecosystems. For example, it has been observed that chemical gradients play a key role in generating complex patterns and in cell differentiation [220].

7.4 Conclusion

In the qualitative analysis of Eq. 7.1, we study the dynamical behavior of the temporal system. It is established that when the rate of mutual interference of the predator (i.e., M and Z), crosses its threshold value (i.e., $M = M_0$ and $Z = Z_0$) then prey, first predator and second predator populations start oscillating around the interior equilibrium as shown in Fig.6.5. The dynamics of spatially inhomogeneous aquatic communities is illustrated in this chapter by studying Turing instability in the *PMZC* model, using the Routh Hurwitz criteria [54]. The Turing criteria did not hold for this study because, as we have remarked earlier, the coexistence point, E_4, possesses four eigenvalues and two of these represent an unstable focus (with $Re(\lambda) > 0$) and the other two stable sinks. Furthermore, based on the numerical experiments, we obtained a spatial homogeneity in Eq. (6.9) which can give way to the appearance of a regular spatiotemporal pattern, depending on the parameter range given in Table 6.2. It is important to clarify that spatiotemporal chaos is typical for two dimensional reaction-diffusion systems with oscillatory dynamics. However, oscillatory behaviour is seen in the four species model even with small amplitudes in Eq. (7.1) and can be seen to be widely possible in terms of the response of the plankton model over time and space. Different patterns may be obtained by setting different initial conditions and using different numerical methods. We address the issue of the non-Turing patterns in Figs. 7.6 and 7.7 –using different initial conditions for the reaction–diffusion

[1]The concentration of the activator (P) is suggested by the dot or spot density

PMZC model (one and two dimensional). The population density of all species in Fig. 7.6 shows oscillatory behavior; this behaviour raises an important question in relation to the phytoplankton population response to the periodic (seasonal) stimuli [199]. Such large scale oscillations may push the system into and out of oscillatory phase during the course of the year [60]. The models short-term oscillations are connected with feedbacks in the ecosystem initiated either by abrupt changes in the phytoplankton or by increased density in spring or by increased spatial depth in autumn [199]. The systematic analysis of the nonlocal interactions in the one dimensional model of Fig. 7.3 and in the two dimensional model of Fig. 7.6 prove the persistence of the oscillation that we have already discovered in the spatially homogeneous model and show the consistency between the density and the average. In relation to this, for mathematical simplicity, the ranges of the nonlocal interactions for prey and predators are assumed to be same (this is consistent with [17]). Also, we could provide a more detailed explanation of the sort of patterns that we have obtained by further studying the dispersion relation of the model as shown in Fig. 7.1. We obtained striped patterns in Fig. 7.6 because we used a periodic function as an initial condition for Eq. (7.7). As found in [85], we can expect the existence of oscillatory travelling waves and more complex, for instance modulated, spatio–temporal dynamics. Spatiotemporal patterns exists for the parameter values given in Table 6.2. In Fig 7.7, using the parameter values shown in Table 6.2 but different initial conditions such as the initial conditions given in Eq. (7.8), we observe a pattern formation with different time steps. Also, it can be observed that stationary "mixtures $\longrightarrow$ stripe–spot mixtures $\longrightarrow$ spots" patterns are time-dependent, as was found in [151]. These observations confirm the fact that the interactions between the temporal and the spatial are unable to drive the system towards spatial and temporal irregularity under any circumstances. Relatively, the existence of the irregular distributions of populations over space and the continuous changes to these over time depends on the complex interactions which take place over both the spatial and temporal scales. Finally, all these spatial patterns show that the qualitative changes lead to spatial density distributions for each species, across the spatial system. Furthermore, we analyse the stability of the linear and non-linear systems with the help of a Turing instability analysis and observe that the spatiotemporal system in Eq. (7.1) does not change its behavior, as revealed by the spatial systematic analysis in Figs. 7.2 and 7.3 in one dimension and Figs. 7.6, 7.6(e), 7.6(f), 7.7 and 7.7(g) in two dimensions, because the trajectories are spiralling in a limit cycle and then they tend to converge into a stable point. Our results show that modeling by reaction –diffusion equation is

an appropriate way to investigate the fundamental mechanisms of the spatio-temporal dynamics in the real world food web system [177] and [14].

7.5 Biological Interpretation

The biological context of these mathematical results is that of a well-mixed food chain, as presented in Eq. (7.1), in a homogeneous environment; A marine environment does not always accord to this description. This is especially so when phytoplankton are distributed heterogeneously, due to light and nutrient limitations, as mentioned in the biological background chapter 2 of this thesis in Sec.2.5. In recent years, marine ecosystems have experienced a number of major changes. One of the most important of these is the acidification that affects the productivity of phytoplankton [244]. The second major source of disturbance is the influence of human activities (other than the production of CO2) on ecological communities; there is increasing recognition of the importance of altered trophic interactions and energy flows in ecosystems which are being degraded by human activities [253]. The discussion in the current chapter has further emphasized the utility of Turing and non-Turing Patterns, as used by many researchers, in relation to understanding the mechanism of pattern formation in various physical processes within the marine ecosystem. The presence of non-Turing patterns, as described in Appendix A.6, depends on a range of influences across a number of different scales which effect plankton growth. [50] further observed that planktonic processes and spatial patterns within the marine ecosystem drive plankton behaviour. However, it is also indicated that the ocean food web can be affected by changes in plankton behaviour. An understanding of the plankton ecology requires an understanding of the various different influences at the various different scales which are spanned, including the effect on plankton growth of micro-scale turbulence. This discussion has mainly focused on four interacting components: namely, the Phytoplankton (P), the Microzooplankton (M), the copepods (Z) and (C) infochemical release. In discussing the different components and how they interact, advanced technologies have been referred to. In terms of the biological research which has been undertaken in this area one of these advanced techniques is remote sensing. As discussed in Sec. 2.6.1, the chapter describing the biological background of this thesis, there are standard methods for remote sensing including various

different types of satellite sensing. The results from these remote sensing methods are used for analyzing and then presenting the different interactions that occur among marine species. Through these technologies, biological and physical dynamics have been used to explain plankton ecology. As discussed by [71], remote sensing has been used as a technique for synoptically mapping aquatic systems.

The four species model presented via Eq. 7.1 used a mathematical modeling approach to analyse the ways in which infochemicals play a critical role in mediating the interactions among plankton. The discussion here has highlighted infochemicals as the main factors which are critical in determining how plankton relate with other organisms. From the results presented in the discussion, it can be seen that there can be a significant alteration in the interactions among plankton and other species following a change in infochemical release. The result of such changes is changes in the dynamics of planktonic food webs: e.g., Figs. 7.2, 7.6, 7.9 and 7.5 show the spatiotemporal patterns which exist for the parameter values given in Table 6.2 and based on the choice of hyperbolic equilibriums given in Table 7.1. Therefore, it is demonstrated that these infochemicals are associated with strong effects on the functioning and structuring of marine ecosystems [107].

As highlighted in the discussion of the spatial models in Eq. 7.1, phytoplankton bloom formation is affected by infochemical-mediated multitrophic interactions. The explanation provided is that the release of grazing induced infochemicals leads to a change in copepod foraging behaviours. This in turn changes the foraging behaviours among other species. Copepods change their foraging behaviour and prefer microzooplankton over the small phytoplankton species [99], due to the abundance of the latter and therefore of the former. Further, the copepods elicit a change in the grazing patterns within the ecosystem because of their prey choice. The release of DMS infochemicals by the small phytoplankton species, among them Emiliania huxleyi and Phaeocystis, presents a wide range of prey choices [225]. It is also argued that as a result of the increased grazing of microzooplankton on the phytoplankton species, there are further releases of infochemicals. The primary result of increased infochemicals release is the enhanced susceptibility of microzooplankton to predation. The copepods are aided in moving to forage on microzooplankton. As explained by [116], the increased grazing by copepods on the microzooplankton leads to bloom formation among the phytoplankton species. It is argued that the community composition of all the species is affected by the grazing induced infochemical release. Furthermore, the abundance and distribution of phytoplankton over the seasons, including their differing physico-chemical characteristics, have been successfully evaluated

using a number of qualitative and quantitative estimates as described in Sec. 2.6.1. These estimates have been used to understand the growth cycles of phytoplankton across the ecosystem [4]. In deriving these estimates [4] observed that plankton samples are collected from different spots within the ecosystem.

[24] are among the few scholars who have managed to investigate the effects of DMS on the marine ecosystem. Their main objective was to determine the production of DMS infochemicals and to discover how these affected the copepods dynamics and foraging behaviours. However, to date, there has been very limited research which evaluates the interactions of species which occur within the ecosystem as a result of DMS release. There is still a wide range of data which is yet to be collected relating to the models and parameters which could explain these interactions, and this is why the current discussion was critical in terms of this topic. The models presented in chapter 6 and the current chapter resulted in biologically reasonable results and allowed the quantification of the behaviours of the models for analysing the interactions among marine species. Through the conceptual-box models, this chapter grouped plankton species into different interacting compartments in order to study their interactions.

One major observation from the discussion is the fact that the models omit bacteria, and these are potential prey for many species in the relevant ecosystems, including the small zooplankton. The bacteria also use the dissolved DMSP as illustrated in the research by [231], leading to its further conversion to DMS. In this chapter, all the processes involving bacteria as a component were grouped into one process and assumed to be proportional to the microzooplankton (M and Z) grazing. This approach was taken in this study in order to allow a focus on the analytical examination of the models.

Based on the models presented in Eqs. 7.1, it is argued that any increase in DMS infochemical results in an increase in the rate at which copepods predate. A study by [220] is amongst the research which presents this argument. [220] conducted a number of different experiments on the relationships between DMS infochemical release and copepod grazing rates. The findings were that tethered copepods respond to microinjections of DMS by increasing their grazing rates. This chapter further highlights that increased copepod predation of microzooplankton can be associated with DMS signaling. Therefore, the main discussion is concerned with predator-mediated coexistence. As explained in the discussion, there is inadequate research which provides information about the actuality of DMS as an infochemical within the ecosystems. This serves to increase the relevance of conducting the current research and so presenting experimental evidence on the topic.

There has also been discussion in this chapter concerning the different factors that result in a change in DMS production. The discussion argues for the use of the CLAW hypothesis to explain the relations between the Earth's climate and the changes in the ocean ecosystems. In regard to this, the information relating to oceanic acidification as being subject to changes in DMS production is presented. The information provided highlights the fact that the formation of sulfuric and methane sulfonic acids in the atmosphere affect the production and emission of DMS [143]. The main result of recent changes to the atmosphere is the oxidation of DMS. Therefore, the discussion was based mainly on the climate changes related to the marine ecosystem as correlated with the changes in the release of DMS and other infochemicals.

It has also been found via this analysis that different factors may affect the abundance of plankton species in the marine ecosystem. Among these factors are nutrient availability, salinity, water temperature and light intensity. These findings are borrowed from a previous study by [217] who evaluated these factors in detail and their roles in the ecosystem. Those author's research finding was that all these factors coexist within the ecosystem. Therefore, research studies must aim at evaluating the different factors. In this study, nutrient availability and light intensity were taken particularly into account. However, the research did not focus on temperature and salinity. The finding from this analysis was that seasonal changes in the different factors affect the variability of species interactions [132].

Chapter 8

Conclusion and Future Work

8.1 Thesis Summary and Discussion

In this thesis, we have studied two reaction–diffusion plankton models with local interaction terms. These models correlate with a previously studied two-component reaction–diffusion system with inter–species reaction and with constant diffusion coefficients. This current study has also investigated instability and bifurcation problems, along with a variational approximation analysis. A linear selection mechanism governing the development and propagation of nonlinear patterns was introduced. This was based on previous work by [15] who investigated the issue of the development and propagation of nonlinear patterns within marine ecosystems. Moreover a detailed analysis of the limit cycle [158] and the instabilities [151] that arise in the system was performed using linear stability analysis. We verified the presence of periodic travelling waves and more complex spatio –temporal dynamics such as modulated and chaotic waves.

The original motivation behind this thesis was to develop and analyze the model introduced in [143], using the general framework provided in [197], [198] and for the analysis and numerical integration, [23,109, 120,134]. Using the above approaches, we were able to derive some new and interesting results which relate to both the previously studied, diffusion-free models, and the less studied extended models. With most of the ecological models studied, even after choosing appropriate initial conditions, the spirals which were initially established broke up into forms of interacting spiral chaos over time [161]. This effect resulted from

the use of reaction-diffusion equations; these constituted the pattern formation mechanism [211]. Moreover if random perturbations are imposed around the homogeneous steady state determined by the parameter values (chosen in order to create a spiral pattern or another target pattern), then only oscillatory behavior is observed and no pattern is generated. Hence it was a challenge to prepare the initial conditions so that a spiral would form and then deform into other structures over time. From the study it can be seen that a correlation exists between the analytical and the numerical results, although the matching can be achieved only until first order perturbation of the analytical results takes place. Thus, there is room for matching the simulation results to higher levels of approximation, and this is an area that could be studied in the future. Here, our main results are that we have provided a theoretical support for the formation of spiral and other target patterns and that the simulation results we have obtained are not due to numerical artifacts. Our analysis could be used in other prey- predator models to obtain useful results and to help in understanding the significance of spiral [60] and other target patterns in the spatio-temporal extension of the general prey predator model. This may have significant implications in the context of ecology. The approximate solutions for spiral and target patterns, when plotted in terms of space variables at a particular point in time, exhibited spiral and other target patterns only. These solutions, when chosen as initial conditions for the complete non-linear model (along with the associated boundary conditions) yielded spiral and other target patterns. This approach can be adopted to generate spiral and other target patterns for any spatio-temporal model with parameter values which produce curves in the vicinity of a Turing–Hopf bifurcation point. The hazards of choosing appropriate initial conditions in order to generate spiral or striped patterns can be avoided by adopting the procedures presented here. We further conducted an investigation into interactions among the three species representing phytoplankton, microzooplankton and copepods. This was achieved through the simple conceptual mathematical models presented in Chapter 6 which were then developed, spatially, in Chapter 7. The investigation further evaluated the predictive power of the model (defined in Chapter 7), based on an analysis of DMSP infochemical cues within the system. As uncovered by [153], an increase in the species and processes which are investigated in the analysis, results in an increase in the predictive power of the model. However, [161] has also argued that increasing the species and the processes covered by the analysis lowers the accuracy of the model. This is caused by the uncertainty in the data collected. A major reason why a conceptual modeling approach was preferred in this chapter (in terms of the analysis)

was because of the ability of such a model to develop a wide range of information relating to infochemical-mediated multitrophic interactions. This is a topic which has not received much attention in plankton modeling research. The perceived relevance of the conceptual modeling approach to this analysis was also based on the ability of these models to explore the full range of model behaviors.

As discussed by [24], there are three spatial scales that explain the foraging of copepods and how this is affected by infochemicals such as DMS. These are the patch scale, the cellular scale, and the water column scale. The models in this thesis inform on the interactions of the different scales by describing the foraging of copepods. The work of [220], in relation to models, was critical in informing the development of the models used in [143] and in this thesis. However, other studies, including [24] have also been used here in terms of informing about foraging behaviours among copepods which the previous two research studies do not address. The suggestion from all the studies is that a number of different interactions exist within the ecosystem in relation to foraging and predation. The most important factors to consider are those such as DMS production and its role in copepod foraging as it manifests at different spatial scales.

The incorporation of infochemical-mediated interactions into ecosystem models is an important extension of this topic. This allows the analysis to account for chemically-mediated interactions. By integrating an analysis of chemical-mediated interactions into the analysis of the models, it became possible to investigate the changes in the functioning of marine food-webs. This also increased the accuracy of the forecasts we could make with these models when applying them to the investigation of the impact of phytoplankton bloom formation on the marine food web.

8.2 Novel Research Finding

We have also discussed a number of assumptions and limitations associated with the work in this thesis.

- **Chapter 4**: Bloom Formation and the Hydra Effect in non-Spatial Infochemical-Mediated Plankton Models.

  We analysed the system of equations which was studied in [143] by looking at a key fact concerning the coexistence equilibrium solution – that only one state is stable when $0.033512 < \nu < 0.051$. Therefore, the system has fourcommon topologically different regions as clarified in Fig.4.3 in Sec.4.3.3 (the general stability diagram after performing the bifurcation related to two main parameters). Furthermore we show that if the net effect of the infochemical-mediated interactions is large enough ($\nu > 0.0335$) then the system changes from an unstable to a stable system through a Hopf bifurcation.

  The presence of infochemicals can act to stabilize an otherwise unstable food-web. This is described in the work of [193] who highlighted the idea that infochemical-mediated interactions are critical for stabilizing the marine wood web. Several cases for different $K's$ have been presented in this chapter, as in Fig. 4.3 and as discussed in section4.3.3. We study the hydra effect in the predator-prey model, Figure 4.6, to show the system maximum P_e and M_e, for the parameters for different values of K and ν. Fig. 4.6(a) in Sec. 4.3.6 shows when and how persistently phytoplankton blooms occur given the effect of nutrient limitation on the system, while Fig. 4.6(b) represents the microzooplankton hydra effect w.r.t a small range of info–chemicalν loads and of K, the carrying capacity.

- **Chapter 5**: The Transient Turing in the spatial infochemical- mediated plankton model.

  In Chapter 5, we studied the quantitative analysis of the non-local interactions using the Turing mechanism. We studied the dynamical behaviour of the spatio temporal system. Based on the work of [143], we observed the oscillation processes in the marine ecosystem which are critical to the understanding of phytoplankton bloom formation. We observed, in Sec. 5.5.1, that when the rate of interaction, i.e., U_e, crosses its threshold value both species populations start oscillating around the interior equilibrium. The above result was shown numerically in Chapter 4 in Sec. 4.3.3 for different values of U_e. Spatial patterns can arise in correspondence with those modes, w, for which $Re(\delta) > 0$. Since (U_e) is stable for the reaction system, then $tr(w) < 0$ and $Det(J) > 0$. The solution of the system becomes unstable when

the prey diffusivity is set to $D_p = 0.02$; this will lead us to an unstable area under the stability curve in Fig. 5.1 in Sec. 5.5.3. For example, in Fig (5.2), we have a stable focus point when $K = 120$ and $\nu = 0.037$. The solution of the system becomes unstable when the prey diffusivity is set to $D_p = 0.02$; this will lead us to an unstable area under the stability curve. When choosing another value for ν in order to reach another, corresponding, equilibrium point, e.g., choosing $\nu = 0.05$ and its corresponding equilibrium point, we find that this is also stable, but $D_p = 0.12$, which means that the area above the stability curve is stable. We found that because of the cubic interaction in the temporal system and its corresponding roots, the region can exhibit another stability, which we call the Transient Turing, which lies in between the two stability curves, as shown in Fig. 5.1 in Sec. 5.5.3.

- **Chapter 6**: Infochemical-mediated PMZC plankton model.

  In chapter 6, we constructed the four species model, deriving this from the model presented in Chapter 4, which in turn is based on the model of [143]. We found the system exhibits five equilibrium points and all of them are hyperbolic. Also, this chapter (Chapter 6) presents the developed two species PM model. This is looked at in relation to [143] who mentioned the role of DMS in trophic interactions. It is shown that there exists a limit cycle with respect to the chemical release, ζ, in the spatially homogeneous system, as shown in Fig.6.5 in Sec.6.6.2. We introduce higher trophic species into the PM model and we modeled a prey defense mechanism infochemical cue produced through microzooplankton grazing. Increasing the value of the carrying capacity, K, in the four species model led to a loss of stability, and this is what has been termed the paradox of enrichment. The paradox was introduced to describe such an effect in six predatorprey models proposed by Michael Rosenzweig. The argument was that when food availability increases, a destabilization of the predator's population is experienced [193], as mentioned in detail in Chapter 3 Section 3.2. We compared our results, numerically and analytically, using asymptotic expansion analysis and we found that both approaches are consistent with each other, as shown in Fig. 6.1 in Sec.6.5. Also, we have studied the stability of the PMZC system using different parameter values. The PMZC model displays a region of instability near the Hopf bifurcations when $K = 20$, $r = 4.455$, $\zeta = 0.01$ and $\omega = 0.01$, as is shown in Table 6.3 in Sec.6.6.3. However, the model does not exhibit any behaviour which accords with the enrichment paradox. While increasing the prey

carrying capacity does take the system through a region of instability, the presence of a higher predator causes the system to be unstable for larger values of K, at least for the parameter values for which Fig. 6.7in Sec.6.6.3 was generated.

- **Chapter 7**: Non Turing Patterns in PMZC Plankton Model.

  In chapter 7 we also studied a quantitative analysis of the four species spatial model which used a Turing mechanism. We used Routh Hurwitzs criteria to aid in this analysis but the patterns formation condition didnt apply here. Therefore, we called this chapter the non-Turing patterns of the PMZC model. The dynamics of spatially inhomogeneous aquatic communities is illustrated in chapter 7. We studied Turing instability in relation to the *PMZC* model using Routh Hurwitzs criteria [15]. This study was based on other work, including [143], who argued that the marine food web is controlled through volatile infochemicals, among them dimethylsulphide (DMS). The understanding is that the structuring and functioning of the interaction among the inhomogeneous aquatic communities is dependent on these infochemicals. The Turing criteria did not hold in this study because the coexistence point, E_4, possess four eigenvalues and two of these represent unstable foci, with $Re(\lambda) > 0$, and the other two are stable sinks, as shown in Sec. 6.3 in Table 7.1. Different patterns may be obtained by setting different initial conditions and using different numerical methods. However, we have addressed the issue of non-Turing patterns in Figs. 7.6 and 7.7 in Sec.7.3, by using different initial conditions for the reaction-diffusion PMZC model in relation to both one and two dimensions. The population densities of all the species show oscillatory solutions, see Fig. 7.6. Systematic analyses in relation to one dimension (Figs. 7.3) and two dimensions (Fig. 7.6) can prove the validity of the persistent oscillation that we already saw in the spatially homogeneous model and could also show the consistency between the density and the average.

8.3 Discussion

In this discussion the analysis was aimed at linking the behaviours of the phytoplankton and copepods. The observation was that the microzooplankton is the main link between the two other species. The models were

also used to further discuss the copepods predatory behaviour. In relation to this, it was observed that 10−40% of primary productivity among the copepods results from consumption across a range of marine ecosystems. It is also observed that copepods prefer microzooplankton, in terms of their predation and foraging, because this source is nutritionally superior. However, the copepods also rely on the small phytoplankton species when these are present at high densities. Therefore, copepod- phytoplankton predation is an important topic for discussion in relation to understanding the interactions within the marine ecosystem. We have also extended the model of [143] for the purposes of exploring spatial diffusion in the horizontal plane. We have highlighted the regions of parameter space wherein a Turing instability can occur and have illustrated how periodic spatial patterns develop within the system. We have also demonstrated that time-dependent spatial patterns can develop which lead to the possibility of transient Turing "Eckhaus instability" (i.e., temporally unstable spatial patterns). From such a model, new observations of copepod foraging can be made. Many, if not all, the previous work in this area considers vertical motility, and [156] defined the vertical movements up and down the water column in response to seasonal changes in marine dynamics as vertical migration. In this thesis (and see, e.g., [115, 209, 255, 256]), our spatial analysis looks at horizontal movement. One particularly original result that we have presented here is the observation of localised solutions which, in biological terms, may indicate the presence of hotspots (i.e., where phytoplankton and/or microzooplankton are abundant in localised areas). Such observations are possible mainly because the model is considered to be in an infinite domain, whereas bounded domain models have been used to investigate vertical motility. Our study can serve as a blueprint, in a very significant way, for the analytic investigation of the dynamics relatively close to bifurcation points; this is addressed as future work. It will be interesting to study the existence and stability of hotspot and coldspot solutions using geometric techniques, as employed in, e.g., [101, 102].

It is also important to note that the spatiality in (5.1) was introduced by quite crudely inserting dispersions into the simple model proposed in [143]. At this stage, we have not analysed the precedence of the dispersion coefficients, as compared to the other parameter values, in terms of being biologically and physically relevant, though mathematically they can always be scaled out. Also, our model is constructed on the assumption of a stable copepod population. Such assumptions and limitations are addressed as future work, which include, e.g., a more realistic model extension.

8.3.1 Closing remarks

Chemical cues are very clearly crucial to the various different mechanisms which support the marine food web. However, in the literature, a detailed understanding of the chemosensory systems involved is not apparent. The info chemicals have not been characterised well, nor has the way in which these chemicals affect the foraging behaviour of planktonic organisms. Thus, the mechanisms are not adequately understood, and the nature of the trophic interactions which occur between the different marine species has not been fully resolved. However, it is known that infochemical release have an impact on the behavioural responses of these various organisms. Given this observation, it may be projected that, based on the current results, a clear comprehension of the effects of this chemical release on the four trophic interactions, as presented in Chapters 6 and 7, may emerge. This will be critical to our understanding of the various different dynamics of the planktonic food webs. Furthermore, from a mathematical point of view, the oscillatory behaviour of the plankton population (observed as a response over time and space to the infochemical release) may be comprehensively investigated via our four species model.

8.4 Future Work

In this section, a variety of proposed plankton models are presented in order to illustrate a number of different ideas concerning how to develop and investigate the plankton model.

- Time Delay Plankton Model.

  In order to further our understanding of the complex dynamics of ecological systems, a time delay can be applied to plankton models so that we can examine some real dynamical behaviours which occur within biological systems [162]. A time delay has been used to show the impact of the zooplankton maturation period on plankton dynamics. The findings by [188] indicate that a time lag of T_1 representing the zooplankton maturation period results in a change in plankton dynamics. A time delay has also been used as a bifurcation parameter in the analysis of ecosystem stability. A research study by [16] indicated that the stability of an ecosystem is denoted by a lower value in time delay as compared to a critical value. The instability in the system occurs when the delay value is relatively high. First we could

propose a model, using a time delay, for studying plankton populations, and then we could compare the results obtained with the results yielded by the previously studied model in Eqs. 4.1 and 4.2 in Chapter four. A plankton time delay model is given by Eqs. 8.1 and 8.2.

$$\frac{\partial \overline{U}}{\partial t} = F_i(\overline{U}), \tag{8.1}$$

where F_i, $(i = 1, 2)$ is the interaction function given by:

$$\begin{aligned} F1(P, M) &= rP(t-\tau)(1 - \frac{P(t-\tau)}{k}) - \frac{aP(t-\tau)M(t-\tau)}{(1 + bP(t-\tau))} + D_P\nabla^2 P, \\ F2(P, M) &= \frac{(\gamma aP(t-\tau))}{(1 + bp(t-\tau))} - mM(t-\tau) - \frac{(vaP(t-\tau)M(t-\tau)^2)}{(1 + bp(t-\tau))} + D_M\nabla^2 M. \end{aligned} \tag{8.2}$$

- The Beddington–DeAngelis Functional Response in Plankton Models.

Understanding the dynamical relationships between prey and the predator is important for explaining the dynamics of an ecosystem. The BeddingtonDeAngelis functional response plays a critical role in modeling plankton. It is an advance on the prey-dependent Holling's type II functional response. It can be used to explain the predators per capita feeding rates on prey [204]. This functional response can also be used to provide better descriptions of predatorprey abundances and how these affect predator feeding. [212] discussed that in their predatorprey system, BeddingtonDeAngelis was used to describe mutual interference by predators within the ecosystem. In relation to this, the concept was used to highlight the effect of changes in prey density on the predator density attached per unit time [204]. Further investigation by [100] found that in plankton models, the BeddingtonDeAngelis functional response can be used to perform a detailed mathematical analysis of the intra-specific competition among predators. An important topic for future research would be to study the effects of changing the functional response type of the model in [143] and of the PMZC model developed here.

$$F1(P,M) = rP(1-\frac{P}{k}) - \frac{aPM}{(b+P+EM)} + D_P\nabla^2 P$$
$$F2(P,M) = \frac{(\gamma aPM)}{(b+P+EM)} - mM - \frac{(vaPM^2)}{(b+P+EM)} + D_M\nabla^2 M \tag{8.3}$$

where t denotes time and P and M stand for prey and predator density, respectively. All parameters are positive constants: r stands for the maximum per capita growth rate of the prey; a, the capture rate; m, the predator death rate; E, a predator interference parameter; and K, the carrying capacity (which is the nonzero equilibrium population size). The diffusion coefficients are denoted by D_P and D_M, respectively. $\nabla^2 = \frac{\partial}{\partial^2 x} + \frac{\partial}{\partial^2 y}$ is the usual Laplacian operator for two-dimensional space .

- Advection or Convection Diffusion Model

  The Convection –diffusion equation plays important roles in the modeling of several physical and biological phenomena where energy is transformed inside a physical system due to the two processes: convection and diffusion [235].

$$\nabla U_t = F_i(\overline{U}) + \nabla U + D_U\nabla^2 U,$$

One can consider the non-spatial (interaction) term, $F_i(\overline{U})$, $i = 1,2$ in Eqs. (8.4) as the interaction term of Eq.(8.3) or alternatively as the non- spatial model studied earlier in Chapter 3. $\nabla = \frac{\partial}{\partial x} + \frac{\partial}{\partial y}$ and $\nabla^2 = \frac{\partial}{\partial^2 x} + \frac{\partial}{\partial^2 y}$ is the usual Laplacian operator for two-dimensional space.

—

Appendix A

Mathematical Models for Population Growth and Basic Bifurcation Analysis

A.1 Exponential (Malthusian) Growth

The simplest and most naive population model is the exponential growth or 'homogeneous green gunk' model as it is described in [134]; [120] used it to describe individual population densities with a positive intrinsic growth rate. The exponential growth model is highly unrealistic because population can never tend to infinity. We can represent the single species model via exponential growth as follows:

$$\frac{dN}{dt} = rN. \tag{A.1.1}$$

Where N is the the density of a single species in a group, and where the individual rate of change is given by $\frac{1}{N}\frac{dN}{dt} = r$ r is the intrinsic growth rate, determined from the difference between the per capita birth and death rates [134].

$$N(t) = N_0 e^{(rt)}. \tag{A.1.2}$$

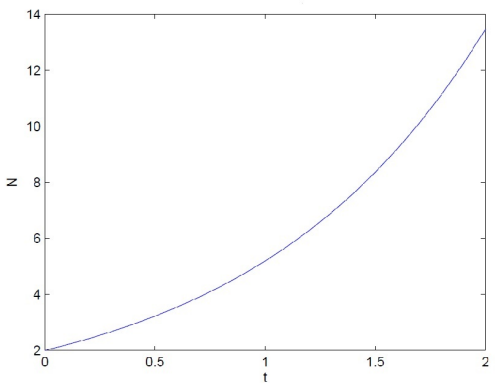

(a)

Figure A.1: *A population which grows at ever increasing rates: plot of Eq. (A.1.2) with r=1 , $N_0 = 2$ and time step (h=0.1).*

Fig. A.2(a) shows a population which grows continuously. Exponential (Malthusian) growth is considered to be ecologically unrealistic as it does not take into account any density-dependent effects [120], [134].

A.2 Logistic Model

The logistic model is a quadratic, rather than a linear, equation of population size; it is sometimes known as a Pearl-Verhulst equation [15]. This model is based on the common s-curve logistic function that shows how a population grows slowly, then rapidly, before de-escalating (peaking), as it reaches carrying capacity. The logistic function uses a differential equation that treats time as continuous as does the exponential model in the previous section. The logistic map instead uses a nonlinear difference equation to look at discrete time steps. It is called the logistic map because it maps the population value at any time step to its value at the next time step [129]; the following formula is for the logistic model:

$$\frac{dN}{dt} = rN(1 - \frac{N}{K}) \tag{A.2.3}$$

Where N represents the population at any given time t, and r represents the growth rate. In other words, the population level at any given time is a function of the growth rate parameter and the previous time steps population level. If the growth rate is set too low, the population will die out and go extinct. Higher growth rates may settle toward a stable value or fluctuate across a series of population blooms and busts. Equation A.2.3 defines the rules, or dynamics, of a single species system. This is a first order differential

equation which has two equilibrium points: when $N = 0$ and $N = K$. The linearized equation about the first equilibrium point is unstable, after considering small perturbations, around $N = 0$ s.t $N = N_0 + \widehat{N}$:

$$\frac{d\widehat{N}}{dt} = r\widehat{N} > 0 \tag{A.2.4}$$

In contrast, the linearized equation about K is asymptotically stable, because:

$$\frac{d\widehat{N}}{dt} = -r\widehat{N} < 0 \tag{A.2.5}$$

Fig. A.2 represents a numerical solution of the logistic model, determined by using the finite difference method.

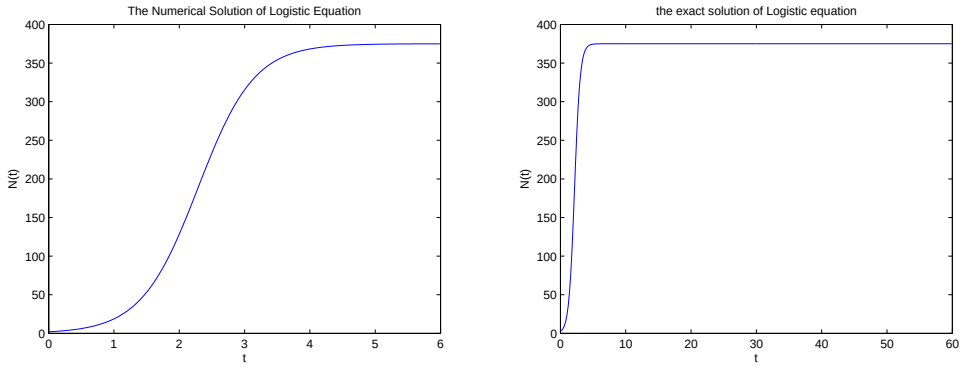

(a)

Figure A.2: *Logistic equation: the numerical and the analytic solution in relation to a growth rate* $r = 2.31$*, and a carrying capacity* $K = 375$*; the initial population growth is* $N_0 = 2$*.*

The logistic equation is used to describe the growth terms of many different models [120]. Moreover, the population level at any given time is a function of the growth rate parameter and the previous time steps population level. If the growth rate is set too low, the population will die out and go extinct. Higher growth rates may settle toward a stable value or fluctuate across a series of population blooms and busts.

A.3 Prey-Predator Population Model

The Lotka Volterra model and its modification will be considered as a two species ecological model, the model's name belongs to the authors: Volterra, who based his considerations on the unexpected results of the

biologist D'Ancona (1954) in relation to the fishing catches in the Adriatic sea after the first world war [151]. In this model only two populations are accounted for, the prey and the predator populations, denoted by $N(t)$ and $P(t)$, respectively; the predators are assumed to have sources of food other than the prey. In the absence of interactions, the two populations would grow independently as follows [151]:

$$\frac{dN}{dt} = aN - bNP, \tag{A.3.6}$$

$$\frac{dP}{dt} = cNP - dP, \tag{A.3.7}$$

where all the constants a, b, c and d are positive.

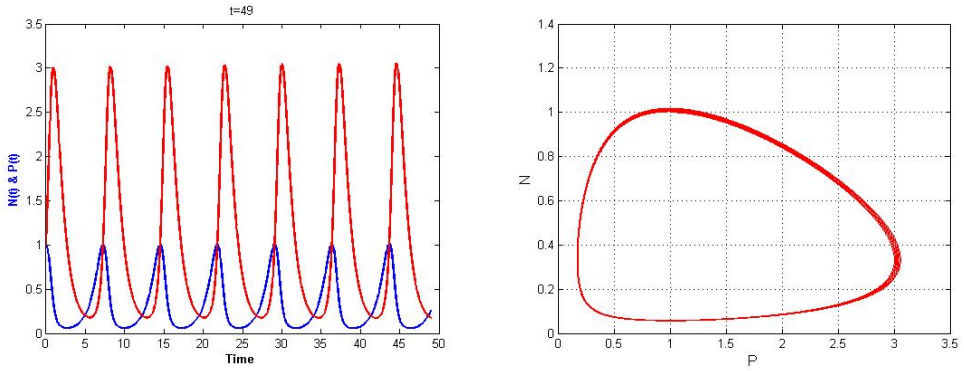

(a) (b)

Figure A.3: *A.3(a) is a time-dynamics (trajectories) analysis of the Lotka Voltera model Eq.A.3.7 with* $a = b = d = 1$ *and* $c = 3$*, and the initial condition* $N_0 = P_0 = 1$*. A.3(b) is a phase portrait of the Lotka Volterra model, using Maple-*18 *to show the equilibrium point* $(1, 1)$ *is at the centre with a pair of complex conjugate eigenvalues.*

This model makes the following assumptions:

- In the absence of any predation, the prey population grows unboundedly in a Malthusian manner (i.e., via the aN term in Eq. A.3.7.
- Predation reduces the per capita growth rate of the prey population by a term proportional to the prey and predator populations (i.e., the $-bNP$ term in Eq. A.3.7).
- The predator population decreases exponentially in the absence of any prey (i.e., via the $-dP$ term in Eq. A.3.7).

- The prey's contribution to the predator's growth rate is cNP; it is proportional to the available prey population as well as the size of the predator population. The NP terms represent a conversion of energy from the prey population to the predator.

A first step in analysing the system is to rescale the model by writing:

$$u(\tau) = \frac{cN(t)}{d}, \qquad v(\tau) = \frac{bp(t)}{a}, \tau = at, \qquad \alpha = \frac{d}{a}, \tag{A.3.8}$$

and then the Lotka-Volterra equations in Eq. (A.3.7), become

$$\frac{du}{d\tau} = u(1-v) = u - uv, \tag{A.3.9}$$

$$\frac{dv}{d\tau} = \alpha v(u-1) = \alpha uv - \alpha v. \tag{A.3.10}$$

In (u, v) phase space, the trajectory curves for this particular system can be written:

$$\frac{dv}{du} = \alpha \frac{v(u-1)}{u(1-v)}, \tag{A.3.11}$$

after solving this system by separate and integrate variables, [111], [120], we obtain exactly the following form:

$$\alpha u + v - \ln(u^{\alpha} v) = H, \tag{A.3.12}$$

where H is a fixed constant determined by initial conditions, $u(0)$ and $v(0)$. If $(u, v) = (1, 1)$, then Eq. (A.3.12) is at a minimum, $H_m = 1 + \alpha$. There are slightly different solution curves in the (u, v) space for different values of $H > H_m$. The solution curves must be closed and bounded to satisfy Eq. (A.3.12), and hence Eq.(A.3.10) is known as a maintained system [134]; this is because the constant, H, is conserved along a solution trajectory [111]. Having an equilibrium point with a centre means that we can expect periodic solutions oscillating around $(u, v) = (1, 1)$. One way in which this can happen is through a bifurcation process called a Hopf bifurcation in which a parameter passes through a critical value and there is then a change from equilibrium solutions to periodic solutions [120], [15].

A.4 The Classical Holling-Tanner model (Michael Menten)

Holling described three different functional response curves, the functional response (Solomon, 1949) is the rate at which each predator captures prey [134].

The **Holling type I** functional response is a linear relationship between the number of prey consumed per predator per unit time and the prey density, the result may increase up to some fixed maximum or it may increase indefinitely, Figs. A.4 in A.4(a) illustrates this.

$$\Phi(N) = cN \tag{A.4.13}$$

Holling type II Functional response is a hyperbolic function that saturates because of the time it takes to handle prey. One could be written as:

$$\Phi(N) = \frac{cN}{a + N} \tag{A.4.14}$$

a is referred to as the *half-saturation* constant, which is the carrying capacity divided by two $a = \frac{K}{2}$ Fig. A.4 in A.4(b) illustrates this.

Holling type III

$$\Phi(N) = \frac{cN^2}{a^2 + N^2} \tag{A.4.15}$$

this is a ”sigmoidal” curve that implements inefficient predators foraging at low prey densities. This functional response is highly appropriate for predators that must encounter enough prey to form a ’search image’ [134], Fig. A.4 in A.4(c) illustrates this. The following figures represent the first type of Holling functional response:

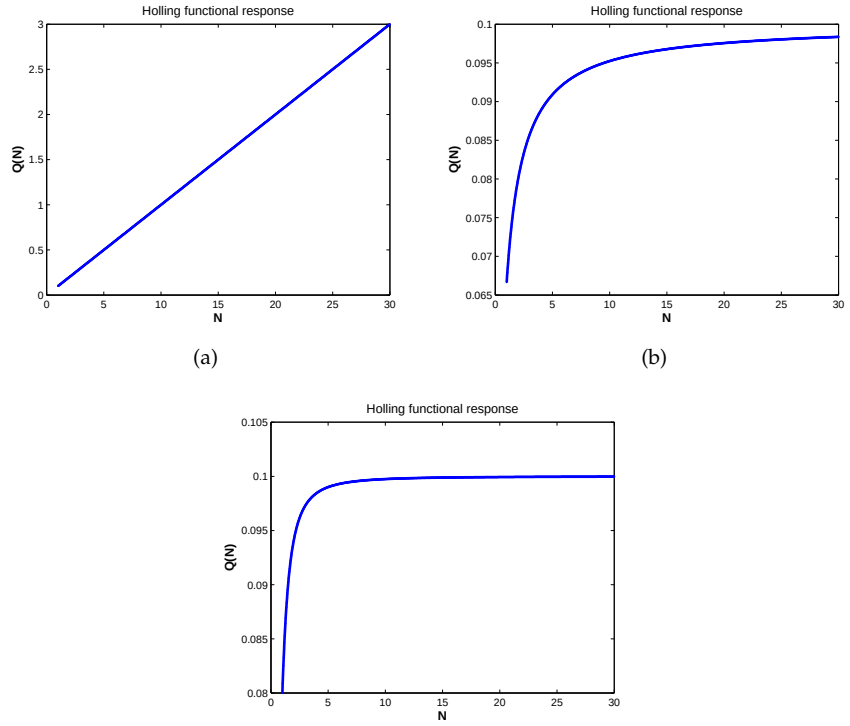

Figure A.4: *Holling functional response type-1, 2 and 3 when* $N \in [1, 30]$ *,* $a = 0.5$ *and* $c = 0.1$.

A.5 Local bifurcation theory

To study local bifurcation is to study the long term behaviour of a system of equations. When a small smooth change made to the parameter values (the bifurcation parameters) of a system causes a sudden 'qualitative' change in its behaviour, this leads the stability of an equilibrium (or fixed point) to change [154]. When a slight change in parameter values causes a drastic, qualitative change in the systems behaviour this is bifurcation and the values around which this change occurs are called critical thresholds. There are many different kinds of Bifurcation. Generically, bifurcation (such as Hopf and cusp bifurcatuion) appears in codimension-two manifolds in the parameter space. A manifold is a topological space that is locally Euclidean (i.e., around every point, there is a neighborhood that is topologically the same as the open unit ball in R^n). The concept of a manifold is central to many topics in geometry and modern mathematical physics because it allows complicated structures to be described and understood in terms of the simpler, local topological properties of a Euclidean space [111], [210]. There are many different types of bifurcation, the following are the types that we study in this thesis:

- Saddle-node bifurcation.
- Cusp bifurcation.
- Hopf bifurcation.

Simple examples of the first three types of local bifurcation will be presented by using some relatively simple equations, see [248], [10], [1] for more details.

A.5.1 The saddle-node bifurcation

Consider the dynamical system defined by:

$$\frac{dx}{dt} = a - x^2 \tag{A.5.16}$$

where a,x are real and a is a control parameter that can be changed externally. The solution at the steady state, x_e, is as follows: $x = x_e = \pm\sqrt{a}$ therefore, for different values of a we have:

- $a < 0$ we have no real solutions.
- $a > 0$ we have two real solutions.

If we consider $a > 0$, an analysis of linear stability can be used to examine the systems stability in the usual way. Firstly, we add a small perturbation: $x = x_e + \widehat{x}$. Substitute into Eq. (A.5.16) to get:

$$\frac{d\widehat{x}}{dt} = (a - x_e^2) - 2x_e\widehat{x} - \widehat{x}^2$$

The first term on the RHS is equal to zero. Thus, we will have

$$\frac{d\widehat{x}}{dt} = -2x_e\widehat{x}$$

with solution:

$$\widehat{x} = Ae^{(-2x_e t)}$$

. From this, we see that:

- for $x_e = +\sqrt{a}, \widehat{|x|} \rightarrow 0$as $t \rightarrow \infty$(linear stability).

- for $x_e = -\sqrt{a}, \widehat{|x|} \rightarrow \infty$as $t \rightarrow \infty$(linear stability).

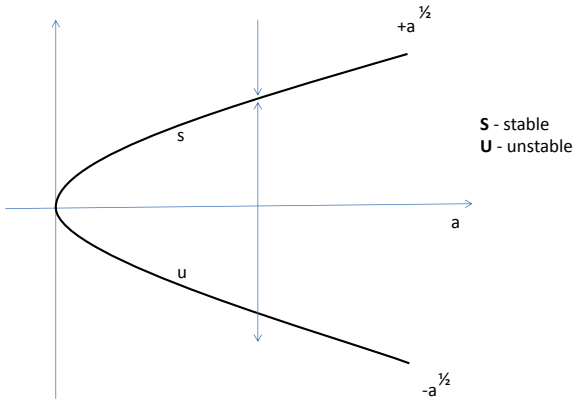

Figure A.5: *Saddle-node bifurcation diagram .*

Fig. A.5 shows the saddle node bifurcation at $a = 0$ corresponding to the two solution branches, one is linearly stable and the other is linearly unstable [248], [10].

A.5.2 Cusp bifurcation

A cusp bifurcation is a bifurcation of equilibria in a two-parameter family of autonomous *ODEs* Eq .(A.5.17) at which the critical equilibrium has one zero eigenvalue and the quadratic coefficient for the saddle-node bifurcation vanishes [89].

$$\dot{x} = f(x, \alpha). \tag{A.5.17}$$

At the cusp bifurcation point two branches of the saddle-node bifurcation curve meet tangentially, forming a semi-cubic parabola. For nearby parameter values, the system can have three equilibria which collide and disappear pairwise via the saddle-node bifurcations. The cusp bifurcation implies the presence of a hysteresis phenomenon. Cusp bifurcation may occur in its simplest form in a one-dimensional state space

with a two-dimensional parameter space. A simple, model differential equation for the cusp bifurcation is in the cubic [103]:

$$f(x, \alpha) = x^3 + \alpha x + \beta, \tag{A.5.18}$$

where $x \in \mathfrak{R}$ and α, β are the bifurcation parameters. This differential equation has equilibrium points which lie on a two-dimensional manifold $M \in \mathfrak{R} \times \mathfrak{R}^2$ given by:

$$M = \{(x, \alpha, \beta) | x^3 + \alpha x + \beta = 0\} \tag{A.5.19}$$

We call this manifold, M, the cusp manifold. The cusp bifurcation variety, consists of two algebraic curves in the parameter plane meeting tangentially at the cusp point $(0, 0)$, the result of cusp bifurcation is presented in chapter three.

A.5.3 Hopf Bifurcation

Consider the dynamical system:

$$\frac{dx}{dt} = -y + (a - x^2 - y^2)x \tag{A.5.20}$$

$$\frac{dy}{dt} = x + (a - x^2 - y^2)y. \tag{A.5.21}$$

for real x, y, a. The first trivial steady state at $x = y = 0$. Using the same process to examine the linear stability, we write $x = 0 + \widehat{x}, y = 0 + \widehat{y}$. Substituting this into the main equation, and linearising, we get:

$$\frac{d\widehat{x}}{dt} = -\widehat{y} + a\widehat{x} \tag{A.5.22}$$

$$\frac{d\widehat{y}}{dt} = \widehat{x} + a\widehat{y} \tag{A.5.23}$$

$$\tag{A.5.24}$$

The solution of these linearised equations has the following form:

$$\begin{pmatrix} \widehat{x} \\ \widehat{y} \end{pmatrix} = \begin{pmatrix} \alpha \\ \beta \end{pmatrix} e^{(st)} + c.c \tag{A.5.25}$$

Substituting this Eq. (A.5.24) to find the eigenvalue s and the eigenvector (α, β) to be determined by the following system of linear equations.

$$\alpha s = -\beta + a\alpha \tag{A.5.26}$$

$$\beta s = \alpha + a\beta. \tag{A.5.27}$$

After eliminating α and β, we will get the characteristic equation of s at any a:

$$s^2 - 2as + (a^2 + 1) = 0$$

. depending on this equation, we can determine the eigenvalue:

$$s = a \pm i$$

We can easily determine the corresponding eigenvector (α, β) by substituting the eigenvalues back into Eq. (A.5.27). From Eq. (A.5.25) and the eigenvalue equation, we can see:

- If $a > 0$ then $\Re(s) > 0$ and so $|\widehat{x}|, |\widehat{y}| \to \infty$ (Linear instability).
- If $a < 0$ then $\Re(s) < 0$ and so $|\widehat{x}|, |\widehat{y}| \to 0$ (linear stability).

Which means, that for $a < 0$, the progress of $\widehat{x}$ and $\widehat{y}$ towards the origin is via a damped oscillation, as sketched in Fig. A.6.

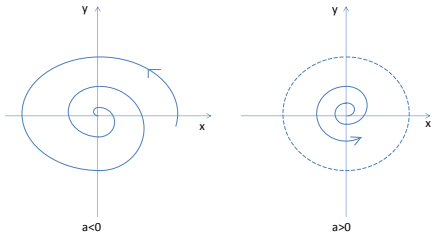

Figure A.6: *Hopf bifurcation for $a < 0$ and the dashed line in the right hand side represents the limit cycle.*

If $a > 0$, we will have a periodic solution.

$$x = \sqrt{a}\cos(t + t_0) \tag{A.5.28}$$

$$y = \sqrt{a}\sin(t + t_0) \tag{A.5.29}$$

Figure(A.7) represent Hopf-bifurcation diagram as follows:

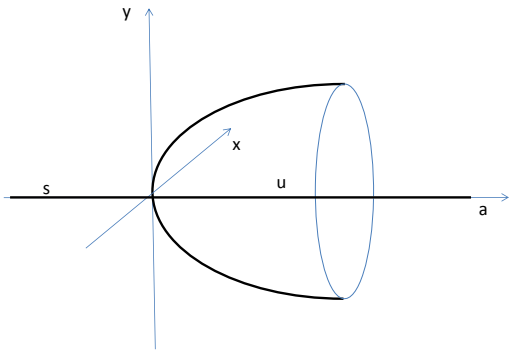

Figure A.7: *Hopf bifurcation diagram.*

Finally, a Hopf bifurcation can be classified as either supercritical or subcritical depending on the system stability type, [248], [10].

A.6 Reaction Diffusion (Turing) Mechanisms in Prey Predator Models

The non-linear evolution equations and their linear stability analysis will be discussed in detail in this section, Chemicals can react and diffuse under certain conditions to produce steady state heterogeneous spatial patterns of chemical or morphogen concentrations, as Alan Turing (1952) discussed [49],

$$\frac{\partial U}{\partial t} = f(U) + D\nabla^2 U \tag{A.6.30}$$

where U is the vector of morphogen concentration, f represent the reaction kinetic and D is the diagonal matrix of the positive constant diffusion coefficient [121]. Reaction diffusion systems are perhaps the easiest to study mathematically of the many experimental systems considered [15]. Reaction diffusion systems are a broad and important class of non-equilibrium systems, used in biology, chemistry ecology, and engineering. The Turing instability analysis examined, analytically, the linear stability of the simplest possible reaction-diffusion system. This analysis led to several insights concerning what forms a uniform state, some were unexpected [49]; they are as follows:

- At least two interacting chemicals are needed in order to form a pattern.
- Diffusion can be a destabilizing influence in reacting chemical systems.
- Instability caused by diffusion can cause the growth of a structure at a particular wave length, such as the segmentation patterns in the developing fly embryo or zebra stripes.
- Pattern formation in a chemical system will not occur unless the diffusion coefficient of at least two reagents differ substantially.

  A Turing model for two reacting and diffusing chemicals takes the form:

$$\frac{\partial u_1}{\partial t} = f_1(u_1, u_2) + D_1 \frac{\partial {u_1}^2}{\partial x^2}, \tag{A.6.31}$$

$$\frac{\partial u_2}{\partial t} = f_2(u_1, u_2) + D_2 \frac{\partial {u_2}^2}{\partial x^2}, \tag{A.6.32}$$

where $0 < x < L$. Eq's.(A.6.32) and (A.6.32) in a vector form similar to Eq. (A.6.30).

$$\frac{\partial u}{\partial t} = f(u) + D\frac{\partial u^2}{\partial x^2} \tag{A.6.33}$$

with Neumann BC's:

$$\frac{\partial u_1(0,t)}{\partial x} = 0, \tag{A.6.34}$$

$$\frac{\partial u_2(L,t)}{\partial x} = 0, \tag{A.6.35}$$

and IC:

$u_1(0,x) = f_0(x)$,

$u_2(0,x) = f_0(x)$.

The first two equations describe the evolution of two concentration fields, $u_i(t,x)$, along the real line $-\infty < x < \infty$. The nonlinear functions $f_1(u_1,u_2)$ are the reaction rates of the two chemicals while D_i, $(i = 1,2)$ are the corresponding diffusion coefficients [15]. The simplest possible model is obtained by assuming that there is no prior spatiotemporal structure in the system so that the function f_i and the diffusion coefficients D_i do not depend explicitly on time, t, or on position, x. For simplicity, we further assume that the diffusion coefficients are constant and so do not depend on the field values u_i [15]. These assumptions are considered reasonable for many experiment situations.

Where:

$$J = \begin{pmatrix} a_{11} & a_{12} \\ a_{21} & a_{22} \end{pmatrix}_{(u_{1e},u_{2e})} \tag{A.6.36}$$

is a Jacobian matrix, and a_{ij} are its elements, represented by partial derivatives of Eqs. (A.6.32) and (A.6.32) and (u_{1e},u_{2e}) is the system equilibria. The stability require that in the absence of diffusion the system is stable. This is equivalent to $Re(\lambda(0)) < 0$, as setting $k^2 = 0$ removes the diffusion term in equation, where k^2 is the

wave number [1], [121]. We have $\lambda(0)$ satisfies

$$\lambda(0)^2 + (a_{11} + a_{22})\lambda(0) + (a_{11}a_{22} - a_{12}a_{21}) = 0. \tag{A.6.37}$$

The stability without diffusion depends on $trace(J)$ and $\det(J)$ such that:

$$trace(J) = a_{11} + a_{22} < 0, \tag{A.6.38}$$

$$\det(J) = a_{11}a_{22} - a_{12}a_{21} > 0, \tag{A.6.39}$$

when diffusion present the stability require $\lambda(k^2) > 0$, We have that $\lambda(k^2)$ satisfies

$$\lambda(k)^2 + (D_1 + D_2)k^2 - (a_{11} + a_{22})\lambda(k) + H(k^2) = 0. \tag{A.6.40}$$

Where

$$H(k^2) = D_1D_2k^4 - (D_1a_{22} + D_2a_{11})k^2 + (a_{11}a_{22} - a_{12}a_{21}) < 0 \tag{A.6.41}$$

after several steps we can derive the diffusion length from Eq. (A.6.41), where $l_1 = \sqrt{\frac{D_1}{a_{11}}}$ and $l_2 = \sqrt{\frac{D_2}{-a_{22}}}$. in the form

$$k^2 = \frac{1}{2}\left(\frac{1}{l_1^2} - \frac{1}{l_2^2}\right) \tag{A.6.42}$$

This implies that the length l_2 must be sufficiently larger than the length l_1. Having Jacobian element $a_{11} > 0$ implies that chemical 1 enhances its own instability and so could be called an *activator*. Similarly when $a_{22} < 0$, chemical 2 inhibits its own growth and could be called an *inhibitor*. The necessary condition $l_2 > l_1$ for Turing instability is then sometimes referred to as **(Local activation with long range inhibition)** and have an equivalent form such that

$$\frac{D_2}{D_1} > (\frac{-a_{22}}{a_{11}}) \tag{A.6.43}$$

Which means that the diffusion coefficient D_2 of the inhibitor has to exceed the diffusion coefficient D_1 by

[1] Is equal to 2π divided by the wavelength in meters, it is defined as the reciprocal of the wavelength in centimeters, as the wavelength grows shorter, the wave number becomes larger

the factor $(\frac{-a_{22}}{a_{11}})$.

A.6.1 Two spatial dimensions and finite domains

A two dimensional model will be considered in order to analyse more realistic geometries such as patterning on the skin of an animal, which have a finite length and width. The reaction diffusion system is generalized to include two spatial dimensions:

$$\frac{\partial U_1}{\partial t} = f(U_1, U_2) + D_1(\frac{\partial^2 U_1}{\partial x^2}) + (\frac{\partial^2 U_2}{\partial y^2}) \tag{A.6.44}$$

$$\frac{\partial U_2}{\partial t} = f(U_1, U_2) + D_2(\frac{\partial^2 U_1}{\partial x^2}) + (\frac{\partial^2 U_2}{\partial y^2}) \tag{A.6.45}$$

with Neumann BC's:

$$\frac{\partial U_1}{\partial x} = 0, \tag{A.6.46}$$

$$\frac{\partial U_2}{\partial x} = 0, \tag{A.6.47}$$

and IC: $U_1(0, x) = f_0(x)$,

$U_2(0, x) = f_0$,

Using the same criteria of the one spatial dimension, the system has a uniform steady state $(\overline{U_1}, \overline{U_2})$. We seek a solution of the form

$$U_i' = \alpha_i e^{\sigma t} \cos k_1 x \cos k_2 y$$

. non trivial solution should satisfy Neumann homogeneous boundary conditions, to obtain the following:

$$k_1 = m\pi/L_x \quad (m = 0, 1, 2, ...) \tag{A.6.48}$$

$$k_2 = n\pi/L_y \quad (n = 0, 1, 2, ...) \tag{A.6.49}$$

We now define

$$K^2 = k_1^2 + k_2^2$$

Turing's conditions in two dimensional are exactly the same as the one dimensional case, except that k^2.

$$a_{11} + a_{22} < 0, \qquad a_{11}a_{22} - a_{12}a_{21} \tag{A.6.50}$$

and

$$H^{2D} \equiv (a_{11} - D_1K^2)(a_{22} - D_2K^2) - a_{12}a_{21} < 0$$

which is the third condition of Turing instability and leads to:

$$a_{11}D_2 + a_{22}D_1 > 2(D_1D_2)^{1/2}(a_{11}a_{22} - a_{21}a_{12})^{1/2} > 0. \tag{A.6.51}$$

Thus, the instability criteria are unchanged as we go from $1-D$ to $2-D$ but the minimum of $H(2D)$ occurs at

$$K_{min}^2 = k_1^2 + k_2^2 = \pi^2\left(\frac{m^2}{L_x^2} + \frac{n^2}{L_y^2}\right) = \frac{1}{2}\left(\frac{a_{11}}{D_1} + \frac{a_{22}}{D_2}\right). \tag{A.6.52}$$

From Eq. (A.6.52), we now can conclude that patterns could arise at the onset of instability, and for more details see [121].

$$m^2 + \frac{n^2}{\gamma^2} = \frac{L_x^2 a_{11}}{2\pi^2 D_1}\left(1 + \frac{\eta}{\delta}\right) \tag{A.6.53}$$

where $\delta = D_2/D_1, \quad \eta = a_{22}/a_{11}, \quad \gamma = \frac{L_y}{L_x}$.

Eq. (A.6.53) is critically important: it clarifies that near the onset of instability, the pattern wave number depends on the size of the domain, though:

$$E^2 \propto \frac{\text{area of the domain}}{(\text{range of activation})^2}(1 - (\frac{\text{range of activation}}{\text{range of inhibition}})^2$$

Recall that $\sqrt{\frac{D_1}{|a_{11}|}}$ and $\sqrt{\frac{D_2}{|a_{22}|}}$ give ranges of activation and inhibition. The minus sign arises because $\eta < 0$.

Appendix B

Details of Chapter 4

B.1 The Coefficients of the Real Part of the Eigenvalue of the Coexistence Point.

$$\widehat{\beta} = C_1 P_e^6 + C_2 P_e^5 + C_3 P_e^4 + C_4 P_e^3 + C_5 P_e^2 + C_6 P_e + C_7 P_e. \tag{B.1.1}$$

Where $C_i, i = 1, 2, 3, 4, 5, 6$ are Cascading parameters, that have a hierarchical relationship, as shown:

$$C_1 = 4r^2 b^4 \tag{B.1.2}$$

$$C_2 = -4rb^4 Km + 16r^2 b^3 - 8rb^3 K\nu aM - 4r^2 b^4 K + 4rb^3 K\gamma a \tag{B.1.3}$$

$$\begin{aligned} C_3 = & -4K^2 b^2 \nu^2 a^2 M^2 - 2rK^2 b^4 m + K^2 b^4 m^2 - K^2 b^2 \gamma^2 a^2 + 24rb^2 K\nu aM \\ & + 24r^2 b^2 - 4rK^2 b^3 \nu aM + r^2 K^2 b^4 + 2rK^2 b^3 \gamma a - 16r^2 b^3 K \\ & - 4K^2 b^3 m\nu aM - 16rb^3 Km + 4K^2 b^2 \gamma a^2 \nu M - 12rb^2 K\gamma a \\ & + 2K^2 b^3 m\gamma a \end{aligned} \tag{B.1.4}$$

$$C_4 = 24rbKvaM - 12K^2b^2mvaM + 8K^2b\gamma a^2vM + 24rb^2Km - 24r^2b^2K - 8K^2bv^2a^2M^2 - 12Kb\gamma ar + 6K^2b^2m\gamma a - 8rK^2b^3m + 4rKb^2aM - 12rK^2b^2vaM + 6rK^2b^2\gamma a + 4r^2K^2b^3 + 2K^2b\gamma^2a^2 + 4K^2b^3m^2 + 16r^2b \tag{B.1.5}$$

$$C_5 = 2K^2b\gamma a^2M + 16rbKm + 4r^2 + 6r^2K^2b^2 - 16r^2bK + 4K^2\gamma a^2vM - 12K^2bvaMm + 8rKbaM + 4rK\gamma a - 12K^2bvaMr - 8rKvaM + 6K^2b\gamma ar + 2K^2b^2maM - 4K^2v^2a^2M^2 + 6K^2b\gamma am + 2rK^2b^2aM + K^2\gamma^2a^2 + 6K^2b^2m^2 - 12rK^2b^2m \tag{B.1.6}$$

$$C_6 = 2K^2\gamma am + 2K^2\gamma ar - 4K^2vaMm + 2a^2MK^2\gamma + 4rK^2baM - 4K^2vaMr - 4r^2K - 4rKm + 4r^2K^2b - 8K^2mbr + 4K^2mbaM + 4rKaM + 4K^2m^2b \tag{B.1.7}$$

$$C_7 = a^2M^2K^2 + r^2K^2 + 2rK^2m - 2aMK^2r - 2aMK^2m + K^2m^2 \tag{B.1.8}$$

B.2 Saddle Node Bifurcation Roots.

$$\nu_{Sd1} = \widehat{\omega} + \frac{2}{3}\sqrt{\frac{B^2}{A} - 3CD}\sin\left(\frac{\pi}{6} + \widehat{\theta_1}\right) \tag{B.2.9}$$

$$\nu_{Sd2} = \widehat{\omega} + \frac{2}{3}\sqrt{\frac{B^2}{A} - 3CD}\cos\left(\frac{\pi}{3} + \widehat{\theta_2}\right) \tag{B.2.10}$$

$$\nu_{Sd3} = \widehat{\omega} + \frac{2}{3}\sqrt{\frac{B^2}{A} - 3CD}\cos\left(\frac{\pi}{3} + \widehat{\theta_3}\right) \tag{B.2.11}$$

where $\widehat{\omega}$ and $\widehat{\theta}$ are as follows:

$$\widehat{\omega} = \frac{-B}{3A} \tag{B.2.12}$$

$$\widehat{\theta} = \frac{1}{3}\arccos\left(\frac{27}{2}\rho\right) \tag{B.2.13}$$

$$\rho = \left(\frac{B^3}{A^2} - \frac{DB - E}{3A}RA\right) \tag{B.2.14}$$

where $R = \sqrt{\frac{(B^2-3CD)^3}{A}}$ $f(v)$ in Eq.(4.18) depends on the following cascading (sequence of) parameters:

$$A = (-K^3b^2 - 2K^2b)r^3 \tag{B.2.15}$$

$$B = (2K^3b^3m - 2K^2b^2m - 8Kbm - 4m + 8K^2b\gamma a + 2K\gamma a + 2K^3b^2\gamma a)r^2 \tag{B.2.16}$$

$$\begin{aligned} C = (&-K^3b^4m^2 + 2K^3b^3\gamma am + 2K^2b^2\gamma am + 20\gamma aKbm + 8K^2b^3m^2 \\ &+ 8b^2m^2K - K^3b^2\gamma^2a^2 - \gamma^2a^2K - 10K^2b\gamma^2a^2)r \end{aligned} \tag{B.2.17}$$

$$D = 4b^4m^3K^2 - 12\gamma^2a^2K^2b^2m + 12\gamma aK^2b^3m^2 + 4\gamma^3a^3K^2b \tag{B.2.18}$$

Appendix C

Details of Chapter 6

C.1 The Coefficients of the Quartic Polynomial

The quartic polynomial given in Eq.6.13, has A_i, $i = 0, .., 4$ as cascading parameters given by:

$$A_0 = \gamma_2 b_1 \beta \eta r^2 + \zeta b_1 \beta \eta r^2 - b_1 b_2 \eta m_2 r^2,$$

$$\begin{aligned} A_1 = &-2\gamma_2 b_1 \beta \eta k r^2 - 2\zeta b_1 \beta \eta k r^2 + 2 b_1 b_2 \eta k m_2 r^2 - \gamma_2 b_1 \beta k \omega r - \zeta b_1 \beta k \omega r \\ &+ b_1 b_2 k m_2 \omega r + \gamma_2 \beta \eta r^2 + \zeta \beta \eta r^2 - b_2 \eta m_2 r^2, \end{aligned}$$

$$\begin{aligned} A_2 = &-\gamma_2 b_1 \beta \eta k^2 r^2 + \zeta b_1 \beta \eta k^2 r^2 - b_1 b_2 \eta k^2 m_2 r^2 + \gamma_2 b_1 \beta k^2 \omega r \\ &+ \zeta b_1 \beta k^2 \omega r - b_1 b_2 k^2 m_2 \omega r - \gamma_2 b_1 \beta k m_3 r - 2\gamma_2 \beta \eta k r^2 - 2\zeta \beta \eta k r^2 \\ &+ b_1 b_2 k m_2 m_3 r + 2 b_2 \eta k m_2 r^2 - \gamma_2 \beta k \omega r - \zeta \beta k \omega r + a \eta k m_2 r + b_2 k m_2 \omega r, \end{aligned}$$

$$A_3 = \gamma_2 b_1 \beta k^2 r m_3 + \gamma_2 \beta \eta k^2 r^2 + \zeta \beta \eta k^2 r^2 - b_1 b_2 k^2 r m_2 m_3 - b_2 \eta k^2 r^2 m_2 + \gamma_2 \beta k^2 \omega r + \zeta \beta k^2 \omega r - a \eta k^2 r m_2 - b_2 k^2 \omega r m_2 - \gamma_2 \beta k r m_3 - a k^2 \omega m_2 + b_2 k r m_2 m_3,$$

$$A_4 = \gamma_2 \beta k^2 m_3 r - b_2 k^2 m_2 m_3 r - a k^2 m_2 m_3,$$

The coefficient A, B and G in Eq.(6.14) are cascading parameters and shown:

$$A_5 = \zeta^2 \beta r b_1 b_2 m_2 m_3 - \zeta \beta^2 r \gamma_2^2 b_1 m_3 + 2\zeta \beta r \gamma_2 b_1 b_2 m_2 m_3 - \zeta r b_1 b_2^2 m_2^2 m_3 + \zeta^2 a \beta \eta r m_2 - \zeta^2 \beta^2 r b_1 m_3 + \zeta a \beta \eta r \gamma_2 m_2 - \zeta a \eta r b_2 m_2^2 - \zeta \beta^2 r \gamma_2 b_1 m_3 + \zeta \beta r b_1 b_2 m_2 m_3 - \zeta a \beta \eta r m_2 - a \beta \eta r \gamma_2 m_2 + a \eta r b_2 m_2^2$$

$$B = \zeta^2 \beta^2 K r \gamma_2 b_1 m_3 - \zeta^2 \beta K r b_1 b_2 m_2 m_3 + \zeta \beta^2 K r \gamma_2^2 b_1 m_3 - 2\zeta \beta K r \gamma_2 b_1 b_2 m_2 m_3 - \zeta^2 a \beta \eta K r m_2 - \zeta a \beta \eta K r \gamma_2 m_2 + \zeta a \eta K r b_2 m_2^2 + \zeta \beta^2 K r \gamma_2 b_1 m_3 - \zeta \beta K r b_1 b_2 m_2 m_3 - \zeta^2 a \beta K \omega m_2 - \zeta^2 \beta^2 r \gamma_2 m_3 - \zeta^2 \beta^2 r b_1 m_3 + \zeta^2 \beta r b_2 m_2 m_3 + \zeta a \beta \eta K r m_2 - \zeta a \beta K \omega \gamma_2 m_2 + \zeta a K \omega b_2 m_2^2 - \zeta \beta^2 r \gamma_2^2 m_3 + 2\zeta \beta r \gamma_2 b_2 m_2 m_3 - \zeta r b_2^2 m_2^2 m_3 + a \beta \eta K r \gamma_2 m_2 - a \eta K r b_2 m_2^2 - \zeta^2 \beta^2 r m_3 + \zeta a \beta K \omega m_2 - \zeta \beta^2 r \gamma_2 m_3 + \zeta \beta r b_2 m_2 m_3 + a \beta K \omega \gamma_2 m_2 - a K \omega b_2 m_2^2$$

$$G = \beta^2 K r \zeta^2 \gamma_2 m_3 - \beta K r \zeta^2 m_3 m_2 b_2 + \beta^2 K r \zeta \gamma_2^2 m_3 - 2\beta K r \zeta \gamma_2 m_3 m_2 b_2 + K r \zeta m_3 m_2^2 b_2^2 - a \beta K \zeta^2 m_3 m_2 + \beta^2 K r \zeta^2 m_3 - a \beta K \zeta \gamma_2 m_3 m_2 + a K \zeta m_3 m_2^2 b_2 + \beta^2 K r \zeta \gamma_2 m_3 - \beta K r \zeta m_3 m_2 b_2 + a \beta K \zeta m_3 m_2 + a \beta K \gamma_2 m_3 m_2 - a K m_3 m_2^2 b_2$$

C.2 Stability of the Steady-States in PMZC Model

The coefficient of Jacobian matrix in Sec.6.4.

$$a_{11} = r\frac{(1-2P_e)}{k} - \frac{aM_e}{(1+b_1P_e)} + \frac{aP_eM_eb_1}{(1+b_1P_e)^2}, \tag{C.2.1}$$

$$a_{12} = \frac{-aP_e}{(1+b_1P_e)}, \tag{C.2.2}$$

$$a_{21} = \frac{\gamma_1 aM_e}{(1+b_1P_e)} - \frac{\gamma_1 aP_eM_eb_1}{(1+b_1P_e)^2}, \tag{C.2.3}$$

$$\begin{aligned} a_{22} &= \frac{\gamma_1 aP_e}{(1+b_1P_e)} - m1 - \frac{\beta Z_e}{(1+b_2M_e)} + \frac{\beta Z_eM_eb_2}{(1+b_2M_e)^2} \\ &+ \frac{\beta Z\zeta C_e}{((1+C_e)(1+b_2M_e))} - \frac{\beta Z_eM_e\zeta C_eb_2}{((1+C_e)(1+b_2M_e)^2)}, \end{aligned} \tag{C.2.4}$$

$$a_{23} = \frac{-\beta M_e}{(1+b2M_e)} + \frac{\beta M_e\zeta C_e}{((1+C_e)(1+b_2M_e))}, \tag{C.2.5}$$

$$a_{24} = \frac{\beta Z_eM_e\zeta}{((1+C_e)(1+b_2M_e))} - \frac{\beta Z_eM_e\zeta C_e}{((1+C_e)^2(1+b_2M_e))}, \tag{C.2.6}$$

$$\begin{aligned} a_{32} &= \frac{\gamma_2\beta Z_e}{(1+b_2M_e)} - \frac{\gamma_2\beta Z_eM_eb_2}{(1+b_2M_e)^2} \\ &+ \frac{\beta Z_e\zeta C_e}{((1+C_e)(1+b_2M_e))} - \frac{\beta Z_eM_e\zeta C_eb_2}{((1+C_e)(1+b_2M_e)^2)}, \end{aligned} \tag{C.2.7}$$

$$a_{33} = \frac{\gamma_2\beta M_e}{(1+b_2M_e)} - \frac{\beta M_e\zeta C_e}{((1+C_e)(1+b_2M_e))} - m_2, \tag{C.2.8}$$

$$a_{34} = \frac{\beta Z_eM_e\zeta}{((1+C_e)(1+b_2M_e))} - \frac{\beta Z_eM_e\zeta C_e}{((1+C_e)^2(1+b_2M_e))}, \tag{C.2.9}$$

$$\begin{aligned} a_{41} &= \frac{\eta aM_e}{(1+b_1P_e} - \frac{\eta aP_eM_eb_1}{(1+b_1P_e)^2} + \omega, \\ a_{42} &= \frac{\eta aP_e}{(1+b_1P_e)}, \\ a_{44} &= -m_3. \end{aligned} \tag{C.2.10}$$

C.3 The Coefficient of the Copepod Free Equilibrium E_3

$$
\begin{aligned}
A = & -\gamma_1^4\gamma_2 a^3\beta k^2 m_3 r + \gamma_1^4 a^3 b_2 k^2 m_2 m_3 r + 3\gamma_1^3\gamma_2 a^2 b_1\beta k^2 m_1 m_3 r \\
& - \gamma_1^3\gamma_2 a^2\beta\eta k^2 m_1 r^2 - \gamma_1^3\zeta a^2\beta\eta k^2 m_1 r^2 \\
& - 3\gamma_1^3 a^2 b_1 b_2 k^2 m_1 m_2 m_3 r + \gamma_1^3 a^2 b_2\eta k^2 m_1 m_2 r^2 - 3\gamma_1^2\gamma_2 a b_1^2\beta k^2 m_1^2 m_3 r \\
& + 2\gamma_1^2\gamma_2 a b_1\beta\eta k^2 m_1^2 r^2 + 2\gamma_1^2\zeta a b_1\beta\eta k^2 m_1^2 r^2 \\
& + 3\gamma_1^2 a b_1^2 b_2 k^2 m_1^2 m_2 m_3 r - 2\gamma_1^2 a b_1 b_2\eta k^2 m_1^2 m_2 r^2 + \gamma_1\gamma_2 b_1^3\beta k^2 m_1^3 m_3 r \\
& + \gamma_1\gamma_2 b_1^2\beta\eta k^2 m_1^3 r^2 - \gamma_1\zeta b_1^2\beta\eta k^2 m_1^3 r^2 + \gamma_1 b_1^3 b_2 k^2 m_1^3 m_2 m_3 r \\
& + \gamma_1 b_1^2 b_2\eta k^2 m_1^3 m_2 r^2 + \gamma_1^4 a^4 k^2 m_2 m_3 - \gamma_1^3\gamma_2 a^2\beta k^2 m_1\omega r \\
& - \gamma_1^3\zeta a^2\beta k^2 m_1\omega r + 4\gamma_1^3 a^3 b_1 k^2 m_1 m_2 m_3 - \gamma_1^3 a^3\eta k^2 m_1 m_2 r \\
& + \gamma_1^3 a^2 b_2 k^2 m_1 m_2\omega r - 2\gamma_1^2\gamma_2 a b_1\beta k^2 m_1^2\omega r - 2\gamma_1^2\zeta a b_1\beta k^2 m_1^2\omega r \\
& + 6\gamma_1^2 a^2 b_1^2 k^2 m_1^2 m_2 m_3 + 3\gamma_1^2 a^2 b_1\eta k^2 m_1^2 m_2 r + 2\gamma_1^2 a b_1 b_2 k^2 m_1^2 m_2\omega r \\
& - \gamma_1\gamma_2 b_1^2\beta k^2 m_1^3\omega r + \gamma_1\zeta b_1^2\beta k^2 m_1^3\omega r + 4\gamma_1 a b_1^3 k^2 m_1^3 m_2 m_3 \\
& + 3\gamma_1 a b_1^2\eta k^2 m_1^3 m_2 r - \gamma_1 b_1^2 b_2 k^2 m_1^3 m_2\omega r - b_1^4 k^2 m_1^4 m_2 m_3 \\
& - b_1^3\eta k^2 m_1^4 m_2 r - \gamma_1^3\gamma_2 a^2\beta k m_1 m_3 r - \gamma_1^3 a^3 k^2 m_1 m_2\omega \\
& - \gamma_1^3 a^2 b_2 k m_1 m_2 m_3 r + 2\gamma_1^2\gamma_2 a b_1\beta k m_1^2 m_3 r - 2\gamma_1^2\gamma_2 a\beta\eta k m_1^2 r^2 \\
& + 2\gamma_1^2\zeta a\beta\eta k m_1^2 r^2 - 3\gamma_1^2 a^2 b_1 k^2 m_1^2 m_2\omega - 2\gamma_1^2 a b_1 b_2 k m_1^2 m_2 m_3 r \\
& - 2\gamma_1^2 a b_2\eta k m_1^2 m_2 r^2 + \gamma_1\gamma_2 b_1^2\beta k m_1^3 m_3 r - 2\gamma_1\gamma_2 b_1\beta\eta k m_1^3 r^2 \\
& - 2\gamma_1\zeta b_1\beta\eta k m_1^3 r^2 + 3\gamma_1 a b_1^2 k^2 m_1^3 m_2\omega - \gamma_1 b_1^2 b_2 k m_1^3 m_2 m_3 r \\
& + 2\gamma_1 b_1 b_2\eta k m_1^3 m_2 r^2 - b_1^3 k^2 m_1^4 m_2\omega - \gamma_1^2\gamma_2 a\beta k m_1^2\omega r \\
& + \gamma_1^2\zeta a\beta k m_1^2\omega r - \gamma_1^2 a^2\eta k m_1^2 m_2 r - \gamma_1^2 a b_2 k m_1^2 m_2\omega r \\
& - \gamma_1\gamma_2 b_1\beta k m_1^3\omega r - \gamma_1\zeta b_1\beta k m_1^3\omega r + 2\gamma_1 a b_1\eta k m_1^3 m_2 r \\
& + \gamma_1 b_1 b_2 k m_1^3 m_2\omega r - b_1^2\eta k m_1^4 m_2 r - \gamma_1\gamma_2\beta\eta {m_1}^3 r^2 - \gamma_1\zeta\beta\eta {m_1}^3 r^2 \\
& - \gamma_1 b_2\eta m_1^3 m_2 r^2,
\end{aligned}
$$

and

$$
\begin{aligned}
B = {} & \gamma_1^4 a^3 b_2 k^2 m_3 r - 3\gamma_1^3 a^2 b_1 b_2 k^2 m_1 m_3 r + \gamma_1^3 a^2 b_2 \eta k^2 m_1 r^2 \\
& + 3\gamma_1^2 a b_1^2 b_2 k^2 m_1^2 m_3 r - 2\gamma_1^2 a b_1 b_2 \eta k^2 m_1^2 r^2 - \gamma_1 b_1^3 b_2 k^2 m_1^3 m_3 r \\
& + \gamma_1 b_1^2 b_2 \eta k^2 m_1^3 r^2 + \gamma_1^4 a^4 k^2 m_3 - 4\gamma_1^3 a^3 b_1 k^2 m_1 m_3 + \gamma_1^3 a^3 \eta k^2 m_1 r \\
& + \gamma_1^3 a^2 b_2 k^2 m_1 \omega r + 6\gamma_1^2 a^2 b_1^2 k^2 m_1^2 m_3 - 3\gamma_1^2 a^2 b_1 \eta k^2 m_1^2 r \\
& - 2\gamma_1^2 a b_1 b_2 k^2 m_1^2 \omega r - 4\gamma_1 a b_1^3 k^2 m_1^3 m_3 + 3\gamma_1 a b_1^2 \eta k^2 m_1^3 r \\
& + \gamma_1 b_1^2 b_2 k^2 m_1^3 \omega r + b_1^4 k^2 m_1^4 m_3 - b_1^3 \eta k^2 m_1^4 r + \gamma_1^3 a^3 k^2 m_1 \omega \\
& - \gamma_1^3 a^2 b_2 k m_1 m_3 r - 3\gamma_1^2 a^2 b_1 k^2 m_1^2 \omega + 2\gamma_1^2 a b_1 b_2 k m_1^2 m_3 r \\
& - 2\gamma_1^2 a b_2 \eta k m_1^2 r^2 + 3\gamma_1 a b_1^2 k^2 m_1^3 \omega - \gamma_1 b_1^2 b_2 k m_1^3 m_3 r \\
& + 2\gamma_1 b_1 b_2 \eta k m_1^3 r^2 - b_1^3 k^2 m_1^4 \omega - \gamma_1^2 a^2 \eta k m_1^2 r - \gamma_1^2 a b_2 k m_1^2 \omega r \\
& + 2\gamma_1 a b_1 \eta k m_1^3 r + \gamma_1 b_1 b_2 k m_1^3 \omega r - b_1^2 \eta k m_1^4 r + \gamma_1 b_2 \eta m_1^3 r^2,
\end{aligned}
$$

$$
A_0 = \gamma_1 a k (\gamma_1 a - b_1 m_1), \tag{C.3.11}
$$

$$
\alpha = -m_1(\gamma_1 a b_1 k r + b_1^2 k m_1 r + r\gamma_1 a + b_1 m_1 r),
$$

$$
\begin{aligned}
\beta = {} & -4\gamma_1^4 a^4 k^2 m_1 r + 12\gamma_1^3 a^3 b_1 k^2 m_1^2 r - 12\gamma_1^2 a^2 b_1^2 k^2 m_1^3 r \\
& + \gamma_1^2 a^2 b_1^2 k^2 m_1^2 r^2 + 4\gamma_1 a b_1^3 k^2 m_1^4 r - 2\gamma_1 a b_1^3 k^2 m_1^3 r^2 \\
& + b_1^4 k^2 m_1^4 r^2 + 4\gamma_1^3 a^3 k m_1^2 r - 8\gamma_1^2 a^2 b_1 k m_1^3 r \\
& - 2\gamma_1^2 a^2 b_1 k m_1^2 r^2 + 4\gamma_1 a b_1^2 k m_1^4 r + 2 b_1^3 k m_1^4 r^2 \\
& + \gamma_1^2 a^2 m_1^2 r^2 + 2\gamma_1 a b_1 m_1^3 r^2 \\
& + b_1^2 m_1^4 r^2.
\end{aligned}
$$

C.4 The Coefficient of the Coexistence Equilibrium E_4

$$A_1 = -a_{11} - a_{22} - a_{33} - a_{44}, \tag{C.4.12}$$

$$A_2 = a_{11}a_{22} + a_{11}a_{33} + a_{11}a_{44} - a_{12}a_{21} + a_{22}a_{33} + a_{22}a_{44} - a_{23}a_{32} - a_{24}a_{42} +_{33} a_{44}, \tag{C.4.13}$$

$$\begin{aligned} A_3 = &-a_{11}a_{22}a_{33} - a_{11}a_{22}a_{44} + a_{11}a_{23}a_{32} + a_{11}a_{24}a_{42} - a_{11}a_{33}a_{44} + a_{12}a_{21}a_{33} + a_{12}a_{21}a_{44} \\ &- a_{12}a_{24}a_{41} - a_{22}a_{33}a_{44} + a_{23}a_{32}a_{44} - a_{23}a_{34}a_{42} +_{24} a_{33}a_{42}, \end{aligned} \tag{C.4.14}$$

$$\begin{aligned} A_4 = &a_{11}a_{22}a_{33}a_{44} - a_{11}a_{23}a_{32}a_{44} +_{11} a_{23}a_{34}a_{42} - a_{11}a_{24}a_{33}a_{42} - a_{12}a_{21}a_{33}a_{44} \\ &- a_{12}a_{23}a_{34}a_{41} + a_{12}a_{24}a_{33}a_{41}. \end{aligned} \tag{C.4.15}$$

C.5 The Coefficients of the Quadratic Z Polynomial

The coefficients of Eq.(6.14) in Sec.6.3 in Chapter 6.

$$\begin{aligned} A_5 = &\zeta^2\beta r b_1 b_2 m_2 m_3 - \zeta\beta^2 r\gamma_2^2 b_1 m_3 + 2\zeta\beta r\gamma_2 b_1 b_2 m_2 m_3 - \zeta r b_1 b_2^2 m_2^2 m_3 \\ &+ \zeta^2 a\beta\eta r m_2 - \zeta^2\beta^2 r b_1 m_3 + \zeta a\beta\eta r\gamma_2 m_2 - \zeta a\eta r b_2 m_2^2 - \zeta\beta^2 r\gamma_2 b_1 m_3 \\ &+ \zeta\beta r b_1 b_2 m_2 m_3 - \zeta a\beta\eta r m_2 - a\beta\eta r\gamma_2 m_2 + a\eta r b_2 m_2^2 \end{aligned}$$

$$\begin{aligned} B = &\zeta^2\beta^2 K r\gamma_2 b_1 m_3 - \zeta^2\beta K r b_1 b_2 m_2 m_3 + \zeta\beta^2 K r\gamma_2^2 b_1 m_3 - 2\zeta\beta K r\gamma_2 b_1 b_2 m_2 m_3 \\ &- \zeta^2 a\beta\eta K r m_2 - \zeta a\beta\eta K r\gamma_2 m_2 + \zeta a\eta K r b_2 m_2^2 + \zeta\beta^2 K r\gamma_2 b_1 m_3 - \zeta\beta K r b_1 b_2 m_2 m_3 \\ &- \zeta^2 a\beta K\omega m_2 - \zeta^2\beta^2 r\gamma_2 m_3 - \zeta^2\beta^2 r b_1 m_3 + \zeta^2\beta r b_2 m_2 m_3 + \zeta a\beta\eta K r m_2 - \zeta a\beta K\omega\gamma_2 m_2 \\ &+ \zeta a K\omega b_2 m_2^2 - \zeta\beta^2 r\gamma_2^2 m_3 + 2\zeta\beta r\gamma_2 b_2 m_2 m_3 - \zeta r b_2^2 m_2^2 m_3 + a\beta\eta K r\gamma_2 m_2 - a\eta K r b_2 m_2^2 \\ &- \zeta^2\beta^2 r m_3 + \zeta a\beta K\omega m_2 - \zeta\beta^2 r\gamma_2 m_3 + \zeta\beta r b_2 m_2 m_3 + a\beta K\omega\gamma_2 m_2 - a K\omega b_2 m_2^2 \end{aligned}$$

$$G = \beta^2 Kr\zeta^2\gamma_2 m_3 - \beta Kr\zeta^2 m_3 m_2 b_2 + \beta^2 Kr\zeta\gamma_2^2 m_3 - 2\beta Kr\zeta\gamma_2 m_3 m_2 b_2 + Kr\zeta m_3 m_2^2 b_2^2 \tag{C.5.16}$$

$$- a\beta K\zeta^2 m_3 m_2 + \beta^2 Kr\zeta^2 m_3 - a\beta K\zeta\gamma_2 m_3 m_2 + aK\zeta m_3 m_2^2 b_2 + \beta^2 Kr\zeta\gamma_2 m_3 - \beta Kr\zeta m_3 m_2 b_2 \tag{C.5.17}$$

$$+ a\beta K\zeta m_3 m_2 + a\beta K\gamma_2 m_3 m_2 - aKm_3 m_2^2 b_2 \tag{C.5.18}$$

Bibliography

[1] Eyad H Abed and Jyun-Horng Fu. Local feedback stabilization and bifurcation control, ii. stationary bifurcation. *Systems & Control Letters*, 8(5):467–473, 1987.

[2] Peter A Abrams and Carl J Walters. Invulnerable prey and the paradox of enrichment. *Ecology*, 77(4):1125–1133, 1996.

[3] Pasternak AF., VN Mikheev, and J Wanzenböck. How plankton copepods avoid fish predation: From individual responses to variations of the life cycle. *Journal of Ichthyology*, 46:S220–S226, 2006.

[4] Ahmed, SU KKU, MRA Hossain, T Ahmed, and S Barman. Quantitative and qualitative assessment of plankton: some ecological aspect and water quality parameters of the river meghna, bangladesh. *Bangladesh Journal of Fisheries Research*, 7(2):131–140, 2003.

[5] David Alonso, Frederic Bartumeus, and Jordi Catalan. Mutual interference between predators can give rise to turing spatial patterns. *Ecology*, 83(1):28–34, 2002.

[6] Charles D Amsler. *Algal chemical ecology*, volume 468. Springer, 2008.

[7] Miguel B Araujo and Antoine Guisan. Five (or so) challenges for species distribution modelling. *Journal of biogeography*, 33(10):1677–1688, 2006.

[8] Archer, CE Stelfox-Widdicombe, SD, G Malin, and PH Burkill. Is dimethyl sulphide production related to microzooplankton herbivory in the southern north sea? *Journal of Plankton Research*, 25(2):235–242, 2003.

[9] Mathieu Ardyna, Marcel Babin, Michel Gosselin, Emmanuel Devred, Luc Rainville, and Jean-Éric Tremblay. Recent arctic ocean sea ice loss triggers novel fall phytoplankton blooms. *Geophysical Research Letters*, 41(17):6207–6212, 2014.

[10] David Arrowsmith and Colin M Place. *Dynamical systems: differential equations, maps, and chaotic behaviour*, volume 5. CRC Press, 1992.

[11] Isabel Averill, King-Yeung Lam, and Yuan Lou. *The role of advection in a two-species competition model: a bifurcation approach*, volume 245. American Mathematical Society, 2017.

[12] Greg P Ayers and Jill M Cainey. The *claw* hypothesis: a review of the major developments. *Environmental Chemistry*, 4(6):366–374, 2008.

[13] Hansen B., KS Tande, and UC Berggreen. On the trophic fate of phaeocystis pouchetii (harlot). iii. functional responses in grazing demonstrated on juvenile stages of calanus finmarchicus (copepoda) fed diatoms and phaeocystis. *Journal of Plankton Research*, 12(6):1173–1187, 1990.

[14] Randhir Singh Baghel, Joydip Dhar, Marek Berezowski, Marcin Lawnik, Maher Berzig, Mircea-Dan Rus, Anar Huseyin, Justina Jachimavičienė, Mifodijus Sapagovas, Artūras Štikonas, et al. Pattern formation in three species food web model in spatiotemporal domain with beddingtondeangelis functional response. *Nonlinear Anal Model Control*, 19:155–171, 2014.

[15] Ruth Baker. Mathematical biology and ecology lecture notes, 2011.

[16] Malay Banerjee. Turing and non-turing patterns in two-dimensional prey-predator models. In *Applications of Chaos and Nonlinear Dynamics in Science and Engineering-Vol. 4*, pages 257–280. Springer, 2015.

[17] Malay Banerjee and Santo Banerjee. Turing instabilities and spatio-temporal chaos in ratio-dependent holling–tanner model. *Mathematical biosciences*, 236(1):64–76, 2012.

[18] Malay Banerjee and Ezio Venturino. A phytoplankton–toxic phytoplankton–zooplankton model. *Ecological Complexity*, 8(3):239–248, 2011.

[19] Baurmann, W Ebenhoh, M, and U Feudel. Turing instabilities and pattern formation in a benthic nutrient-microoganism system. *Mathematical biosciences and engineering: MBE*, 1(1):111–130, 2004.

[20] Beibei, Min Zhao, Wang, Chuanjun Dai, Hengguo Yu, Nan Wang, and Pengfei Wang. Dynamics analysis of a nutrient-plankton model with a time delay. *Discrete Dynamics in Nature and Society*, 2016, 2016.

[21] David Blondeau-Patissier, Thomas Schroeder, Vittorio E Brando, Stefan W Maier, Arnold G Dekker, and Stuart Phinn. Esa-meris 10-year mission reveals contrasting phytoplankton bloom dynamics in two tropical regions of northern australia. *Remote Sensing*, 6(4):2963–2988, 2014.

[22] Carl Boettiger and Alan Hastings. Quantifying limits to detection of early warning for critical transitions. *Journal of the Royal Society Interface*, 9(75):2527–2539, 2012.

[23] William E Boyce, Richard C DiPrima, and Charles W Haines. *Elementary differential equations and boundary value problems*, volume 9. Wiley New York, 1992.

[24] Lisa M Breckels, Laurent Gatto, Andy Christoforou, Arnoud J Groen, Kathryn S Lilley, and Matthew WB Trotter. The effect of organelle discovery upon sub-cellular protein localisation. *Journal of proteomics*, 88:129–140, 2013.

[25] Mark N Breckels, Emily C Roberts, Stephen D Archer, Gill Malin, and Michael Steinke. The role of dissolved infochemicals in mediating predator–prey interactions in the heterotrophic dinoflagellate oxyrrhis marina. *Journal of plankton research*, 33(4):629–639, 2011.

[26] WCM Klein Breteler, N Schogt, M Baas, S Schouten, and GW Kraay. Trophic upgrading of food quality by protozoans enhancing copepod growth: role of essential lipids. *Marine Biology*, 135(1):191–198, 1999.

[27] Nicholas F Britton et al. *Reaction-diffusion equations and their applications to biology.* Academic Press, 1986.

[28] Woodson C. Brock, Donald R Webster, Marc J Weissburg, and Jeannette Yen. The prevalence and implications of copepod behavioral responses to oceanographic gradients and biological patchiness. *Integrative and Comparative biology*, 47(6):831–846, 2007.

[29] Burkill, RFC Mantoura, Burkill, CA Llewellyn, and NJP Owens. Microzooplankton grazing and selectivity of phytoplankton in coastal waters. *Marine biology*, 93(4):581–590, 1987.

[30] Stavros Busenberg, S Kishore Kumar, Paul Austin, and Graeme Wake. The dynamics of a model of a plankton-nutrient interaction. *Bulletin of Mathematical Biology*, 52(5):677–696, 1990.

[31] Levennore C David. The complex ginzburg-landau equation as a model problem. In *Dynamical Systems and Probabilistic Methods in Partial Differential Equations: 1994 Summer Seminar on Dynamical Systems and Probabilistic Methods for Nonlinear Waves, June 20-July 1, 1994, MSRI, Berkeley, CA*, volume 31, page 141. American Mathematical Soc., 1996.

[32] Jill M Cainey, Herman Sievering, and Greg P Ayers. Where to now? a synthesis of current views of the claw hypothesis. *Environmental Chemistry*, 4(6):406–409, 2008.

[33] Albert Calbet. Mesozooplankton grazing effect on primary production: a global comparative analysis in marine ecosystems. *Limnology and Oceanography*, 46(7):1824–1830, 2001.

[34] Albert Calbet. The trophic roles of microzooplankton in marine systems. *ICES Journal of Marine Science*, 65(3):325–331, 2008.

[35] Albert Calbet, Michael R Landry, et al. Phytoplankton growth, microzooplankton grazing, and carbon cycling in marine systems. *Limnology and Oceanography*, 49(1):51–57, 2004.

[36] Robert Stephen Cantrell and Chris Cosner. *Spatial ecology via reaction-diffusion equations*. John Wiley & Sons, 2004.

[37] Jacob Carstensen. *Statistical analysis and modelling of phytoplankton dynamics: exploitation of data in the Nordic and Baltic monitoring programs*. Nordic Council of Ministers, 2002.

[38] Causon and CG Mingham, DM. *Introductory Finite Difference Methods for PDEs*. Bookboon, 2010.

[39] Jenny L Chapman and Michael Jonathan Reiss. *Ecology: principles and applications*. Cambridge University Press, 1998.

[40] Charles, Alain Vezina, Hannah, and Mike St John. The case for marine ecosystem models of intermediate complexity. *Progress in Oceanography*, 84(1):121–128, 2010.

[41] Robert J Charlson, James E Lovelock, Meinrat O Andreaei, and Stephen G Warren. Oceanic phytoplankton, atmospheric sulphur, cloud. *Nature*, 326(6114):655–661, 1987.

[42] Roger Chou, Gilbert J Fanciullo, Perry G Fine, Jeremy A Adler, Jane C Ballantyne, Pamela Davies, Marilee I Donovan, David A Fishbain, Kathy M Foley, Jeffrey Fudin, et al. Clinical guidelines for the use of chronic opioid therapy in chronic noncancer pain. *The Journal of Pain*, 10(2):113–130, 2009.

[43] Christian, Philippe Cury, Mullon, and Lynne Shannon. Viability model of trophic interactions in marine ecosystems. *Natural Resource Modeling*, 17(1):71–102, 2004.

[44] Fred Cooper, So-Young Pi, and Paul N Stancioff. Quantum dynamics in a time-dependent variational approximation. *Physical Review D*, 34(12):3831, 1986.

[45] Michael H Cortez and Peter A Abrams. Hydra effects in stable communities and their implications for system dynamics. *Ecology*, 97(5):1135–1145, 2016.

[46] Caitlin M Crain, Benjamin S Halpern, Mike W Beck, and Carrie V Kappel. Understanding and managing human threats to the coastal marine environment. *Annals of the New York Academy of Sciences*, 1162(1):39–62, 2009.

[47] Edmund J Crampin, Eamonn A Gaffney, and Philip K Maini. Reaction and diffusion on growing domains: scenarios for robust pattern formation. *Bulletin of mathematical biology*, 61(6):1093–1120, 1999.

[48] Roger Cropp, John Norbury, and Roger Braddock. Dimethylsulphide, clouds, and phytoplankton: Insights from a simple plankton ecosystem feedback model. *Global Biogeochemical Cycles*, 21(2), 2007.

[49] Michael D Cross. Notes on the turing instability and chemical instabilities, 2006.

[50] Davide, Giovanni Denaro, Valenti, Rosalia Ferreri, Simona Genovese, Salvatore Aronica, Salvatore Mazzola, Angelo Bonanno, Gualtiero Basilone, and Bernardo Spagnolo. Spatio-temporal dynamics of a planktonic system and chlorophyll distribution in a 2d spatial domain: matching model and data. *Scientific Reports*, 7, 2017.

[51] Paul Davidson. *Post Keynesian macroeconomic theory*. Edward Elgar Publishing, 2011.

[52] Jonathan HP Dawes and Hadi Susanto. Variational approximation and the use of collective coordinates. *Physical Review E*, 87(6):063202, 2013.

[53] Jennifer L DeBose, Sean C Lema, and Gabrielle A Nevitt. Dimethylsulfoniopropionate as a foraging cue for reef fishes. *Science*, 319(5868):1356–1356, 2008.

[54] Edmund X DeJesus and Charles Kaufman. Routh-hurwitz criterion in the examination of eigenvalues of a system of nonlinear ordinary differential equations. *Physical Review A*, 35(12):5288, 1987.

[55] Elisabeth SM Deschaseaux, Graham B Jones, Myrna A Deseo, Kellie M Shepherd, RP Kiene, HB Swan, Peter Lynton Harrison, and Bradley D Eyre. Effects of environmental factors on dimethylated sulfur compounds and their potential role in the antioxidant system of the coral holobiont. *Limnology and Oceanography*, 59(3):758–768, 2014.

[56] Alex J Dumbrell, Ewen J Clark, Gillian A Frost, Thomas E Randell, Jonathan W Pitchford, and Jane K Hill. Changes in species diversity following habitat disturbance are dependent on spatial scale: theoretical and empirical evidence. *Journal of Applied Ecology*, 45(5):1531–1539, 2008.

[57] William M Durham, Eric Climent, Michael Barry, Filippo De Lillo, Guido Boffetta, Massimo Cencini, and Roman Stocker. Turbulence drives microscale patches of motile phytoplankton. *Nature communications*, 4:2148, 2013.

[58] Edward and J Brindley. Zooplankton mortality and the dynamical behaviour of plankton population model. *Bulletin of Mathematical Biology*, 61:303–339, 1999.

[59] Edwards and Andrew M Brindley, John. Zooplankton mortality and the dynamical behaviour of plankton population models. *Bulletin of mathematical biology*, 61(2):303–339, 1999.

[60] Andrew M Edwards and John Brindley. Oscillatory behaviour in a three-component plankton population model. *Dynamics and stability of Systems*, 11(4):347–370, 1996.

[61] Andrew M Edwards and Andrew Yool. The role of higher predation in plankton population models. *Journal of Plankton Research*, 22(6):1085–1112, 2000.

[62] Christopher A Edwards, Harold P Batchelder, and Thomas M Powell. Modeling microzooplankton and macrozooplankton dynamics within a coastal upwelling system. *Journal of Plankton Research*, 22(9):1619–1648, 2000.

[63] Egilmez and A Yu Morozov, HI. Tri-trophic plankton models revised: importance of space, food web structure and functional response parametrisation. *Mathematical Modelling of Natural Phenomena*, 11(4):16–33, 2016.

[64] Milner Gulland EJ. Interactions between human behaviour and ecological systems. *Phil. Trans. R. Soc. B*, 367(1586):270–278, 2012.

[65] Ellen, Adrianna Ianora, Van Donk, and Matthijs Vos. Induced defences in marine and freshwater phytoplankton: a review. *Hydrobiologia*, 668(1):3–19, 2011.

[66] Aiman Elragig and Stuart Townley. A new necessary condition for turing instabilities. *Mathematical biosciences*, 239(1):131–138, 2012.

[67] Bard Ermentrout. Nullclines and phaseplanes, 2002.

[68] Fengqi, Junjie Wei, Yi, and Junping Shi. Bifurcation and spatiotemporal patterns in a homogeneous diffusive predator–prey system. *Journal of Differential Equations*, 246(5):1944–1977, 2009.

[69] Edyta Fiałkowska and Agnieszka Pajdak-Stós. Chemical and mechanical signals in inducing phormidium (cyanobacteria) defence against their grazers. *FEMS microbiology ecology*, 89(3):659–669, 2014.

[70] Fidia Fibriana and Andin Vita Amalia. Potensi kitchen microbiology untuk meningkatkan keterampilan teknik hands-on dalam pembelajaran mikrobiologi. *Unnes Science Education Journal*, 5(2), 2016.

[71] Helen S Findlay, Andrew Yool, Marianna Nodale, and Jonathan W Pitchford. Modelling of autumn plankton bloom dynamics. *Journal of plankton research*, 28(2):209–220, 2006.

[72] Patrick Fink. Ecological functions of volatile organic compounds in aquatic systems. *Marine and Freshwater Behaviour and Physiology*, 40(3):155–168, 2007.

[73] Matthew A Foretich, Claire B Paris, Martin Grosell, John D Stieglitz, and Daniel D Benetti. Dimethyl sulfide is a chemical attractant for reef fish larvae. *Scientific Reports*, 7, 2017.

[74] Peter JS Franks. Phytoplankton blooms in a fluctuating environment: the roles of plankton response time scales and grazing. *Journal of Plankton Research*, 23(12):1433–1441, 2001.

[75] Freedman and RM Mathsen, HI. Persistence in predator-prey systems with ratio-dependent predator influence. *Bulletin of Mathematical Biology*, 55(4):817–827, 1993.

[76] Freedman and Paul Waltman, HI. Persistence in models of three interacting predator-prey populations. *Mathematical Biosciences*, 68(2):213–231, 1984.

[77] Herbert I Freedman. *Deterministic mathematical models in population ecology*, volume 57. Marcel Dekker Inc, 1980.

[78] Holmes G. C. The use of hyperbolic cosines in solving cubic polynomials. *The Mathematical Gazette*, pages 473–477, 2002.

[79] Alison P Galvani, Chris T Bauch, Madhur Anand, Burton H Singer, and Simon A Levin. Human–environment interactions in population and ecosystem health, 2016.

[80] Gambino, MC Lombardo, S Lupo, and M Sammartino. Super-critical and sub-critical bifurcations in a reaction-diffusion schnakenberg model with linear cross-diffusion. *Ricerche di Matematica*, 65(2):449–467, 2016.

[81] Gambino, MC Lombardo, and M Sammartino. Pattern formation driven by cross-diffusion in a 2d domain. *Nonlinear Analysis: Real World Applications*, 14(3):1755–1779, 2013.

[82] Gambino, MC Lombardo, and M Sammartino. Turing instability and pattern formation in an activator-inhibitor system with nonlinear diffusion. *arXiv preprint arXiv:1403.0351*, 2014.

[83] Gambino, MC Lombardo, G, and M Sammartino. Turing instability and traveling fronts for a nonlinear reaction–diffusion system with cross-diffusion. *Mathematics and Computers in Simulation*, 82(6):1112–1132, 2012.

[84] Marcus R Garvie. Finite-difference schemes for reaction–diffusion equations modeling predator–prey interactions in matlab. *Bulletin of mathematical biology*, 69(3):931–956, 2007.

[85] Stéphane Genieys, Vitaly Volpert, and Pierre Auger. Pattern and waves for a model in population dynamics with nonlocal consumption of resources. *Mathematical Modelling of Natural Phenomena*, 1(1):63–80, 2006.

[86] Jeroen Gerritsen and J Rudi Strickler. Encounter probabilities and community structure in zooplankton: a mathematical model. *Journal of the Fisheries Board of Canada*, 34(1):73–82, 1977.

[87] John J Gilbert. The cost of predator-induced morphological defense in rotifers: experimental studies and synthesis. *Journal of plankton research*, 35(3):461–472, 2013.

[88] Michael E Gilpin and ML Rosenzweig. Enriched predator-prey systems: theoretical stability. *Science*, 177(4052):902–904, 1972.

[89] Guckenheimer and Y. A. Kuznetsov, J. Cusp bifurcation. *Scholarpedia*, 2(4):1852, 2007.

[90] Jeremy Gunawardena. Models in biology:accurate descriptions of our pathetic thinking. *BMC biology*, 12(1):29, 2014.

[91] Andrés Gutiérrez-Rodríguez, Karen E Selph, and Michael R Landry. Phytoplankton growth and microzooplankton grazing dynamics across vertical environmental gradients determined by transplant in situ dilution experiments. *Journal of plankton research*, 38(2):271–289, 2015.

[92] Scott A Hadley and Larry K Forbes. Dynamical systems analysis of a two level trophic food web in the southern oceans. *ANZIAM Journal*, 50:24–55, 2009.

[93] Scott A Hadley and Lawrence K Forbes. Dynamical systems analysis of a five-dimensional trophic food web model in the southern oceans. *Journal of Applied Mathematics*, 2009, 2010.

[94] Benjamin S Halpern, Shaun Walbridge, Kimberly A Selkoe, Carrie V Kappel, Fiorenza Micheli, Caterina D'agrosa, John F Bruno, Kenneth S Casey, Colin Ebert, Helen E Fox, et al. A global map of human impact on marine ecosystems. *Science*, 319(5865):948–952, 2008.

[95] Hammer and JW Pitchford, AC. Mixotrophy, allelopathy and the population dynamics of phagotrophic algae (cryptophytes) in the darss zingst bodden estuary, southern baltic. *Marine Ecology Progress Series*, 328:105–115, 2006.

[96] Astrid C Hammer and Jonathan W Pitchford. The role of mixotrophy in plankton bloom dynamics, and the consequences for productivity. *ICES Journal of Marine Science*, 62(5):833–840, 2005.

[97] Norhayati Hamzah, A Ross, and Graeme C Wake. A bifurcation analysis of a simple phytoplankton and zooplankton model. *Mathematical and computer modelling*, 45(3):449–458, 2007.

[98] Matthew J Hancock. The 1-d heat equation. 2004.

[99] Hansen, M Reckermann, FC WCM Klein Breteler, and R Riegman. Phaeocystis blooming enhanced by copepod predation on protozoa: evidence from incubation experiments. *Marine Ecology Progress Series*, pages 51–57, 1993.

[100] Mainul Haque. A detailed study of the beddington–deangelis predator–prey model. *Mathematical Biosciences*, 234(1):1–16, 2011.

[101] Kristen Harley, Peter van Heijster, and Graeme John Pettet. A geometric construction of travelling wave solutions to the keller–segel model. *ANZIAM Journal*, 55:399–415, 2014.

[102] G. Pettet Harley van Heijster, R. Marangell and M. Wechselberger. Numerical computation of an evans function for travelling waves. *Math. Biosci.*, pages 266, 3651, 2015.

[103] John Harlim and WILLIAM F LANGFORD. The cusp–hopf bifurcation. *International Journal of Bifurcation and Chaos*, 17(08):2547–2570, 2007.

[104] Chris J Harvey, Sean P Cox, Timothy E Essington, Sture Hansson, and James F Kitchell. An ecosystem model of food web and fisheries interactions in the baltic sea. *ICES Journal of Marine Science*, 60(5):939–950, 2003.

[105] Elizabeth L Harvey and Susanne Menden-Deuer. Predator-induced fleeing behaviors in phytoplankton: a new mechanism for harmful algal bloom formation? 2012.

[106] Alan Hastings. Transient dynamics and persistence of ecological systems. *Ecology Letters*, 4(3):215–220, 2001.

[107] Mark E Hay. Marine chemical ecology: chemical signals and cues structure marine populations, communities, and ecosystems. *Annual Review of Marine Science*, 1:193–298, 2009.

[108] Van Hecke, PC Hohenberg, and W Van Saarloos, M. Amplitude equations for pattern forming systems. *Fundamental Problems in Statistical Mechanics VIII*, pages 245–278, 1994.

[109] Keller Herbert B. Lectures on numerical methods in bifurcation problems. *Applied Mathematics*, 217:50, 1987.

[110] John Hilton, Matthew O'Hare, Michael J Bowes, and J Iwan Jones. How green is my river? a new paradigm of eutrophication in rivers. *Science of the Total Environment*, 365(1-3):66–83, 2006.

[111] Morris W Hirsch, Stephen Smale, and Robert L Devaney. *Differential equations, dynamical systems, and an introduction to chaos*, volume 60. Academic press, 2004.

[112] Crawford S Holling. Some characteristics of simple types of predation and parasitism1. *The Canadian Entomologist*, 91(7):385–398, 1959.

[113] Robert D Holt. Population dynamics in two-patch environments: some anomalous consequences of an optimal habitat distribution. *Theoretical population biology*, 28(2):181–208, 1985.

[114] Huffaker, Kb Shea, CB S Herman, et al. Experimental studies on predation: complex dispersion and levels of food in an acarine predator-prey interaction. *California Agriculture*, 34(9):305–330, 1963.

[115] Huisman, N. N. D. M. Karl Pham Thi, J., and B. P. Sommeijer. Reduced mixing generates oscillations and chaos in the oceanic deep chlorophyll maximum. *Nature*, 439:322325, 2006.

[116] Irigoien, X Harris, and RP Flynn, KJ. Phytoplankton blooms: a loopholein microzooplankton grazing impact? *Journal of Plankton Research*, 27(4):313–321, 2005.

[117] Xabier Irigoien, Robert Head, Ulrike Klenke, Bettina Meyer-Harms, Derek Harbour, Barbara Niehoff, Hans-Jürgen Hirche, and Roger Harris. A high frequency time series at weathership m, norwegian sea, during the 1997 spring bloom: feeding of adult female calanus finmarchicus. *Marine Ecology Progress Series*, 172:127–137, 1998.

[118] Xabier Irigoien, Jef Huisman, and Roger P Harris. Global biodiversity patterns of marine phytoplankton and zooplankton. *Nature*, 429(6994):863–867, 2004.

[119] Katrina J, Philip L Bond, Edwards, Greg K Druschel, Molly M McGuire, Robert J Hamers, and Jillian F Banfield. Geochemical and biological aspects of sulfide mineral dissolution: lessons from iron mountain, california. *Chemical Geology*, 169(3-4):383–397, 2000.

[120] Murray J D. *Mathematical Biology I: An Introduction, vol. 17 of Interdisciplinary Applied Mathematics*. Springer, New York, NY, USA,, 2002.

[121] Murray J D. *Mathematical Biology II: Spatial Models and Biomedical Applications*. Springer, New York, NY, USA,, 2003.

[122] Tommi S Jaakkola. 10 tutorial on variational approximation methods. *Advanced mean field methods: theory and practice*, page 129, 2001.

[123] Alex James, Jonathan W Pitchford, and John Brindley. The relationship between plankton blooms, the hatching of fish larvae, and recruitment. *Ecological Modelling*, 160(1):77–90, 2003.

[124] Janse, JH Kuiper, MJ Weijters, EP Westerbeek, MHJL Jeuken, M Bakkenes, R Alkemade, WM Mooij, and JTA Verhoeven. Globio-aquatic, a global model of human impact on the biodiversity of inland aquatic ecosystems. *Environmental Science & Policy*, 48:99–114, 2015.

[125] Vincent AA Jansen and Alun L Lloyd. Local stability analysis of spatially homogeneous solutions of multi-patch systems. *Journal of mathematical biology*, 41(3):232–252, 2000.

[126] Houshuo Jiang, Thomas R Osborn, and Charles Meneveau. Chemoreception and the deformationof the active space in freely swimming copepods: a numerical study. *Journal of Plankton Research*, 24(5):495–510, 2002.

[127] Michel J Kaiser. *Marine ecology: processes, systems, and impacts*. Oxford University Press, 2011.

[128] Hassan K Khalil. *Noninear Systems*. Prentice-Hall, New Jersey, 1996.

[129] L Douglas Kiel and Euel W Elliott. *Chaos theory in the social sciences: Foundations and applications*. University of Michigan Press, 1996.

[130] Thomas Kiørboe. *A mechanistic approach to plankton ecology*. Princeton University Press, 2008.

[131] Richard R Kirby. *Ocean Drifters: A Secret World Beneath the Waves*. Firefly Books, 2011.

[132] Christopher A Klausmeier. Successional state dynamics: a novel approach to modeling nonequilibrium foodweb dynamics. *Journal of Theoretical Biology*, 262(4):584–595, 2010.

[133] Shigeru Kondo and Takashi Miura. Reaction-diffusion model as a framework for understanding biological pattern formation. *Science*, 329(5999):1616–1620, 2010.

[134] Mark Kot. *Elements of mathematical ecology*. Cambridge University Press, 2001.

[135] Sylvia Kowalewsky, Martin Dambach, Björn Mauck, and Guido Dehnhardt. High olfactory sensitivity for dimethyl sulphide in harbour seals. *Biology Letters*, 2(1):106–109, 2006.

[136] Pavel Kratina, Ralph Mac Nally, Wim J Kimmerer, James R Thomson, and Monika Winder. Human-induced biotic invasions and changes in plankton interaction networks. *Journal of applied ecology*, 51(4):1066–1074, 2014.

[137] Steven L and Lawrence M Dill, Lima. Behavioral decisions made under the risk of predation: a review and prospectus. *Canadian journal of zoology*, 68(4):619–640, 1990.

[138] Arancha Lana, TG Bell, R Simó, SM Vallina, J Ballabrera-Poy, AJ Kettle, J Dachs, L Bopp, ES Saltzman, J Stefels, et al. An updated climatology of surface dimethlysulfide concentrations and emission fluxes in the global ocean. *Global Biogeochemical Cycles*, 25(1), 2011.

[139] Karen Lebret, María Fernández Fernández, Camilla HC Hagman, Karin Rengefors, and Lars-Anders Hansson. Grazing resistance allows bloom formation and may explain invasion success of gonyostomum semen. *Limnology and Oceanography*, 57(3):727–734, 2012.

[140] Lee, CT-MF Hoopes, J Diehl, W Gilliland, G Huxel, EV Leaver, K McCann, J Umbanhowar, and A Mogilner. Non-local concepts and models in biology. *Journal of theoretical biology*, 210(2):201–219, 2001.

[141] Istvan Lengyel and Irving R Epstein. Modeling of turing structures in the chlorite-iodide-malonic acid-starch reaction system. *Science*, 251(4994):650, 1991.

[142] Lewis, M N Breckels, N D, M Steinke, and E A Codling. Role of infochemical mediated zooplankton grazing in a phytoplankton competition model. *Ecological Complexity*, 16:41–50, 2013.

[143] Lewis, Mark N Breckels, N D, S D Archer, A Morozov, J W Pitchford, M Steinke, and E A Codling. Grazing-induced production of dms can stabilize food-web dynamics and promote the formation of phytoplankton blooms in a multitrophic plankton model. *Biogeochemistry*, 110(1-3):303–313, 2012.

[144] Lewis, Andrew Morozov, N. D, Mark N Breckels, Michael Steinke, and Edward A Codling. Multitrophic interactions in the sea: assessing the effect of infochemical-mediated foraging in a 1-d spatial model. *Mathematical Modelling of Natural Phenomena*, 8(6):25–44, 2013.

[145] Fang Hua Lin. Some recent trends of nonlinear partial differential equations. *Courant Institute*, 32(2):8–13, 2001.

[146] Harry J Lipkin, N Meshkov, and AJ Glick. Validity of many-body approximation methods for a solvable model:(i). exact solutions and perturbation theory. *Nuclear Physics*, 62(2):188–198, 1965.

[147] Veronica Lundgren. *Phytoplankton Defense Mechanisms Against Grazing: The Role of Grazing Infochemicals*. Institutionen för naturvetenskap, Linnaeus University Press, 2011.

[148] Jinhuo Luo. Phytoplankton–zooplankton dynamics in periodic environments taking into account eutrophication. *Mathematical Biosciences*, 245(2):126–136, 2013.

[149] Richard M, Anthony Lagalante, Turcotte, Jonathan Jones, Frank Cook, Thomas Elliott, Anthony A Billings, and Yong-Lak Park. Spatial and temporal distribution of imidacloprid within the crown of eastern hemlock. *Journal of Insect Science*, 17(1), 2017.

[150] Suqi Ma and Qishao Lu. Dynamical bifurcation for a predator-prey metapopulation model with delay. *International Journal of Nonlinear Sciences and Numerical Simulation*, 6(1):13–18, 2005.

[151] Malchow, S V Petrovskii, H, and E Venturino. *Spatiotemporal patterns in ecology and epidemiology: theory, models, and simulation*. Chapman & Hall/CRC Press London, 2008.

[152] Horst Malchow. Spatio-temporal pattern formation in nonlinear non-equilibrium plankton dynamics. *Proceedings of the Royal Society of London. Series B: Biological Sciences*, 251(1331):103–109, 1993.

[153] Horst Malchow, Frank M Hilker, Ivo Siekmann, Sergei V Petrovskii, and Alexander B Medvinsky. Mathematical models of pattern formation in planktonic predation-diffusion systems: a review. In *Aspects of Mathematical Modelling*, pages 1–26. Springer, 2008.

[154] Manoj Mali, Neha Goyal, and Himanshu Trivedi. Geometric methods in the theory of ordinary differential equations: A review.

[155] Manfredi Manizza, Corinne Le Quéré, Andrew J Watson, and Erik T Buitenhuis. Ocean biogeochemical response to phytoplankton-light feedback in a global model. *Journal of Geophysical Research: Oceans*, 113(C10), 2008.

[156] C Manno, Manno and AK Pavlov. Living planktonic foraminifera in the fram strait (arctic): absence of diel vertical migration during the midnight sun. *Hydrobiologia*, 721(1):285–295, 2014.

[157] Jerrold E Marsden and Marjorie McCracken. *The Hopf bifurcation and its applications*, volume 19. Springer-Verlag, 1976.

[158] Robert M May. Limit cycles in predator-prey communities. *Science*, 177(4052):900–902, 1972.

[159] Robert M May et al. Biological populations with nonoverlapping generations: stable points, stable cycles, and chaos. *Science*, 186(4164):645–647, 1974.

[160] Robert McCredie May. *Stability and complexity in model ecosystems*, volume 6. Princeton University Press, 1973.

[161] Alexander B Medvinsky, S V Petrovskii, Irene A Tikhonova, Horst Malchow, and Bai-Lian Li. Spatiotemporal complexity of plankton and fish dynamics. *SIAM review*, 44(3):311–370, 2002.

[162] DeBing Mei, Min Zhao, Hengguo Yu, Chuanjun Dai, and Yi Wang. Nonlinear dynamics of a nutrient-phytoplankton model with time delay. *Discrete Dynamics in Nature and Society*, 25, 2015.

[163] Nicholas Meskhidze and Athanasios Nenes. Phytoplankton and cloudiness in the southern ocean. *Science*, 314(5804):1419–1423, 2006.

[164] Charles B Miller. *Biological oceanography*. John Wiley & Sons, 2009.

[165] Andrew Morozov, Elena Arashkevich, Anastasia Nikishina, and Konstantin Solovyev. Nutrient-rich plankton communities stabilized via predator–prey interactions: revisiting the role of vertical heterogeneity. *Mathematical medicine and biology: a journal of the IMA*, 28(2):185–215, 2010.

[166] Andrew Morozov, Sergei Petrovskii, and Bai-Lian Li. Bifurcations and chaos in a predator-prey system with the allee effect. *Proceedings of the Royal Society of London B: Biological Sciences*, 271(1546):1407–1414, 2004.

[167] Muniyagounder, Krishnan Balachandran, Sambath, and Murugan Suvinthra. Stability and hopf bifurcation of a diffusive predator-prey model with hyperbolic mortality. *Complexity*, 21(S1):34–43, 2016.

[168] Lewis N. D. *Modelling the Infochemical Role of Dimethylsulphide in Pelagic Multitrophic Interactions*. PhD thesis, University of Essex, 2014.

[169] Michael G Neubert, Hal Caswell, and JD Murray. Transient dynamics and pattern formation: reactivity is necessary for turing instabilities. *Mathematical biosciences*, 175(1):1–11, 2002.

[170] Gabrielle A Nevitt. Olfactory foraging by antarctic procellariiform seabirds: life at high reynolds numbers, 2000.

[171] Nielsen, J Rasmus Eric Thunberg, Daniel S Holland, Jorn O Schmidt, Elizabeth A Fulton, François Bastardie, André E Punt, Icarus Allen, Heleen Bartelings, Michel Bertignac, et al. Integrated ecological–economic fisheries modelsevaluation, review and challenges for implementation. *Fish and Fisheries*, 2017.

[172] Richard S Ostfeld, Gregory E Glass, and Felicia Keesing. Spatial epidemiology: an emerging (or re-emerging) discipline. *Trends in ecology & evolution*, 20(6):328–336, 2005.

[173] Narendra K Pareek, Vinod Patidar, and Krishan K Sud. Image encryption using chaotic logistic map. *Image and Vision Computing*, 24(9):926–934, 2006.

[174] Franks Peter JS. Npz models of plankton dynamics: their construction, coupling to physics, and application. *Journal of Oceanography*, 58(2):379–387, 2002.

[175] Sergei Petrovskii and BAI-LIAN LI. Increased coupling between subpopulations in a spatially structured environment can lead to population outbreaks. *Journal of theoretical biology*, 212(4):549–562, 2001.

[176] Sergei Petrovskii, Bai-Lian Li, and Horst Malchow. Quantification of the spatial aspect of chaotic dynamics in biological and chemical systems. *Bulletin of mathematical biology*, 65(3):425–446, 2003.

[177] Sergei V Petrovskii and Horst Malchow. A minimal model of pattern formation in a prey-predator system. *Mathematical and Computer Modelling*, 29(8):49–63, 1999.

[178] Sergei V Petrovskii and Horst Malchow. Wave of chaos: new mechanism of pattern formation in spatio-temporal population dynamics. *Theoretical population biology*, 59(2):157–174, 2001.

[179] David Pimentel, Edwin H Feinberg, Peter W Wood, and John T Hayes. Selection, spatial distribution, and the coexistence of competing fly species. *American Naturalist*, pages 97–109, 1965.

[180] Jonathan Pitchford and John Brindley. Intratrophic predation in simple predator-prey models. *Bulletin of Mathematical Biology*, 60(5):937–953, 1998.

[181] Jonathan W Pitchford, Edward A Codling, and Despina Psarra. Uncertainty and sustainability in fisheries and the benefit of marine protected areas. *Ecological Modelling*, 207(2):286–292, 2007.

[182] Jonathan W Pitchford, Alex James, and John Brindley. Quantifying the effects of individual and environmental variability in fish recruitment. *Fisheries Oceanography*, 14(2):156–160, 2005.

[183] Georg Pohnert, Michael Steinke, and Ralph Tollrian. Chemical cues, defence metabolites and the shaping of pelagic interspecific interactions. *Trends in Ecology & Evolution*, 22(4):198–204, 2007.

[184] Brian Porter. *Stability criteria for linear dynamical systems*. Academic Press, 1968.

[185] Jennifer C Prairie, Kelly R Sutherland, Kerry J Nickols, and Amanda M Kaltenberg. Biophysical interactions in the plankton: A cross-scale review. *Limnology and Oceanography: Fluids and Environments*, 2(1):121–145, 2012.

[186] Corinne Le Quere, Sandy P Harrison, I Colin Prentice, Erik T Buitenhuis, Olivier Aumont, Laurent Bopp, Hervé Claustre, Leticia Cotrim Da Cunha, Richard Geider, Xavier Giraud, et al. Ecosystem

dynamics based on plankton functional types for global ocean biogeochemistry models. *Global Change Biology*, 11(11):2016–2040, 2005.

[187] Quinn and PK Bates, TS. The case against climate regulation via oceanic phytoplankton sulphur emissions. *Nature*, 480(7375):51–56, 2011.

[188] Mehbuba Rehim and Mudassar Imran. Dynamical analysis of a delay model of phytoplankton–zooplankton interaction. *Applied Mathematical Modelling*, 36(2):638–647, 2012.

[189] Mehbuba Rehim, Zhenzhen Zhang, and Ahmadjan Muhammadhaji. Mathematical analysis of a nutrient–plankton system with delay. *SpringerPlus*, 5(1):1–22, 2016.

[190] Torben C Rick and Jon M Erlandson. *Human impacts on ancient marine ecosystems: a global perspective*. Univ of California Press, 2008.

[191] Upadhyay RK. and J Chattopadhyay. Chaos to order: role of toxin producing phytoplankton in aquatic system. *Nonlinear Analysis: Modelling and Control*, 10(4):383–396, 2005.

[192] Caroline Robert, Luc Thomas, Igor Bondarenko, Steven O'day, Jeffrey Weber, Claus Garbe, Celeste Lebbe, Jean-François Baurain, Alessandro Testori, Jean-Jacques Grob, et al. Ipilimumab plus dacarbazine for previously untreated metastatic melanoma. *New England Journal of Medicine*, 364(26):2517–2526, 2011.

[193] Michael L Rosenzweig et al. Paradox of enrichment: destabilization of exploitation ecosystems in ecological time. *Science*, 171(3969):385–387, 1971.

[194] Michael L Rosenzweig and Robert H MacArthur. Graphical representation and stability conditions of predator-prey interactions. *The American Naturalist*, 97(895):209–223, 1963.

[195] Rubao, Christoph Stegert, Ji, and Cabell S Davis. Sensitivity of copepod populations to bottom-up and top-down forcing: a modeling study in the gulf of maine region. *Journal of Plankton Research*, 35(1):66–79, 2012.

[196] Ruberg, HA Vanderploeg, SA, JF Cavaletto, GA Lang, JR Liebig, TC Miller, and M Agy. Plankton survey system. In *OCEANS, 2001. MTS/IEEE Conference and Exhibition*, volume 3, pages 1899–1903. IEEE, 2001.

[197] Nickalls RWD. A new approach to solving the cubic: Cardan's solution revealed. *The Mathematical Gazette*, pages 354–359, 1993.

[198] Nickalls RWD. The quartic equation: invariants and euler's solution revealed. *The Mathematical Gazette*, 93(526):66–75, 2009.

[199] Ryabchenko, MJR Fasham, BA Kagan, VA, and EE Popova. What causes short-term oscillations in ecosystem models of the ocean mixed layer? *Journal of Marine Systems*, 13(1-4):33–50, 1997.

[200] John P Ryan, Curtiss O Davis, Nicholas B Tufillaro, Raphael M Kudela, and Bo-Cai Gao. Application of the hyperspectral imager for the coastal ocean to phytoplankton ecology studies in monterey bay, ca, usa. *Remote Sensing*, 6(2):1007–1025, 2014.

[201] Schreiber S. Allee effects, chaotic transients, and unexpected extinctions. *Theor. Pop. Biol*, 64:201–209, 2003.

[202] Enric Saiz and Albert Calbet. Scaling of feeding in marine calanoid copepods. *Limnology and Oceanography*, 52(2):668–675, 2007.

[203] Mathias Sandulescu, Cristóbal López, E Hernández-García, and Ulrike Feudel. Plankton blooms in vortices: The role of biological and hydrodynamic time scales. *arXiv preprint arXiv:0802.3973*, 2008.

[204] Sarwardi, Sahabuddin Md Reduanur Mandal, and Nurul Huda Gazi. Dynamical behaviour of an ecological system with beddington–deangelis functional response. *Modeling Earth Systems and Environment*, 2(2):106, 2016.

[205] Shubha Sathyendranath, Louis Prieur, and André Morel. A three-component model of ocean colour and its application to remote sensing of phytoplankton pigments in coastal waters. *International Journal of Remote Sensing*, 10(8):1373–1394, 1989.

[206] Marten Scheffer, Jordi Bascompte, William A Brock, Victor Brovkin, Stephen R Carpenter, Vasilis Dakos, Hermann Held, Egbert H Van Nes, Max Rietkerk, and George Sugihara. Early-warning signals for critical transitions. *Nature*, 461(7260):53–59, 2009.

[207] Rui Seabra, David S Wethey, António M Santos, and Fernando P Lima. Understanding complex biogeographic responses to climate change. *Scientific reports*, 5, 2015.

[208] Lee A Segel and Julius L Jackson. Dissipative structure: an explanation and an ecological example. *Journal of Theoretical Biology*, 37(3):545–559, 1972.

[209] Sewalt, A Doelman, Hil Gaétan Ellart Meijer, L, V Rottschäfer, and Antonios Zagaris. Tracking pattern evolution through extended center manifold reduction and singular perturbations. *Physica D: Nonlinear Phenomena*, 298:48–67, 2015.

[210] Strogatz SH. Nonlinear dynamics and chaos: With applications to physics, biology, chemistry, and engineering, edition, 2014.

[211] Jonathan A Sherratt. Periodic travelling wave selection by dirichlet boundary conditions in oscillatory reaction-diffusion systems. *SIAM Journal on Applied Mathematics*, 63(5):1520–1538, 2003.

[212] Sun Shulin and Guo Cuihua. Dynamics of a beddington-deangelis type predator-prey model with impulsive effect. *Journal of Mathematics*, 2013, 2013.

[213] Michael Sieber and Frank M Hilker. The hydra effect in predator–prey models. *Journal of mathematical biology*, 64(1-2):341–360, 2012.

[214] Song, RB Ji, HJ, Charles Stock, Kelly Kearney, and Zongling Wang. Interannual variability in phytoplankton blooms and plankton productivity over the nova scotian shelf and in the gulf of maine. *Marine Ecology Progress Series*, 426:105–118, 2011.

[215] Hongjun Song, Rubao Ji, Charles Stock, and Zongling Wang. Phenology of phytoplankton blooms in the nova scotian shelf–gulf of maine region: remote sensing and modeling analysis. *Journal of Plankton research*, 32(11):1485–1499, 2010.

[216] John H Steele and Eric W Henderson. The role of predation in plankton models. *Journal of Plankton Research*, 14(1):157–172, 1992.

[217] Jacqueline Stefels, Michael Steinke, Suzanne Turner, Gill Malin, and Sauveur Belviso. Environmental constraints on the production and removal of the climatically active gas dimethylsulphide (dms) and implications for ecosystem modelling. *Biogeochemistry*, 83(1-3):245–275, 2007.

[218] Michael Steinke, Gill Malin, Stephen D Archer, Peter H Burkill, and Peter S Liss. Dms production in a coccolithophorid bloom: evidence for the importance of dinoflagellate dmsp lyases. *Aquatic Microbial Ecology*, 26:259–270, 2002.

[219] Michael Steinke, Gill Malin, and Peter S Liss. Trophic interactions in the sea: An ecological role for climate relevant volatiles. *Journal of Phycology*, 38(4):630–638, 2002.

[220] Michael Steinke, Jacqueline Stefels, and Eize Stamhuis. Dimethyl sulfide triggers search behavior in copepods. *Limnology and oceanography*, 51(4):1925–1930, 2006.

[221] Michael Steinke, Gordon V Wolfe, and Gunter O Kirst. Partial characterisation of dimethylsulfoniopropionate (dmsp) lyase isozymes in 6 strains of emiliania huxleyi. *Marine Ecology Progress Series*, 175:215–225, 1998.

[222] Lewi Stone. Phytoplankton-bacteria-protozoa interactions: A qualitative model portraying indirect effects. *Marine ecology progress series. Oldendorf*, 64(1):137–145, 1990.

[223] Suzanne L Strom and T Aaron Morello. Comparative growth rates and yields of ciliates and heterotrophic dinoflagellates. *Journal of Plankton Research*, 20(3):571–584, 1998.

[224] William G Sunda and Susan A Huntsman. Processes regulating cellular metal accumulation and physiological effects: phytoplankton as model systems. *Science of the Total Environment*, 219(2):165–181, 1998.

[225] Tang, Hans Henrik Jakobsen, and AW Visser, KW. Phaeocystis globosa (prymnesiophyceae) and the planktonic food web: feeding, growth, and trophic interactions among grazers. *Limnology and Oceanography*, 46(8):1860–1870, 2001.

[226] Kam W Tang and Maiyai Taal. Trophic modification of food quality by heterotrophic protists: species-specific effects on copepod egg production and egg hatching. *Journal of Experimental Marine Biology and Ecology*, 318(1):85–98, 2005.

[227] Tamás Tél and Márton Gruiz. *Chaotic dynamics: an introduction based on classical mechanics*. Cambridge University Press, 2006.

[228] Irena V Telesh. Plankton of the baltic estuarine ecosystems with emphasis on neva estuary: a review of present knowledge and research perspectives. *Marine Pollution Bulletin*, 49(3):206–219, 2004.

[229] Elisa Thébault and Michel Loreau. Trophic interactions and the relationship between species diversity and ecosystem stability. *The American Naturalist*, 166(4):E95–E114, 2005.

[230] David C Thomas. Seaweeds. london: Natural history museum. *ISBN 0-565-09175-1*, 2002.

[231] Jonathan D Todd, Rachel Rogers, You Guo Li, Margaret Wexler, Philip L Bond, Lei Sun, Andrew RJ Curson, Gill Malin, Michael Steinke, and Andrew WB Johnston. Structural and regulatory genes required to make the gas dimethyl sulfide in bacteria. *Science*, 315(5812):666–669, 2007.

[232] Truscott and JE Brindley, J. Ocean plankton populations as excitable media. *Bulletin of Mathematical Biology*, 56(5):981–998, 1994.

[233] Alan Mathison Turing. The chemical basis of morphogenesis. *Bulletin of mathematical biology*, 52(1-2):153–197, 1990.

[234] Upadhyay, RK Naji, and RK Kumari, N. Dynamical complexity in some ecological models: effect of toxin production by phytoplankton. *Nonlinear Analysis: Modelling and Control*, 12(1):123–138, 2007.

[235] Ranjit Kumar Upadhyay, NK Thakur, and B Dubey. Nonlinear non-equilibrium pattern formation in a spatial aquatic system: Effect of fish predation. *Journal of Biological Systems*, 18(01):129–159, 2010.

[236] Volterra V. Variazioni e fluttuazioni del numero d individui in specie animali conviventi. memoire della r. accademia nazionale dei lincei, anno ccccxxiii, ii. 1926.(fluctuations in the abundance of a species considered mathematically). *Nature*, 118:558–560, 1926.

[237] Rafael Vallina, SM Anderson, TR Simó, Albert Gabric, Roger Cropp, and José M Pacheco. A dynamic model of oceanic sulfur (dmos) applied to the sargasso sea: Simulating the dimethylsulfide (dms) summer paradox. *Journal of Geophysical Research: Biogeosciences*, 113(G1), 2008.

[238] Sergio M Vallina and Rafel Simó. Re-visiting the claw hypothesis. *Environmental Chemistry*, 4(6):384–387, 2008.

[239] Kathryn L Van Alstyne, Gordon V Wolfe, Tess L Freidenburg, Anna Neill, and Corrine Hicken. Activated defense systems in marine macroalgae: evidence for an ecological role for dmsp cleavage. *Marine Ecology Progress Series*, 213:53–65, 2001.

[240] Ellen Van Donk, Miquel Lürling, and Winfried Lampert. *Consumer-induced changes in phytoplankton: inducibility, costs, benefits and the impact on grazers.* Princeton University Press, 1999.

[241] Vogt, Vallina M. SM, ET Buitenhuis, L Bopp, and C Le Quéré. Simulating dimethylsulphide seasonality with the dynamic green ocean model planktom5. *Journal of Geophysical Research: Oceans*, 115(C6), 2010.

[242] Volpert and V Petrovskii, S. Reaction–diffusion waves in biology. *Physics of life reviews*, 6(4):267–310, 2009.

[243] Matthijs Vos, Louise EM Vet, Felix L Wäckers, Jack J Middelburg, Wim H Van Der Putten, Wolf M Mooij, Carlo HR Heip, and Ellen Van Donk. Infochemicals structure marine, terrestrial and freshwater food webs: implications for ecological informatics. *Ecological Informatics*, 1(1):23–32, 2006.

[244] Mathis Wackernagel and William Rees. *Our ecological footprint: reducing human impact on the earth*. Number 9. New Society Publishers, 1998.

[245] Yong Wang, Hongbin Wang, and Weihua Jiang. Hopf-transcritical bifurcation in toxic phytoplankton–zooplankton model with delay. *Journal of Mathematical Analysis and Applications*, 415(2):574–594, 2014.

[246] HORST Weikert. Plankton and the pelagic environment. *Red Sea*, pages 90–111, 1987.

[247] Linda Weiss, Christian Laforsch, and Ralph Tollrian. The taste of predation and the defences of prey. *Chemical Ecology in Aquatic Systems*, pages 111–126, 2012.

[248] Stephen Wiggins, Stephen Wiggins, and Martin Golubitsky. *Introduction to applied nonlinear dynamical systems and chaos*, volume 2. Springer, 1990.

[249] Lampert Winfried. Ultimate causes of diel vertical migration of zooplankton: new evidence for the predator-avoidance hypothesis. In *Diel vertical migration of zooplankton*, pages 79–88, 1993.

[250] Gordon V Wolfe. The chemical defense ecology of marine unicellular plankton: constraints, mechanisms, and impacts. *The Biological Bulletin*, 198(2):225–244, 2000.

[251] Sarah A Woodin, Thomas J Hilbish, Brian Helmuth, Sierra J Jones, and David S Wethey. Climate change, species distribution models, and physiological performance metrics: predicting when biogeographic models are likely to fail. *Ecology and evolution*, 3(10):3334–3346, 2013.

[252] Hongyan Xi, Martin Hieronymi, Hajo Krasemann, and Rüdiger Röttgers. Phytoplankton group identification using simulated and in situ hyperspectral remote sensing reflectance. *Frontiers in Marine Science*, 4:272, 2017.

[253] Yariv, Shoshana Naiman, Kanfi, Gail Amir, Victoria Peshti, Guy Zinman, Liat Nahum, Ziv Bar-Joseph, and Haim Y Cohen. The sirtuin sirt6 regulates lifespan in male mice. *Nature*, 483(7388):218–221, 2012.

[254] Peter Yodzis and Stuart Innes. Body size and consumer-resource dynamics. *The American Naturalist*, 139(6):1151–1175, 1992.

[255] Antonios Zagaris and Arjen Doelman. Emergence of steady and oscillatory localized structures in a phytoplankton–nutrient model. *Nonlinearity*, 24(12):3437, 2011.

[256] Antonios Zagaris, Arjen Doelman, NN Pham Thi, and Ben P Sommeijer. Blooming in a nonlocal, coupled phytoplankton-nutrient model. *SIAM journal on applied mathematics*, 69(4):1174–1204, 2009.

[257] Richard K Zimmer and Cheryl Ann Butman. Chemical signaling processes in the marine environment. *The Biological Bulletin*, 198(2):168–187, 2000.

[258] Mikhail V Zubkov, Bernhard M Fuchs, Stephen D Archer, Ronald P Kiene, Rudolf Amann, and Peter H Burkill. Linking the composition of bacterioplankton to rapid turnover of dissolved dimethylsulphoniopropionate in an algal bloom in the north sea. *Environmental Microbiology*, 3(5):304–311, 2001.